IS-T--1529

DE91 012025

Vacuum Ultraviolet Photodissociation and Photoionization of Selected Organosulfur Compounds

by

Nourbakhsh, S.

PHD Thesis submitted to Iowa State University

Ames Laboratory, U.S. DOE

Iowa State University

Ames, Iowa 50011

Date Transmitted: April 26, 1991

PREPARED FOR THE U.S. DEPARTMENT OF ENERGY

UNDER CONTRACT NO. W-7405-Eng-82.

DISCLAIMER

Printed in the United States of America

Available from
National Technical Information Service
U.S. Department of Commerce
5265 Port Royal Road
Springfield, VA 22161

Vacuum ultraviolet photodissociation and photoionization of selected organosulfur compounds

Sohail Nourbakhsh

Under the supervision of C.-Y. Ng
From the Department of Chemistry
Iowa State University

Using translational spectroscopy and photoionization techniques some organosulfur compounds have been studied in the vacuum ultraviolet spectral region. The photofragmentation technique has been used to obtain data from which bond energies, product quantum state distribution, and energy partitioning among photofragments has been calculated. The photofragmentation experiment also provides information on the secondary photodissociation of primary photofragments such as $SSCH_3$, SCH_3, and SH. Photoelectron-photoion coincidence (PEPICO) spectra have been measured in the wavelength region of 900-1475 Å. The PEPICO measurements provide detailed information about the unimolecular decomposition dynamics of state or energy-selected CH_3SH^+ and $CH_3SCH_3^+$. The energetic information obtained in the photoionization and photodissociation experiments allows estimates of the ionization energies for some radicals. Finally, a new laser photolysis method has been developed to study free radicals. Intersecting a high repetition rate excimer laser beam with a pulsed molecular beam, a cold pseudocontinuous beam of free radicals can be generated. Combining photoionization with this technique S, CS, CH_3 and SCH_3 photoionization efficiency curves have been obtained.

Vacuum ultraviolet photodissociation and photoionization

of selected organosulfur compounds

by

Sohail Nourbakhsh

A Dissertation Submitted to the

Graduate Faculty in Partial Fulfillment of the

Requirements for the Degree of

DOCTOR OF PHILOSOPHY

Department: Chemistry
Major: Physical Chemistry

Approved:

In Charge of Major Work

For the Major Department

For the Graduate College

Members of the Committee:

Iowa State University
Ames, Iowa
1991

TABLE OF CONTENTS

ACKNOWLEDGEMENTS

Numerous people have helped me with my accomplishments in graduate school at Iowa State University and the Ames Laboratory. I mention only a few of the many to whom I am indebted.

I deeply thank Professor Cheuk-Yiu Ng for his encouragement, support, understanding, generosity, and sincerity. Dr. Ng has not only taught me about science, but more importantly, has explained many experiences in his life, and this has had a great impact on my life. His motivation, good attitude, determination, and constant striving to be the best is an inspiration to me. I especially enjoyed my last year and half of graduate studies. I appreciate the considerable help he has given me.

I acknowledge Jerry Flesch for the time he took teaching and patiently explaining the instruments to me. Jerry is a genuinely good man who always did his best for me - I learned much from him about being content and good. In the same way, I thank the Chemistry machine shop crew of Eldon Ness, Terry Soseman, and Richard Egger for their prompt service and for always doing an excellent job for me. Eldon has been very helpful in the performance of my research projects. He took my scribbled drawings and came up with ingenious ideas to solve experimental difficulties. Their work is recognized and valued.

I also appreciate the friendship of Kevin Norwood, Win-Bih Tzeng, Ren Xu, Chung-Lin Liao, Homing Yin, Yuguang Li, and Guo-Zhong He. Kevin especially helped me

with my last project. As my academic colleague and a friend, I thank Kevin for helping me and for cheering me up whenever I needed it. His friendship is always remembered.

Finally, I thank my parents, brother, uncle, aunt, and cousins for being there for me. My uncle and aunt made my studies possible by sacrificing from their own life and family. Without their encouragement and support I could not have attended college or graduate school. I am heartfully indebted to my uncle Massoud for sharing his many life experiences. I am also thankful to my brother Ramin for his deep sense of caring.

I acknowledge the Ames Laboratory, operated for the USDOE by Iowa State University, and the Iowa State Chemistry Dėpartment for supporting me and this research. This work was performed at Ames Laboratory under contract no. W-7405-eng-82 with the U. S. Department of Energy. The United States government has assigned the DOE Report number IS-T 1529 to this thesis.

GENERAL INTRODUCTION

In a photofragment translational spectroscopy experiment,[1,2] radiant energy ($h\nu$) is used to cause a bond rupture in a molecule. The recoiling fragments may be translationally and/or internally excited, sharing a total available energy $E_{avl} = h\nu - D_o$ (D_o is the bond dissociation energy). By measuring the flight time between the dissociation and detection regions, the translational energy distribution of the photofragments can be obtained.

The goal is to determine the primary dissociation channels, bond dissociation energies, relative product yields, two-photon processes, and the translational and internal energy partitioning among fragments. The internal energy of the photofragment can be derived from its translational energy, due to conservation of energy and linear momentum in the center of mass. The energy distribution among the photofragments is important in the interpretation of their further reaction.

Theoretical studies of photofragmentation internal energy distributions have been investigated using semiclassical[3] and quantum mechanical models.[4-10] In order to understand better the process of photodissociation, the division of available energy between translational and internal excitation can be compared to the predictions of various models. Theoretical progress in predicting experimental measurements of cross sections is another motivation behind this experiment.

Typically, in this type of experiment an excimer laser beam is crossed with a

molecular beam. Excimer lasers are used because they have high output energy and narrow bandwidth in the ultraviolet region of the spectrum, where most electronic transitions take place. Jet-cooled molecular beams generate an intense beam of molecules with narrow spread in translational energy and negligible internal energies. After the molecule is promoted to a dissociative electronically excited state by absorbing a laser photon, it may fall apart either by direct or indirect dissociation. The product state distribution is determined using a time-of-flight (TOF) quadrupole mass spectrometer, which has the advantage of high sensitivity and universal detection ability. This technique was first introduced by Wilson and co-workers,[11,12] and improved by others.[2,13] Our high resolution rotating beam source laser photofragmentation apparatus is equipped with a translationally movable mass spectrometer which allows an increase in the flight path to achieve high resolution in a TOF measurement.

Using photofragment translational spectroscopy one can learn about the photochemistry of free radicals and determine thermochemical data.[14,15] Combining photofragmentation translational spectroscopy with photoionization mass spectrometry, thermochemical cycles can be completed and one can obtain ionization energies for free radicals.[16,17]

Most of the chemistry in the upper atmosphere starts with an interaction of solar radiation with gases, which could lead to photoionization or photodissociation. Thus the identification and measurement of the primary photofragments resulting from ultraviolet photofragmentation of atmospheric molecules are important in understanding the events that take place in the upper atmosphere. Photofragment translational spectroscopy has

been used to study the photochemistry of selected organosulfur molecules, such as CS_2, CH_3SH, CH_3SCH_3, CH_3CH_2SH, and CH_3SSCH_3. We have chosen to study the photofragmentation of these compounds because they are major air pollutants and therefore have atmospheric importance. Organosulfur compounds absorb ultraviolet radiation in the atmosphere and oxidize to form SO_2. For example, many factories emit methanethiol into the atmosphere, where it is believed to photo-oxidize to SO, SO_2, and SO_3, which is washed out through precipitation to the earths surface.[18] Sulfur pollution is one of the major factors affecting the acidity of moisture and rain water. Perhaps a knowledge of the fundamental information about the ultraviolet photodissociation processes of organosulfur molecules will lead to the development of control methods for processes involving sulfur containing pollutants. Photolysis followed by scrubbing of SO_2 has already been proposed as one way of removing dimethylsulfide in Kraft pulping emission control.[19]

A supersonically cooled radical beam source has been developed. In this beam source, radicals are produced by 193 nm excimer laser photodissociation of stable precursors. Photoionization efficiency spectra of rotationally and vibrationally cold CS and SCH_3 radicals have been measured for the first time.

EXPLANATION OF THESIS FORMAT

This thesis consist of seven sections. Each section is an independent paper and is prepared in a format ready for publication. The tables, figures, and references mentioned in each section pertain only to that section. The specific experimental conditions used in each study are described in each section. The references cited in the general introduction and general conclusion are listed after the general conclusion. The essential signal and velocity transformations from laboratory to center of mass signal and energy are compiled in Appendix A. Appendix B contains the computer programs used for interpretation of experimental data.

SECTION I.

A 193 nm LASER PHOTOFRAGMENTATION TIME-OF-FLIGHT MASS SPECTROMETRIC STUDY OF CS_2 AND CS_2 CLUSTERS

ABSTRACT

A crossed laser and molecular beam photofragmentation apparatus is described. The apparatus is equipped with a rotatable molecular beam source and a translationally movable ultrahigh vacuum mass spectrometer for time-of-flight (TOF) measurements. Using this apparatus we have measured the TOF spectra of S and CS resulting from the photofragmentation processes, $CS_2 + h\nu$ (193 nm) $\rightarrow$ CS(X, v) + S(^{1}D or ^{3}P). The translational energy distributions of photofragments derived from the S and CS TOF spectra are in good agreement. This observation, together with the finding that the TOF spectra of S and CS are independent of laser power in the 25-150 mJ range, shows that the further absorption of a laser photon by CS to form C(^{3}P) + S(^{3}P) within the laser pulse is insignificant. The TOF spectra of S obtained at electron ionization energies of 20 and 50 eV are indiscernible, indicating that the contribution to the TOF spectrum of S from dissociative ionization of CS is negligible at electron impact energies $\leq$ 50 eV. The thermochemical thresholds for the S(^{1}D) and S(^{3}P) channels are determined to be 18.7 and 45.0 $\pm$ 0.4 kcal/mol, respectively, consistent with literature values. Structures found in the translational energy distribution can be correlated with vibrational structures of CS(X, v = 0-5) associated with the S(^{1}D) channel. The translational energy distribution supports the previous observation that the vibrational state distribution of CS(X, v) is peaked at v = 3. The TOF experiment is also consistent with the S(^{3}P)/S(^{1}D) ratio of 2.8 $\pm$ 0.3 determined in a recent vacuum ultraviolet laser induced fluorescence measurement on the S

photofragment. Photofragments from CS_2 clusters are observed at small laboratory angles with respect to the CS_2 beam direction and are found to have velocity distributions peaked at the CS_2 cluster beam velocity.

INTRODUCTION

Photodissociation studies of triatomic molecules have been a rich and mature subfield in photofragment dynamics.[1-6] Due to the advances in laser technology, spectroscopic techniques, and molecular beams, the photodissociation studies of many triatomic molecules have been performed to the detail of state-to-state levels. The precise experimental data obtained have allowed direct comparisons with rigorous theoretical predictions. The satisfactory agreement between experimental and theoretical results for photofragment dynamics of diatomic and triatomic molecules is an important step for further understanding of photodissociation processes involving polyatomic molecules.

Although the photochemistry of CS_2 in the wavelength region of 180-210 nm has been investigated by various spectroscopic techniques,[7-22] detailed agreement between these experiments is lacking. The most controversial result is the branching ratio for the $S(^3P)$ and $S(^1D)$ channels formed by the photodissociation of CS_2 at 193 nm:

$$CS_2 + h\nu\ (193\ nm) \rightarrow CS(X, v) + S(^3P_J) \qquad (1)$$

$$CS2 + h\nu\ (193\ nm) \rightarrow CS(X, v) + S(^1D_2) \qquad (2)$$

The ratio for $S(^3P)/S(^1D)$ obtained previously varies by more than an order of magnitude. The problem in determining the vibrational distribution of CS(X, v) by the laser induced fluorescence method is the strong absorption of CS(X, v) at 193 nm within the dissociating laser pulse resulting in the $A \leftarrow X$ transition. The subsequent emission of CS(A, v′) to CS(X, v) makes the laser induced fluorescence experiment difficult. The

absorption of a 193 nm excimer laser photon by CS(X, $v \geq 5$) may also induce the decomposition of CS(X, $v \geq 5$) to give $S(^3P)$ and $C(^3P)$.[16] If the latter process occurs, the result of the branching ratio measurement will be erroneous. Furthermore, the efficient quenching of $S(^1D)$ by CS_2 may affect the measured branching ratio if $S(^1D)$ and $S(^3P)$ are not monitored at a sufficiently short delay time after the excimer laser pulse.

The most recent photodissociation studies[20-22] of CS_2 at 193 nm have added to the controversy concerning the $S(^3P)/S(^1D)$ branching ratio. By examining the time-resolved vibration-rotation spectral lines of CS(X, v, J), Kanamori and Hirota[21] estimated the branching ratio as 1. A value of 0.66 for $S(^3P)/S(^1D)$ was obtained by McCrary et al.[20] based on the time-of-flight (TOF) spectrum for CS measured at 0° laboratory angle with respect to the CS_2 beam direction and laser induced fluorescence measurements of CS. The laser induced fluorescence detection of $S(^3P)$ and $S(^1D)$ using a vacuum ultraviolet (VUV) laser by Waller et al.[22] gives a value of 2.8 for the $S(^3P)/S(^1D)$ ratio.

The previous experimental results are consistent with the conclusion that the vibrational population of the CS fragment is peaked at $v \sim 3$. This conclusion is not confirmed by the infrared laser kinetic spectroscopic study of Kanamori and Hirota.[21]

Since the pioneering work of Wilson and co-workers,[23-27] the crossed laser and molecular beam photofragmentation spectroscopy with TOF mass spectrometric detection was established to be a universal and detailed method of investigating photodissociation dynamics. Two TOF mass spectrometric experiments have been performed on 193 nm photodissociation of CS_2. The earlier experiment of Yang et al.[18] measured the TOF spectrum of CS at 90° laboratory angle with respect to the CS_2 beam direction. Therefore,

CS fragments having center-of-mass (c.m.) velocities lower than the CS_2 beam velocity are not detected. The translational energy distribution derived from the 90° TOF spectrum of CS is peaked at ~ 5 kcal/mol. However, the more recent measurement of the TOF spectrum of CS at 0° laboratory angle gives a translational energy distribution which is nearly a monotonically decreasing function of translational energy. The greatest population of photofragments are found to be near thermal energy.

In order to shed light on the different results of the previous TOF experiments, we have performed a 193 nm laser photofragment TOF mass spectrometric experiment on CS_2 using a newly constructed rotating beam source laser photofragmentation apparatus in our laboratory. A similar rotating beam source laser photofragmentation apparatus has been reported recently.[28] The unique feature of our apparatus is the translationally movable mass spectrometer which allows the flight path (L) to be varied. At a high signal level, a long flight path can be used to achieve high resolution in TOF measurements. In this study, the TOF spectra for both CS and S are measured. The effects of ionization electron energy and laser power on the measured TOF spectra are examined. Time-of-flight spectra of photofragments from CS_2 clusters are also presented in this report.

EXPERIMENTAL

The cross section of the rotatable beam source laser photofragmentation apparatus is shown in Fig. 1. The apparatus can be divided into three main components: an ArF excimer laser, a photodissociation chamber in which a rotatable supersonic molecular beam intersects with the laser beam, and a linearly movable ultrahigh vacuum electron ionization mass spectrometric detector.

A pure CS_2 beam or a beam of CS_2 seeded in He(Ne) is produced by supersonic expansion through a stainless nozzle (1) with a diameter of 0.127 mm. The nozzle stagnation partial pressure of CS_2 is kept constant at ~ 150 Torr, the vapor pressure of CS_2 at 273 K, by placing CS_2 in a stainless-steel container submerged in a water-ice bath. The seeded CS_2 beam is formed by bubbling the He(Ne) carrier gas through liquid CS_2 before allowing the mixture of CS_2 vapor and He(Ne) to expand through the nozzle. The molecular beam source is pumped by a 20 in. diffusion pump (DP) (Varian HS20) with a pumping speed of ~ 20000 ℓ/s. At a nozzle stagnation pressure (P_o) of 15 psi for the CS_2/He seed beam, a pressure of $\leq 1 \times 10^{-4}$ Torr is maintained in the beam source chamber. The CS_2 beam has an angular divergence of 3° which is defined by the opening of a conical skimmer and a circular aperture as it passes through the differential pumping chamber (7) into the photodissociation chamber (4). The 3° angular spread of the beam corresponds to a beam width of 3 mm at the photodissociation region. The differential pumping chamber is evacuated by a liquid-nitrogen (LN_2) trapped 6 in. DP (Varian VHS6)

Figure 1. Cross-sectional view of the rotating beam source photofragmentation apparatus (1) nozzle, (2) rotatable molecular beam source chamber, (2a) shaft, (3) excimer laser beam, (4) photodissociation chamber, (5) liquid-nitrogen-cooled cold trap, (6) rotatable differential pumping chamber, (7) differential pumping chamber, (8) molecular beam source chamber, (9) bearing, (10) detector axis, (11) liquid-nitrogen cold trap, (12) flexible bellow, (13) valve, (14) extension tube, (15) adjustable aperture, (16) detector chamber, (17) first differential pumping region, (18) second differential pumping region, (19) ionization region, (20) ionizer, (21) to turbomolecular pump (Balzer TPU310), (22) to ion pump (Ultek DI pump, 220 ℓ/s), (23) quadrupole mass filter, (24) photomultiplier assembly, (25) to liquid-nitrogen trapped turbomolecular pump (Balzer TPU50), (26) ion target

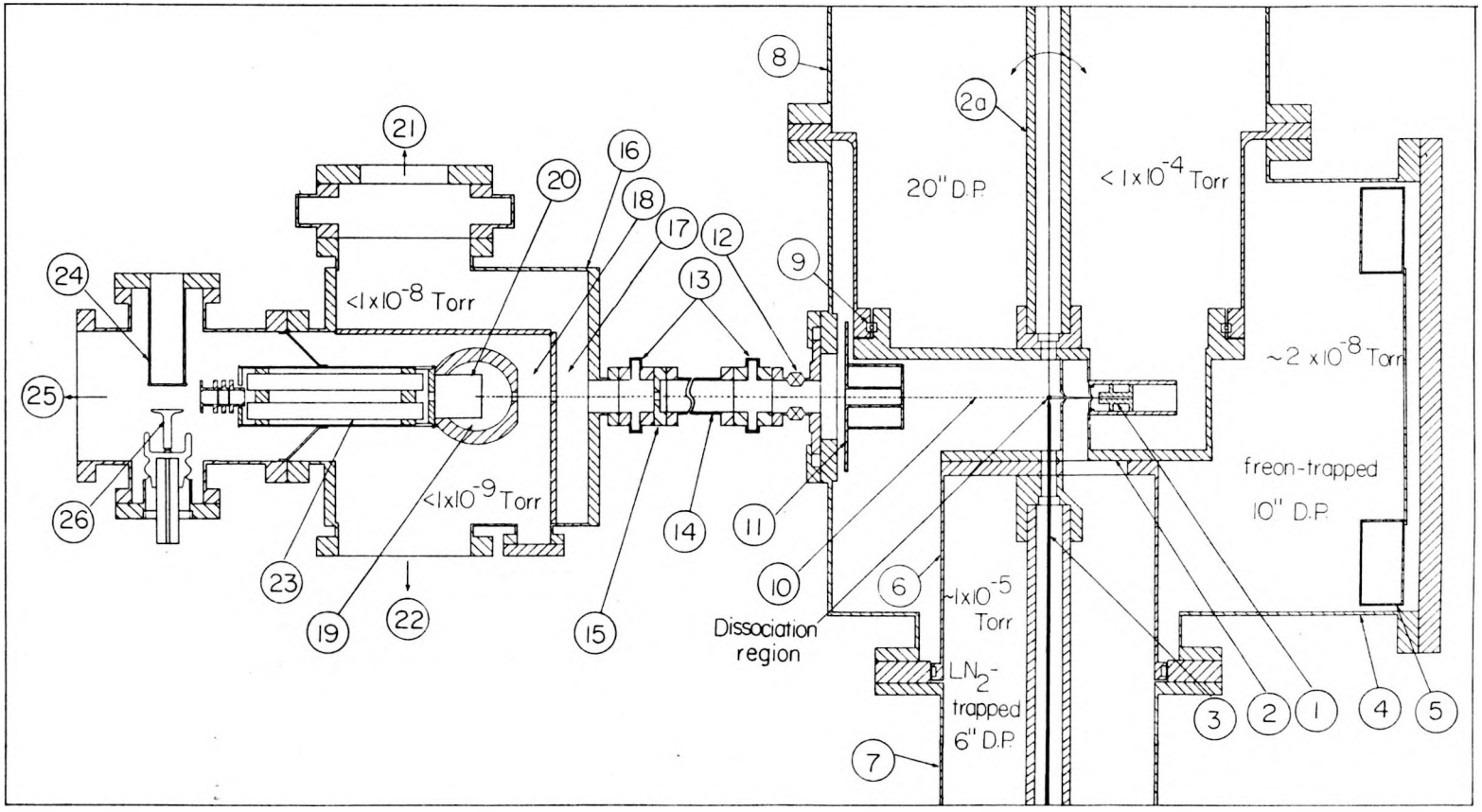
8
2a
21
16
20
18
17
12
13
9
24
25
26
23
19
22
15
14
11
10
6
7
20" D.P.
< 1 x 10⁻⁴ Torr
< 1 x 10⁻⁸ Torr
< 1 x 10⁻⁹ Torr
~2 x 10⁻⁸ Torr
freon-trapped
10" D.P.
~1 x 10⁻⁵ Torr
Dissociation region
LN2-trapped
6" D.P.
3
2
1
4
5

with a pumping speed of ~ 2000 ℓ/s, while the photodissociation chamber is pumped by a freon-trapped 10 in. DP (Varian VHS10) having a pumping speed of ~ 5000 ℓ/s. The photodissociation chamber has two LN_2 cold traps, (5) and (11). When these cold traps are cooled to LN_2 temperature, the photodissociation chamber has a base pressure of ~ 1 x 10^{-8} Torr. During the experiment, the pressures in the differential and photodissociation chambers are maintained at ~ 1 x 10^{-5} and $\lesssim$ 8 x 10^{-8} Torr, respectively. When a pure CS_2 beam is used, the pressure in the photodissociation chamber is $\lesssim$ 2 x 10^{-8} Torr.

The nozzle is mounted on the rotatable beam source chamber (2) which is coupled to the molecular beam source chamber (8) using a bearing (9) and rotating O-ring seal assembly. The rotatable differential pumping chamber (6) is fabricated from a stainless-steel tube. One end of the rotatable differential pumping chamber is rigidly attached to and sealed against the rotatable molecular beam source chamber with an O-ring, while the other end is opened to the differential pumping chamber. The seal between the rotatable differential pumping chamber and the photodissociation chamber is accomplished by a rotating O-ring seal as shown in the figure. A shaft (2a) secured to the center of the rotatable beam source chamber and placed along the common axis of the rotatable beam source and rotatable differential pumping chamber makes possible the rotation of the molecular beam in a plane perpendicular to the common axis. Since the rotatable beam source and rotatable differential pumping chambers rotate together as the shaft is turned, differential pumping for the molecular beam production is achieved without the rotation of any pumps. The rotation of the shaft outside the vacuum chamber can be made manually or automatically by a stepping motor.

The excimer laser used is either a Lambda Physik (MSC201) laser or a Questek (Model 2260) laser, which have a maximum repetition rate of 80 and 200 Hz at an output power of ~ 300 and 100 mJ at 193 nm, respectively. The output power of the Lambda Physik laser can be maintained at a constant value of 100 mJ operating at 80 Hz by a microprocessor (Lambda Physik ILC) for 3-4 h for one gas fill. The excimer laser beam has a cross section of ~ 8 x 24 mm^2.

The laser beam enters the differential pumping chamber through a MgF_2 focusing lens and traverses along the central axis of the rotatable differential pumping chamber before intersecting the CS_2 molecular beam at 90° at the photodissociation region. The fact that the CS_2 molecular beam is adjusted to intersect the common central axis of the rotatable beam source and the rotatable differential pumping chambers ensures the crossing of the laser and the CS_2 beams at all directions of the CS_2 beam.

The mass spectrometric detector has four stages of differential pumpings. The first (17) and second (18) differential pumping regions are evacuated by a turbomolecular pump (Balzer TPU310) and an ion pump (Ultek 220 ℓ/s DI pump), respectively. The ionizer (20) is mounted inside the ionization chamber which is cooled to LN_2 temperature during the experiment. The ionizer is an axial ionizer (Extranuclear Model 041-1) which has an acceptance aperture of ~ 4.8 mm in diameter and a length of ~ 1 cm. The emission current of the ionizer used is ≤ 2.5 mA in this experiment. The ionization region (19) is pumped by a 120 ℓ/s ion pump (Ultek DI pump) and has a base pressure of ~ 5 x 10^{-11} Torr. The apertures between the first and second differential and the ionization chambers are 6 mm in diameter. During this experiment, the pressures in the

first and second differential and ionization regions are $\lesssim 1 \times 10^{-8}$, $\sim 5 \times 10^{-10}$, and $\sim 2 \times 10^{-10}$ Torr, respectively. The quadrupole mass filter (QMF) is constructed of four stainless-steel rods which have a diameter of 1.9 cm and a length of 21 cm and are symmetrically held in a circle of 3.55 cm diameter. The ion detector is a Daly-type scintillation detector[29] which consists of an ion target (26) and a scintillator-photomultiplier assembly (24). The ion detector chamber is separated from the second differential pumping region by the QMF and a sheet metal wall. The vacuum in the ion detector chamber is maintained by a LN_2 trapped turbomolecular pump (Balzer TPU50).

The detector chamber (16) is mounted on a platform which is supported on a linearly movable rail assembly (not shown in the figure). Using the rail assembly, the distance between the photodissociation region and the ionizer can be varied continuously in the range of ~ 35-110 cm. The CS_2 molecular beam axis in the horizontal direction and the central axis of the ionizer define the detector axis. The positions of the platform and rail assembly are carefully adjusted such that the central axis of the ionizer remains in alignment with the detector axis as the detector chamber moves along the full range of rail. The laboratory angle (θ_{lab}) is the angle between the CS_2 molecular beam and the detector axis. The detector chamber is coupled to the photodissociation chamber with a flexible bellows (12) which serves to relieve the slight mechanical misalignment of the two chambers.

The detector and photodissociation chambers can be isolated by isolation valves (13). In order to change the distance between the photodissociation region and the ionizer, i.e., the flight path, an extension tube of the desired length can be placed between the valves.

The isolation valves allow the replacement of the extension tube without venting the detector and photodissociation chambers.

In addition to the two apertures on the differential pumping walls in the detector, there are two more defining apertures along the detector axis. The first aperture (3 mm in diameter) is attached to the LN_2 cold trap (11) in the photodissociation chamber. The adjustable aperture (15), located between the extension tube and the isolation valve of the detector chamber, has an aperture of 6 mm in diameter in the normal photodissociation experiment. In the case when it is necessary to orient the CS_2 beam at the detector (θ_{lab} = 0°) such as in the experiment of measuring the velocity distribution of the CS_2 molecular beam, the adjustable aperture is reduced to a diameter of 0.127 mm.

The data acquisition and operation of the apparatus is controlled by a LSI-11/23 minicomputer. The TOF spectrum is recorded on a homemade 1024 channel scaler which has a minimum channel width of 0.3 μs. The multichannel scaler (MCS) is started by a trigger pulse signifying the firing of the laser. Time-of-flight spectra have also been recorded using a pulsed molecular beam valve (Newport Research Corp.). In a pulsed molecular beam beam experiment, the trigger pulse to the MCS and the excimer laser is delayed by ~ 600 μs with respect to the trigger pulse for opening the pulsed valve.

In order to obtain the translational energy distribution from TOF spectra of photofragments, it is necessary to measure the velocity distribution of the CS_2 molecular beam. Two methods are used to determine the velocity distribution of the CS_2 in this experiment. The first method involves using a TOF chopper wheel to chop the CS_2 beam and record the TOF spectrum of CS_2 from the wheel to the ionizer. In such an

experiment, an aluminum chopper wheel with a diameter of 20 cm and two opening slots is placed between the photodissociation region and the first aperture along the detector. The two opening slots on the edge of the wheel are 0.2 mm wide and 5 mm deep and are separated by 180°. For a chopping frequency of 200 Hz, the chopper produces a CS_2 pulse of 1.6 μs wide every 2.5 ms. The MCS is initiated by a trigger pulse from a photodiode which marks the production of the CS_2 pulse by the chopper wheel. The second method is the laser hole burning method. By firing the excimer laser at the CS_2 molecular beam, one finds that the intensity of the CS_2 beam along the detector axis is reduced for a time equal to the pulse width (15 ns) of the laser. The reduction of the CS_2 signal is due to the dissociation of CS_2 after the absorption of a 193 nm photon. The evolution of the laser burn hole from the photodissociation region to the ionizer recorded by the MCS gives an accurate measure of the velocity spread (Δv) and velocity (v) of the CS_2 molecular beam.

To find the flight time of a photofragment that traveled from the photodissociation region to the ionizer, the time required for the ion to drift from the ionizer to the ion detector must be accounted for. The ion drift time through the QMF depends on the ion mass m and ion energy to the QMF. The ion drift times for several ions (m/e = 2, 18, 32, 44, and 76) have been determined by applying a voltage pulse to the ion extraction lens of the ionizer and measuring the arrival times of the ions at the ion detector with respect to the triggered voltage pulse using an oscilloscope. As expected, at a given ion entrance energy to the QMF, the ion drift time is linearly proportional to $\sqrt{m}$. The actual flight

time of the neutral CS_2 or photofragments is equal to the difference in time measured by the MCS and the ion drift time of the corresponding ion.

DATA ANALYSIS

The analysis of the TOF data involves the transformation of the laboratory TOF spectra into c.m. translational energy distributions. The transformation equation for laboratory to c.m. coordinates has been discussed in detail previously.[30, 31] The electron impact ionizer used here is a number density detector. The c.m. flux $I_{c.m.}(E_{c.m.}, \theta_{c.m.})$ at a given c.m. angle ($\theta_{c.m.}$) and a c.m. translational energy ($E_{c.m.}$) is related to the measured laboratory TOF signal $N_{lab}(t, \theta_{lab})$ and the corresponding θ_{lab} and arrival time t by the equation

$$I_{c.m.}(E_{c.m.}, \theta_{c.m.}) \propto t^3 \, u \, N_{lab}(t, \theta_{lab}), \qquad (3)$$

where u is the c.m. velocity of the photofragment. The translational energy distributions presented here are obtained by the direct application of Eq. (3). The velocities for CS_2 are assumed to be equal to the most probable velocities (v_{mp}) measured by the chopper wheel method or laser hole burning technique. We have ignored the effect of the apparatus resolution factors on the observed TOF distributions.

RESULTS

Velocity Distributions of the CS_2 and $(CS_2)_2$ Beams

Figures 2(a)-2(d) show the laser hole burning spectra of CS_2 observed in a pure CS_2 beam at P_o = 150 Torr, a CS_2/Ne seeded beam at P_o = 517 Torr, a CS_2/He seeded beam at P_o = 362 Torr, and a CS_2/He seeded beam at P_o = 776 Torr, respectively. The most probable velocities (v_{mp}) and the ratio $\Delta v/v_{mp}$ for the CS_2 beam determined by the spectra are summarized in Table 1. Here, Δv represents the velocity spread (FWHM) of the CS_2 beam. In this experiment, the velocity spread of CS_2 is a major limitation to the resolution of the photofragment TOF measurements. The TOF spectrum of CS_2 from the pure CS_2 beam has also been measured by the chopper wheel method. The values of v_{mp} and $\Delta v/v_{mp}$ for the pure CS_2 beam obtained from the TOF spectrum of CS_2 are consistent with those determined from the laser hole burning spectrum shown in Fig. 2(a). Since the masses of the carrier gases are lighter than that of CS_2, the values of v_{mp} for CS_2 from the seeded beams are greater than that for the pure CS_2 beam. The $\Delta v/v_{mp}$ value for the CS_2/He seeded beam at P_o = 776 Torr is ~ 2.5 times smaller than that for the pure CS_2 beam. Considerable amounts of CS_2 dimer and clusters are formed in the CS_2/He seeded beam at P_o = 776 Torr. The laser hole burning spectrum for $(CS_2)_2$ formed in the CS_2/He seeded beam at P_o = 776 Torr is depicted in the lower panel of Fig. 2(d). Due to the slippage effect in the seeded supersonic beam, the velocity of $(CS_2)_2$ is slightly lower than

Figure 2. Laser hole burning spectra for CS_2 in (a) a pure CS_2 beam (P_o = 150 Torr), (b) a CS_2/Ne seeded beam (P_o = 517 Torr), (c) a CS_2/He seeded beam (P_o = 362 Torr), and (d) a CS_2/He seeded beam (P_o = 776 Torr) (upper spectrum); (d) laser hole burning spectra for $(CS_2)_2$ in a CS_2/He seeded beam (P_o = 776 Torr) (lower spectrum)

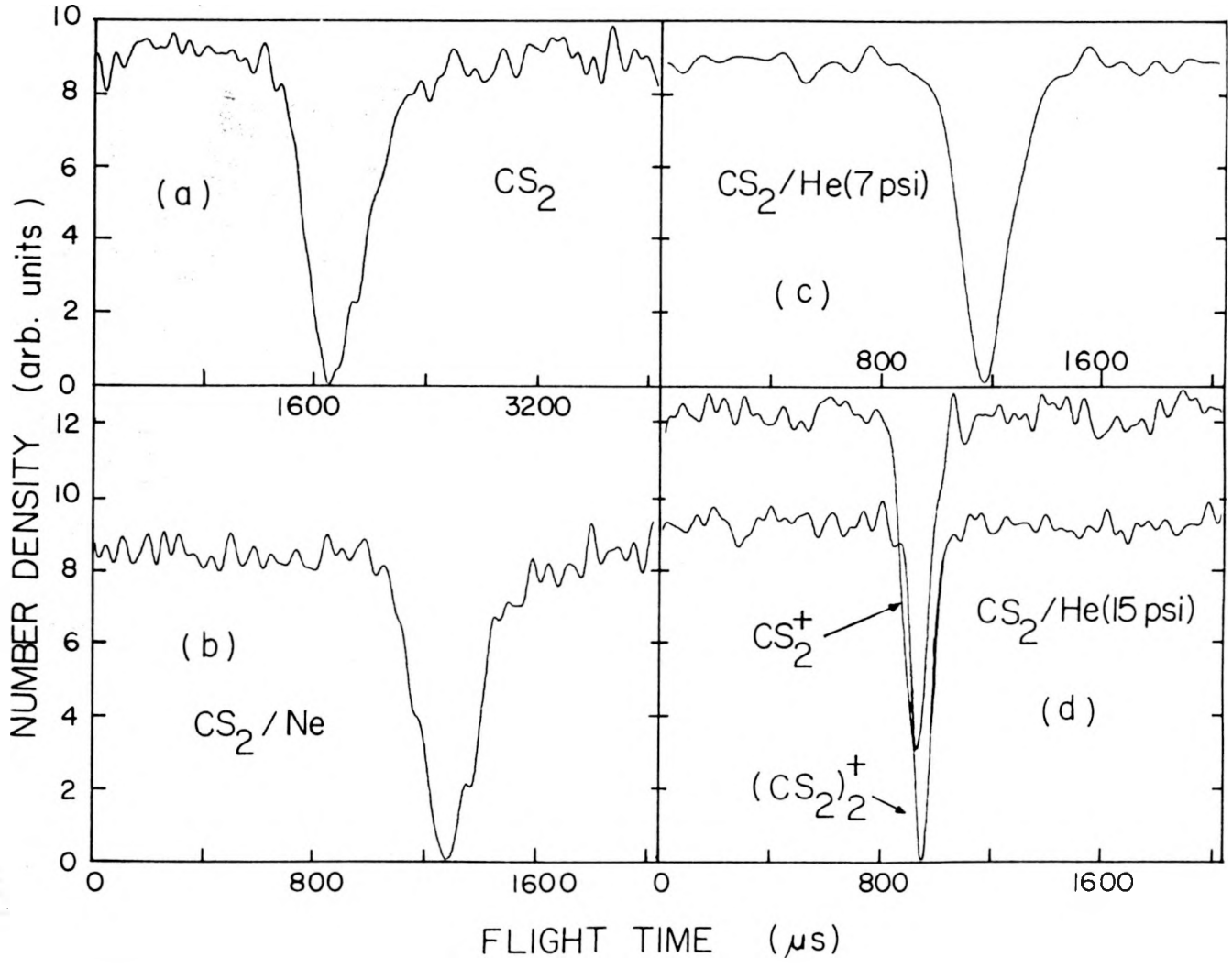
NUMBER DENSITY (arb. units)
FLIGHT TIME (μs)
(a)
CS2
(b)
CS2 / Ne
(c)
CS2/He(7 psi)
(d)
CS2/He(15 psi)
CS2+
(CS2)2+
0
800
1600
3200
2
4
6
8
10
12

Table 1. Characteristics of the CS_2 and $(CS_2)_2$ beams

Nozzle conditions[a]	v_{mp}[b,d]	$\Delta v/v_{mp}$[c,d]
Pure CS_2 beam P_o = 150 Torr, T_o = 300 K	$v_{mp}(CS_2) = 4.68 \times 10^4$ cm/s[e]	0.25[e]
CS_2/Ne seeded beam P_o = 517 Torr, T_o = 300 K	$v_{mp}(CS_2) = 6.68 \times 10^4$ cm/s	0.15
CS_2/He seeded beam P_o = 362 Torr, T_o = 300 K	$v_{mp}(CS_2) = 7.42 \times 10^4$ cm/s	0.15
CS_2/He seeded beam P_o = 776 Torr, T_o = 300 K	$v_{mp}(CS_2) = 9.36 \times 10^4$ cm/s $v_{mp}[(CS_2)_2] = 9.09 \times 10^4$ cm/s	0.10 0.08

[a]Nozzle diameter = 0.127 mm.

[b]Most probable velocity.

[c]Δv represents the velocity spread (FWHM).

[d]Values measured using the laser hole burning method, L = 84.5 cm.

[e]Values of $\Delta v_{mp}/v_{mp}$ determined from the laser hole burning spectrum and the TOF chopper wheel method are in agreement.

that of CS_2. The $\Delta v/v_{mp}$ value for $(CS_2)_2$ is found to be smaller than that for CS_2. The shoulder observed at the longer flight time side for the CS_2^+ dip is probably contributed by CS_2 dimer and higher CS_2 clusters. It is likely that the contribution to the CS_2^+ dip from CS_2 dimer and clusters has broadened the CS_2^+ dip. We believe that the $\Delta v/v_{mp}$ values for CS_2 are upper bounds.

Effect of Ionizer Conditions on TOF Measurements

In the TOF measurements neutral photofragments are ionized in the ionizer before mass filtering and detection. We find that the conditions of the ionizer can affect significantly the appearance of the TOF spectrum of a photofragment. Figures 3(a) and 3(b) compare the TOF spectra of S from CS_2 recorded at two ion extraction voltages of ~ 8 and 0 V, respectively. The ion extraction voltage is the difference in voltage applied to the grid cage where the ions are formed and the ion extraction lens next to the cage. To extract ions from the cage, the potential of the ion extraction lens is lower than the cage. Other than the ion extraction voltage, these two spectra are recorded at the same experimental conditions. The spectrum in Fig. 3(a) exhibits two step like structures and a sharp peak, whereas the spectrum in Fig. 3(b) only reveals a single broad peak. Furthermore, the first onset of the spectrum in Fig. 3(b) is delayed by ~ 80 μs compared to that of the spectrum in Fig. 3(a). We believe that the delay of the TOF of S observed in Fig. 3(b) is due to the space charge effect in the ionizer at 0 V ion extraction voltage. Under this condition the S^+ ion trapped by the space charge potential in the ionizer may

Figure 3. TOF spectra for S obtained using an ion extraction voltage of (a) 8 V, (b) 0 V with respect to the ionizer cage [L = 52.7 cm, θ_{lab} = 15°, P_o = 150 Torr (pure CS_2), T_o = 298 K, electron energy = 50 eV, laser power = 20-120 mJ]

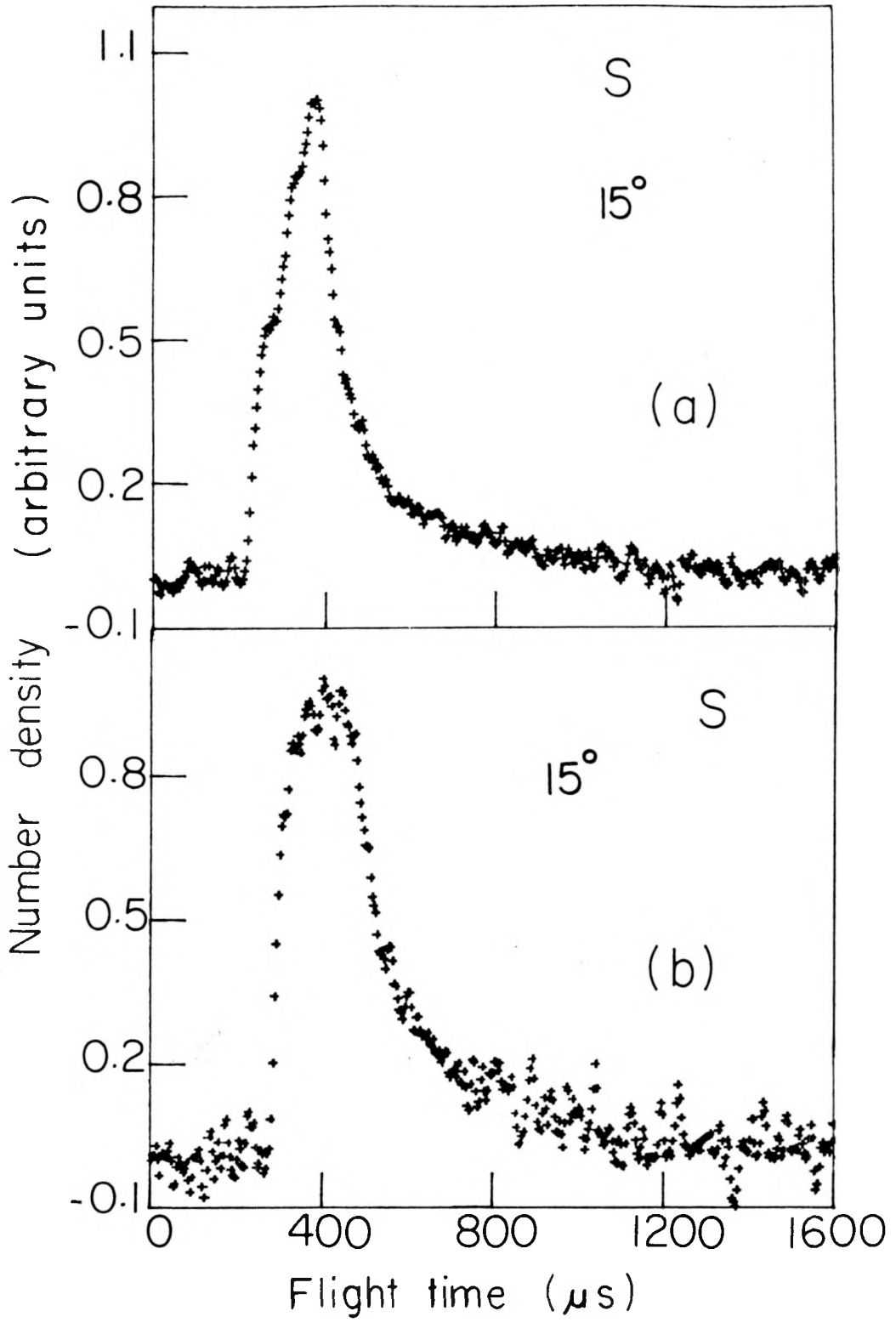
1.1
0.8
0.5
0.2
-0.1
S
15°
(a)
Number density (arbitrary units)
0.8
0.5
0.2
-0.1
S
15°
(b)
0
400
800
1200
1600
Flight time (μs)

be responsible for washing out the TOF structure of the neutral photofragment. A similar observation is found in the comparison of the TOF spectrum of CS obtained using ion extraction voltages of 0 and 8 V. The comparison of TOF spectra recorded at different ion extraction voltages suggests that it is important to minimize the effect of the space charge potential minimum in the ionizer by applying a sufficiently high extraction voltage when performing TOF measurements. All TOF spectra presented in this report were obtained with an ion extraction voltage of ~ 8 V.

Effects of Electron Energy and Laser Power on TOF Measurements

From energetic considerations, CS(X, v) can be produced in v = 0-13 and v = 0-5 by reactions (1) and (2), respectively. In the TOF measurements of S and CS, it is important to examine the effects of the ionization reactions

$$CS(X, v) + e^- \rightarrow CS^+ + 2e^- \quad (4)$$

$$CS(X, v) + e^- \rightarrow C + S^+ + 2e^- \quad (5)$$

on the TOF spectra. If processes (4) and (5) depend on v and/or the cross section for process (5) is high, the measured TOF spectra of CS and S would be erroneous. To minimize the extent of process (5), we have used an ionization electron energy of 50 eV in this experiment. Since the yield of S^+ from CS(X, v) is expected to depend on the ionization electron energy, it is possible to estimate the effect of process (5) by comparing the TOF spectra of S and CS measured at different electron energies. Figures 4(a) and

4(b) depict the TOF spectra of CS and S recorded at θ_{lab} = 10° and an electron energy of 50 eV, respectively. The two spectra have similar structure except that the spectrum of CS is shifted toward longer arrival time compared to the S spectrum. Taking into account the counting statistics, the S spectrum measured at an electron energy of 50 eV is in agreement with that obtained at an electron energy of 20 eV [Fig. 4(c)]. This observation leads us to conclude that process (5) at the electron energy of 50 eV has little effect on the TOF measurements. We arrive at the same conclusion in the comparison of the TOF spectra of CS measured at electron energies of 20 and 50 eV.

The translational energy distributions derived from the TOF spectra of CS and S at θ_{lab} = 10° and an electron energy of 50 eV are compared in Fig. 5(a). The two distributions have been normalized to one at the most probable translational energy of ~ 8 kcal/mol. Taking into account the experimental uncertainties of both spectra, the translational energy distributions are in agreement, indicating that process (4) only depends weakly on v and has little effect on the measured TOF spectra.

Time-of-flight spectra of S and CS have been recorded at different laser powers ranging from ~ 20 to 150 mJ. The laser power is found to have no discernible effect on the TOF spectra of S and CS. This observation shows that the further decomposition of CS(X, v > 5) by absorbing a second excimer photon within the photodissociating laser pulse is insignificant under the present experimental conditions. A similar conclusion was reached in the recent laser kinetic spectroscopic study of Kanamori and Hirota.[21] The majority of TOF spectra reported here are recorded using a constant laser power of 100 mJ.

Figure 4. (a) TOF spectrum of CS observed using an electron energy of 50 eV; (b) TOF spectrum of S observed using an electron energy of 50 eV; (c) TOF spectrum of S observed using an electron energy of 20 eV [P_o = 150 Torr (pure CS_2), T_o = 298 K, L = 52.7 cm, θ_{lab} = 10°, laser power = 20-120 mJ]

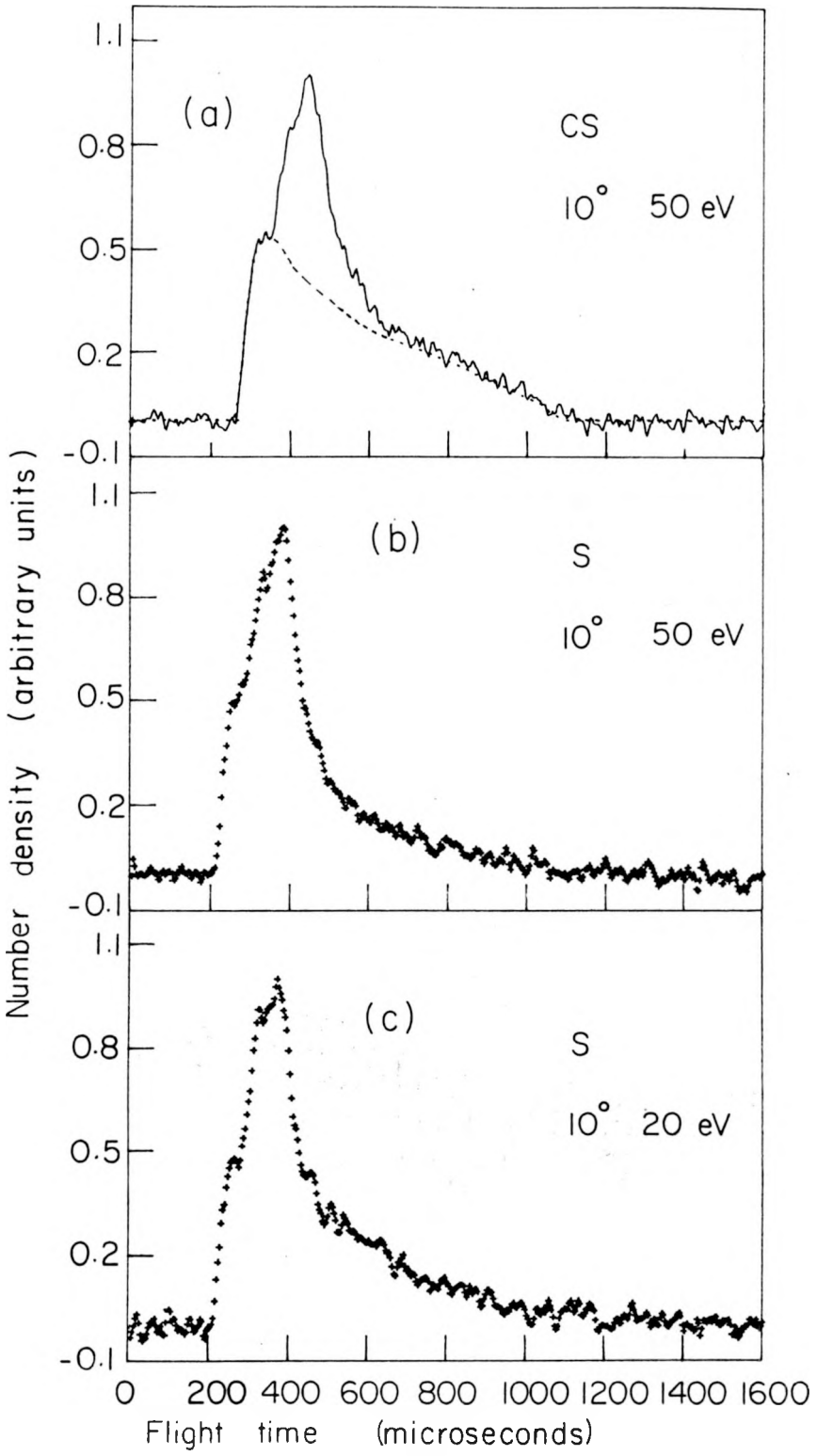
(a)
CS
10° 50 eV
(b)
S
10° 50 eV
(c)
S
10° 20 eV
Number density (arbitrary units)
1.1
0.8
0.5
0.2
-0.1
0 200 400 600 800 1000 1200 1400 1600
Flight time (microseconds)

Figure 5. (a) Translational energy distributions: — derived from TOF spectrum of CS [see Fig. 4(a)]; +++ derived from TOF spectrum of S [see Fig. 4(b)]; --- Ref. 18; -.- Ref. 20 (b) correlation of the translational energy distribution with the expected translational energies for the formation of CS(X, v = 0-5) + $S(^1D)$ and CS(X, v = 0-13) + $S(^3P)$

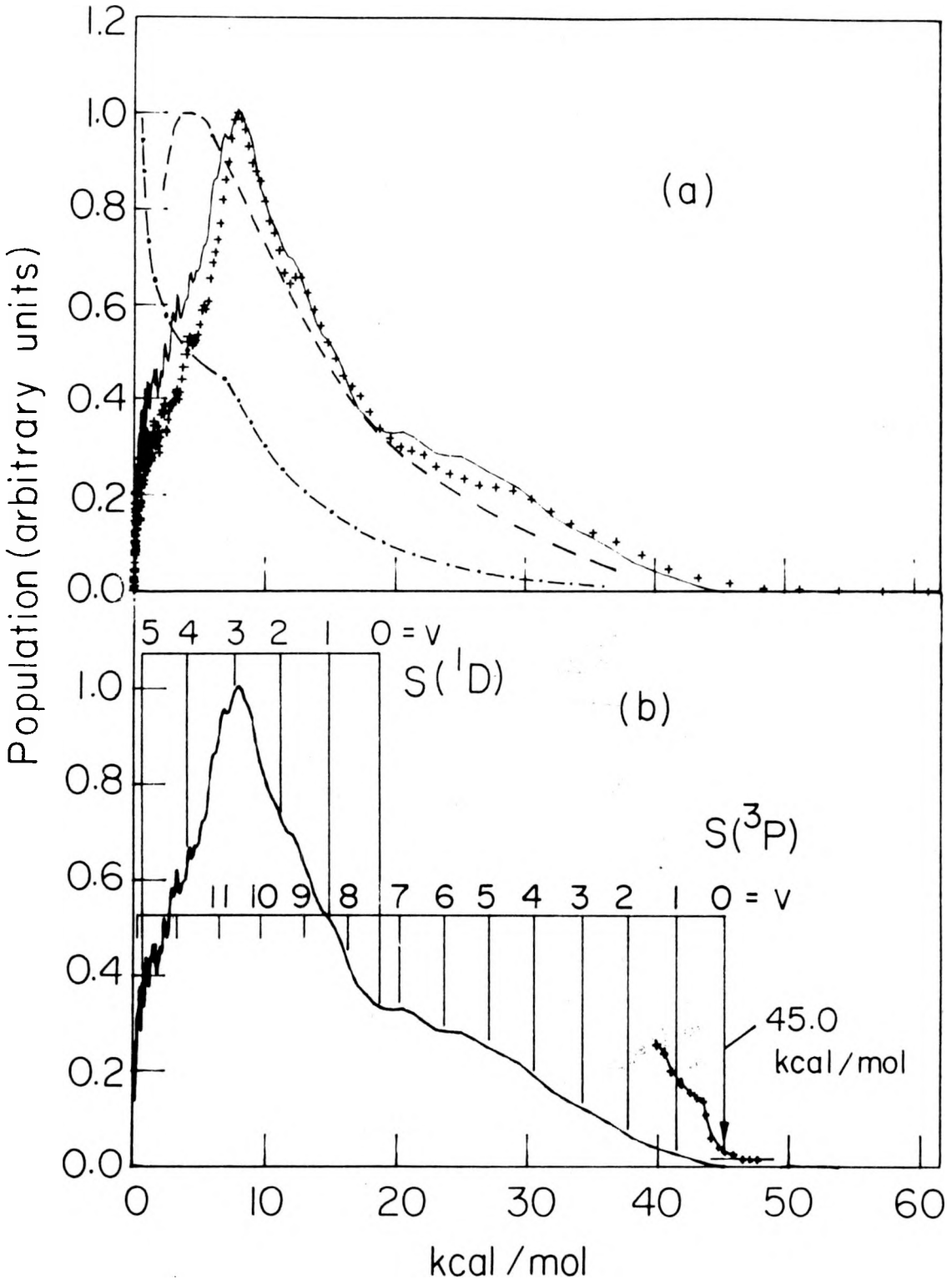
Population (arbitrary units)
1.2
1.0
0.8
0.6
0.4
0.2
0.0
(a)
5 4 3 2 1 0 = v
S(¹D)
(b)
S(³P)
11 10 9 8 7 6 5 4 3 2 1 0 = v
45.0
kcal/mol
0
10
20
30
40
50
60
kcal/mol

TOF Spectra of Photofragments from CS_2/He(Ne) Seeded Beams

The TOF spectra of S obtained at θ_{lab} = 7°, 15°, 30°, 45°, 60°, and 75° using the CS_2/He seeded beam at P_o = 776 Torr are plotted in Figs. 6(a)-6(f), respectively. The TOF spectra of CS are found to be consistent with the S spectra. Since the ion background in the QMF for mass 32 is lower compared to that for mass 44 and a better signal to noise can be obtained at a given accumulation time for the S spectrum than the CS spectrum, we only show the TOF spectra of S here. Figures 7(a) and 7(b) depicted the S spectrum recorded at θ_{lab} = 7° and 15° using the seeded CS_2/Ne beam at P_o = 517 Torr and CS_2/He beam at 357 Torr, respectively. The TOF spectrum of S obtained at θ_{lab} = 30° using the pulsed CS_2/He seeded beam at P_o = 780 Torr is plotted in Fig. 7(c). We found that a signal-to-noise improvement of ~ 100 was achieved by using a pulsed CS_2/He beam in comparison with that obtained with a continuous pure CS_2 beam at P_o = 150 Torr.

The translational energy distributions derived from the TOF spectra of S at θ_{lab} = 30°, 45°, 60°, and 75° [Figs. 6(c)-6(f)] are shown in Figs. 8(c)-8(f), while the translational energy distributions obtained from the spectra in Figs. 7(a) and 7(b) are shown in Figs. 8(a) and 8(b), respectively.

When the seeded CS_2/He(Ne) beams are used, photofragments from CS_2 dimer and clusters are also observed at small θ_{lab} ($\lesssim$ 20°). The TOF spectra for S_2^+ observed at θ_{lab} = 7° and 15° using the seeded CS_2/He beam at P_o ~ 776 Torr are depicted in Figs. 9(a) and

9(b), respectively. The TOF spectra for the $(CS_2)_2^+$, $C_2S_2^+$, and CS_3^+ ions are shown in Figs. 10(a)-10(c), respectively. No effort was made to measure TOF spectra for ions heavier than $(CS_2)_2^+$.

Figure 6. TOF spectra of S observed at (a) θ_{lab} = 7°; (b) 15°; (c) 30°; (d) 45°; (e) 60°; and (f) 75° (L = 84.5 cm, CS_2/He seeded beam at P_o = 776 Torr)

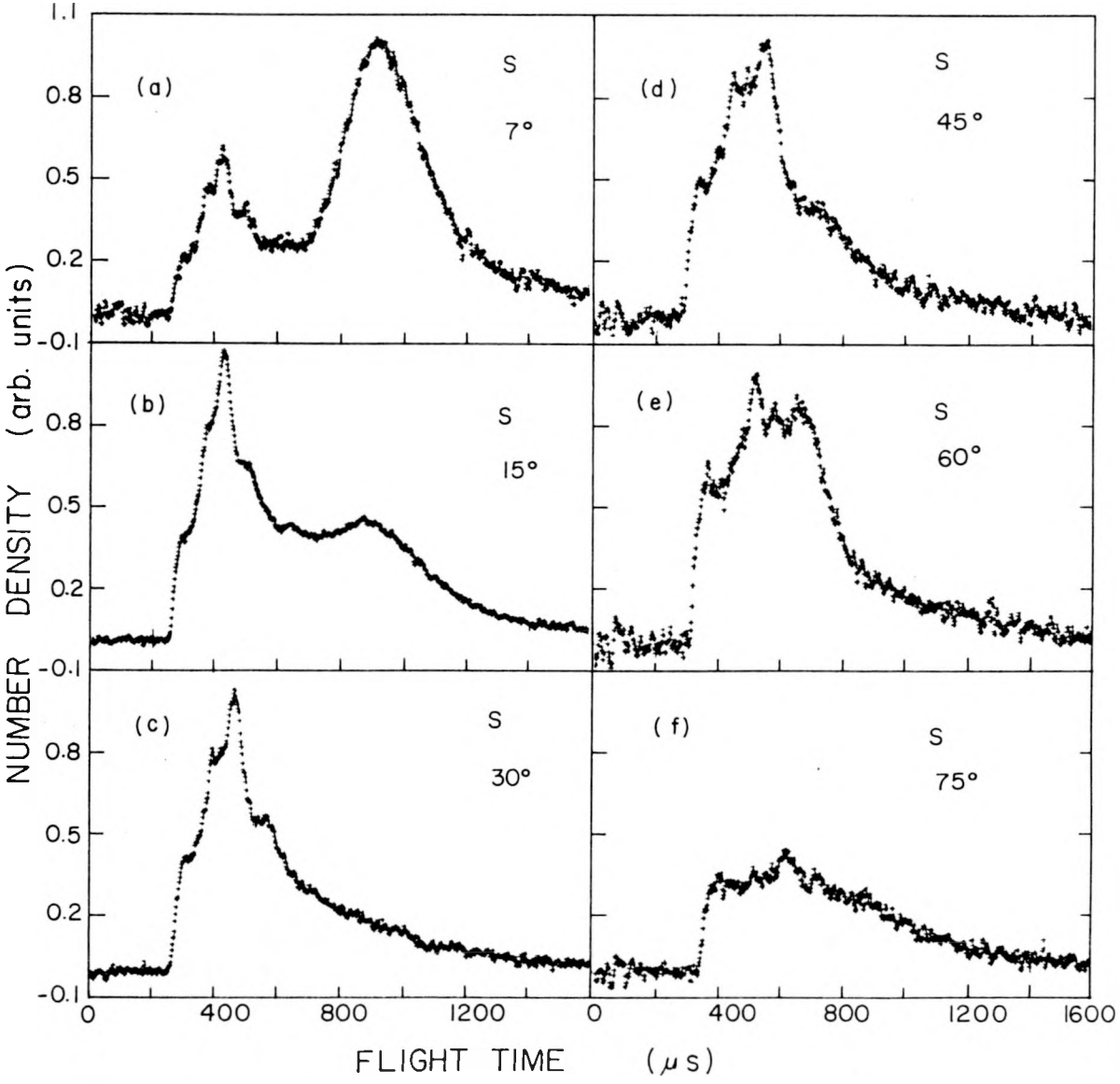
(a)
S
7°
(d)
S
45°
(b)
S
15°
(e)
S
60°
(c)
S
30°
(f)
S
75°
NUMBER DENSITY (arb. units)
1.1
0.8
0.5
0.2
-0.1
0
400
800
1200
1600
FLIGHT TIME (μs)

Figure 7. TOF spectra of S (a) θ_{lab} = 7°, CS_2/Ne seeded beam at P_o = 517 Torr; (b) θ_{lab} = 15°, CS_2/He seeded beam at P_o = 357 Torr; and (c) θ_{lab} = 30°, pulsed CS_2/He seeded beam at P_o = 780 Torr, pulse rate = 48 Hz (L = 84.5 cm)

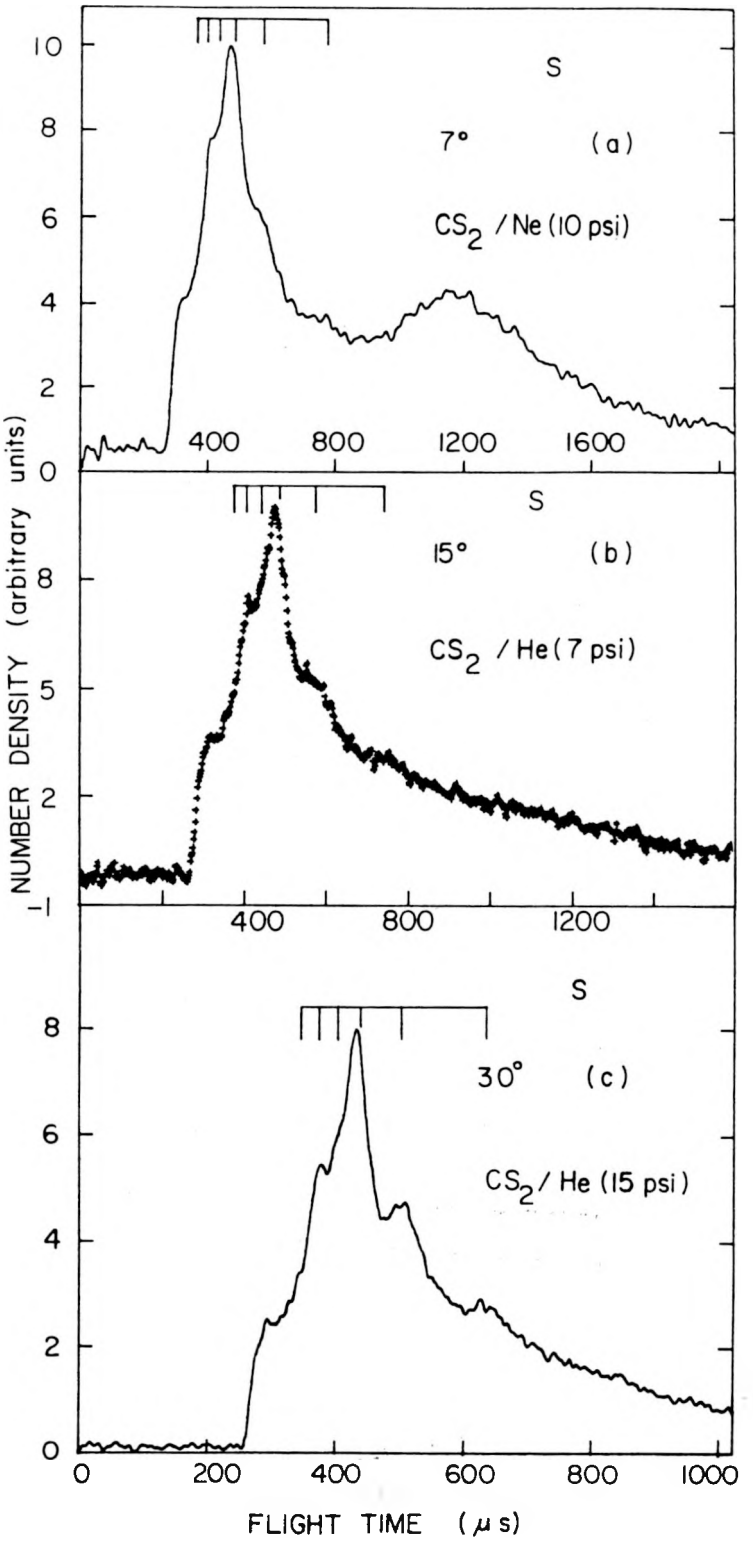
S
7°
(a)
CS2 / Ne (10 psi)
S
15°
(b)
CS2 / He (7 psi)
S
30°
(c)
CS2 / He (15 psi)
NUMBER DENSITY (arbitrary units)
FLIGHT TIME (μs)

Figure 8. Translational energy distribution derived from TOF spectra of S measured at (a) θ_{lab} = 7°, CS_2/Ne seeded beam at P_o = 517 Torr, (b) θ_{lab} = 15°, CS_2/He seeded beam at P_o = 357 Torr, (c) θ_{lab} = 30°, CS_2/He seeded beam at 776 Torr, (d) θ_{lab} = 45°, CS_2/He seeded beam at P_o = 776 Torr, (e) θ_{lab} = 60°, CS_2/He seeded beam at P_o = 776 Torr and (f) θ_{lab} = 75°, CS_2/He seeded beam at P_o = 776 Torr

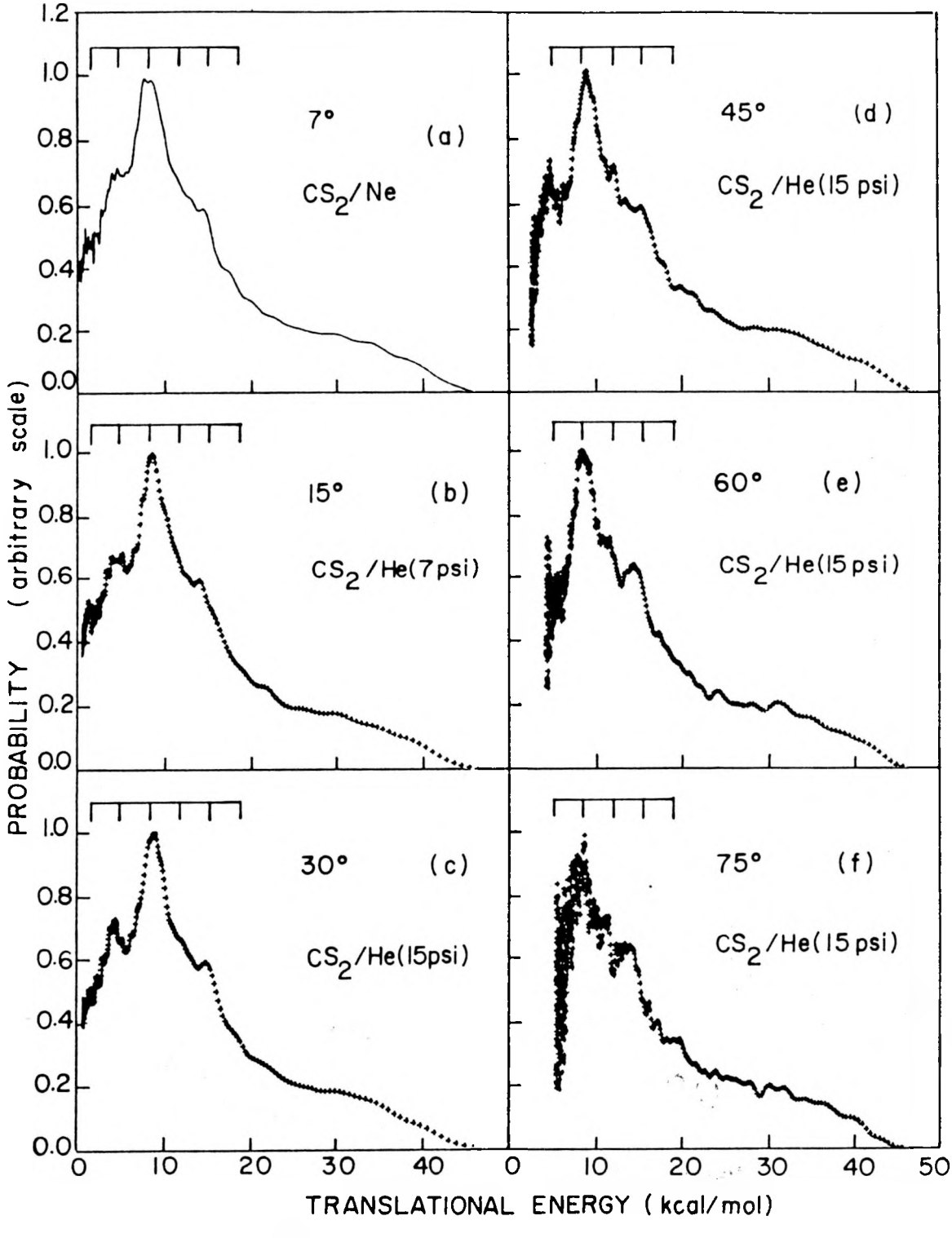
7° (a)
CS2/Ne
45° (d)
CS2/He(15 psi)
15° (b)
CS2/He(7psi)
60° (e)
CS2/He(15psi)
30° (c)
CS2/He(15psi)
75° (f)
CS2/He(15 psi)
PROBABILITY (arbitrary scale)
TRANSLATIONAL ENERGY (kcal/mol)
0.0
0.2
0.4
0.6
0.8
1.0
1.2
0
10
20
30
40
50

Figure 9. TOF spectra for S_2^+ observed at (a) $\theta_{lab} = 7°$ and (b) $\theta_{lab} = 15°$ (L = 84.5 cm, CS_2/He seeded beam at P_o = 776 Torr)

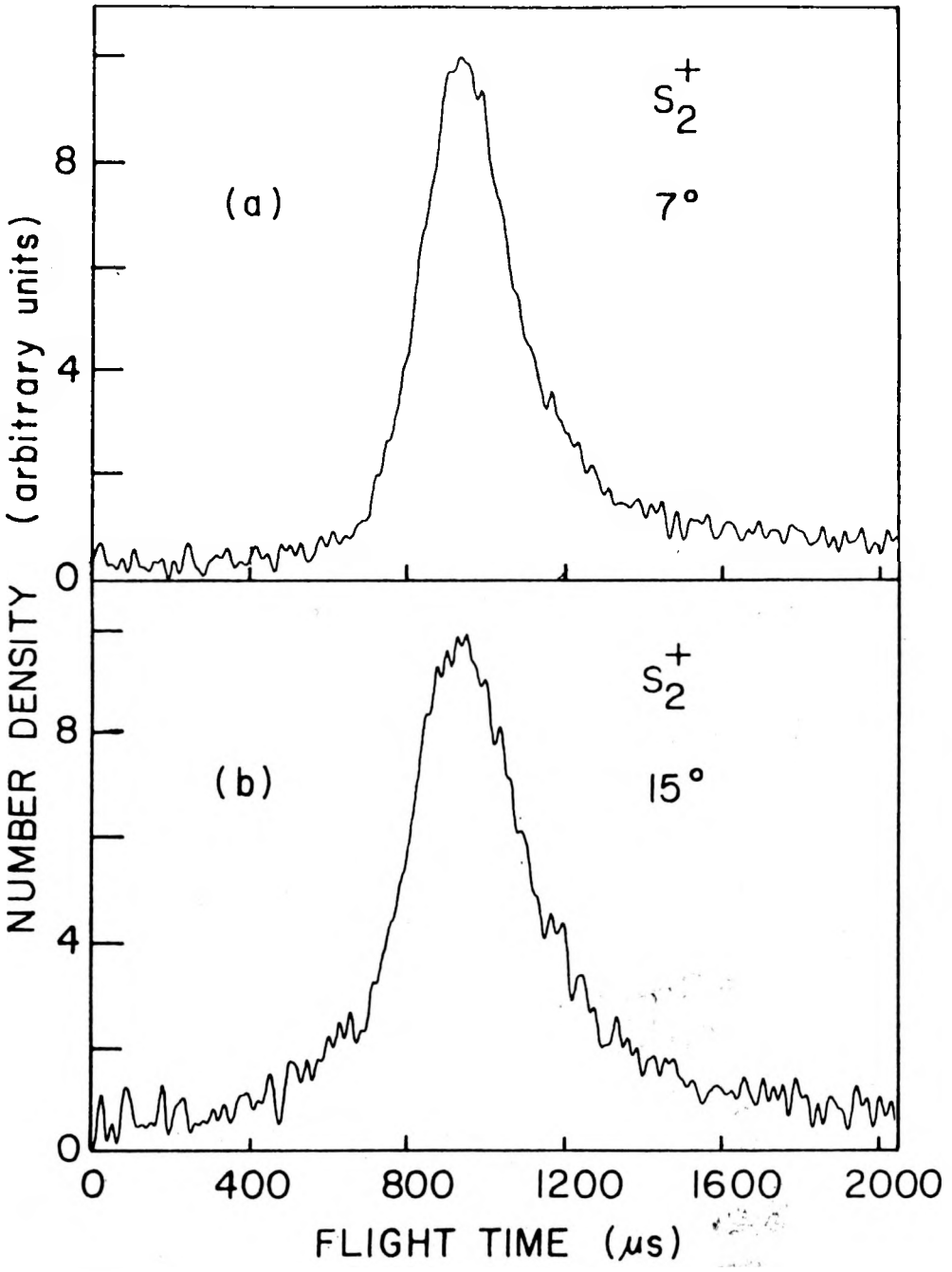
(a)
S_2^+
7°
(b)
S_2^+
15°
NUMBER DENSITY (arbitrary units)
0
4
8
0
400
800
1200
1600
2000
FLIGHT TIME (μs)

Figure 10. TOF spectra for (a) $(CS_2)_2^+$, (b) $C_2S_2^+$, and (c) CS_3^+ observed at θ_{lab} = 7° (L = 84.5 cm, CS_2/He seeded beam at P_o = 776 Torr)

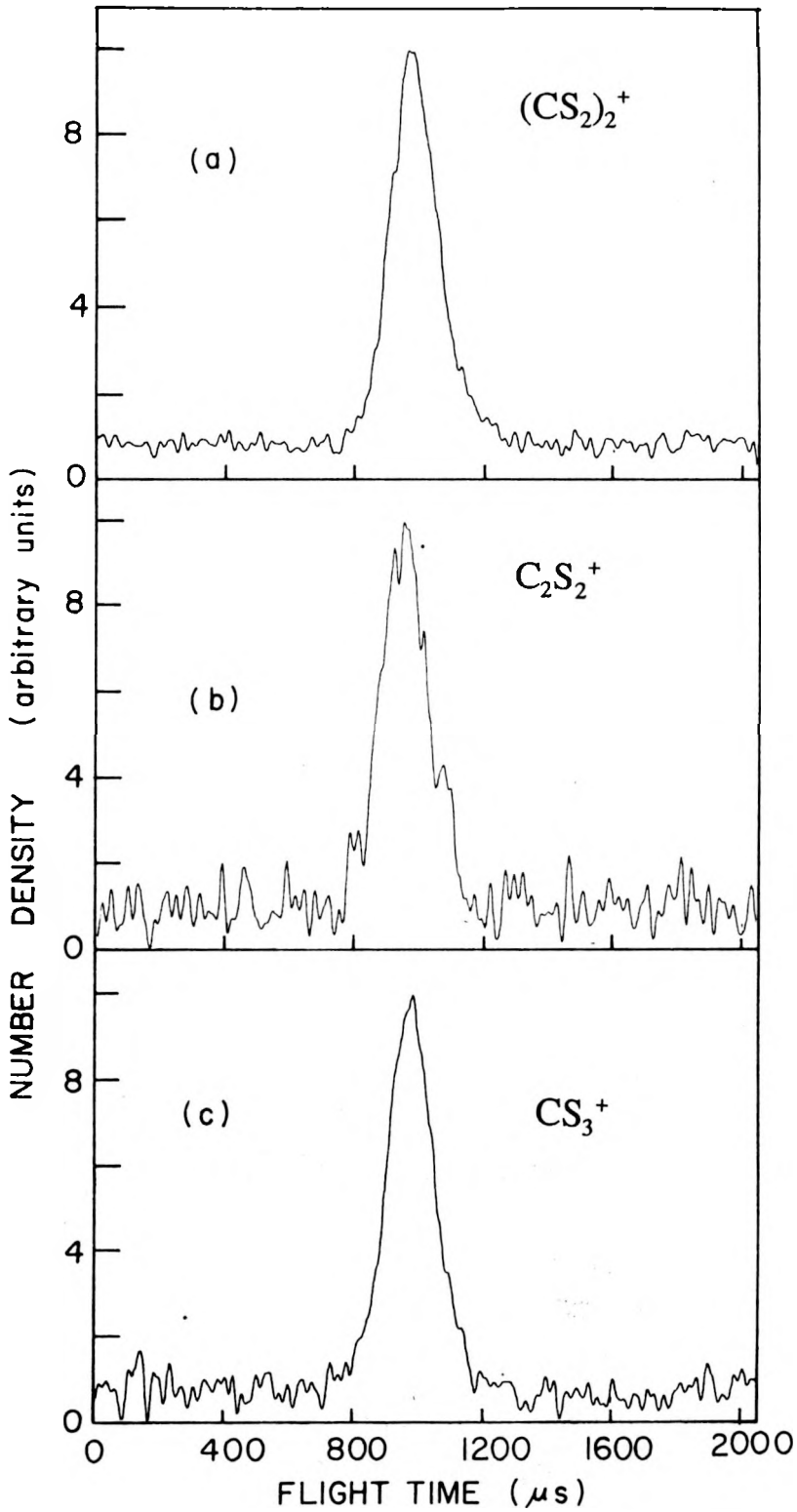
(a)
$(CS_2)_2^+$
(b)
$C_2S_2^+$
(c)
CS_3^+
NUMBER DENSITY (arbitrary units)
0
4
8
0
400
800
1200
1600
2000
FLIGHT TIME (μs)

DISCUSSION

Based on the conservation of energy, we have the relation

$$h\nu + E_{int} = D_o(SC\text{-}S) + E_e + E_v + E_r + E_{c.m.}, \qquad (6)$$

where $h\nu$ is the photodissociation energy, E_{int} is the initial internal energy of the parent CS_2 molecule (which is assumed to be negligible due to the cooling effect in a supersonic beam), $D_o(SC\text{-}S)$ is the SC-S bond dissociation energy, and E_e, E_v, and E_r are the electronic, vibrational, and rotational energy of the photofragments, respectively. The energy separation of the $S(^1D_2)$ and $S(^3P_2)$ states is known to be 26.4 kcal/mol.[2] From the threshold energy for $A \rightarrow X$ emission of CS formed in the irradiation of CS_2 with VUV light, Okabe[11] has determined an upper bound of 102.9 ± 0.32 kcal/mol for $D_o(SC\text{-}S)$. This value is found to be in excellent agreement with the value of 102.7 ± 0.7 kcal/mol obtained from the photoionization experiment.[32] The vibrational spacings of CS(X) have been reported previously.[33] The Newton diagram for the formation of $S(^1D)$ and $S(^3P)$ by 193 nm photodissociation of the pure CS_2 beam at P_o = 150 Torr, constructed using Eq. (6), is depicted in Fig. 11. The two dashed circles show the expected maximum velocities of the S fragments produced by reactions (1) and (2). The magnitudes of the velocities for $S(^3P)$ with CS(X) in v = 0-13 and $S(^1D)$ with CS(X) in v = 0-5 are also shown in the figure. The velocities for S are calculated by assuming $E_r = 0$. The values for θ_{lab} shown are where data were taken. The signal for S was found to decrease rapidly as θ_{lab} is increased (see Fig. 12).

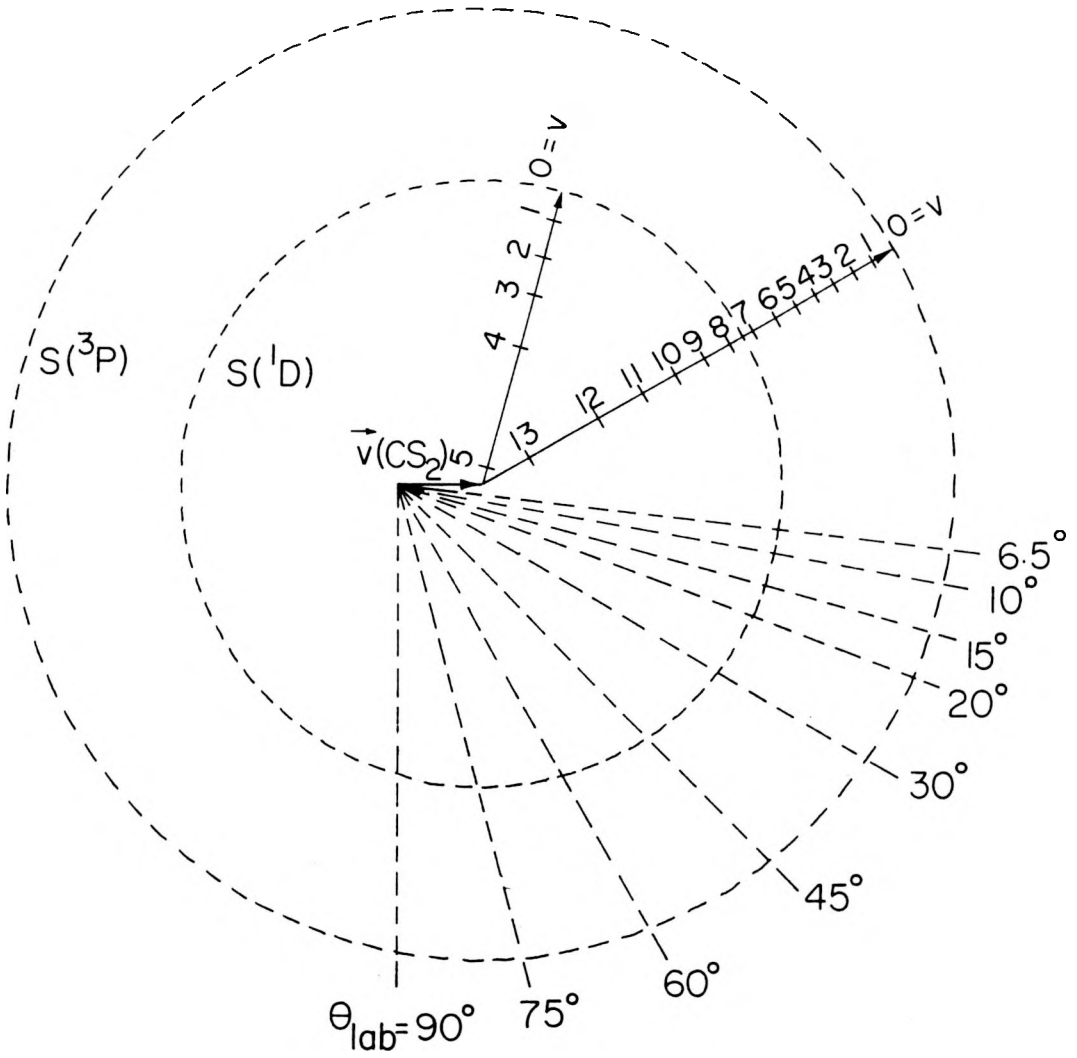

Figure 11. Kinematics for the 193 nm photodissociation of a pure CS_2 beam

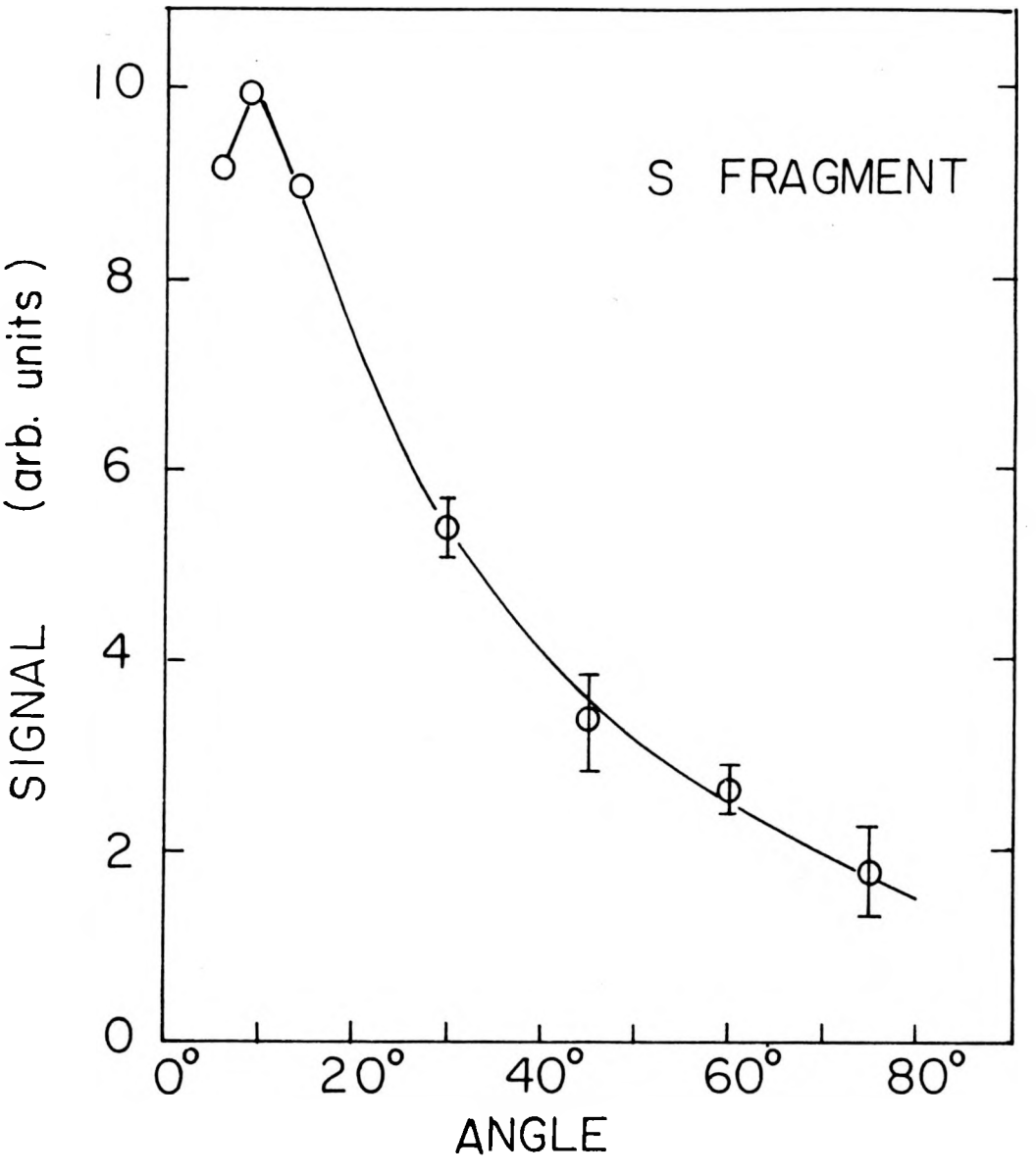

Figure 12. Laboratory angular distribution of S

It is clear from the Newton diagram that when the S fragment is detected at large θ_{lab}, e.g., $\theta_{lab} = 90°$, slow S fragments with velocities less than the CS_2 beam velocity cannot reach the detector. The primary motivation of the coaxial TOF experiment of McCrary et al.[20] is to detect photofragments at all translational energies. They concluded from their coaxial TOF measurement that a considerable fraction of photofragments are formed at low translational energies and these slow photofragments were not observed in the perpendicular TOF measurement of Yang et al.[18] Figure 5(a) compares the translational energy distributions obtained by McCrary et al., Yang et al., and this work. The translational energy distribution of this work is derived from the CS spectrum shown in Fig. 4(a), which is measured at $\theta_{lab} = 10°$. The peaks of the distributions are arbitrarily normalized to one. The results of Yang et al. and this work are in qualitative agreement except that the peak of their distribution is lower by ~ 3 kcal/mol compared to that of ours. The nearly exponential increase in population towards low translational energy found by McCrary et al. is not confirmed in this experiment. However, the translational energy distribution derived from their TOF spectrum of CS measured at $\theta_{lab} = 90°$, which is not shown in the figure, is consistent with our results. When the neutral CS_2 beam is aimed directly at the ionizer, i.e., $\theta_{lab} = 0°$, the ion background for CS^+ is expected to be very high. The coaxial TOF spectrum of CS recorded by McCrary et al. might have been affected by the space charge effect in the ionizer.

The relative populations of the spin-orbit sublevels of $S(^3P_J)$ were determined to be $^3P_2 : {}^3P_1 : {}^3P_0 = 4.0 : 2.1 : 1.0$ in the VUV laser induced fluorescence experiment of Waller et al.[22] The position in translational energy correlating to the formation of CS(X, v = 0-5) +

$S(^1D_2)$ and $CS(X, v = 0\text{-}13) + S(^3P_2)$ are indicated in Fig. 5(b). The threshold for the formation of $CS(X, v = 0) + S(^3P_2)$ is found to be 45.0 ± 0.4 kcal/mol in this experiment. Assuming $E_{int} = 0$, we calculate a value of 102.9 ± 0.4 kcal/mol for $D_o(SC\text{-}S)$ which is in excellent agreement with those determined previously in the fluorescence[11] and photoionization[32] experiments. The uncertainties of ± 0.4 kcal/mol are in accordance with the variation of the threshold values observed in the translational energy distributions shown in Figs. 8(a)-8(f) which are derived from the TOF spectra of S measured using the seeded CS_2/He(Ne) beam method. At 18.7 kcal/mol, there is a clear break in the translational energy distribution which coincides with the thermochemical threshold for the formation of $CS(X, v = 0) + S(^1D_2)$. This break was observed, but less clearly, in the translational energy distribution reported by Yang et al.

Because of the narrower velocity spreads for parent CS_2 achieved in the CS_2/He(Ne) seeded beams compared to that in the pure CS_2 beam, the resolutions of the TOF spectra recorded using the seeded CS_2/He(Ne) beams are higher than those of the spectra shown in Figs. 4(a) and 4(b). Structures which can be correlated with the formation of $CS(X, v = 0\text{-}5) + S(^1D_2)$ are discernible in the TOF spectra of S [Figs. 6(a)-6(f) and Figs. 7(a)-7(c)] using seeded CS_2/He(Ne) beams. The stick marks in Figs. 7(a)-7(c) and Figs. 8(a)-8(f) indicate the expected flight times and translational energies, respectively, for the formation of $CS(X, v = 0\text{-}5) + S(^1D_2)$. The structures corresponding to v = 4 and 5 are most well-resolved in the TOF spectrum of S [Fig. 7(c)] measured using the pulsed CS_2/He seeded beam. The fragment laboratory velocity $\mathbf{v}_{lab}$ is equal $\mathbf{u} + \mathbf{v}_{mp}$. As θ_{lab} increases, the magnitude of $\mathbf{v}_{lab}$ decreases. Thus, the TOF resolution improves as θ_{lab}

increases. This effect can be seen in Figs. 8(a)-8(f). The broad peaks appearing at longer flight times in Figs. 6(a), 6(b), and 7(a) are due to the photodissociation of CS_2 dimer and clusters and will be discussed in a later section. Although the TOF spectra of S observed at $\theta_{lab} = 45°$, 60°, and 75° are quite different from those at $\theta_{lab} \leq 30°$, the translational energy distributions derived from these spectra are essentially identical. The transformation of the slow broad peaks in the TOF spectra into energy space gives a low energy peak at translational energy well below 1 kcal/mol. The low energy peak originating from the slow broad peak in Fig. 7(a) has been deleted from the translational energy distribution of Fig. 8(a).

The absorption band of CS_2 in the region between 185-230 nm has been assigned as the linear $\rightarrow$ bent, $X^1\Sigma_g^+ \rightarrow \tilde{A}^1B_2$, transition.[34-36] The transition results in excitation of both the symmetric stretch and bending vibrations and gives rise to a complex absorption spectrum. The $\tilde{A}^1B_2$ state has a lifetime of ~ 1 ps and a very low fluorescence quantum yield ($< 10^{-3}$).[18,37] The rapid predissociation of $CS_2(\tilde{A}^1B_2)$ is believed to be the mechanism for the formation of CS + S. The bent structure of $CS_2(\tilde{A}^1B_2)$ is consistent with the observation that CS(X, v) fragments are produced in a broad distribution of rotational states.[21] The lack of vibrational structure in the TOF spectra for the CS(X, v) + $S(^3P)$ channel can be attributed to the rotational excitation of CS(X, v) and the population of $S(^3P)$ in the spin-orbit sublevels. Although CS(X, v) fragments associating with the $S(^1D_2)$ channel were also found to be rotationally excited, the rotational excitation energy ranges for CS(X, v) formed in the singlet channel allowed by energy conservation are much narrower than those in the triplet channel. The TOF experiment of Yang et al. revealed

an isotropic angular distribution of CS and estimated a lower limit of 0.6 ps for the predissociation lifetime of CS_2. However, the recent experiment of Waller et al. using Doppler spectroscopic techniques observed an anisotropy in dissociation and provided a lifetime of 2 ps for the excited $\tilde{A}^1B_2$ state. The discrepancy between the two experiments has been attributed to rotational cooling of CS_2 molecules by supersonic expansion in the experiment of Waller et al., while a thermal CS_2 effusive beam was used in the work of Yang et al. The 193 nm excimer laser beam used in this experiment is not polarized. The CS and S fragments are expected to scatter isotropically in space. The finding that translational energy distributions [Figs. 8(a)-8(f)] derived from TOF spectra at different θ_{lab} are identical is consistent with this expectation.

The TOF measurement cannot provide a clear separation between the singlet and triplet channels. Thus, the $S(^3P)/S(^1D)$ ratio cannot be determined unambiguously from the translational energy distribution. Since the intensities of CS_2 dimers and clusters produced in the pure CS_2 beam are negligible compared to that of the CS_2 monomer, the TOF spectrum of CS shown in Fig. 4(a) is predominantly due to the dissociation of CS_2. The sharp rise in the CS spectrum at ~ 354 μs which corresponds to the break at 18.7 kcal/mol in the translational energy distribution is assigned as the thermochemical threshold for reaction (2). Assuming the photodissociation products with translational energies below 18.7 kcal/mol are all formed in the singlet channel, we calculate a lower limit of 0.4 for the $S(^3P)/S(^1D)$ ratio. There seems to be a break at ~ 650 μs, midway at the drop-off of the TOF signal from the peak at ~ 440 μs. If one connects the breaks at 354 and 650 μs by the dashed line as shown in Fig. 4(a) and assumes the signals above

and below the dashed line to be due to the singlet and triplet channels, respectively, an estimate of 2.6 is obtained for the $S(^3P)/S(^1D)$ ratio. The division of the populations for the two channels in the translational energy distribution can be seen in Fig. 5(b). Similar exercises based on the translational energy distributions, shown in Figs. 8(a)-8(c), give values between 2.5 to 2.7 for the ratio. The estimate of 2.6 for the $S(^3P)/S(^1D)$ ratio is in agreement with a value of 2.8 ± 0.3 determined by Waller et al. This observation can be taken as a support for the data analysis described above.

Assuming the data analysis to be correct, we have deduced a bimodal vibrational distribution for CS(X, v = 0-13) produced by reactions (1) and (2). Figure 13 compares this distribution and those obtained in previous studies. The relative populations for CS(X, v = 5) have been normalized to have the same value. The relative vibrational populations for CS(X, v = 1-5) have been measured earlier by Butler et al.[17] in a laser induced fluorescence experiment. They found that the CS(X, v) fragments are formed with a maximum population at v = 3. As shown in the figure, this finding is consistent with the conclusion of the later experiments.[18,22] Taking into account the experimental uncertainties, the relative populations for CS(X, v = 0-5) measured by Butler et al., Waller et al., and this work are in good agreement. Our results for v = 6-10 are also in accord with those obtained most recently by Waller et al. using Doppler spectroscopic techniques. The relative populations for CS(X, v = 11-12) estimated in this study are higher than those of Waller et al. As shown in Fig. 5(a), the populations of fragments at translational energies below ~ 8 kcal/mol derived from the TOF spectrum of S [Fig. 4(b)] are lower than those from the CS spectrum by ~ 10%-20%. Therefore, it is possible that our values

Figure 13. Experimental values for the relative vibrational population of CS(X); ⊙:this work; ⊡:Ref. 22; [ ]:values obtained using the translational energy distribution of Ref. 22 and the correct translational energies corresponding to the formation of CS(X, v = 11-13) (see text); Δ:Ref. 17; +:Ref. 18; ●:Ref. 20

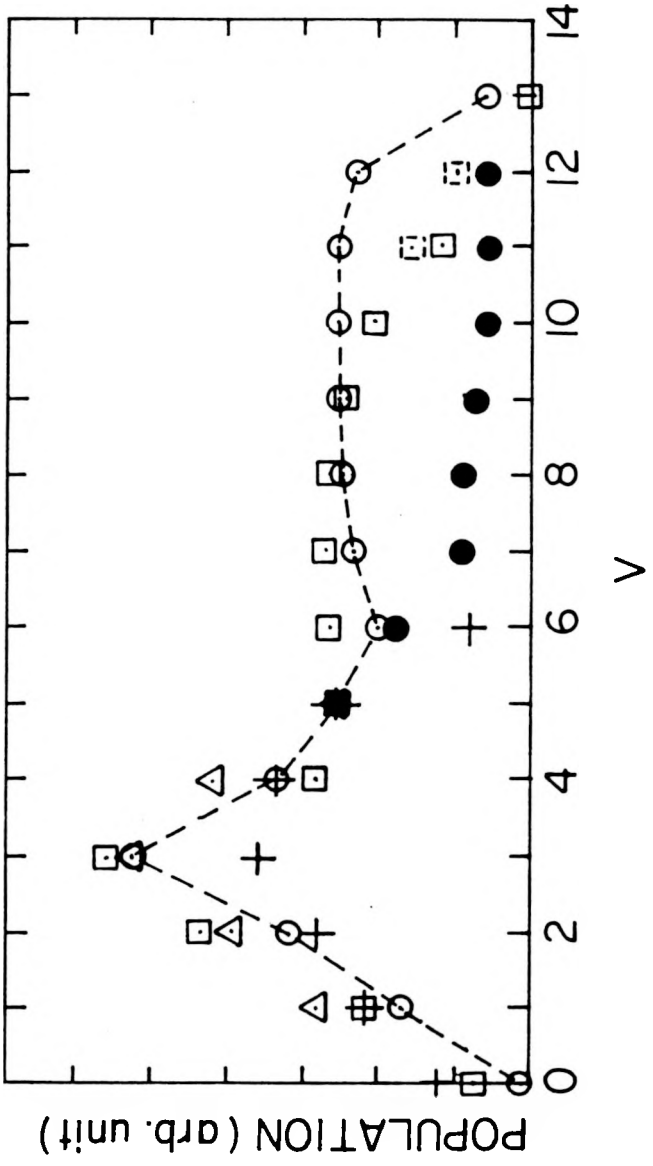
POPULATION (arb. unit)
0
2
4
6
8
10
12
14
v

for v = 11-13 are ~ 10%-20% too high. We note that the values for the translational energies of fragments corresponding to the formation of CS (X, v = 11-12) used by Waller et al. to determine the relative vibrational populations for v = 11-12 are incorrect. Using the correct translational energies for v = 11-13, together with their translational energy distribution, we obtained higher values for the populations of CS (X, v = 11-13) which are included in Fig. 13. The above considerations bring the results for v = 11-13 of the two experiments in satisfactory agreement. The relative populations for v = 7-12 measured by McCrary et al. seem to be too low.

The formation of C + S_2 from CS_2 requires 7.5 eV (Ref. 38). Thus, S_2 cannot be produced by one photon absorption at 193 nm. Signals observed at ion masses corresponding to S_2^+, $(CS_2)_2^+$, $C_2S_2^+$, and CS_3^+ necessarily originate from photofragmentation of CS_2 dimers and clusters. All the TOF spectra of these ions are peaked at 930-970 μs (see Figs. 9 and 10). The slight variations in position of the peaks can be mostly accounted for by the different drift times of the ions from the ionizer to the ion detector. The slower broad peak resolved in the TOF spectrum of S at θ_{lab} = 7° [Fig. 6(a)] has the maximum at the same position in flight time (~ 930 μs), indicating that it is also produced by photofragments of CS_2 dimers and clusters. As mentioned above, a similar broad peak was found in the TOF spectrum of CS at θ_{lab} = 7° which is not shown here. The heights of the slower broad peaks relative to the fast peaks in the S and CS spectra reduce substantially as P_o is decreased. This is the most convincing evidence that the slower broad peak is due to CS_2 dimers and clusters. The magnitude of the slow broad peak diminishes quickly as θ_{lab} is increased. At θ_{lab} = 30°, the broad peak is

indiscernible in the S and CS spectra [see Fig. 6(c)]. The TOF peaks attributed to cluster fragmentation appear at essentially the same flight time position (925-950 μs) of the CS_2 beam, i.e., the cluster photofragments have nearly the same velocities as the parent CS_2 dimers and clusters and are strongly focused in the forward direction. This is the expected kinematic situation when the heavy fragment is detected in a light-heavy dissociation process.

The widths (FWHM) of the S_2^+ TOF peak and the slower broad peaks in the S and CS spectra are identical and have a value of ~ 260 μs. The TOF peaks for $(CS_2)_2^+$, $C_2S_2^+$, and CS_3^+ are also found to have the same width (~ 170 μs) which is closer to the width (~ 104 μs) of the CS_2 parent beam. The width of the TOF peak for an ion is a measure of the translational energy spread of the neutral photofragment from which the ion is produced. No attempt was made to characterize the distribution of CS_2 clusters in the experiment. According to the previous molecular beam photoionization study of CS_2 (Ref. 39), CS_2 clusters $(CS_2)_n$, n = 2-5, are formed with appreciable concentrations in the supersonic expansion of a CS_2/Ar seeded beam at P_o = 450 Torr. Using a CS_2/He seeded beam at P_o ~ 776 Torr, we expected that higher CS_2 clusters, n > 5 are produced. To a first approximation, one may consider the photodissociation of a CS_2 cluster as involving only one CS_2 molecule of the cluster

$$(CS_2)_n + h\nu \rightarrow S + CS(v).(CS_2)_{n-1} \qquad (7)$$

$$(CS_2)_n + h\nu \rightarrow CS(v) + S.(CS_2)_{n-1}. \qquad (8)$$

This approximation implies that the photodissociation cross section is linearly proportional to n. Thus the cluster photofragmentation can be dominated by those from higher clusters

even though the dimer has the highest concentration in a supersonic expansion. Since the binding energies for $CS(v).(CS_2)_{n-1}$ and $S.(CS_2)_{n-1}$ are weak, the further dissociation of these fragments is possible. For $v \geq 1$, vibrational predissociation of $CS(v).(CS_2)_{n-1}$ can be a highly efficient process. It is most likely that the TOF spectra for $(CS_2)_2^+$, $C_2S_2^+$, and CS_3^+ are due to the heavier fragments of reactions (7) and (8). The reaction

$$S + CS_2 \rightarrow S_2 + CS \qquad (9)$$

is nearly thermal neutral.[39] The half reaction

$$S.(CS_2)_{n-1} \rightarrow S_2 + CS.(CS_2)_{n-2} \qquad (10)$$

is a feasible process. The lighter fragments, S, CS, and S_2 formed in reactions (7), (8), and (10), respectively, may account for the greater widths of the S, CS, and S_2 TOF peaks in comparison with those of the $(CS_2)_2^+$, $C_2S_2^+$, and CS_3^+ TOF peaks. Undoubtedly, the S^+, CS^+, and S_2^+ signals also have contributions from heavier photofragments.

SUMMARY

Higher resolution TOF spectra for CS and S from 193 nm photodissociation of CS_2 have been recorded using a crossed laser and molecular beam photofragmentation apparatus. The thermochemical thresholds for the formation of CS(X) + S($^1D_2$) and CS(X) + S($^3P_2$) are determined to be 18.7 and 45.0 ± 0.4 kcal/mol, respectively, in excellent agreement with literature values. Using the translational energy distribution derived from the TOF data and the data analysis procedures described in the text, we estimate a value of 2.6 for the branching ratio S(^3P)/S(^1D) which is consistent with the value determined most recently by Waller et al. using the VUV laser induced fluorescence method. The vibrational distribution for CS(X, v = 0-13) measured in this study is also in satisfactory accord with the results of the latter experiment. Photofragments from CS_2 clusters are found to appear at small laboratory angles ($\theta_{lab} \lesssim 20^o$) with narrow energy spreads.

REFERENCES

1. M. N. R. Ashfold, M. T. Macpherson, and J. P. Simons, Top. Curr. Chem. 86, 1 (1979).

2. H. Okabe, in "Photochemistry of Small Molecules" (Wiley, New York, 1978).

3. R. Bersohn, J. Phys. Chem. 88, 5145 (1984), and references therein.

4. S. R. Leone, Adv. Chem. Phys. 51, 255 (1982).

5. M. N. R. Ashfold, in "Photophysics and Photochemistry in the Vacuum Ultraviolet", edited by S. P. McGlynn et al. (Reidel, Boston, 1985), p. 409.

6. G. G. Balint-Kurti and M. Shapiro, Chem. Phys. 61, 137 (1981).

7. R. G. W. Norrish and G. Porter, Proc. R. Soc. London Ser. A 200, 284 (1950).

8. F. J. Wright, J. Phys. Chem. 64, 1648 (1960).

9. A. B. Callear, Proc. R. Soc. London Ser. A 276, 401 (1963).

10. M. deSorgo, A. J. Yarwood, O.P. Strausz, and H. E. Gunning, Can. J. Chem. 43, 1886 (1965).

11. H. Okabe, J. Chem. Phys. 56, 4381 (1972).

12. L. C. Lee and D. L. Judge, J. Chem. Phys. 63, 2782 (1975).

13. M. C. Addison, C. D. Byrne, and R. J. Donovan, Chem. Phys. Lett. 64, 57 (1979).

14. M. C. Addison, R. J. Donovan, and C. Fotakis, Chem. Phys. Lett. 74, 58 (1980).

15. T. R. Loree, J. H. Clark, K. B. Butterfield, J. L. Lyman, and R. Engleman, Jr., J. Photochem. 10, 359 (1979).

16. G. DornHofer, W. Hack, and W. Langel, J. Phys. Chem. 88, 3060 (1984).

17. J. B. Butler, W. S. Drozdoski, and J. R. McDonald, Chem. Phys. 50, 413 (1980).

18. S. Yang, A. Freedman, M. Kawasaki, and R. Bersohn, J. Chem. Phys. 72, 4048 (1980).

19. T. Ebata, M. Kawasaki, K. Obi, and I. Tanaka, Bull. Chem. Soc. Jpn. 52, 3226 (1979).

20. V. R. McCrary, R. Lu, D. Zakheim, J. A. Russell, J. B. Halpern, and W. M. Jackson, J. Chem. Phys. 83, 3481 (1985).

21. H. Kanamori and E. Hirota, J. Chem. Phys. 86, 3901 (1987).

22. I. M. Waller and J. W. Hepburn, J. Chem. Phys. 87, 3261 (1987).

23. G. E. Busch, J. F. Cornelius, R. T. Mahoney, R. I. Morse, D. W. Schlosser, and K. R. Wilson, Rev. Sci. Instrum. 41, 1066 (1970).

24. G. E. Busch and K. R. Wilson, J. Chem. Phys. 56, 3626 (1972); 56, 3638 (1972); 56, 3655 (1972).

25. R. K. Sander and K. R. Wilson, J. Chem. Phys. 63, 4242 (1975).

26. R. J. Oldman, R. K. Sander, and K. R. Wilson, J. Chem. Phys. 63, 4252 (1975).

27. R. D. Clear, S. J. Riley, and K. R. Wilson, J. Chem. Phys. 63, 1340 (1975).

28. A. M. Wodtke and Y. T. Lee, J. Phys. Chem. 89, 4744 (1985).

29. N. R. Daly, Rev. Sci. Instrum. 31, 264 (1960).

30. T. T. Warnock and R. B. Bernstein, J. Chem. Phys. 49, 1878 (1968).

31. G. L. Catchen, J. Husain, and R. N. Zare, J. Chem. Phys. 69, 1737 (1968).

32. V. H. Dibeler and J. A. Walker, J. Opt. Soc. Am. 57, 1007 (1967).

33. T. Bergeman and D. Cossart, J. Mol. Spectrosc. 87, 119 (1981).

34. A. E. Douglas and J. Zanon, Can. J. Phys. 42, 627 (1964).

35. J. W. Rabalais, J. R. McDonald, V. Scherr, and S. P. McGlynn, Chem. Rev. 71, 73 (1971).

36. R. J. Hemley, D. G. Leopold, J. L. Roebber, and V. Vaida, J. Chem. Phys. 79, 5219 (1983).

37. K. Hara and D. Phillips, J. Chem. Soc. Faraday Trans. 2 74, 1441 (1978).

38. D. R. Stull and H. Prophet, Natl. Stand. Rev. Data Ser., Natl. Bur. Stand. 37 (U. S. GPO Washington, D. C., 1971).

39. Y. Ono, S. H. Linn, H. F. Prest, M. E. Gress, and C. Y. Ng, J. Chem. Phys. 73, 2523 (1980).

SECTION II.

A 193 nm LASER PHOTOFRAGMENTATION TIME-OF-FLIGHT MASS SPECTROMETRIC STUDY OF CH_3SSCH_3, $SSCH_3$, AND SCH_3

ABSTRACT

We have measured the time-of-flight (TOF) spectra for SCH_3, CH_3, and $SSCH_3$ formed in the photodissociation processes, $CH_3SSCH_3 + h\nu$ (193 nm) $\rightarrow 2SCH_3$ and $CH_3 + SSCH_3$. The dissociation energies for the CH_3S-SCH_3 and CH_3SS-CH_3 bonds determined at 0 K by the TOF measurements are 72.4 ± 1.5 and 55.0 ± 1.5 kcal/mol, in agreement with the literature values. The threshold value for the formation of S_2 measured by the TOF spectrum for S_2 is in accord with the thermochemical threshold for the process, $SSCH_3 + h\nu$ (193 nm) $\rightarrow S_2 + CH_3$. The threshold energy determined from the TOF spectrum for S is found to be consistent with the thermochemical threshold for the photodissociation process, $SCH_3 + h\nu$ (193 nm) $\rightarrow S(^1D) + CH_3$, an observation supporting that S atoms are not produced in the ground $S(^3P)$ state in the 193 nm photodissociation of SCH_3. This observation is rationalized by symmetry correlation arguments applied between the $S + CH_3$ product and SCH_3 states.

INTRODUCTION

Sulfur occurs naturally in crude oil and in coals in the range from 0.2% to 10%. A great deal of effort has been directed toward the desulfurization of coals and oil so as to minimize the emission of sulfur-containing species to the atmosphere.[1] The modelling of the combustion and oxidation of sulfur compounds represents important steps for the control of both the production and the elimination of sulfur-containing pollutants.[2]

Detailed and accurate knowledge of the thermochemistry of sulfur compounds is required for the modelling efforts.[3-7] Despite the fact that the thermochemistry of the organosulfur chemistry is considered to be fairly well established,[3,7] heats of formation data for many sulfur-containing species are only estimates based on empirical rules of group additivity.[8] Direct measurements of bond dissociation energies are desirable to test the validity of the empirical rules. Much less information exists about the thermochemical data for sulfur-containing radicals compared to those for stable sulfur compounds.

Hoping to provide an accurate thermochemical data base for sulfur-containing compounds, we have devoted considerable effort previously to measure the photoionization efficiency[9] and laser photofragmentation[10] time-of-flight (TOF) spectra of many inorganic sulfur molecules. Recently, we have developed a pulsed photoion-photoelectron coincidence scheme which is shown to have sufficiently high sensitivity for the measurements of the photoelectron spectra of minor sulfur-containing radical species generated in a SO_2 discharge plasma.[11] We have initiated a project to measure

systematically the energetics and photodissociation dynamics of organosulfur molecules and radicals. The combination of the energetic information for organosulfur molecules and radicals obtained in the photoionization, photoion-photoelectron coincidence, and neutral photofragmentation studies will allow us to examine the consistency of thermochemical data for many neutral and ion species by completing the thermochemical cycles.

Dimethyl disulphide is among the industrial organosulfur pollutants emitted to the atmosphere.[12-14] The absorption spectrum for CH_3SSCH_3 exhibits a strong band centered at approximately 200 nm.[15] Thus the study of the ultraviolet photochemistry of CH_3SSCH_3 is relevant to the understanding of the atmospheric sulfur chemistry cycles. Previous studies[16-19] show that upon absorption of an ultraviolet photon, the primary decomposition of CH_3SSCH_3 is the S-S bond scission to produce $2SCH_3$ radicals.

In this article, we present the results and an analysis of the 193 nm laser photofragmentation study of CH_3SSCH_3. The results of the photoionization study of CH_3SSCH_3 will be presented in a separate paper.[20]

EXPERIMENTAL

The rotatable beam source laser photofragmentation apparatus used in this study has been described in detail previously.[10] The apparatus consists of three main components: an ArF excimer laser, a photodissociation chamber in which a rotatable supersonic molecular beam intersects with the laser beam, and a linearly movable ultrahigh vacuum electron ionization mass spectrometric detector.

In this experiment, a pulsed beam of CH_3SSCH_3 seeded in He is produced by supersonic expansion through a commercial pulsed valve (General Valve, No.9) with a nozzle diameter of 0.5 mm at 298 K and a total stagnation pressure of approximately 2280 Torr. The ratio for the pressure of CH_3SSCH_3 to that of He is about 0.25. The molecular beam source chamber is pumped by a 20 in. diffusion pump (DP) with a pumping speed of 20000 ℓ/s. The seeded CH_3SSCH_3 beam has an angular divergence of 3° which is defined by the opening of the conical skimmer and the circular aperture as it passes through the differential chamber into the photodissociation chamber. The 3° angular spread of the beam corresponds to a beam width of 3 mm at the photodissociation region. The differential pumping chamber is evacuated by a liquid-nitrogen (LN_2) trapped 6 in. DP with a pumping speed of 2000 ℓ/s, while the photodissociation chamber is pumped by a freon-trapped 10 in. DP with a pumping speed of 5000 ℓ/s. During the experiment, the beam source, differential, and photodissociation chambers are maintained at pressures of approximately 1×10^{-6}, 2×10^{-7}, and 5×10^{-8} Torr, respectively.

The excimer laser used is a Questek (Model 2460) laser, which has a maximum repetition rate of 200 Hz and a maximum output energy of 250 mJ at 193 nm. The laser energy used is varied in the range of 100-130 mJ. The laser beam enters the photodissociation chamber through a MgF_2 focusing lens and intersects the seeded CH_3SSCH_3 beam at 90°.

The detector chamber, which houses the mass spectrometer, has four stages of differential pumping. The first and second differential pumping regions are evacuated by a turbomolecular pump and an ion pump having pumping speeds of 300 and 220 ℓ/s, respectively. The ionizer is located inside the ionization chamber which is cooled to LN_2 temperature. The ionization chamber is pumped by the combination of a 120 ℓ/s ion pump and a 500 ℓ/s turbomolecular pump. The neutral fragments produced by photodissociation in the photodissociation region pass through the first and second differential pumping regions of the detector chamber before entering the ionization region. The emission current of the ionizer is $\leq$ 2.5 mA and the ionization electron energy is 100 eV. During the experiment, the pressures in the first and second differential and ionization chambers are $\leq 2 \times 10^{-9}$, 5×10^{-10}, and 2×10^{-11} Torr, respectively. The mass spectrometer used is a quadrupole mass filter constructed of 1.9 cm diameter rods. The ion detector is a Daly-type scintillation detector. The ion detector chamber is separated from the second differential pumping region by the quadrupole mass filter and a sheet metal wall. The vacuum in the ion detector chamber is maintained by a turbomolecular pump with a pumping speed of 50 ℓ/s.

The detector chamber is mounted on a movable platform which is supported on a linear rail assembly. Using the rail assembly, the distance between the photodissociation region and the ionizer can be varied continuously in the range of 35-110 cm. In this experiment, all TOF spectra are taken at a flight path distance of 73.7 cm. The detector and photodissociation chambers are connected by a flexible bellows which allows the variation of the flight path length without venting any of the experimental chambers.

The data acquisition and operation of the apparatus is controlled by a LSI-11/23 minicomputer. The TOF spectrum is recorded on a homemade 1024 channel scaler which has a minimum channel width of 0.3 μs. In this experiment, the pulsed valve is operated at 40 Hz. The firing of the excimer laser is delayed by approximately 500 μs with respect to the triggering pulse for the opening of the pulsed valve. The multichannel scaler is started by a second trigger pulse signifying the firing of the laser. The delay timings are controlled by a digital delay unit (SRS, Model DG 535).

The laboratory angle (θ) is defined to be the angle between the seeded CH_3SSCH_3 molecular beam and the detector axis. The laboratory velocity for the parent CH_3SSCH_3 beam (v_p) is determined by measuring the TOF of the CH_3SSCH_3 beam pulse at $\theta = 0°$ at two known nozzle-ionizer distances. An aperture of 0.075 mm is used between the photodissociation and detector chambers during the measurement of v_p. The value for v_p (1.65×10^5 cm/s) is determined before and after the laser photodissociation experiment and the agreement of the two measurements is usually better than 2%. Under these beam expansion conditions, the ratio $\Delta v/v_p$ is estimated to be less than 0.08, where Δv represents the velocity spread (full width at half maximum) of the CH_3SSCH_3 beam.

The ion drift times through the quadrupole mass filter have been determined by applying a voltage pulse to the ion extraction lens and using an oscilloscope to measure the arrival times of the ions at the ion detector with respect to the trigger voltage pulse. The actual flight time of the neutral CH_3SSCH_3 or photofragments is equal to the difference between the time measured by the multichannel scaler and the ion drift time of the corresponding ion.

The analysis of the TOF data, involving the transformation of the laboratory TOF spectra into center-of-mass (c.m.) translational energy distributions, has been described in detail. We have ignored the effect of the apparatus resolution factors on the observed TOF distributions.

RESULTS AND DISCUSSION

Upon the absorption of a 193 nm photon, CH_3SSCH_3 may dissociate according to processes (1) and (2):

$$CH_3SSCH_3 + h\nu\ (193\ nm) \rightarrow 2SCH_3 \qquad (1)$$

$$CH_3SSCH_3 + h\nu\ (193\ nm) \rightarrow CH_3 + SSCH_3. \qquad (2)$$

TOF Spectra for SCH_3

Under the pulsed nozzle expansion conditions used in this experiment, dimers and clusters of CH_3SSCH_3 are expected to be formed in the supersonic beam. The photodissociation of the dimer and cluster species may give rise to the same fragments as those due to the monomer. As we have shown in a photodissociation study of CS_2,[10] the fragments resulting from photodissociation of dimers and clusters are mainly confined to small θ values because of kinematic constraints. Therefore, the background signal arising from photodissociation of dimer and cluster species can be reduced substantially by measuring the TOF spectra of photofragments at sufficiently large laboratory angles. As a consequence of the slippage effect in the supersonic expansion, the velocity for CH_3SSCH_3 is expected to be slightly greater than those for the dimer and higher clusters. We find that it is possible to minimize the interference of dimer and cluster photodissociations by choosing carefully the delay time between the trigger pulses for the

pulsed molecular beam valve and the excimer laser. Figures 1(a) and 1(b) show the TOF spectrum for SCH_3 measured at $\theta = 30°$ and at a delay time of 550 and 500 μs, respectively. The broad peak in the temporal range of approximately 350-800 μs observed in the spectrum shown in Fig. 1(a) is attributed to fragments from dimer and cluster species of CH_3SSCH_3. The TOF spectrum for SCH_3 depicted in Fig. 1(b) is believed to be due mostly to process (1). Figures 1(c) and 1(d) show the TOF spectra for SCH_3 measured at $\theta = 45°$ and 60° using a delay time of 500 μs between the trigger pulses for opening the nozzle valve and firing of the laser.

Based on the conservation of energy, we have the relation,

$$h\nu\ (193\ nm) + E_{int}^{*} = D_o(CH_3S\text{-}SCH_3) + E_e + E_v + E_r + E_{c.m.}, \qquad (3)$$

where hν is the photodissociation energy (147.9 kcal/mol); E_{int}^{*} is the initial internal energy of the parent CH_3SSCH_3 molecule, which is assumed to be negligible due to supersonic cooling; $D_o(CH_3S\text{-}SCH_3)$ is the dissociation energy for the $CH_3S\text{-}SCH_3$ at 0 K; and E_e, E_v, E_r, and $E_{c.m.}$ are the electronic, vibrational, rotational, and c.m. translational energies of the photofragments. A value of 74 ± 2 kcal/mol has been given previously for the dissociation energy of the $CH_3S\text{-}SCH_3$ bond at 298 K ($DH°(CH_3SSCH_3)$), based on heats of formation data.[3] In a later review,[7] McMillen and Golden have assigned a lower value of 72 ± 2 kcal/mol for $DH°(CH_3S\text{-}SCH_3)$. Using the latter value, we have constructed the Newton diagram (Fig. 2) for the formation of SCH_3 by process (1) using Eq. (3). Here $v_l(SCH_3)$ and $v_{c.m.}(SCH_3)$ represent the maximum laboratory and c.m. velocities for SCH_3 expected at $\theta = 30°$.

Figure 1. TOF spectra for SCH_3 (a) $\theta = 30°$, delay between the trigger pulse for opening the pulse valve and that for firing of the excimer laser is equal to 550 μs; (b) $\theta = 30°$, delay = 500 μs; (c) $\theta = 45°$, delay = 500 μs; (d) $\theta = 60°$, delay = 500 μs

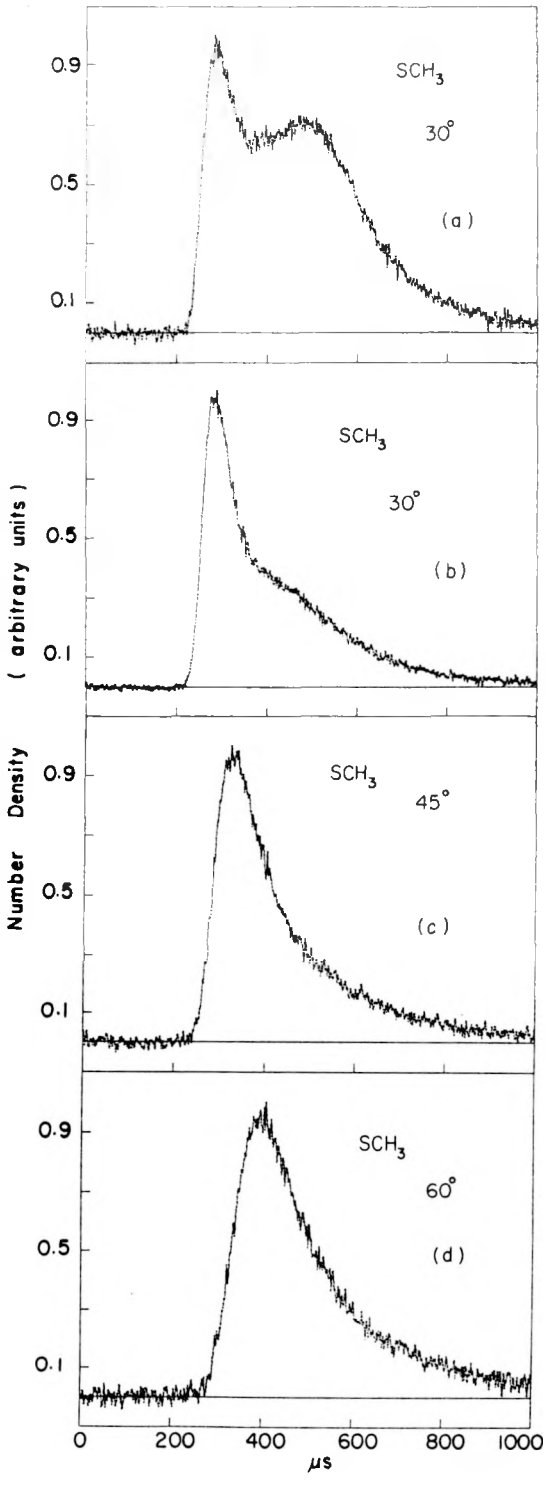
SCH3
30°
(a)
SCH3
30°
(b)
SCH3
45°
(c)
SCH3
60°
(d)
Number Density (arbitrary units)
0.9
0.5
0.1
0
200
400
600
800
1000
μs

Figure 2. Kinematics are shown for the formation of $2SCH_3$ by process (1) and the formation of $S + CH_3$ by process (6) at $\theta = 30°$. Here, v_p is the laboratory velocity for CH_3SSCH_3; $v_{c.m.}(SCH_3)$ and $v_l(SCH_3)$ are the maximum c.m. and laboratory velocities for SCH_3, respectively; $v_{c.m.}(S(^3P))$, $v_{c.m.}(S(^1D))$, $v_{c.m.}(S(^1S))$, and $v'_{c.m.}(CH_3)$ represent the maximum c.m. velocities for $S(^3P)$, $S(^1D)$, $S(^1S)$, and CH_3 formed by process (6).

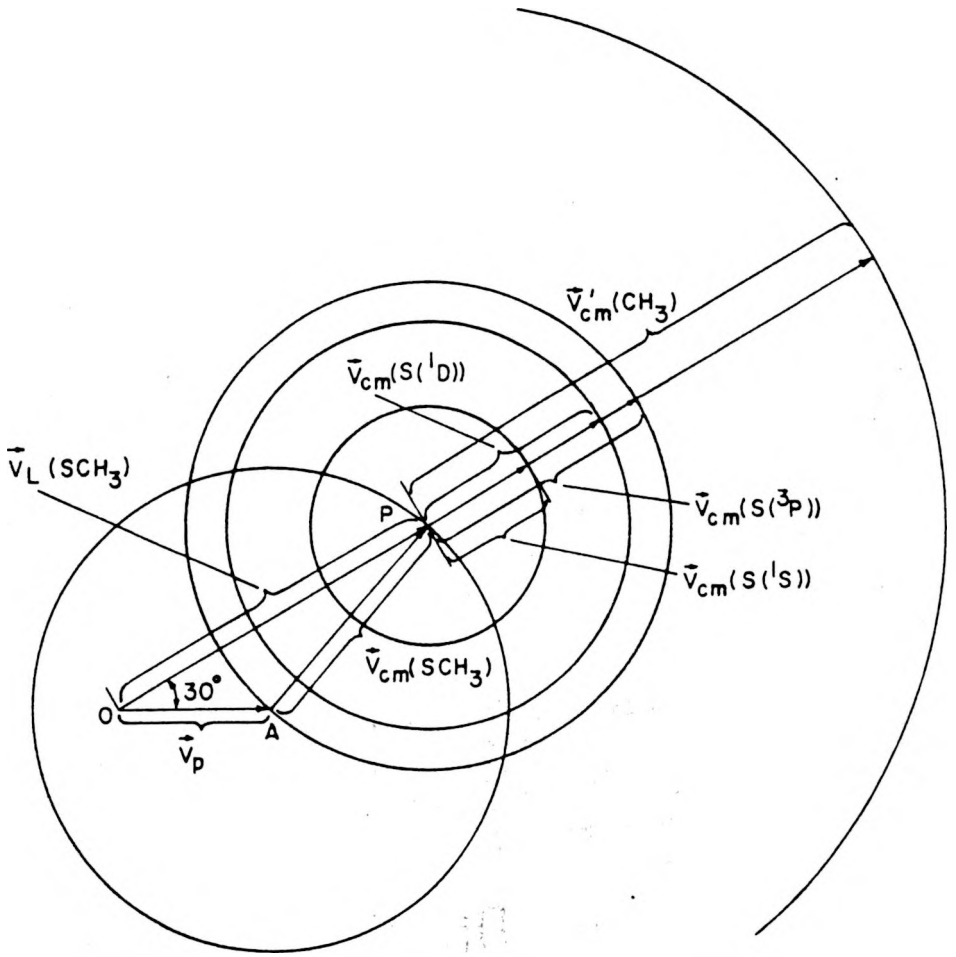
$\vec{V}_{cm}'(CH_3)$
$\vec{V}_{cm}(S(^1D))$
$\vec{V}_L(SCH_3)$
P
$\vec{V}_{cm}(S(^3P))$
$\vec{V}_{cm}(S(^1S))$
$\vec{V}_{cm}(SCH_3)$
30°
O
A
$\vec{V}_p$

The c.m. translational energy distributions transformed from the TOF spectra for SCH_3 measured at $\theta = 30°$, 45°, and 60° are shown in Figs. 3(a), 3(b), and 3(c), respectively. Because of kinematic constraints, the spectra measured at $\theta = 30°$, 45°, and 60° only provide information about the translational energy distribution at $E_{c.m.}$ ranges ≥ 10, ≥ 23, and ≥ 39 kcal/mol, respectively. The distributions shown in Figs. 3(a)-3(c) are in agreement in revealing a broad peak centered at $E_{c.m.} \sim 30$ kcal/mol. A value of 30 kcal/mol for $E_{c.m.}$ corresponds to a total internal excitation $E_{int}(= E_e + E_v + E_r)$ of 46 kcal/mol for the SCH_3 fragments.

The threshold energy for process (1) is determined to be $E_{c.m.} = 75.5 \pm 1.5$ kcal/mol, corresponding to a value of 72.4 ± 1.5 kcal/mol for $D_o(CH_3S\text{-}SCH_3)$. The conversion of $D_o(CH_3S\text{-}SCH_3)$ to $DH°(CH_3S\text{-}SCH_3)$ requires the addition of 2.4 kcal/mol to the latter value assuming that the vibrational and electronic degrees of freedom for CH_3SSCH_3 and SCH_3 are not populated at 298 K.[21] The value of 74.8 ± 1.5 kcal/mol for $DH°(CH_3S\text{-}SCH_3)$ obtained in this experiment supports the value of 74 ± 2 kcal/mol given previously by Benson.[3]

TOF Spectra for CH_3 and $SSCH_3$

The TOF spectra for CH_3 and $SSCH_3$ measured at $\theta = 30°$ are depicted in Figs. 4(a) and 4(b), respectively. The strong peak observed at approximately 280 μs in the TOF spectrum for CH_3 coincides with the peak found in the SCH_3 TOF spectrum (Fig. 1(b)). This observation indicates that, using an electron energy of 100 eV for the ionization

Figure 3. Translational energy distributions for fragments of process (1) derived from TOF spectra for SCH_3 measured at (a) $\theta = 30°$, (b) $\theta = 45°$, and (c) $\theta = 60°$

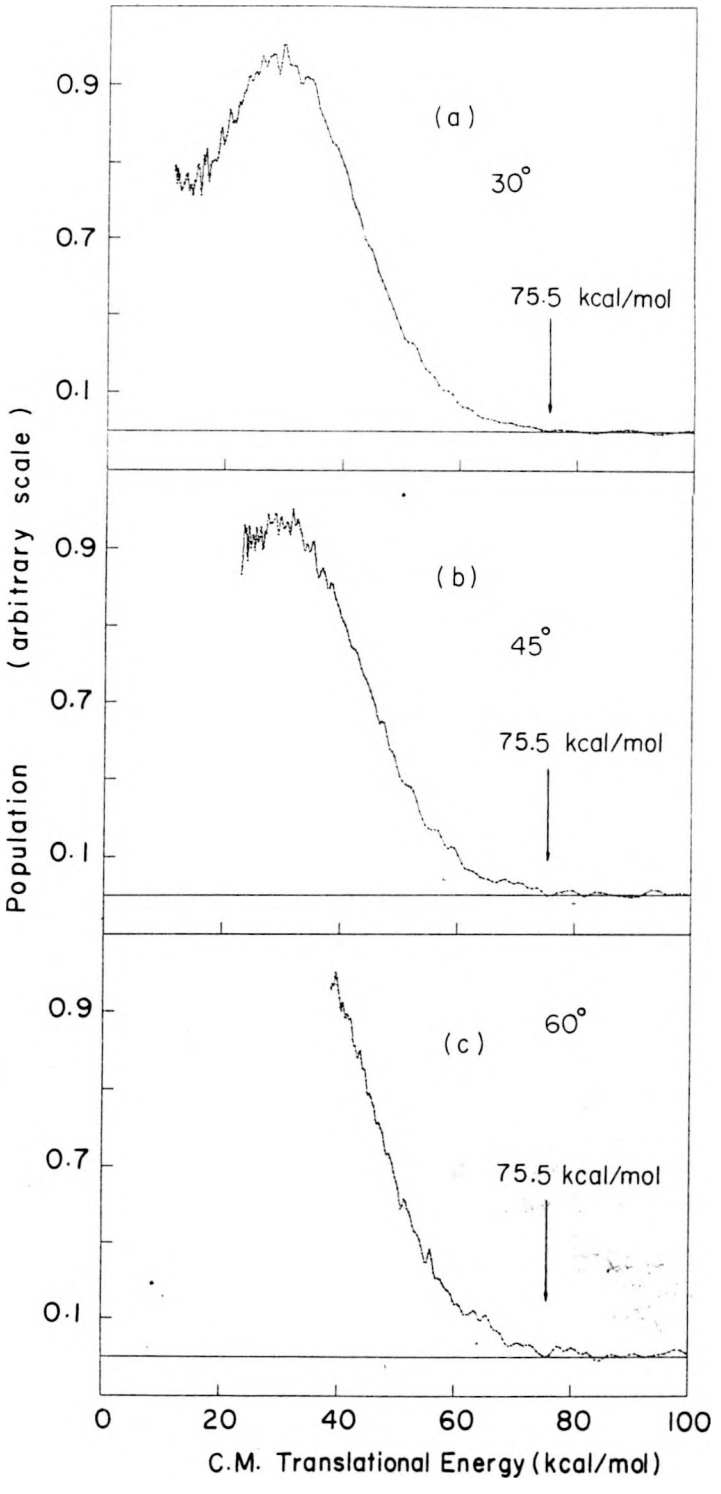
0.9
0.7
0.1
(a)
30°
75.5 kcal/mol
0.9
0.7
0.1
(b)
45°
75.5 kcal/mol
0.9
0.7
0.1
(c)
60°
75.5 kcal/mol
Population (arbitrary scale)
0
20
40
60
80
100
C.M. Translational Energy (kcal/mol)

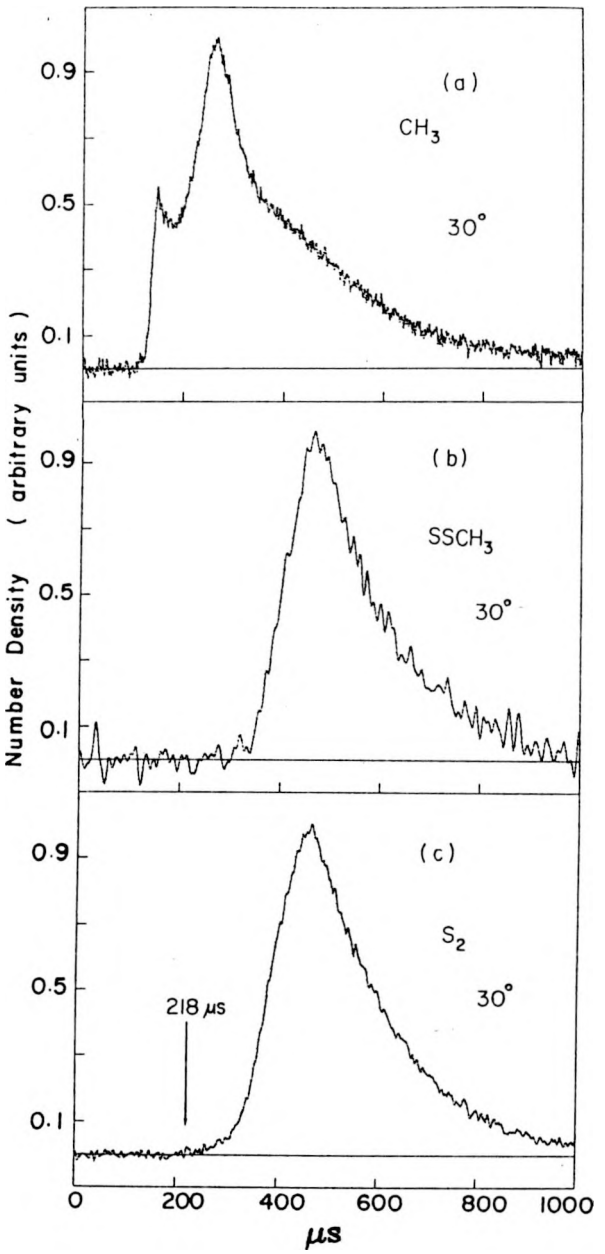

Figure 4. TOF spectra measured at $\theta = 30°$ (a) CH_3; (b) $SSCH_3$; (c) S_2

sampling in this experiment, the formation of CH_3^+ by the dissociative ionization process,

$$SCH_3 + e^- \rightarrow S + CH_3^+ + 2e^-, \quad (4)$$

is significant. Efforts have been made to examine the effect of ionization electron energy on the appearance of the CH_3 TOF spectrum. A TOF spectrum for CH_3, obtained using an ionization electron energy of 50 eV, is found to be similar to that shown in Fig. 4(a). Since the TOF spectrum for SCH_3 appears in a temporal range greater than that for CH_3, the threshold for the formation of CH_3 determined by the TOF spectrum corresponds to that of process (2).

The Newton diagram for process (2) is shown in Fig. 5. Here, $\mathbf{v}_{c.m.}(CH_3)$ and $\mathbf{v}_{c.m.}(SSCH_3)$ are the maximum c.m. velocities for CH_3 and $SSCH_3$ formed by process (2) and $\mathbf{v}_l(CH_3)$ and $\mathbf{v}_l(SSCH_3)$ are corresponding maximum laboratory velocities at $\theta = 30°$. As indicated in Fig. 4(a), the threshold in flight time for process (2) is 107.5 μs, which corresponds to a value of 92.8 kcal/mol for $E_{c.m.}$. Thus, the value for $D_o(CH_3SS\text{-}CH_3)$ is determined to be 55.1 kcal/mol, which is consistent with the literature value of 57.0 ± 1.5 kcal/mol for $DH°(CH_3SS\text{-}CH_3)$.[3,7] The TOF spectrum for CH_3 shows a peak at approximately 150 μs (see Fig. 4(a)), indicating that the translational energy distribution for process (2) has a maximum at $E_{c.m.}$ ~ 38 kcal/mol (or E_{int} ~ 55 kcal/mol).

The translational energy distribution obtained using the TOF spectrum for $SSCH_3$ is shown in Fig. 6. The threshold for the formation of $SSCH_3$ is determined to be 93.0 ± 1.5 kcal/mol, which gives a value of 55.0 ± 1.5 kcal/mol for $D_o(CH_3SS\text{-}CH_3)$. This value is in excellent agreement with that derived from the TOF measurement of CH_3.

Figure 5. Kinematics are shown for the formation of CH_3 and $SSCH_3$ by process (2) and the formation of S_2 + CH_3 by process (9). Here, v_p is the laboratory velocity for CH_3SSCH_3, $v_{c.m.}(SSCH_3)$ and $v_l(SSCH_3)$ are the maximum c.m. and laboratory velocities for $SSCH_3$, respectively; $v_{c.m.}(CH_3)$ and $v_l(CH_3)$ are the c.m. and laboratory velocities for CH_3, respectively, formed by process (2); $v_{c.m.}(S_2)$ and $v'_{c.m.}(CH_3)$ represent the maximum c.m. velocities for S_2 and CH_3 formed by process (9).

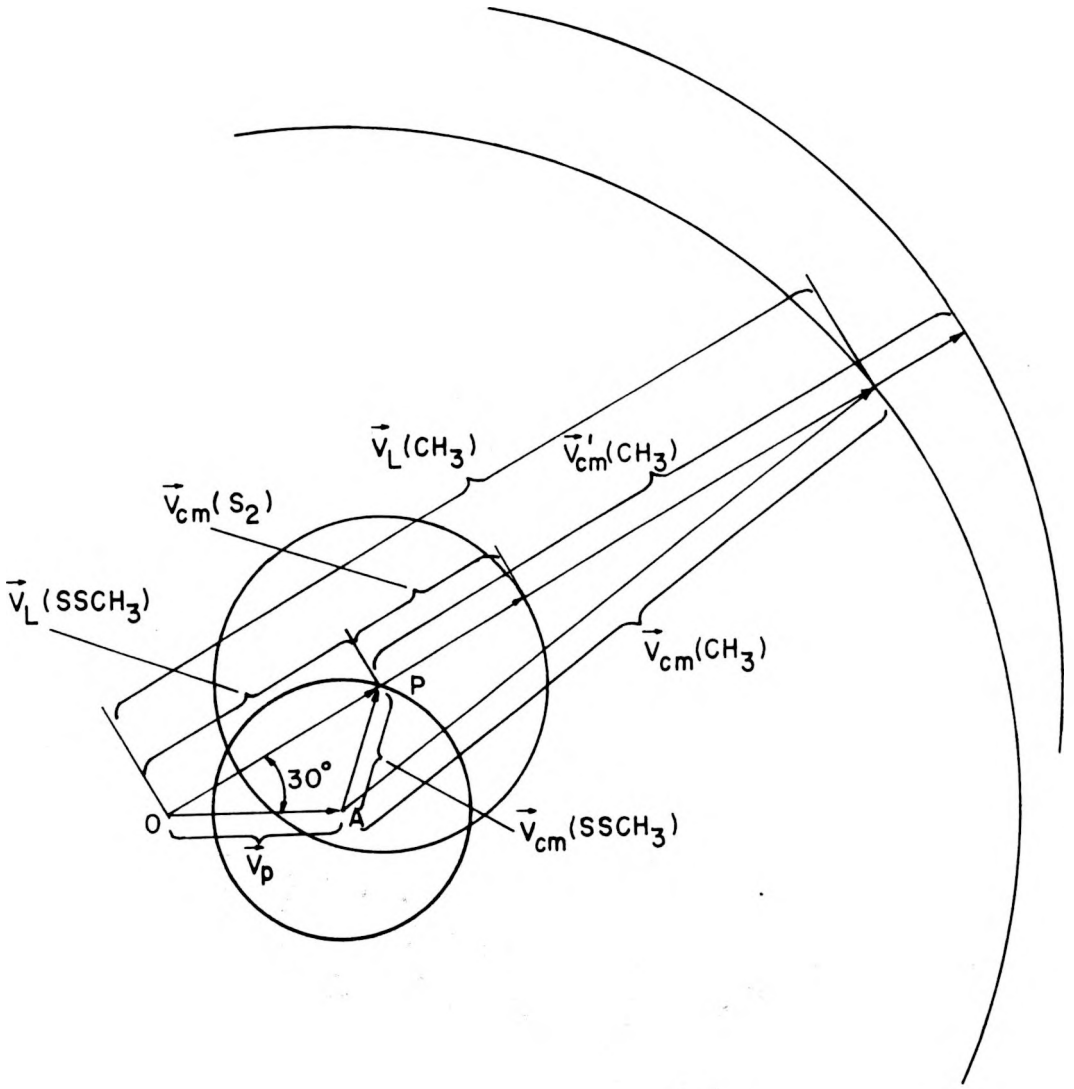
$\vec{V}_L(CH_3)$
$\vec{V}'_{cm}(CH_3)$
$\vec{V}_{cm}(S_2)$
$\vec{V}_L(SSCH_3)$
$\vec{V}_{cm}(CH_3)$
P
30°
O
A
$\vec{V}_{cm}(SSCH_3)$
$\vec{V}_p$

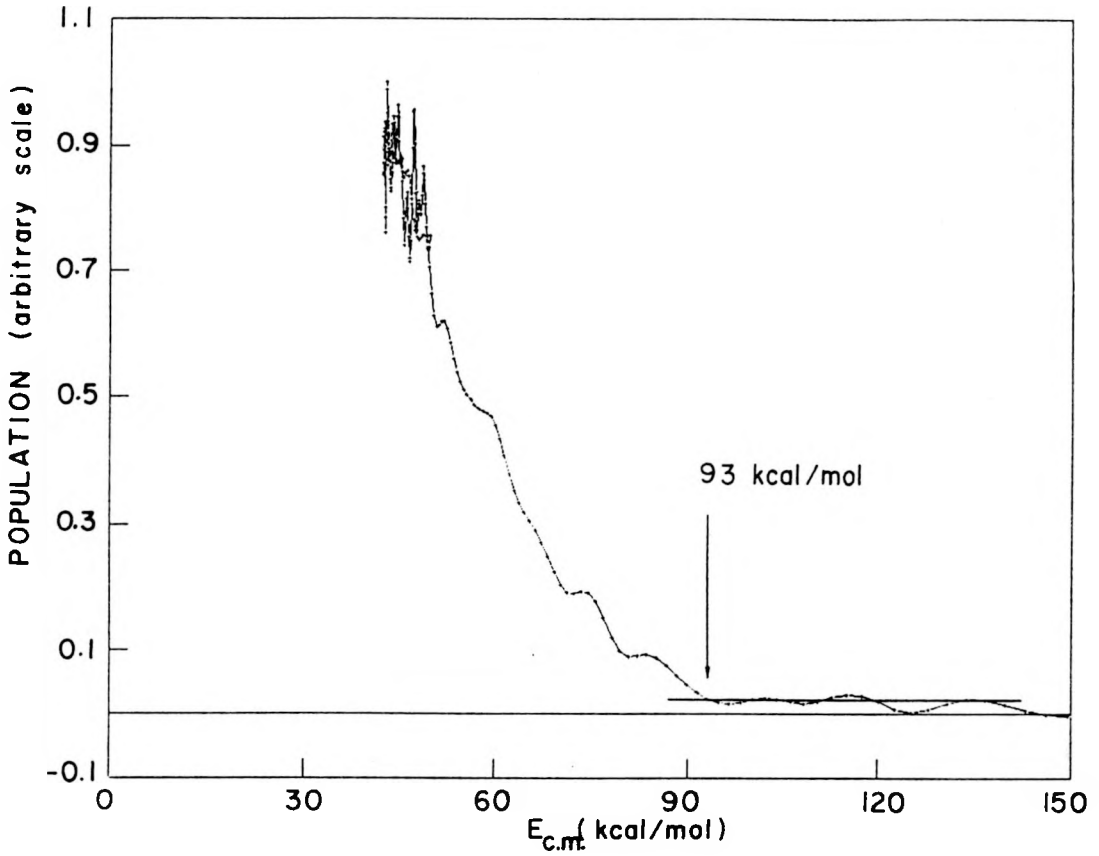

Figure 6. Translational energy distribution for fragments of process (2) derived from the TOF spectrum for $SSCH_3$ measured at $\theta = 30°$

TOF Spectrum for S

Figures 7(a) and 7(b) compare the TOF spectra for SCH_3 and S measured at $\theta = 30°$, and show that the TOF spectrum for S is not solely the result of fragmentation from SCH_3. Figure 7(c) shows a magnified view of the TOF spectrum for S in the threshold region. The threshold in flight time for S is found to be at 145 μs, which corresponds to a velocity much faster than that for the S atoms formed in the process,

$$CH_3SSCH_3 + h\nu\ (193\ nm) \rightarrow CH_3 + S + SCH_3. \qquad (5)$$

Using the literature value of 66 ± 1.5 kcal/mol[3,7] for $DH°(S\text{-}CH_3)$ or 64.5 ± 1.5 kcal/mol for $D_o(S\text{-}CH_3)$, process (5) is predicted to be exothermic by only about 8.5 kcal/mol at 0 K. The only possible process which can account for the energetics of the observed S atoms is the photodissociation of SCH_3 according to the process,

$$SCH_3 + h\nu\ (193\ nm) \rightarrow S + CH_3. \qquad (6)$$

Energetically, S can be formed in the $S(^3P)$, $S(^1D)$, and $S(^1S)$ states. The excited metastable $S(^1D)$ and $S(^1S)$ states are 26.4 and 63.4 kcal/mol higher, respectively, than the $S(^3P)$ ground state.[22] The exothermicities for S formed in the $S(^3P)$, $S(^1D)$, and $S(^1S)$ states and CH_3 in the $CH_3(\tilde{X}^2A''_2)$ ground state are 83.4, 57.0, and 20.0 kcal/mol, respectively.

The kinematics for the photodissociation process (6) at $\theta = 30°$ is shown in the Newton diagram of Fig. 2. In the diagram, $v_l(SCH_3)$ is the maximum laboratory velocity for SCH_3 resulting from the photodissociation process (1). For SCH_3 moving at $v_l(SCH_3)$,

Figure 7. (a) TOF spectrum for SCH_3 measured at $\theta = 30°$; (b) TOF spectrum for S measured at $\theta = 30°$; (c) a magnified view of the TOF spectrum for S near the threshold region

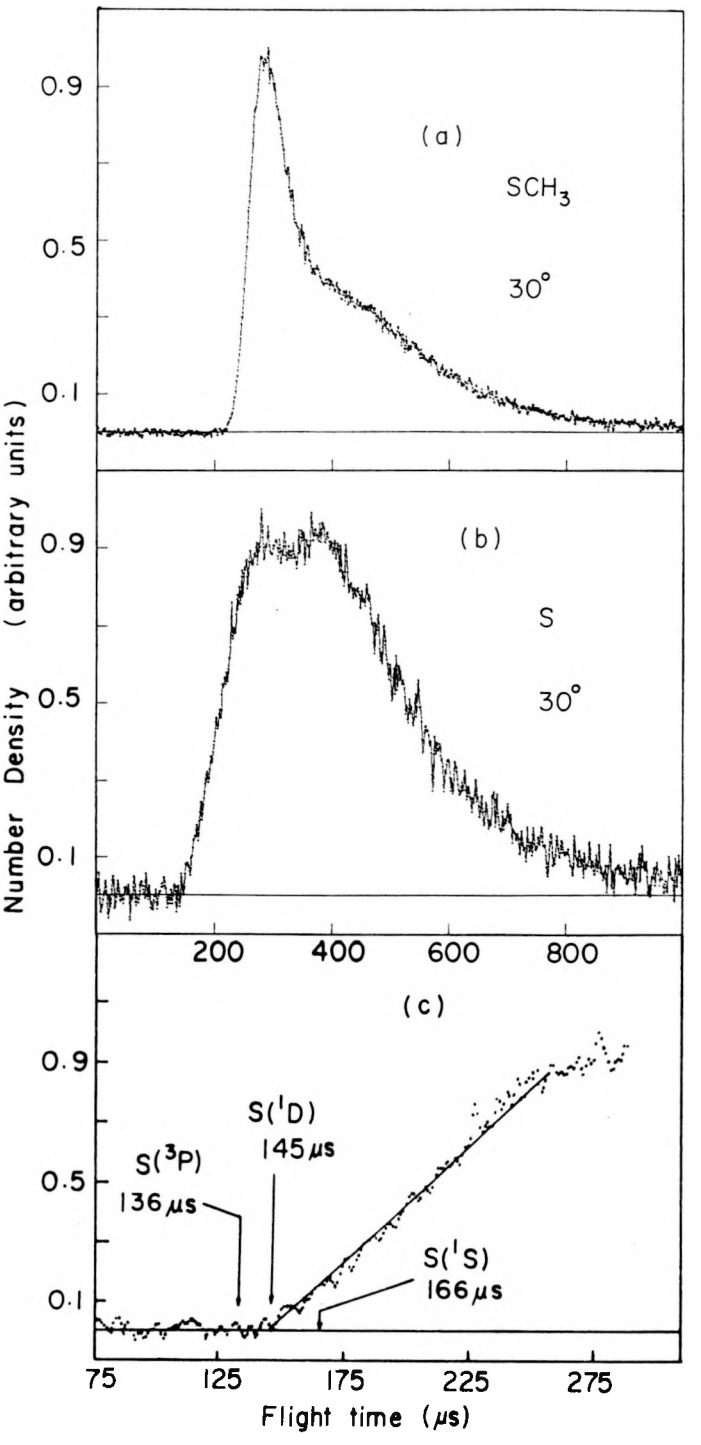
(a)
SCH3
30°
(b)
S
30°
(c)
S(3P)
136 μs
S(1D)
145 μs
S(1S)
166 μs
Number Density (arbitrary units)
0.9
0.5
0.1
200
400
600
800
75
125
175
225
275
Flight time (μs)

the value for $E_{int}(SCH_3)$ is zero. If these SCH_3 radicals with zero internal excitations further dissociate according to process (6), the maximum c.m. recoil velocity circles due to the formation of $S(^3P)$, $S(^1D)$, and $S(^1S)$ are as indicated in the figure. The maximum laboratory velocities for S formed in the $S(^3P)$, $S(^1D)$, and $S(^1S)$ states predicted at $\theta = 30^o$ are equal to $\mathbf{v}_l(S(^3P)) = \mathbf{v}_l(SCH_3) + \mathbf{v}_{c.m.}(S(^3P))$, $\mathbf{v}_l(S(^1D)) = \mathbf{v}_l(SCH_3) + \mathbf{v}_{c.m.}(S(^1D))$, and $\mathbf{v}_l(S(^1S)) = \mathbf{v}_l(SCH_3) + \mathbf{v}_{c.m.}(S(^1S))$, respectively. The values for $\mathbf{v}_l(S(^3P))$, $\mathbf{v}_l(S(^1D))$, and $\mathbf{v}_l(S(^1S))$ correspond to thresholds in flight time of 136.1, 144.6, and 165.8 μs, respectively, which are marked in Fig. 7(c). The S^+ ion drift time of 22.8 μs is included in these flight times.

The overwhelming majority of the SCH_3 radicals formed by process (1) are internally excited. As pointed out above, the translational energy distribution for photofragments shown in Fig. 3(a) indicates that the most probable translational distribution for SCH_3 corresponds to a value of approximately 46 kcal/mol for E_{int} of SCH_3 fragments. Since the two fragments of process (1) are identical, we expect that each SCH_3 fragment has about 23 kcal/mol of internal energy. A simple calculation shows that the laboratory velocities predicted for the production of $S(^3P)$, $S(^1D)$, and $S(^1S)$ by photodissociation of these internally excited SCH_3 fragments are lower than the respective values for $\mathbf{v}_l(S(^3P))$, $\mathbf{v}_l(S(^1D))$, and $\mathbf{v}_l(S(^1S))$. As E_{int} for SCH_3 increases from zero, the laboratory velocity for S formed in $S(^3P)$ decreases correspondingly from $\mathbf{v}_l(S(^3P))$. The good agreement between the observed threshold (145 μs) and the predicted threshold (144.6 μs) for the formation of $S(^1D)$ supports the conclusion that $S(^3P)$ is not formed in the 193 nm photodissociation of SCH_3. However, we consider this conclusion to be tentative. Future experiments to

measure directly the states of S are necessary to confirm this conclusion. The previous photodissociation studies of OCS[23] and ethylene sulfide[24] have shown that S atoms are produced exclusively in the $S(^1D)$ state.

With the exception of the first excited $SCH_3(\tilde{A}^2A_1)$ state,[25-28] which is approximately 76 kcal/mol higher than the $SCH_3(\tilde{X}^2E)$ ground state, experimental information about excited states for SCH_3 is not known. The spin-orbit splitting of the $SCH_3(^2E_{3/2})$ and $SCH_3(^2E_{1/2})$ states[25,28] has been determined to be 280 cm^{-1}. The thiomethoxyl radical is subject to a slight Jahn-Teller distortion, splitting the ^2E state into the nearly degenerate $^2A'$ and $^2A''$ states. An ab initio calculation[29] assuming a C_s symmetry for SCH_3 shows that in the excitation energy range covered by the 193 nm laser radiation, the states, in the order of increasing energy, are $\tilde{X}(^2A', ^2A'')$, $\tilde{A}^2A'$, $\tilde{B}^4A''$, $\tilde{C}^2A''$, and $\tilde{D}^2A'$. The calculation predicts that the $\tilde{A}^2A'$ state lies at an energy of 92.7 kcal/mol above the ground state, compared to the experimental value of 76 kcal/mol. In order to gain insight about the photodissociation process (6), we have constructed a correlation diagram between the states for SCH_3 and those for $S(^3P, ^1D, ^1S) + CH_3(\tilde{X}^2A''_2)$, as shown in Fig. 8. The energies are based on the theoretical predictions, except that for the $\tilde{A}^2A'$ state, the experimental energy value is used. Assuming that the energy levels predicted for the excited states for SCH_3 are accurate, and taking into account finite internal excitations for SCH_3 formed in process (1), absorption of a 193 nm photon by SCH_3 may produce SCH_3 in the $\tilde{C}^2A''$ and/or $\tilde{D}^2A'$ states. The $SCH_3(\tilde{D}^2A')$ correlates adiabatically to the $CH_3(\tilde{X}^2A''_2) + S(^1D)$ product channel, whereas the $SCH_3(\tilde{C}^2A'')$ leads to the $CH_3(\tilde{X}^2A''_2) + S(^3P)$ dissociation limit. A similar correlation diagram based on the C_{3v} symmetry without

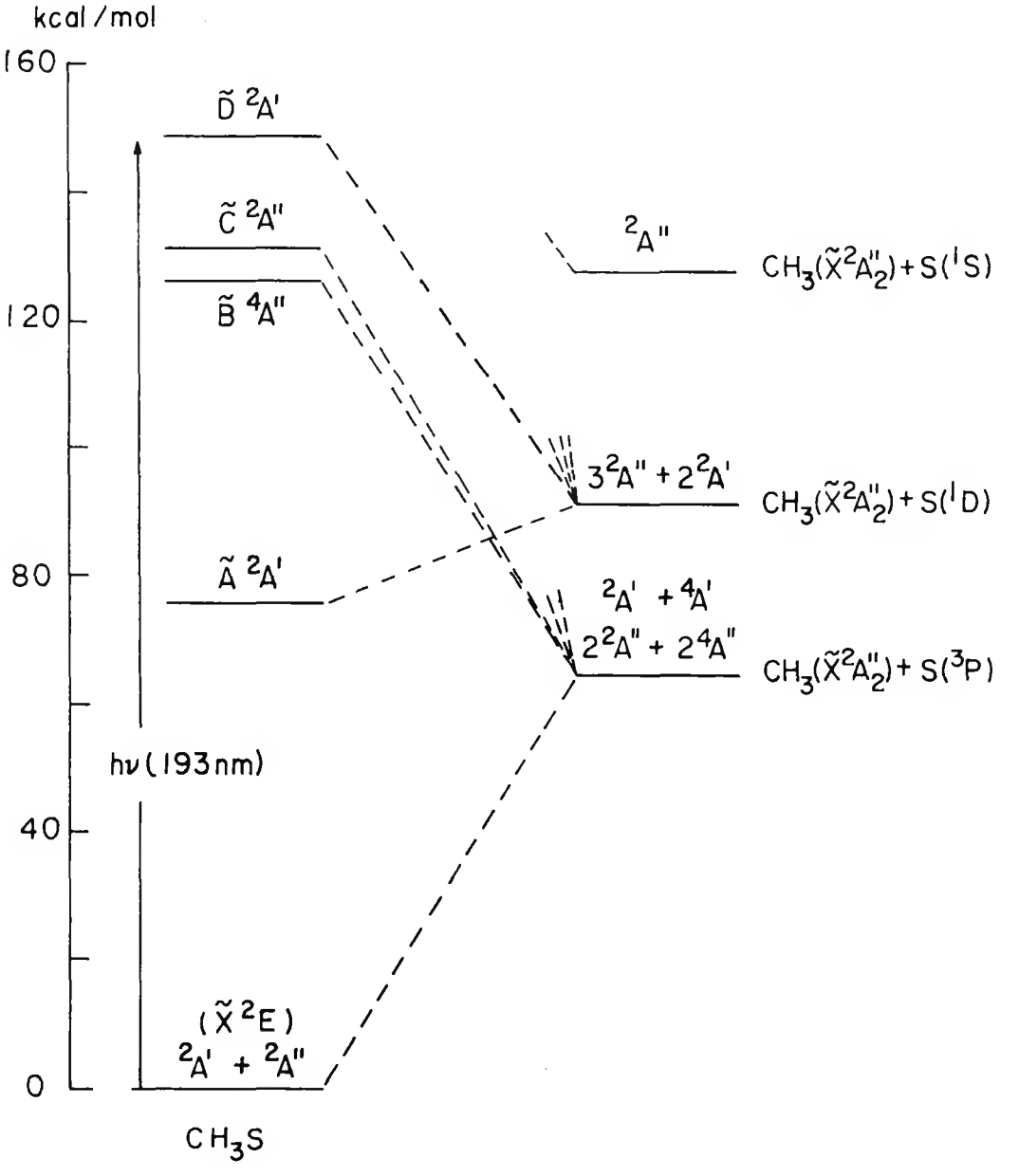

Figure 8. Correlation diagram between the $S(^3P, ^1D, ^1S) + CH_3(\tilde{X}^2A''_2)$ and SCH_3 states, C_s symmetry

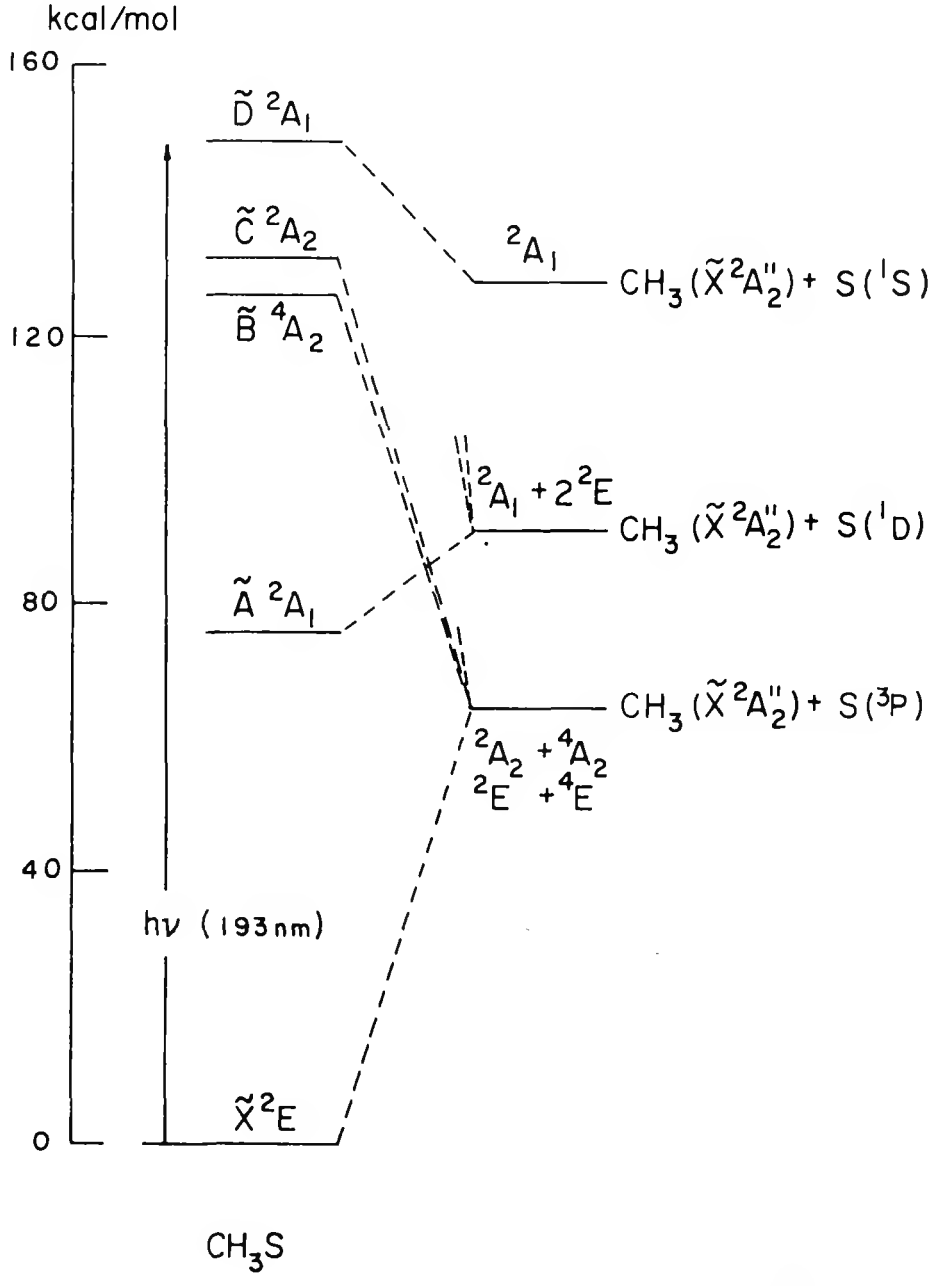

Figure 9. Correlation diagram between the $S(^3P, ^1D, ^1S) + CH_3(\tilde{X}^2A''_2)$ and SCH_3 states, C_{3v} symmetry

the consideration of spin-orbit splittings is shown in Fig. 9. In this case, the $SCH_3(\tilde{D}^2A_1)$ correlates to the formation of $CH_3(\tilde{X}^2A''_2)$ + $S(^1S)$, while the $SCH_3(\tilde{C}^2A_2)$ remains in correlation with the $CH_3(\tilde{X}^2A''_2)$ + $S(^1S)$ product channel. Based on the correlation diagrams, the observation that $S(^3P)$ atoms are not produced by process (6) may be taken as evidence supporting that the $SCH_3(\tilde{C}^2A''$ or $^2A_2)$ state is not involved in the 193 nm photodissociation of SCH_3.

The scenario for the dissociation of SCH_3 is more complicated than that presented by the correlation diagrams when vibrational couplings between electronic states are taken into account. It is also possible that low lying Rydberg states are involved in the photoexcitation process.

The maximum recoil c.m. velocity circle for $CH_3(v'_{c.m.}(CH_3))$ formed in process (6) is also indicated in the Newton diagram of Fig. 2. We note that the maximum laboratory velocity for CH_3 at $\theta = 30^\circ$ ($= v'_{c.m.}(CH_3) + v_l(CH_3)$) produced by process (6) is predicted to be greater than that formed in process (2). In the measurement of the TOF threshold for process (2), it is necessary to reduce the laser power in order to minimize the interference of process (6).

TOF Spectrum for S_2

The TOF spectrum for S_2 is shown in Fig. 4(c). The similarity of the TOF spectra for $SSCH_3$ and S_2 indicates that the spectrum for S_2 is mainly the result of fragmentation of $SSCH_3$ due to electron ionization,

$$SSCH_3 + e^- \rightarrow S_2^+ + CH_3. \quad (7)$$

In fact the signal observed for S_2^+ is greater than that for $SSCH_3^+$. However, the threshold in flight time for S_2 is found to shift to substantially lower flight time than the 346 μs threshold for $SSCH_3$. The observed threshold for S_2 cannot be accounted for by process (8), which has an exothermicity of 48 kcal/mol:[3,7]

$$CH_3SSCH_3 + h\nu\ (193\ nm) \rightarrow 2CH_3 + S_2. \quad (8)$$

Thus, the observed threshold of 218 μs for S_2 is attributed to the photodissociation process,

$$SSCH_3 + h\nu\ (193\ nm) \rightarrow S_2 + CH_3. \quad (9)$$

The kinematics for process (9) are shown in the Newton diagram of Fig. 5. Here, $v_{c.m.}(S_2)$ and $v'_{c.m.}(CH_3)$ represent the c.m. recoil velocities for S_2 and CH_3 formed in process (9). After taking into account the S_2^+ drift time of 32.2 μs, a simple calculation shows that the observed threshold for S_2 corresponds to a value of 103.5 kcal/mol for $E_{c.m.}$ which in turn gives a value of 44.4 kcal/mol for $D_o(SS\text{-}CH_3)$, in good agreement with the literature value.

CONCLUSION

The TOF spectra for CH_3, SCH_3 and $SSCH_3$ resulting from the 193 nm photofragmentation of CH_3SSCH_3 have been measured. The translational energy distributions for photofragments of processes (1) and (2) are found to peak at $E_{c.m.} \sim 30$ and 38 kcal/mol, respectively. The threshold measured for the formation of S_2 is consistent with that of the 193 nm photodissociation of $SSCH_3$. The threshold for S is in agreement with that for the formation of $S(^1D)$ by the photodissociation of SCH_3. We interpret this observation tentatively as evidence that $S(^3P)$ atoms are not produced in the 193 nm photodissociation of SCH_3. Further studies to measure directly the states of S are needed to confirm this conclusion. The values for the bond dissociation energies determined in this experiment are in accord with literature values as summarized in Table 1.

Table 1. Bond dissociation energies (kcal/mol) at 298 K determined in the 193 nm photodissociation studies of CH_3SSCH_3, SCH_3, and $SSCH_3$

Bond dissociation energies	This work	Literature values
$DH°(CH_3S\text{-}SCH_3)$	74.8 ± 1.5	74 ± 2[a] 72 ± 2[b]
$DH°(CH_3SS\text{-}CH_3)$	57.4 ± 1.5	57.0 ± 1.5[b]
$DH°(S\text{-}CH_3)$	~ 66[c]	66.0 ± 1.5[a]
$DH°(SS\text{-}CH_3)$	46.5 ± 3.0	47.5 ± 1.5[a]

[a]Reference 3.
[b]Reference 7.
[c]This value is estimated assuming that the threshold observed for S corresponds to the formation of $S(^1D)$.

REFERENCES

1. A. Levy, E. L. Merryman, and W. T. Reid, Environ. Sci. Technol. 4, 653 (1970).

2. C. F. Cullis and M. F. R. Mulcahy, Combust. Flame 18, 225 (1975).

3. S. W. Benson, Chem. Rev. 78, 23 (1978).

4. S. W. Benson, F. R. Cruickshank, D. M. Golden, G. R. Haugen, H. E. O'Neal, A. S. Rodgers, R. Shaw, and R. Walsh, Chem. Rev. 69, 279 (1969).

5. J. A. Kerr, Chem. Rev. 66, 465 (1966).

6. J. D. Cox and G. Pilcher, in "Thermochemistry of Organic and Organometallic Compounds" (Academic Press, London, 1970).

7. D. F. McMillen and D. M. Golden, Ann. Rev. Phys. Chem. 33, 493 (1982).

8. S. W. Benson, in "Thermochemical Kinetics", 2nd ed. (Wiley, New York, 1976).

9. C. Y. Ng, Adv. Chem. Phys. 52, 265 (1983); M. E. Gress, S. H. Linn, Y. Ono, H. F. Prest, and C. Y. Ng, J. Chem. Phys. 72, 4242 (1980); Y. Ono, S. H. Linn, H. F. Prest, M. E. Gress, and C. Y. Ng, J. Chem. Phys. 73, 2523 (1980); Y. Ono, S. H. Linn, H. F. Prest, M. E. Gress, and C. Y. Ng, J. Chem. Phys. 74, 1125 (1981); Y. Ono, E. A. Osuch, and C. Y. Ng, J. Chem. Phys. 74, 1645 (1981); J. Erickson and C. Y. Ng, J. Chem. Phys. 75, 1650 (1981); C. Y. R. Wu and C. Y. Ng, J. Chem. Phys. 76, 4406 (1982); H. F. Prest, W.-B. Tzeng, J. M. Brom, Jr., and C. Y. Ng, Int. J. Mass Spectrom. Ion Phys. 50, 315 (1983); H. F. Prest, W.-B. Tzeng, J. M. Brom, Jr., and C. Y. Ng, J. Am. Chem. Soc. 105, 7531 (1983); C.-L. Liao and C. Y. Ng, J. Chem. Phys. 84, 778 (1986).

10. W.-B. Tzeng, H.-M. Yin, W.-Y. Leung, J.-Y. Luo, S. Nourbakhsh, G. D. Flesch, and C. Y. Ng, J. Chem. Phys. 88, 1658 (1988).

11. K. Norwood and C. Y. Ng, Chem. Phys. Lett. 156, 145 (1989).

12. T. E. Graedel, Rev. Geophys. and Space Phys. 15, 421 (1977), and reference therein.

13. W. E. Burnett, Environ. Sci. Technol. 8, 744 (1969).

14. M. D. Bentley, I. B. Douglass, J. A. Lacadie, and D. R. Whittier, J. Air Pollution Control Association, 22, 359 (1972).

15. D. F. Sheraton and F. E. Murray, Can. J. Chem. 59, 2750 (1981).

16. A. B. Callear and D. R. Dickon, Trans. Faraday Soc. 66, 1907 (1970).

17. P. M. Rao, J. A. Copeck, and A. R. Knight, Can. J. Chem. 45, 1369 (1967).

18. K. Sayamol and A. R. Knight, Can. J. Chem. 46, 999 (1969).

19. P. M. Rao and A. R. Knight, Can. J. Chem. 46, 2462 (1968).

20. S. Nourbakhsh, C.-L. Liao, K. Norwood, and C. Y. Ng, to be published.

21. S. W. Benson, J. Chem. Ed. 42, 502 (1965).

22. H. Okabe, in "Photochemistry of Small Molecules" (Wiley, New York, 1978).

23. N. Sivakumar, G. E. Hall, and P. L. Houston, J. W. Hepburn, and I. Burak, J. Chem. Phys. 88, 3692 (1988).

24. H. L. Kim, S. Satyapal, P. Brewer, and R. Bersohn, J. Chem. Phys. 91, 1047 (1989).

25. M. Suzuki, G. Inoue, and H. Akimoto, J. Chem. Phys. 81, 5405 (1984).

26. K. Ohbayashi, H. Akimoto, and I. Tanaka, Chem. Phys. Lett. 52, 47 (1977).

27. P. C. Engelking, G. B. Ellison, and W. C. Lineberger, J. Chem. Phys. 69, 1826 (1978).

28. B. K. Janousek and J. I. Brauman, J. Chem. Phys. 72, 694 (1980).

29. B. Mouflih, C. Larrieu, and M. Chaillet, Chem. Phys. 119, 221 (1988).

SECTION III.

VACUUM ULTRAVIOLET PHOTODISSOCIATION AND PHOTOIONIZATION STUDIES OF CH_3SCH_3 AND CH_3S

ABSTRACT

We have measured the translational energy releases of the laser photodissociation processes: CH_3SCH_3 + hν (193 nm) → CH_3 + CH_3S [process (1)] and CH_3SCH_2 + H [process (2)]; and CH_3S + hν (193 nm) → S + CH_3 [process (3)]. The onsets of the translational energy distributions for photofragments of processes (1) and (2) allow the direct determination of 74.9 ± 1.5 and 91 ± 2.5 kcal/mol for the dissociation energies of the CH_3-SCH_3 and H-CH_2SCH_3 bonds at 0 K, respectively. The threshold observed for S formed by process (3) is consistent with the conclusion that S atoms are formed in the ^3P and ^1D states. The photoelectron-photoion coincidence (PEPICO) spectra for $CH_3SCH_3^+$, $CH_3SCH_2^+$, CH_3S^+ (or CH_2SH^+), and CH_2S^+ resulting from CH_3SCH_3 have been measured in the wavelength region of 900-1475 Å. The PEPICO study allows the construction of the breakdown diagram for the formation of $CH_3SCH_2^+$, CH_3S^+ (or CH_2SH^+), and CH_2S^+ from energy-selected $CH_3SCH_3^+$ ions. Combining the energetic information obtained from the photodissociation and photoionization experiments, we have estimated the ionization energy of the CH_3S radical.

INTRODUCTION

Dimethylsulfide is one of the industrial organosulfur pollutants emitted to the atmosphere due to the incomplete combustion of coal and oil.[1-3] Oxidation of organosulfur compounds such as CH_3SCH_3 ultimately leads to the formation of SO_2.[4,5] The absorption spectrum of CH_3SCH_3 shows a strong absorption band in the wavelength region of 190-210 nm.[6-8] Previous ultraviolet photolysis studies[9-12] suggest that the primary ultraviolet photodissociation process of CH_3SCH_3 involves the breaking of the C-S bond. The oxidation rate for CH_3SCH_3 is found to increase in the presence of ultraviolet radiation.[13] Therefore, the study of the ultraviolet photochemistry of CH_3SCH_3 is relevant to the detailed modelling of the atmospheric sulfur chemistry cycles.

Here, we present the results of a 193 nm laser photodissociation time-of-flight (TOF) study of the processes:

$$CH_3SCH_3 + h\nu\ (193\ nm) \rightarrow CH_3 + CH_3S, \qquad (1)$$

$$CH_3SCH_3 + h\nu\ (193\ nm) \rightarrow CH_3SCH_2 + H. \qquad (2)$$

In a recent 193 nm photofragmentation study of CH_3S formed by the photodissociation of CH_3SSCH_3,[14] the threshold observed in the time-of-flight (TOF) spectrum of S is found to be consistent with the formation of S in the excited $S(^1D)$ state. In order to re-examine the previous observation, we have measured the TOF spectrum for S formed by the 193 nm photodissociation of CH_3S formed in process (1).

$$CH_3S + h\nu\ (193\ nm) \rightarrow S + CH_3 \qquad (3)$$

Photoionization mass spectrometry has a distinguished history of providing accurate thermochemical data for molecular and radical ions. Through use of appropriate thermochemical cycles, heats of formation for neutral molecules and radicals can also be obtained. The photoionization efficiency (PIE) spectra for $CH_3SCH_3^+$, $CH_3SCH_2^+$, CH_3S^+ (or CH_2SH^+), and CH_2S^+ formed by the processes,

$$CH_3SCH_3 + h\nu \rightarrow CH_3SCH_3^+ + e^-, \quad (4)$$

$$CH_3SCH_3 + h\nu \rightarrow CH_3SCH_2^+ + H + e^-, \quad (5)$$

$$CH_3SCH_3 + h\nu \rightarrow CH_3S^+ \text{ (or } CH_2SH^+) + CH_3 + e^-, \quad (6)$$

$$CH_3SCH_3 + h\nu \rightarrow CH_2S^+ + CH_4 + e^-, \quad (7)$$

have been measured previously in a gas cell photoionization mass spectrometric study.[15] Because of the scattered light effect of the diffraction grating, the intensity of a specific ion observed in a photoionization experiment remains finite even though the monochromator is set at a photon energy below the ionization energy (IE) or appearance energy (AE) of the ion formation. This, together with the hot band effect, often makes the determination of the true threshold difficult. We have re-examined the thresholds for processes (4)-(7) using the molecular beam photoelectron-photoion coincidence (PEPICO) method. In a previous study,[16] we have pointed out that employing the PEPICO method can significantly reduce the scattered light effect because photoelectrons (PE) produced by scattered light are expected to have kinetic energies different from the accepting energy band width set by the electron energy analyzer. By using the molecular beam method to introduce CH_3SCH_3 into the photoionization region of the mass spectrometer, we reduce the rotational and low frequency vibrational hot band effect.[17] The PEPICO measurements

also yield valuable information about the unimolecular dissociation routes of energy-selected $CH_3SCH_3^+$ ions.

An important motivation for performing both the photoionization and photodissociation studies of CH_3SCH_3 is to obtain energetic information for the radicals such as CH_3S. For example, by combining the AE's for processes (1) and (6) we hope to estimate the IE for CH_3S.

EXPERIMENTAL

Measurements of TOF Spectra for H, S, CH_3, and CH_3S from the Photodissociation of CH_3SCH_3

The rotatable beam source laser photofragmentation apparatus used in this study has been described in detail previously.[14,18] The apparatus consists of three main components: an ArF excimer laser, a photodissociation chamber in which a rotatable supersonic molecular beam intersects the laser beam, and a linearly movable ultrahigh vacuum electron ionization mass spectrometric detector.

In this experiment, a pulsed beam of CH_3SCH_3 seeded in He is produced by supersonic expansion through a pulsed valve (nozzle diameter = 0.5 mm) at ~ 298 K and a total pressure of ~ 2300 Torr. The pressure ratio of CH_3SCH_3 to He is about 0.25. The seeded CH_3SCH_3 beam has an angular divergence of ~ 3°, which corresponds to a beam width of 3 mm in the photodissociation region.

The molecular beam source chamber is pumped by a 20 in. diffusion pump (DP) with a pumping speed of 20000 ℓ/s. The differential pumping chamber is evacuated by a liquid-nitrogen (LN_2) trapped 6 in. DP with a pumping speed of 2000 ℓ/s, while the photodissociation chamber is pumped by a freon-trapped 10 in. DP with a pumping speed of 5000 ℓ/s. During the experiment, the beam source, differential, and photodissociation

chambers are maintained at pressures of ~ 1 x 10^{-6}, 2 x 10^{-7}, and 5 x 10^{-8} Torr, respectively.

The excimer laser used (Questek Model 2460) has a maximum repetition rate of 200 Hz and a maximum output energy of 250 mJ at 193 nm. The laser energy is varied in the range of 90-120 mJ. The laser beam enters the photodissociation chamber through a MgF_2 focusing lens and intersects with the seeded CH_3SCH_3 beam at 90°.

The detector chamber, which houses the mass spectrometer, has four stages of differential pumping. The first and second differential pumping regions are evacuated by a 300 ℓ/s turbomolecular pump and a 220 ℓ/s ion pump, respectively. The ionizer is located inside the LN_2 cooled ionization chamber which is pumped by a 120 ℓ/s ion pump and a 500 ℓ/s turbomolecular pump. The neutral fragments produced in the photodissociation region pass through the first and second differential pumping regions of the detector chamber before entering the ionization region. During the experiment, the pressures in the first and second differential and ionization chambers are ≤ 2 x 10^{-9}, 5 x 10^{-10}, and 2 x 10^{-11} Torr, respectively. The emission current of the ionizer is ≤ 2.5 mA and the ionization electron energy is 100 eV. The mass analyzer is a quadrupole mass filter (QMF) constructed of 1.9 cm diameter rods. The ion detector is a Daly-type scintillation detector. The ion detector chamber is separated from the second differential pumping region by the QMF and a sheet metal wall. The vacuum in the ion detector chamber is maintained by a 50 ℓ/s turbomolecular pump.

The detector chamber is mounted on a movable platform which is supported on a linear rail assembly. Using the rail assembly, the distance between the photodissociation

region and the ionizer can be varied continuously in the range of 35-110 cm. In this experiment, all TOF spectra are taken at a flight path distance of 73.7 cm. The detector and photodissociation chambers are connected by a flexible bellows which allows variation of the flight path length without venting any of the experimental chambers.

The data acquisition and operation of the apparatus are controlled by a LSI-11/23 mini-computer. The TOF spectrum is recorded on a multichannel scaler (MCS) which has a minimum channel width of 0.3 μs. In this experiment, the pulsed valve is operated at 40 Hz. The firing of the excimer laser is delayed by approximately 450 μs with respect to the triggering pulse which activates the pulsed valve. The multichannel scaler is started by a second trigger pulse signifying the firing of the laser. The timing delays are controlled by a digital delay unit (SRS, Model DG 535).

The laboratory angle (θ) is defined as the angle between the seeded CH_3SCH_3 molecular beam and the detector axis. The laboratory velocity for the parent CH_3SCH_3 beam (v_p) is determined by measuring the TOF of the CH_3SCH_3 beam pulse at $\theta = 0°$ at two known nozzle-ionizer distances. The value for v_p (1.2×10^5 cm/s) is determined before and after the laser photodissociation experiment and the deviation of the two measurements is usually < 2%. Under these beam expansion conditions, the ratio $\Delta v/v_p$ is estimated to be less than 0.08, where Δv is the velocity spread [full width at half maximum (FWHM)] of the CH_3SCH_3 beam.

The ion drift times through the QMF have been determined by applying a voltage pulse to the ion extraction lens and the trigger of an oscilloscope. The oscilloscope measures the arrival times of the ions at the ion detector with respect to the trigger

voltage pulse. The photofragment flight time to the ionizer is the difference between the time measured by the MCS and the ion drift time.

The analysis of the TOF data involves the transformation of the laboratory TOF spectra into center-of-mass (c.m.) translational energy ($E_{c.m.}$) distributions and has been described in detail.[14,18] We ignore the effect of the apparatus resolution factors in the transformation.

Measurements of PIE and PEPICO Spectra for CH_2S^+, CH_3S^+, $CH_3SCH_2^+$, and $CH_3SCH_3^+$ from CH_3SCH_3

The experimental arrangement of the molecular beam PEPICO apparatus has been reported in detail in previous publications.[19-21] Briefly, the apparatus consists of a 3 m near normal incidence vacuum ultraviolet (VUV) monochromator, a capillary discharge lamp, a tungsten photoelectric VUV light detector, a molecular beam source, a QMF for ion detection, and an electron energy analyzer for threshold photoelectron (TPE) detection.

The grating employed is a Bausch and Lomb 1200 lines/mm Os coated aluminum grating blazed at 1360 Å. The hydrogen many-lined pseudocontinuum is used as the light source.

The CH_3SCH_3 gas sample is introduced into the photoionization region as a continuous beam of pure CH_3SCH_3 produced by supersonic expansion through a stainless steel nozzle with a diameter of 125 μm at a stagnation pressure of ~ 120 Torr. The

molecular beam is collimated by a conical skimmer before entering the photoionization chamber, which is maintained at $\leq 1 \times 10^{-5}$ Torr.

A differential pulsed PEPICO scheme[21] is used for coincidence measurements. The coincidence detection cycle is initiated by an electronic pulse signifying the arrival of a TPE at the electron detector. The electronic pulse triggers two identical extraction pulses (width = 80 ns and height = 120 V) to extract photoions toward the ion detector. The QMF is used to select the ion of interest for detection. The first and second extraction pulses are delayed by 0 and 40 μs, respectively, with respect to the triggering electronic pulse. The electron flight time from the photoionization region to the electron detector is ≤ 0.1 μs. In such a short time the correlated photoion is expected to remain in the photoionization region. Thus, the first extraction pulse serves to extract the correlated photoion as well as background ions, while the second extraction pulse draws out only background ions. The photoionization region is maintained nearly field free, except during the application of the ion extraction pulse. A potential barrier is used between the photoionization region and the entrance of the QMF such that no ions are transmitted to the ion detector without the application of the extraction pulse. The ions arriving at the ion detector are recorded using an MCS. The difference of the ion intensities detected due to the first and second extraction pulses represents the true coincidence signal. The coincidence cycle is completed in 100 μs. The first TPE electronic pulse generated by the electron detector after this period initiates a new coincidence cycle.

All data are obtained with an optical resolution of 1.4 Å (FWHM). The wavelength

interval used varies in the range of 0.5-2 Å. The counting time at each PEPICO data point is 25 s.

RESULTS AND DISCUSSION

193 nm Photodissociation of CH_3SCH_3

TOF spectra for CH_3S and CH_3

Figures 1(a)-1(c) show the TOF spectra for CH_3S observed at $\theta = 30°$ and delay times of 450, 500, and 550 μs, respectively, between the trigger pulses for opening the pulsed molecular beam valve and for firing the ArF excimer laser. The fast peak centered at ~ 350 μs is due to process (1). The broad peak in the range of ~ 500-1000 μs decreases significantly relative to the fast peak as the nozzle stagnation pressure is decreased, indicating that it arises from the formation of CH_3S^+ fragments in the electron impact ionization of dimer and cluster species of CH_3SCH_3. As a result of slippage in the supersonic expansion, the velocity for CH_3SCH_3 is expected to be slightly greater than those for the dimer and higher clusters. As pointed out in previous reports,[14,18] it is possible to minimize the fragmentation effect of dimers and clusters by selecting a specific delay time between the opening of the nozzle and the firing of the laser. The lower intensity of the slow peak relative to that of the fast peak observed in Fig. 1(a), compared to those observed in Figs. 1(b) and 1(c), indicates that the CH_3SCH_3 beam sampled by the laser at a delay time of 450 μs contains the fewest dimers and clusters. Therefore, the delay time of 450 μs is used for the measurements of all the TOF spectra presented below.

Figure 1. TOF spectra is shown for SCH_3 measured at $\theta = 30°$. The delay time between the trigger pulse for opening the pulse valve and that for firing the excimer laser is (a) 450 μs, (b) 500 μs, and (c) 550 μs

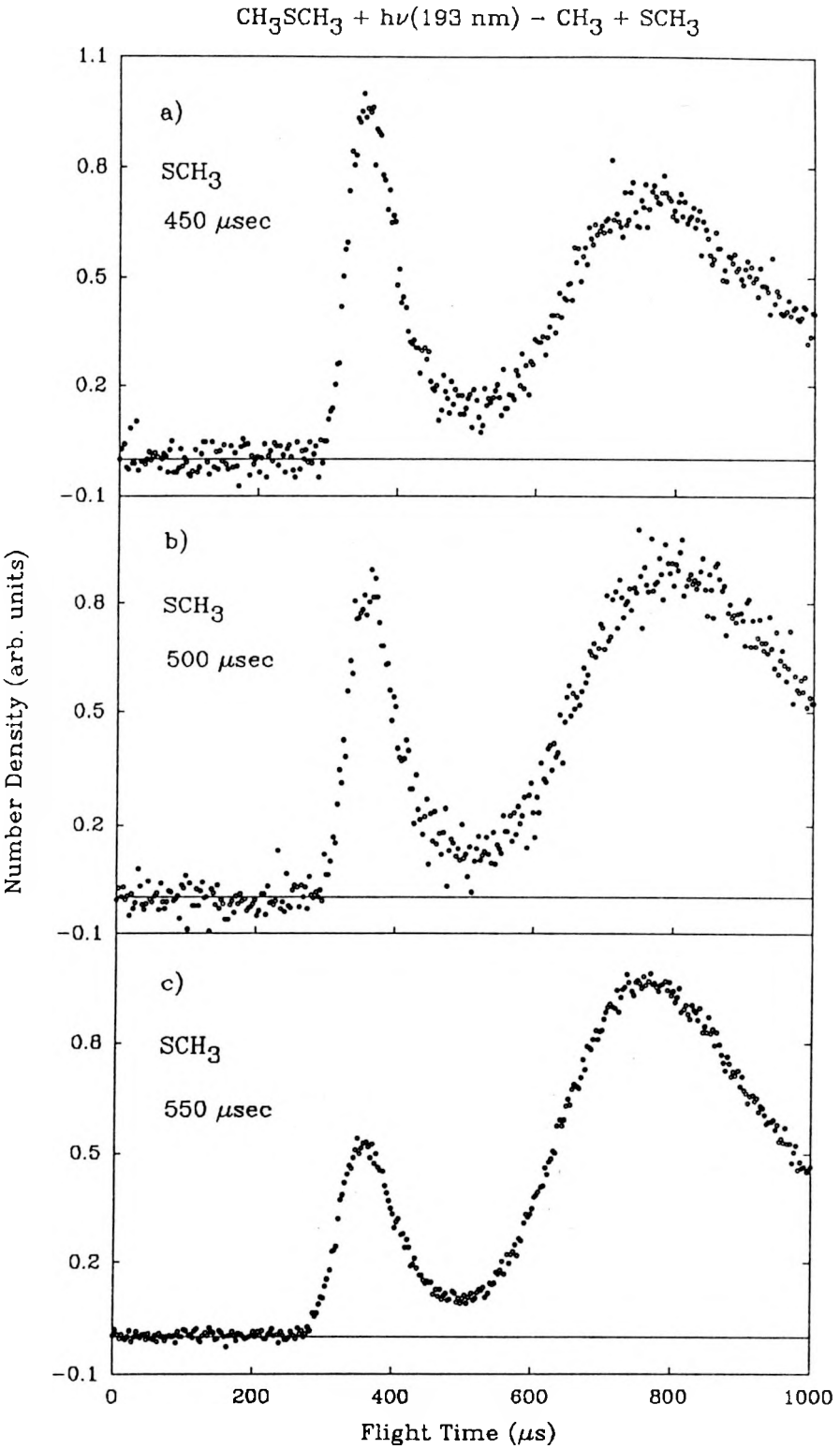
$CH_3SCH_3 + h\nu(193\ nm) \rightarrow CH_3 + SCH_3$
a)
SCH_3
450 μsec
b)
SCH_3
500 μsec
c)
SCH_3
550 μsec
Number Density (arb. units)
Flight Time (μs)
1.1
0.8
0.5
0.2
−0.1
0
200
400
600
800
1000

The TOF spectra for CH_3S recorded at $\theta = 35°$, 40°, and 60° are shown in Figs. 2(a)-2(c). Because of kinematic constraint, the slow peak, attributed to dimer and cluster fragmentation, has negligible intensity at $\theta \geq 60°$.

Figures 3(a) and 3(b) compare the TOF spectra for CH_3S and CH_3 observed at $\theta = 30°$. The comparison reveals that the slow peak in the TOF spectrum for CH_3 results from the fragmentation of CH_3S in the electron impact ionizer.

Based on the conservation of energy,

$$h\nu\ (193\ nm) + E_{int}^{*} = D_o(CH_3S\text{-}CH_3) + E_e + E_v + E_r + E_{c.m.}, \qquad (8)$$

where $h\nu$ is the photodissociation photon energy (147.9 kcal/mol); E_{int}^{*} is the initial internal energy of the parent CH_3SCH_3 molecule, which is assumed to be negligible due to supersonic cooling; $D_o(CH_3S\text{-}CH_3)$ is the dissociation energy of the $CH_3S\text{-}CH_3$ bond at 0 K; and E_e, E_v, and E_r are the electronic, vibrational, and rotational energies of the photofragments, respectively. A value of 77 ± 1.5 kcal/mol has been given for the dissociation energy of the $CH_3S\text{-}CH_3$ bond at 298 K [$DH°(CH_3S\text{-}CH_3)$], based on heats of formation data.[22] In a later review, McMillen and Golden[23] have recommended a value of 77.2 ± 2 kcal/mol[23] for $DH°(CH_3S\text{-}CH_3)$. We have used this value and Eq. 8 to construct the Newton diagram (Fig. 4) for the formation of CH_3S and CH_3 by process (1). Here $v_l(CH_3S)$ and $v_{c.m.}(CH_3S)$ represent the maximum laboratory and c.m. velocities for CH_3S at $\theta = 30°$. The c.m. velocity for CH_3 [$v_{c.m.}(CH_3)$] is also indicated in the figure.

The $E_{c.m.}$ distribution transformed from the TOF spectra for CH_3S and CH_3 at $\theta = 30°$ are shown in Figs. 5(a) and 5(b), respectively. The $E_{c.m.}$ distributions derived from the SCH_3 and CH_3 spectra are in agreement, showing a maximum at ~ 40 kcal/mol. A value

Figure 2. TOF spectra for SCH_3 measured at a delay of 450 μs between the opening of the trigger pulse and the firing of the excimer laser (a) $\theta = 35°$, (b) $\theta = 40°$, and (c) $\theta = 60°$

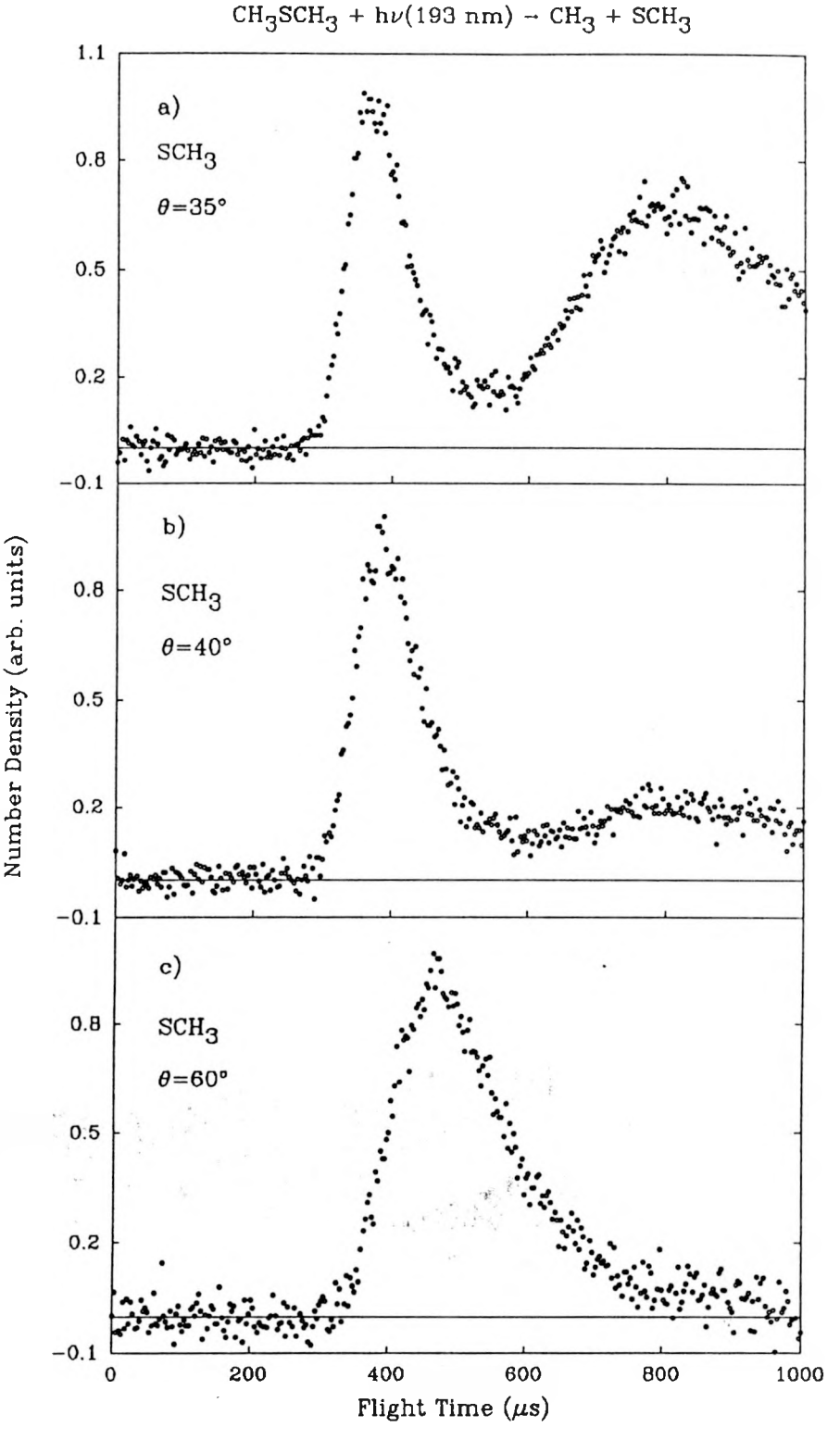
$CH_3SCH_3 + h\nu(193\ nm) \rightarrow CH_3 + SCH_3$
a)
SCH_3
θ=35°
b)
SCH_3
θ=40°
c)
SCH_3
θ=60°
Number Density (arb. units)
Flight Time (μs)
1.1
0.8
0.5
0.2
-0.1
0
200
400
600
800
1000

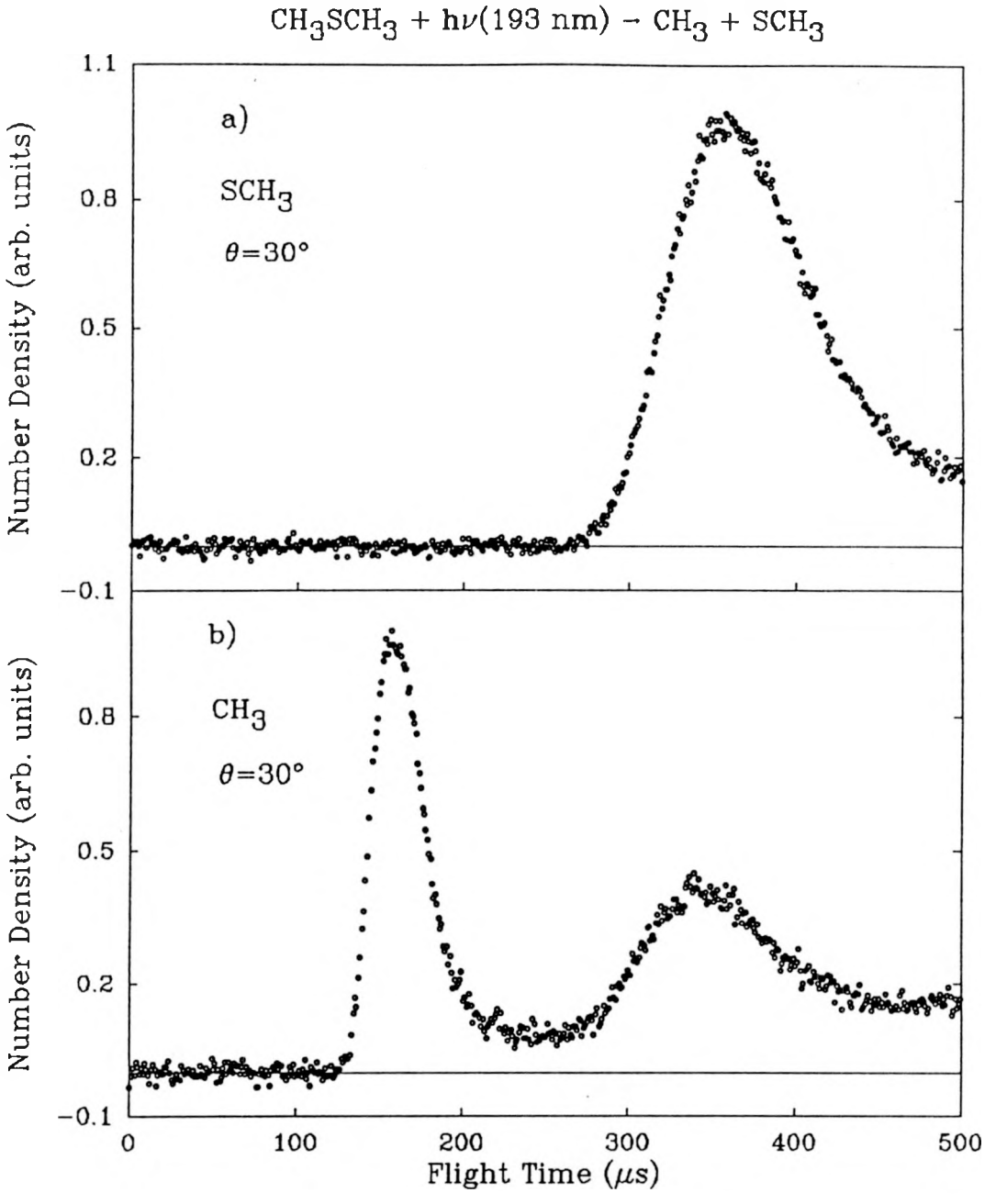

Figure 3. The TOF spectra obtained at θ = 30° for (a) SCH_3 and (b) CH_3

Figure 4. Kinematics for the formation of $SCH_3 + CH_3$ by process (1) and the sequential formation of $S + CH_3$ by processes (1) and (2) at $\theta = 30°$ is shown. Here, v_p is the laboratory velocity for CH_3SCH_3; $v_{c.m.}(SCH_3)$ and $v_l(SCH_3)$ are the maximum c.m. and laboratory velocities for SCH_3, respectively; $v_{c.m.}(CH_3)$ is the c.m. velocity for CH_3; and $v_{c.m.}(S(^3P))$, $v_{c.m.}(S(^1D))$, and $v_{c.m.}(S(^1S))$ are the maximum c.m. velocities for $S(^3P)$, $S(^1D)$, and $S(^1S)$ formed by process (2).

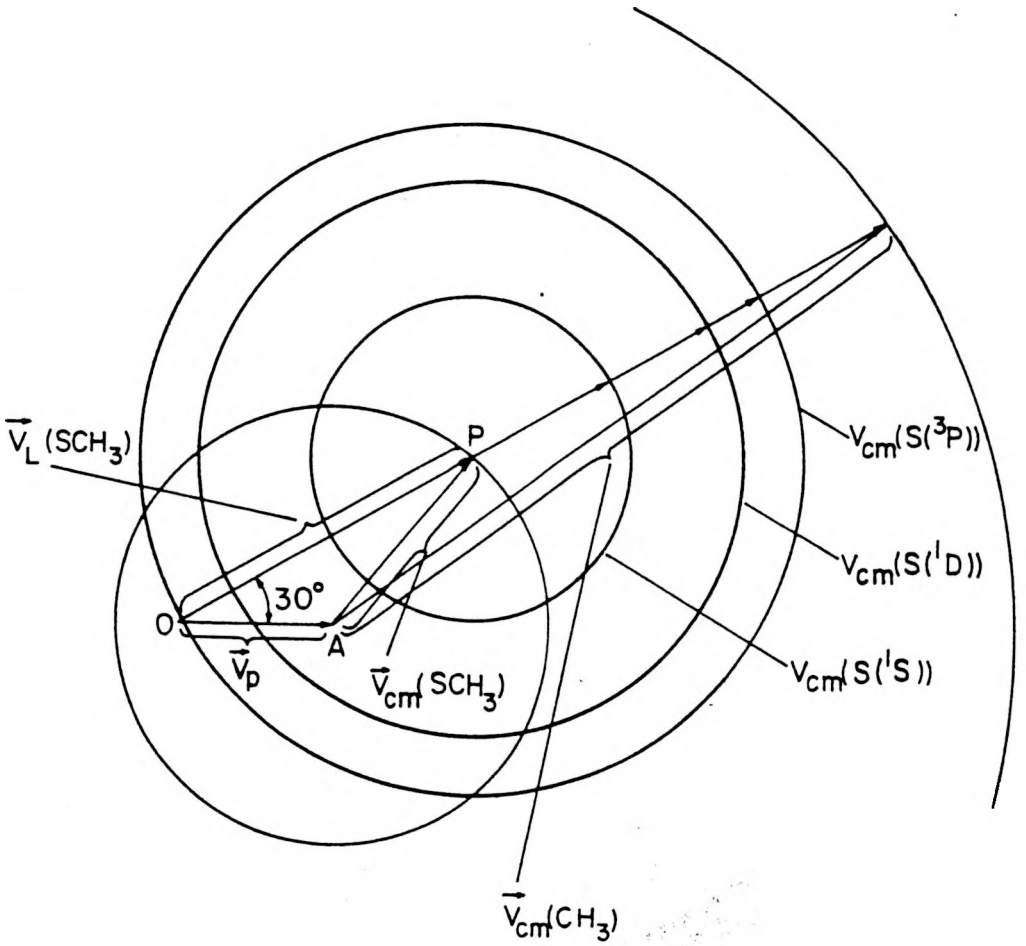
$\vec{V}_L(SCH_3)$
P
$V_{cm}(S(^3P))$
$V_{cm}(S(^1D))$
30°
O
A
$\vec{V}_p$
$\vec{V}_{cm}(SCH_3)$
$V_{cm}(S(^1S))$
$\vec{V}_{cm}(CH_3)$

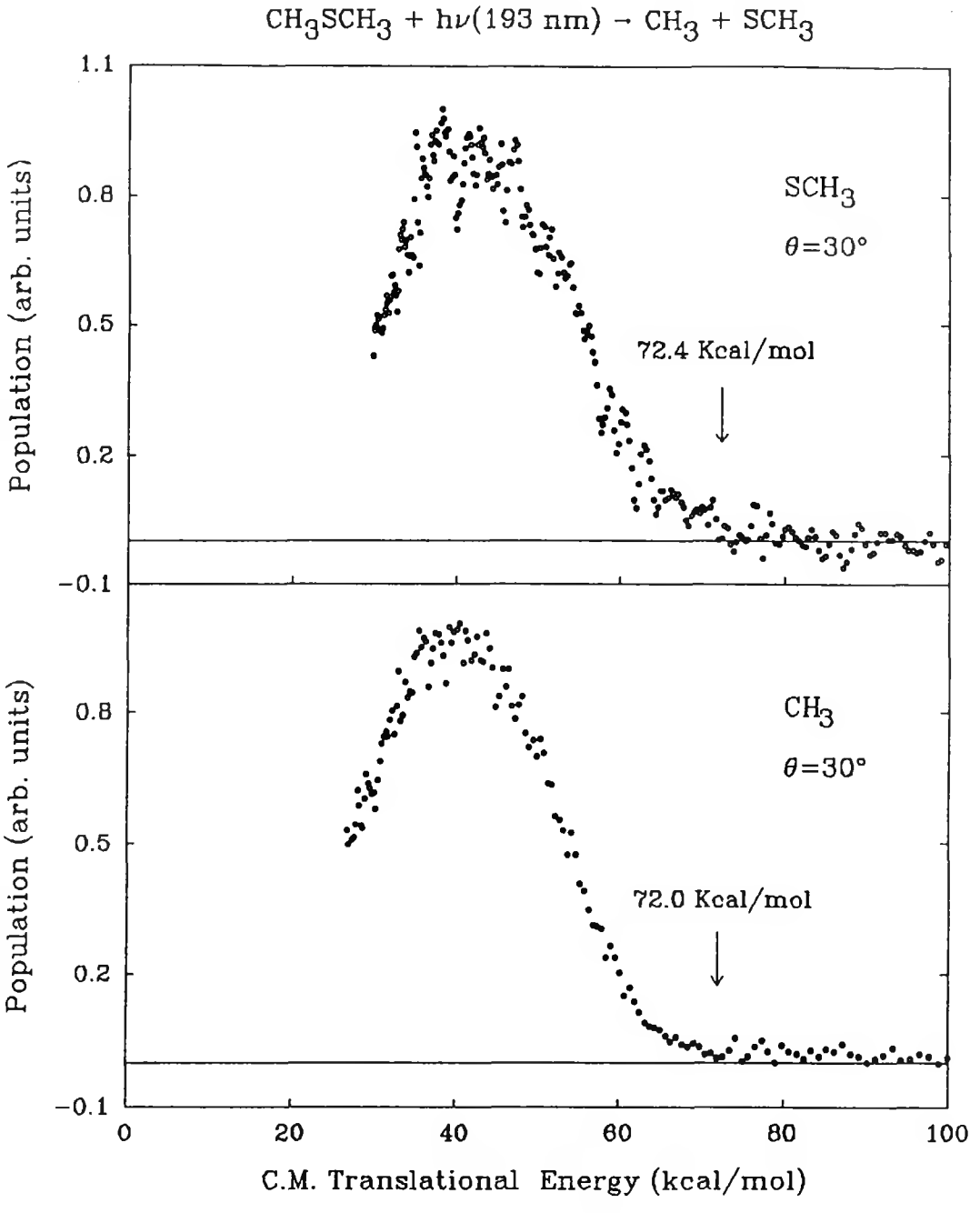

Figure 5. Translational energy distributions measured at θ = 30° for the fragments of process (1) derived from the TOF spectrum for (a) SCH_3 and (b) CH_3

of 40 kcal/mol for $E_{c.m.}$ corresponds to a total internal excitation ($E_e + E_v + E_r$) of 33 kcal/mol for the CH_3 and CH_3S fragments. The threshold energies obtained from the $E_{c.m.}$ distributions of Figs. 5(a) and 5(b) are also in agreement, with values of 72.4 and 72 kcal/mol, respectively. Based on seven TOF spectra for CH_3S and CH_3, the threshold energy for process (1) is 73.0 ± 1.5 kcal/mol, which corresponds to a value of 74.9 ± 1.5 kcal/mol for $D_o(CH_3S\text{-}CH_3)$. Assuming that the vibrational and electronic degrees of freedom are not populated at 298 K for CH_3SCH_3, CH_3, and CH_3S, the conversion of $D_o(CH_3S\text{-}CH_3)$ to $DH°(CH_3S\text{-}CH_3)$ requires the addition of 2.4 kcal/mol to $D_o(CH_3S\text{-}CH_3)$.[24] The value of 77.3 ± 1.5 kcal/mol for $DH°(CH_3S\text{-}CH_3)$ determined in this experiment is in excellent accord with the literature value.[22,23]

TOF spectrum for H

The TOF spectrum for H obtained after 30000 laser shots is shown in Fig. 6. The corresponding $E_{c.m.}$ distribution after 3-point averaging is plotted in Fig. 7. The signal-to-noise ratio of the H spectrum is insufficient for a precise determination of the threshold energy for process (3). The $E_{c.m.}$ distribution shows a rise at $E_{c.m.}$ = 57 kcal/mol and reaches a plateau at $E_{c.m.}$ < 35 kcal/mol. The dissociation energy for the $H\text{-}CH_2SCH_3$ bond is not known. If the rise at $E_{c.m.}$ = 57 kcal/mol is attributed to the threshold energy for process (2), we obtain an estimate of 91 ± 2.5 kcal/mol for $D_o(H\text{-}CH_2SCH_3)$. The latter value is in reasonable accord with the expected bond energy for a C-H bond.[23] The $E_{c.m.}$ distribution shown in Fig. 7 exhibits a tail in the region of ~ 57-88 kcal/mol. We attribute this tail to be the result of H atoms produced by the secondary dissociation

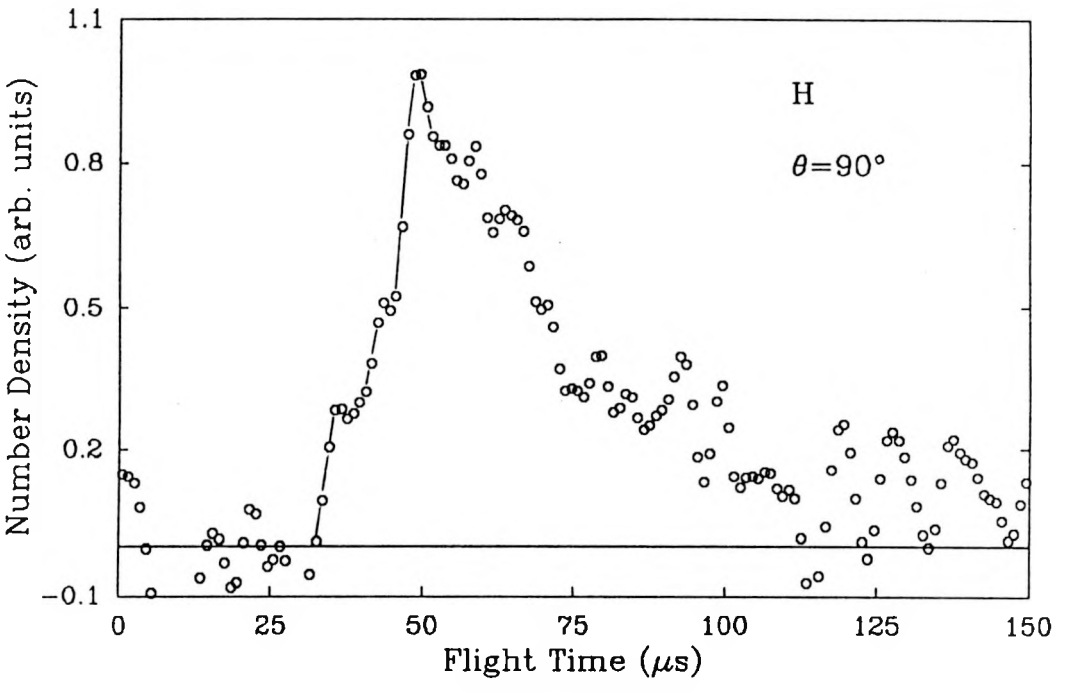

Figure 6. TOF spectrum for H measured at θ = 90°

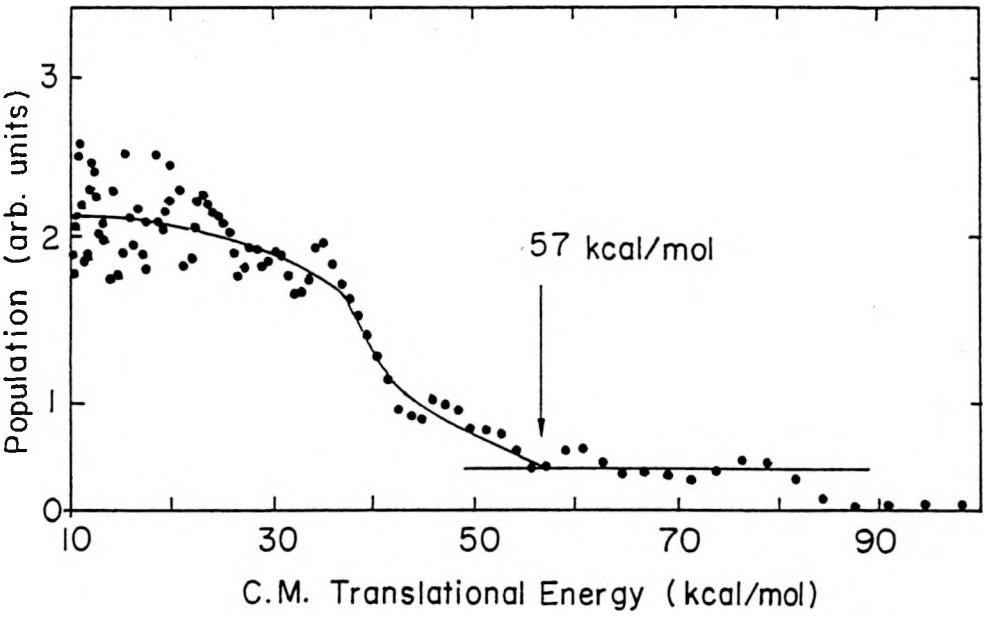

Figure 7. Translational energy distribution for fragments of process (3), derived from the TOF spectrum of H measured at $\theta = 90°$

process

$$CH_3S + h\nu\ (193\ nm) \rightarrow CH_2S + H. \qquad (9)$$

Using the known heats of formation for CH_3S [$\Delta H_{f298}(CH_3S)$ = 34.2 kcal/mol],[22] CH_2S [$\Delta H_{f298}(CH_2S)$ = 24.3 kcal/mol][22], and H [$\Delta H_{f298}(H)$ = 52.1][25], the value for $DH°(H\text{-}CH_2S)$ is calculated to be 42 kcal/mol.

TOF spectrum for S from the photodissociation of CH_3S

Figures 8(a) and 8(b) compare the TOF spectra for CH_3S and S. The peak centered at ~ 370 μs in the TOF spectrum of S is due to fragmentation of CH_3S in the electron impact ionizer. The S signals observed in the range of 150-260 μs are attributed to the dissociation of the primary CH_3S fragment induced by the absorption of a second 193 nm photon.

The S formed by process (3) can be in the $S(^3P)$, $S(^1D)$, and $S(^1S)$ states. The excited metastable $S(^1D)$ and $S(^1S)$ states are 26.4 and 63.4 kcal/mol higher, respectively, than the $S(^3P)$ ground state.[26] Assuming that CH_3 is formed in the $CH_3(\tilde{X}^2A_2'')$ ground state, the exothermicities are predicted to be 83.4, 57.0, and 20.0 kcal/mol for the respective $S(^3P)$, $S(^1D)$, and $S(^1S)$ channels.

The kinematics for the sequential photodissociation processes (1) and (3) at $\theta = 30°$ is shown in the Newton diagram in Fig. 4. For CH_3S moving at $v_l(CH_3S)$, $E_{int}(CH_3S)$ is zero. If these CH_3S radicals further dissociate according to process (3), the maximum c.m. recoil velocity circles due to the formation of $S(^3P)$, $S(^1D)$, and $S(^1S)$ are indicated in the figure. The maximum laboratory velocities for S formed in the $S(^3P)$, $S(^1D)$, and $S(^1S)$

Figure 8. (a) TOF spectrum for SCH_3 measured at $\theta = 30°$; (b) TOF spectrum for S measured at $\theta = 30°$; (c) a magnified view of the TOF spectrum for S near the threshold region

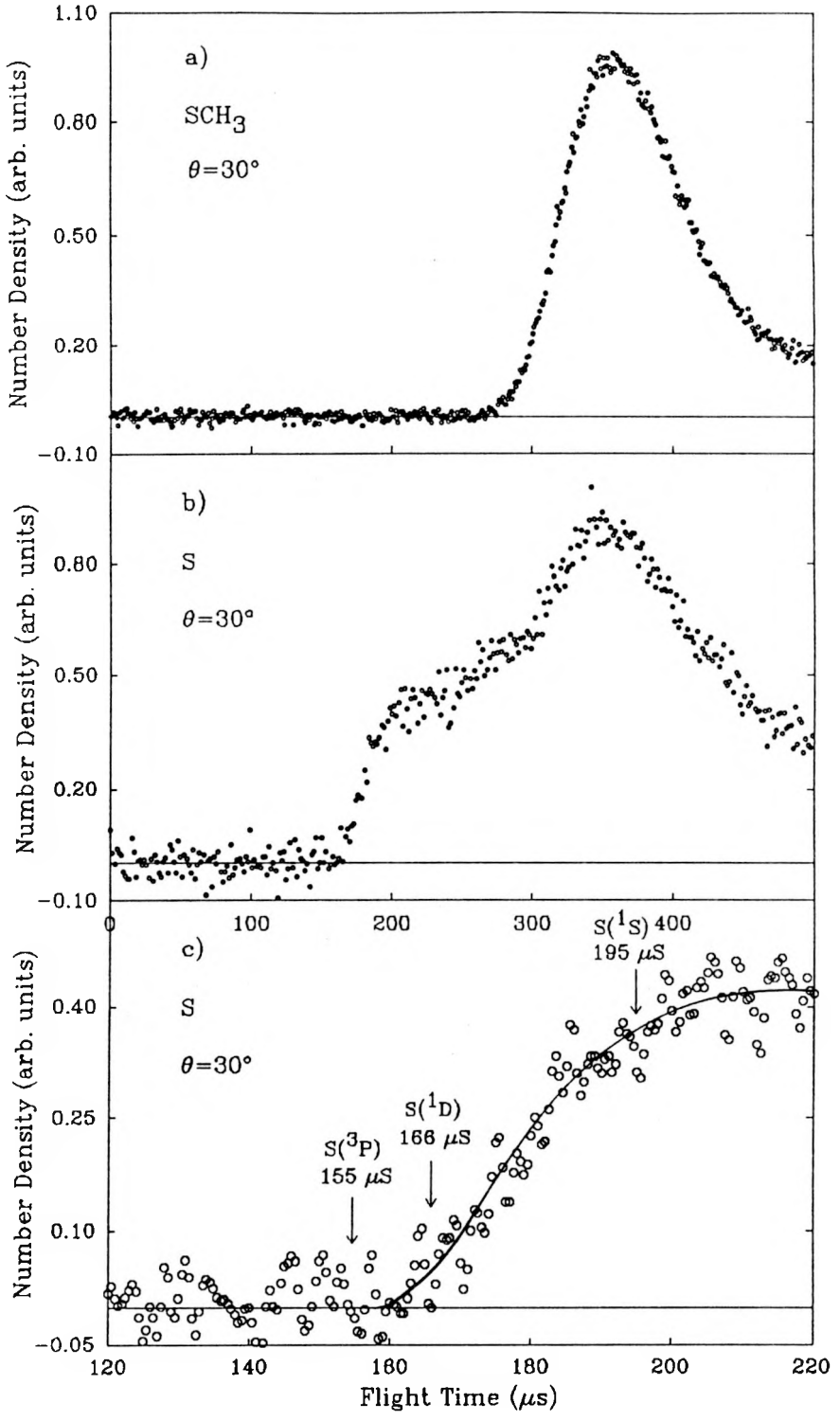
a)
SCH3
θ=30°
b)
S
θ=30°
c)
S
θ=30°
S(1S) 400
195 μS
S(1D)
166 μS
S(3P)
155 μS
Number Density (arb. units)
Flight Time (μs)

states are: $v_l[S(^3P)] = v_l(CH_3S) + v_{c.m.}[S(^3P)]$, $v_l[S(^1D)] = v_l(CH_3S) + v_{c.m.}[S(^1D)]$, and $v_l[S(^1S)] = v_l(CH_3S) + v_{c.m.}[S(^1S)]$. The values for $v_l[S(^3P)]$, $v_l[S(^1D)]$, and $v_l[S(^1S)]$ correspond to thresholds in flight time of 155, 166, and 195 μs, respectively, which are marked in a magnified view of the TOF spectrum for S near the threshold [Fig. 8(c)]. The overwhelming majority of the CH_3S radicals formed by process (1) are internally excited. Due to kinematic constraint, the laboratory velocities for the $S(^3P)$, $S(^1D)$, and $S(^1S)$ states formed from the photodissociation of internally excited CH_3S are less than the respective values for $v_l[S(^3P)]$, $v_l[S(^1D)]$, and $v_l[S(^1S)]$. In the previous 193 nm photodissociation study of CH_3S prepared by the photodissociation of CH_3SSCH_3, the TOF threshold for S is found to be the same as $v_l[S(^1D)]$, within experimental uncertainties. This implies that $S(^3P)$ may not be formed in the 193 nm photodissociation of CH_3S. However, in this study, as shown in Fig. 8(a), the TOF threshold for S appears to fall in between the predicted thresholds for the formation of $S(^3P)$ and $S(^1D)$. This observation is consistent with the conclusion that $S(^3P)$, as well as $S(^1D)$, is formed in process (2). This latter conclusion is supported by a recent resonance enhanced multiphoton ionization experiment[27] designed to identify the product states of S produced via processes (1) and (2).

Photoionization of CH_3SCH_3

Photoionization mass spectrum of CH_3SCH_3

The photoionization mass spectrum for CH_3SCH_3 measured at 820 Å is plotted in Fig. 9. The assignment of the mass peaks is shown in the figure. In addition to the $CH_3SCH_3^+$, $CH_3SCH_2^+$, CH_3S^+,(or CH_2SH^+) and CH_2S^+ ions resulting from processes (4)-(7), SCH^+, H_2S^+, and $C_2H_4^+$ are also observed. These ions are most likely produced by the processes,

$$CH_3SCH_3 + h\nu \rightarrow SCH^+ + H_2 + CH_3 + e^-, \quad (10)$$

$$CH_3SCH_3 + h\nu \rightarrow H_2S^+ + C_2H_4 + e^-, \quad (11)$$

$$CH_3SCH_3 + h\nu \rightarrow C_2H_4^+ + H_2S + e^-. \quad (12)$$

Most of the unassigned minor mass peaks can be identified with organosulfur ions containing the ^{33}S and ^{34}S isotopes.

PIE spectra for $CH_3SCH_3^+$, $CH_3SCH_2^+$, CH_3S^+, and CH_2S^+

Figures 10(a)-10(d) show the respective PIE spectra for $CH_3SCH_3^+$, $CH_3SCH_2^+$, CH_3S^+ (or CH_2SH^+), and CH_2S^+ in the wavelength region of 900-1470 Å. The general profiles of these spectra are in good agreement with those reported previously.[15] The values for the IE of CH_3SCH_3 and for the AE's for processes (5)-(7) determined in this experiment are compared to those of Ref. 15 in Table 1. Good agreement between the two sets of values is observed, except that the AE of CH_3S^+ (CH_2SH^+) determined in Fig. 10(c) is slightly

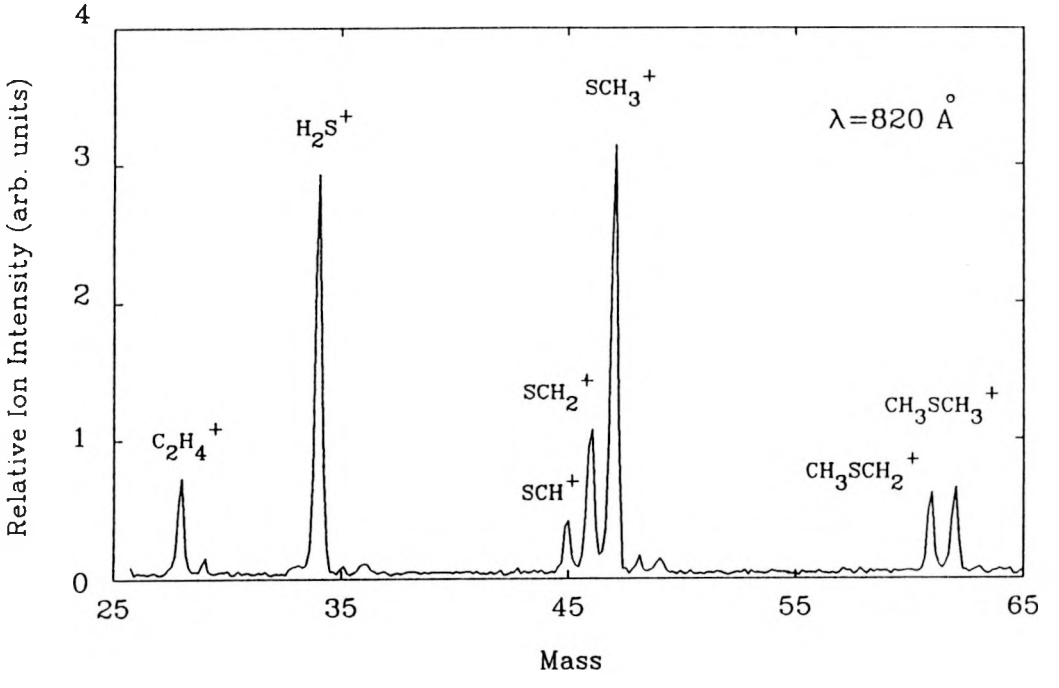

Figure 9. Photoionization mass spectrum of CH_3SCH_3 measured at a photoionization wavelength = 820 Å

Figure 10. PIE spectra in the region of 900-1475 Å (a) $CH_3SCH_3^+$; (b) $CH_3SCH_2^+$; (c) CH_3S^+; (d) CH_2S^+

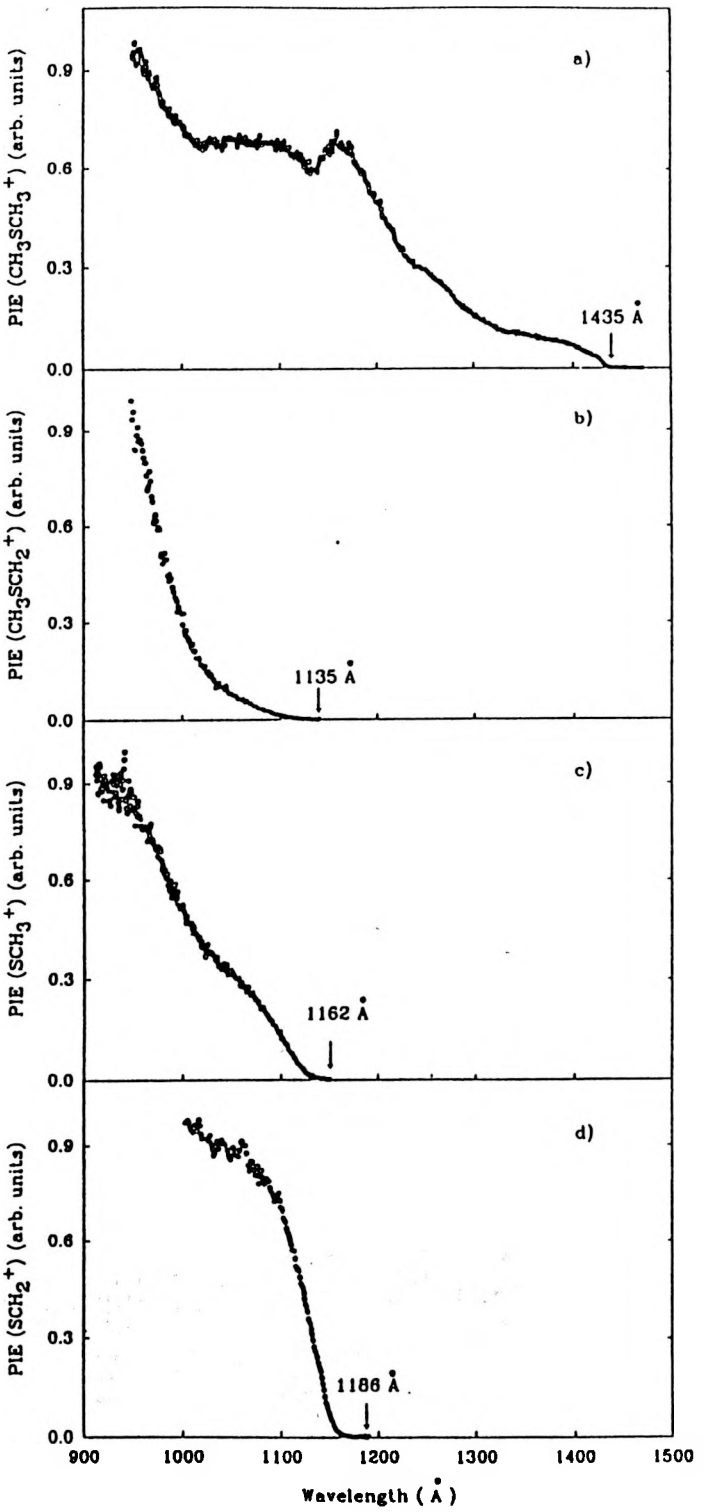
a)
b)
c)
d)
PIE ($CH_3SCH_3^+$) (arb. units)
PIE ($CH_3SCH_2^+$) (arb. units)
PIE (SCH_3^+) (arb. units)
PIE (SCH_2^+) (arb. units)
1435 Å
1135 Å
1162 Å
1186 Å
0.0
0.3
0.6
0.9
900
1000
1100
1200
1300
1400
1500
Wavelength (Å)

Table 1. Ionization and appearance energies for the formation of $CH_3SCH_3^+$, $CH_3SCH_2^+$, SCH_3^+, and SCH_2^+ from CH_3SCH_3, determined from PIE and PEPICO measurements

	IE or AE (eV)	
Ions	PIE	PEPICO
$CH_3SCH_3^+$	8.640 ± 0.012 (1435 ± 2 Å)[a] 8.69 ± 0.01[b]	8.634 ± 0.012 (1436 ± 2 Å)
$CH_3SCH_2^+$	10.924 ± 0.020 (1135 ± 2 Å)[a] 10.93 ± 0.02[b]	10.914 ± 0.020 (1136 ± 2 Å)
SCH_3^+	10.670 ± 0.018 (1162 ± 2 Å)[a] 10.79 ± 0.04[b]	10.670 ± 0.018 (1162 ± 2 Å)
SCH_2^+	10.454 ± 0.018 (1186 ± 2 Å)[a] 10.46 ± 0.08[b]	10.436 ± 0.018 (1188 ± 2 Å)

[a]This work.
[b]Reference 15.

lower than that of the previous measurement.

PEPICO spectra for $CH_3SCH_3^+$, $CH_3SCH_2^+$, CH_3S^+, and CH_2S^+

The PEPICO spectra for $CH_3SCH_3^+$, $CH_3SCH_2^+$, CH_3S^+, and CH_2S^+ in the wavelength region of 900-1450 Å are depicted in Figs. 11(a)-11(d), respectively. The IE of CH_3SCH_3 and the AE's for $CH_3SCH_2^+$, CH_3S^+ (CH_2SH^+), and CH_2S^+ determined from the PIE and PEPICO spectra are in good agreement (see Table 1).

The CH_3SCH_3 molecule has a C_{2v} symmetry. The HeI photoelectron (PE) spectrum of CH_3SCH_3 in the IE region of 8.5-13.7 eV exhibits three peaks at 8.7, 11.3, and 12.7 eV, which are assigned to the removal an electron from the $3b_1$, $8a_1$, and $5b_2$ molecular orbital, respectively.[28] The first electronic band is sharp because the $3b_1$ orbital is essentially a non-bonding 3p orbital of the S atom. The vertical IE's of these three electronic bands are marked by arrows in Fig. 11(a). The low energy peak in the $CH_3SCH_3^+$ PEPICO spectrum is identified as the $CH_3SCH_3^+(3b_1^{-1})$ ground electronic band. The peak at 1160 Å corresponds to the low energy shoulder of the $CH_3SCH_3^+(8a_1^{-1})$ electronic band. In the energy region between the first and second CH_3SCH_3 PE bands, the HeI PE spectrum shows negligible PE intensities. Finite PEPICO $CH_3SCH_3^+$ intensities observed between the first and second PE bands are due to autoionization. The $CH_3SCH_3^+$ PEPICO intensity drops abruptly to the noise level as the $CH_3SCH_2^+$, CH_3S^+ (CH_2SH^+), and CH_2S^+ fragment ions appear.

Figure 11. PEPICO spectra in the region of 900-1450 Å (a) $CH_3SCH_3^+$; (b) $CH_3SCH_2^+$; (c) CH_3S^+; (d) CH_2S^+

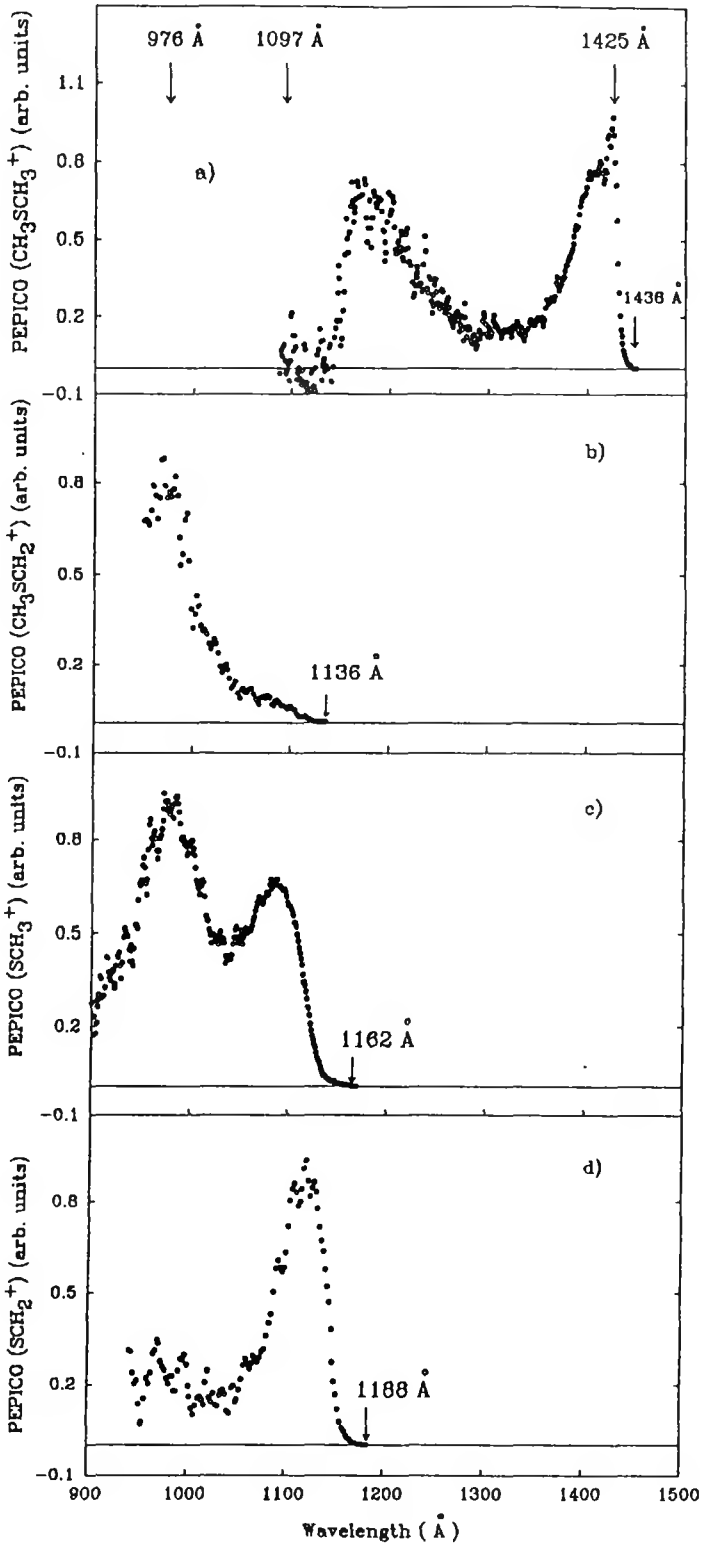
976 Å
1097 Å
1425 Å
1436 Å
a)
b)
1136 Å
c)
1162 Å
d)
1188 Å
PEPICO ($CH_3SCH_3^+$) (arb. units)
PEPICO ($CH_3SCH_2^+$) (arb. units)
PEPICO (SCH_3^+) (arb. units)
PEPICO (SCH_2^+) (arb. units)
1.1
0.8
0.5
0.2
−0.1
900
1000
1100
1200
1300
1400
1500
Wavelength (Å)

Breakdown diagram for the unimolecular decomposition of $CH_3SCH_3^+$

The AE's for processes (5)-(7) are similar. In order to examine the unimolecular decomposition of energy-selected $CH_3SCH_3^+$, we have constructed the breakdown diagram shown in Fig. 12. The shaded areas indicate the uncertainties of the branching ratios introduced by uncertainties of the ion transmissions through the QMF. The internal energy of the parent $CH_3SCH_3^+$ ion corresponding to the ionization photon wavelength is also indicated in the figure. The breakdown diagram clearly reveals the competitive nature of the $CH_3SCH_2^+ + H$, $CH_3S^+ + CH_3$, and $CH_2S^+ + CH_4$ channels. The formation of $CH_2S^+ + CH_4$ from $CH_3SCH_3^+$ necessarily requires H-migration, whereas the production of CH_3S^+ (or CH_2SH^+) + CH_3 and $CH_3SCH_2^+ + H$ involves only simple bond ruptures. Since the dissociation lifetime of $CH_3SCH_3^+$ is expected to decrease as the internal energy of $CH_3SCH_3^+$ is increased, we expect that the yield for CH_2S^+ will decrease with increasing internal energy of $CH_3SCH_3^+$. Contrarily, the yield for a process involving a direct bond rupture increases with increasing internal energy of $CH_3SCH_3^+$. The branching ratios for CH_2S^+, CH_3S^+ (or CH_2SH^+), and $CH_3SCH_2^+$, determined as a function of the $CH_3SCH_3^+$ internal energy, are consistent with the dissociation lifetime consideration. The PEPICO intensity for CH_2S^+ peaks sharply at an internal energy of ~ 52 kcal/mol for $CH_3SCH_3^+$, and becomes negligibly small at $CH_3SCH_3^+$ internal energies greater than 75 kcal/mol. At $CH_3SCH_3^+$ internal energies close to the dissociation thresholds of processes (4)-(7), the relative PEPICO intensities (or branching ratios) for the fragment ions are in the order: $I[PEPICO(CH_2S^+)] > I[PEPICO(CH_3S^+)] > I[PEPICO(CH_3SCH_2^+)]$. This indicates that the yields of the fragment ions are governed by the stabilities of the

Figure 12. Breakdown diagram for the unimolecular decomposition of energy selected $CH_3SCH_3^+$ is shown. Here, I[PEPICO(ion)] is the PEPICO intensity of the ion and Σ = I[PEPICO($CH_3SCH_3^+$ + $CH_3SCH_2^+$ + CH_3S^+ + CH_2S^+)]

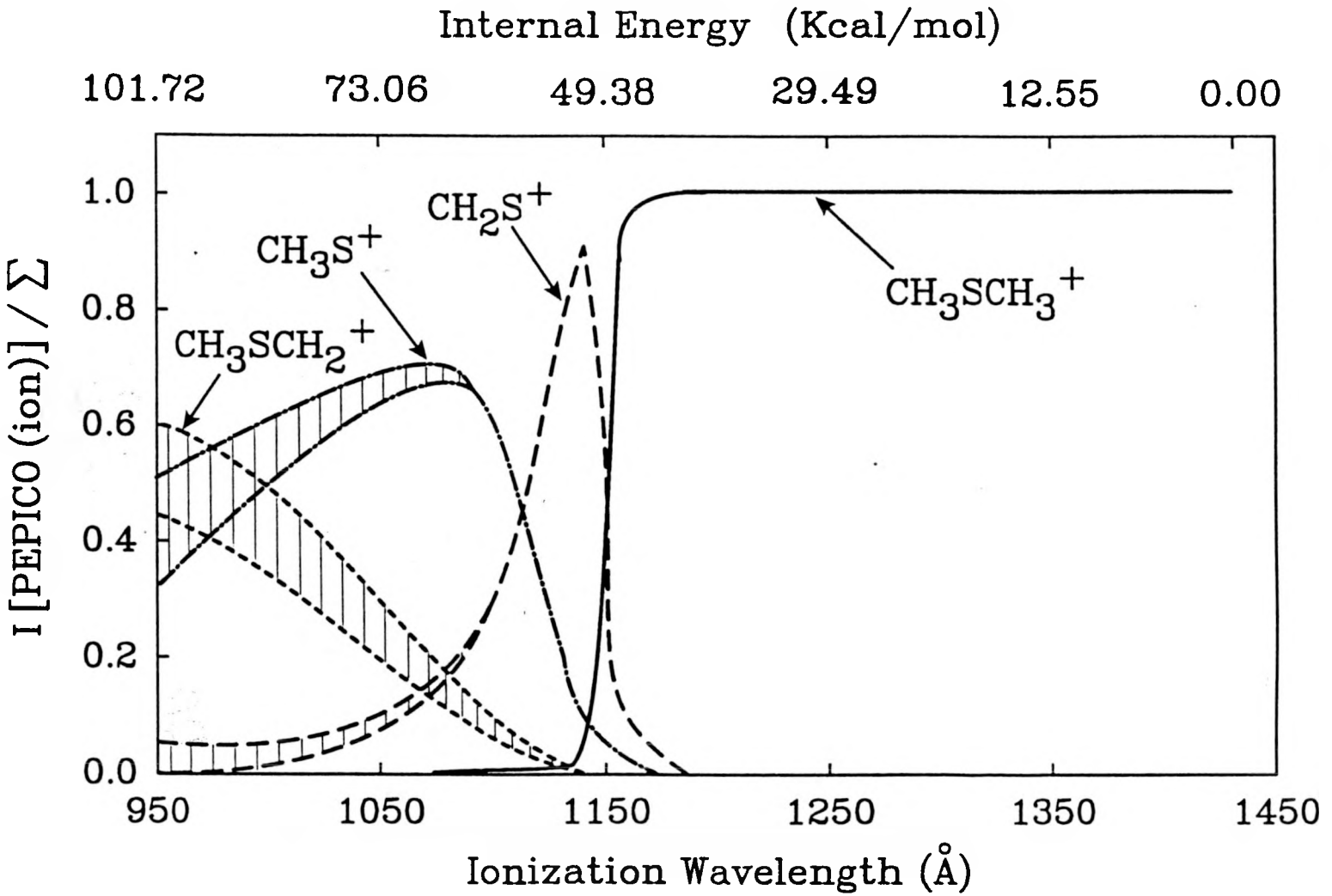
Internal Energy (Kcal/mol)
101.72
73.06
49.38
29.49
12.55
0.00
1.0
0.8
0.6
0.4
0.2
0.0
I [PEPICO (ion)] / Σ
CH2S+
CH3S+
CH3SCH2+
CH3SCH3+
950
1050
1150
1250
1350
1450
Ionization Wavelength (Å)

dissociation channels.

Thermochemistry of CH_3SCH_3 and $CH_3SCH_3^+$ and their Fragments

Heats of formation determined here are summarized and compared to the literature values[22,23,25,29-34] in Table 2. The $\Delta H_{f0}(CH_3S)$ = 35.1 ± 1.5 kcal/mol is consistent with the literature value[22] of $\Delta H_{f298}(CH_3S)$ = 34.2 ± 1.5 kcal/mol. Using the known heats of formation at 0 K for CH_3SCH_3 [$\Delta H_{f0}(CH_3SCH_3)$ = -5.0 kcal/mol][22] and H [$\Delta H_{f0}(H)$ = 51.626 kcal/mol][25], along with the estimated threshold energy (57 ± 2.5 kcal/mol) for process (2), we obtain an estimate of 34 ± 2.5 kcal/mol for $\Delta H_{f0}(CH_3SCH_2)$. The heats of formation calculated for organosulfur ions are based on the IE and AE values obtained from the PEPICO measurements.

A collisional activation experiment and an ab initio calculation suggest that the ΔH_{f0} value for the thiomethoxy ion (CH_3S^+) is ~ 10 kcal/mol above that for the mercaptomethyl ion (CH_2SH^+).[33,34] Assuming that the mass 47 ion observed at its threshold has the CH_2SH^+ structure, we calculate a value of 206.3 kcal/mol for $\Delta H_{f0}(CH_2SH^+)$. The latter value is in agreement with the literature value 207-209 kcal/mol[15,30,31] for $\Delta H_{f0}(CH_2SH^+)$. In a more recent high level ab initio calculation[35] with large polarization basis sets and incorporating electron correlation, the singlet mercaptomethyl ion $CH_2SH^+(^1A')$ is predicted to lie $\gtrsim$ 27 kcal/mol lower in energy than the triplet thiomethoxy ion $CH_3S^+(^3A_1)$. That is, the latter ab initio study predicts that $\Delta H_{f0}(CH_3S^+)$ > 233.3 kcal/mol and IE [CH_3S to $CH_3S^+(^3A_1)$] > 8.62 eV. A value of 8.06 ± 0.1 eV for the IE of CH_3S is

Table 2. Heats of formation for organosulfur molecules and ions involved in the photodissociation and photoionization of CH_3SCH_3

Molecule	ΔH_{f0} (kcal/mol)	D_o (kcal/mol)
CH_3SCH_3	-5.0[a]	$D_o(CH_3S\text{-}CH_3)$ = 74.9 ± 1.5[b] = 74.6 ± 1.5[c] = 74.8 ± 2.0[d] $D_o(H\text{-}CH_2SCH_3)$ = 91 ± 2.5[b]
CH_3SCH_2	34 ± 2.5[b]	
CH_3S	35.1 ± 1.5[b] 35.4 ± 1.5[f] 34.2 ± 1.5[g]	$D_o(H\text{-}CH_2S)$ = 41.6[e]
CH_2S	25.1[h] 24.3[g]	
CH_4	-15.97[a]	
CH_3	34.8 ± 0.3[a]	
H	51.63[a]	
$CH_3SCH_3^+$	194.1[b] 195.4[i]	
$CH_3SCH_2^+$	195.1[b] 195.4[i]	
CH_3S^+	> 233[j]	
CH_2SH^+	206.3[k] 209[i] 208[l] 207[m]	
CH_2S^+	240.5[n] 233[h]	

[a]Reference 25.
[b]This work.
[c]Reference 22.

Table 2. (continued)

[d]Reference 23.

[e]Calculated using known ΔH_{f0} values for CH_3S and CH_2S.

[f]Reference 14. Based on the energy release measurement of the process $CH_3SSCH_3 + h\nu \rightarrow 2CH_3S$.

[g]ΔH_{f298}, Reference 22.

[h]Reference 29.

[i]Reference 15.

[j]The ab initio study of Radom and co-workers (Ref. 35) suggest that $\Delta H_{f0}(CH_3S^+)$ is greater than $\Delta H_{f0}(CH_2SH^+)$ by at least 27 kcal/mol. This lower bound value is obtained by adding 27 kcal/mol to $\Delta H_{f0}(CH_2SH^+)$.

[k]This work. This value is calculated assuming that the mass 46 ion has the protonated thioformaldehyde structure at its AE.

[l]Reference 30.

[m]Reference 31.

[n]Reference 32. This value is calculated based on the IE (9.34 ± 0.01 eV) of CH_2S.

obtained previously[36] using electron impact ionization. It is possible that the mass 47 ions observed in the electron impact ioization of CH_3S near the threshold correspond to $CH_2SH^+(^1A')$. Using the ΔH_{f0} values for CH_3S and CH_2SH^+, we estimate the IE of CH_3S to CH_2SH^+ to be 7.5 eV.

Based on the known ΔH_{f0} values of CH_3SCH_3, CH_4, and CH_2S^+, the thermochemical threshold for process (7) is predicted to be 9.99 eV. The difference between this predicted thermochemical threshold and the measured AE (10.436 eV) may be due to the kinetic shift effect. The difference may also be interpreted as an upper limit for the H-rearrangement potential barrier to yield $CH_2S^+ + CH_4$ from $CH_3SCH_3^+$.

SUMMARY

We have performed photoionization and 193 nm laser photodissociation studies of CH_3SCH_3. The TOF spectra obtained for SCH_3, CH_3, H, and S give a direct measure of the energetics and the energy disposals for processes (1)-(3). The PEPICO measurements allow the construction of a detailed breakdown diagram for the formation of $CH_3SCH_2^+$, CH_3S^+, and CH_2S^+ by the unimolecular decomposition of energy-selected $CH_3SCH_3^+$ in the internal energy range of 0-102 kcal/mol. The energetic information obtained in the photoionization and photodissociation experiments makes the estimate of the IE for CH_3S possible.

REFERENCES

1. T. E. Graedel, Rev. Geophys. and Space Phys. 15, 421 (1977) and references therein.

2. W. E. Burnett, Environ. Sci. Technol. 8, 744 (1969).

3. M. D. Bentley, I. B. Douglass, J. A. Lacadie, and D. R. Whittier, J. Air Pollution Control Association, 22, 359 (1972).

4. J. G. Calvert and J. N. Pitts, Jr., "Photochemistry" (Wiley, New York, 1966).

5. S. D. Thompson, D. G. Carroll, F. Watson, M. O'Donnell, and S. P. McGlynn, J. Chem. Phys. 45, 1367 (1966).

6. L. B. Clark and W. T. Simpson, J. Chem. Phys. 43, 3666 (1965).

7. J. H. Lee, R. B. Timmons, and L. J. Stief, J. Chem. Phys. 64, 300 (1976).

8. C. F. Cullis and L. C. Roselaar, Trans. Faraday Soc. 55, 272, 1554, 1562 (1959).

9. H. B. Rayner and F. E. Murray, Pulp Pap. Mag. Can. 71, 75 (1970).

10. A. B. Callear and D. R. Dickon, Trans. Faraday Soc. 66, 1907 (1970).

11. P. M. Rao, J. A. Copeck, and A. R. Knight, Can. J. Chem. 45, 1369 (1967).

12. K. Sayamol and A. R. Knight, Can. J. Chem. 46, 999 (1969).

13. P. M. Rao and A. R. Knight, Can. J. Chem. 46, 2462 (1968).

14. S. Nourbakhsh, C.-L. Liao, and C. Y. Ng, J. Chem. Phys. 92, 6589 (1990).

15. M. E. Akopyan, Yu. L. Sergeev, and F. I. Vilesov, Khimiya Vysokikh Energil, 4, 305 (1970).

16. K. Norwood, J.-H. Guo, G. Luo, and C. Y. Ng, J. Chem. Phys. 90, 6026 (1989).

17. C. Y. Ng, Adv. Chem. Phys. 52, 265 (1983).

18. W.-B. Tzeng, H.-M. Yin, W.-Y. Leung, J.-Y. Luo, S. Nourbakhsh, G. D. Flesch, and C. Y. Ng, J. Chem. Phys. 88, 1658 (1988).

19. K. Norwood, J.-H, Guo, G. Luo, and C. Y. Ng, Chem. Phys. 129, 109 (1989).

20. K. Norwood, J.-H. Guo, and C. Y. Ng, J. Chem. Phys. 90, 2995 (1989).

21. K. Norwood and C. Y. Ng, Chem. Phys. Lett. 156, 145 (1989).

22. S. W. Benson, Chem. Rev. 78, 23 (1978).

23. D. F. McMillen and D. M. Golden, Ann. Rev. Phys. Chem. 33, 493 (1982).

24. S. W. Benson, J. Chem. Ed. 42, 502 (1965).

25. H. M. Rosenstock, K. Draxl, B. W. Steiner, J. T. Herron, J. Phys. Chem. Ref. Data Suppl. 6, 1977.

26. H. Okabe, "Photochemistry of Small Molecules" (Wiley, New York, 1978).

27. C.-W. Hsu, C.-L. Liao, and P. Tjossom, and C. Y. Ng, to be published.

28. K. Kimura, S. Katsumata, Y. Achiba, T. Yamazaki, and S. Iwata, "Handbook of HeI Photoelectron Spectra of Fundamental Organic Molecules" (Halsted Press, New York, 1981).

29. J. J. Butler and T. Baer, Org. Mass Spectrom. 18, 248 (1983).

30. J. J. Butler, T. Baer, and S. A. Evans, Jr., J. Am. Chem. Soc. 105, 3451 (1983).

31. M. Roy and T. B. McMahon, Org. Mass Spectrom. 17, 392 (1982).

32. H. W. Kroto and R. J. Suffolk, Chem. Phys. Lett. 15, 545 (1972).

33. J. D. Dill and F. W. McLafferty, J. Am. Chem. Soc. 101, 6526 (1979).

34. J. D. Dill and F. W. McLafferty, J. Am. Chem. Soc. 100, 2907 (1978).

35. R. H. Nobes, W. J. Bouma, and L. Radom, J. Am. Chem. Soc. 106, 2774 (1984).

36. T. F. Palmer and F. P. Lossing, J. Am. Chem. Soc. 84, 4661 (1962).

SECTION IV.

VACUUM ULTRAVIOLET PHOTODISSOCIATION AND PHOTOIONIZATION STUDIES OF CH_3SH AND SH

ABSTRACT

The kinetic energy releases of the photodissociation processes, $CH_3SH + h\nu$ (193 nm) $\rightarrow CH_3 + SH$, $CH_3S + H$, and $CH_2S + H_2$, have been measured using the time-of-flight mass spectrometric method. These measurements allow the direct determination of the dissociation energies for the CH_3-SH and CH_3S-H bonds at 0 K as 72.4 ± 1.5 and 90 ± 2 kcal/mol, respectively. The further dissociation of SH according to the process $SH + h\nu$ (193 nm) $\rightarrow S + H$ has also been observed. The appearance energy (AE) of S produced in the latter process is consistent with the formation of $S(^3P) + H$. The photoelectron-photoion coincidence (PEPICO) spectra for CH_3SH^+, CH_3S^+ (or CH_2SH^+), and CH_2S^+ from CH_3SH have been measured in the wavelength range of 925-1460 Å. The PEPICO measurements make possible the construction of the breakdown diagram for the unimolecular decomposition of internal-energy-selected CH_3SH^+ in the range of 0-83 kcal/mol. The AE measured for CH_2S^+ is consistent with the conclusion that the activation energy is negligible for 1,2-H_2 elimination from CH_3SH^+.

INTRODUCTION

Methyl mercaptan (CH_3SH) is among the major organosulfur pollutants emitted to the atmosphere in the industrial combustion of oil and coals.[1] The absorption spectrum of CH_3SH exhibits a strong band at 180-250 nm.[2] The primary decomposition processes[3-7] of CH_3SH induced by the absorption of ultraviolet radiation in this wavelength range are suggested to be:

$$CH_3SH + h\nu \rightarrow CH_3S + H, \quad (1)$$

$$CH_3SH + h\nu \rightarrow CH_3 + SH. \quad (2)$$

The process,

$$CH_3SH + h\nu \rightarrow CH_2S + H_2, \quad (3)$$

is also proposed as a primary dissociation step in 185 nm photolysis.[8] The previous investigations are mostly kinetic in nature and have been made by monitoring the disappearance of the mercaptan and the appearance of stable products. Since the radicals formed in processes (1)-(2) are reaction intermediates of atmospheric sulfur cycles, the studies of the energetics and dynamics of the ultraviolet photodissociation of CH_3SH are relevant to combustion and atmospheric chemistry.

As the simplest mercaptan, CH_3SH has been subjected to detailed ab initio calculations.[9-12] These calculations, which are aimed at understanding the unimolecular decomposition of CH_3SH, have partly motivated the 193 nm photofragmentation time-of-flight (TOF) mass spectrometric study presented here.

The unimolecular decomposition of CH_3SH^+ has also been the topic of several experimental[12-15] and theoretical[16-22] investigations. An interesting question is whether the mass 47 fragment ion from CH_3SH^+ appearing at the threshold corresponds to the thiomethoxy ion (CH_3S^+) structure or the mercaptomethyl ion (CH_2SH^+) structure. Collisional activation studies[15,16] and ab initio molecular orbital calculations[16-22] favor the mercaptomethyl ion as the more stable species.

In order to examine the consistency of the thermochemistry of the CH_3SH/CH_3SH^+ system and to compare the energetics and dynamics of CH_3SH^+ and CH_3SH dissociation, we have also measured the photoionization efficiency (PIE) and photoelectron-photoion coincidence (PEPICO) spectra for CH_3SH^+, CH_3S^+ (or CH_2SH^+), and CH_2S^+ from CH_3SH:

$$CH_3SH + h\nu \rightarrow CH_3SH^+ + e^-, \quad (4)$$

$$CH_3SH + h\nu \rightarrow CH_3S^+ \text{ (or } CH_2SH^+) + H + e^-, \quad (5)$$

$$CH_3SH + h\nu \rightarrow CH_2S^+ + H_2 + e^-. \quad (6)$$

Two gas cell PIE measurements on CH_3SH have been reported previously.[14,15] The breakdown diagram for the unimolecular decomposition of CH_3SH^+ has been estimated from charge transfer experiments[16] and from the normalized derivative curves of PIE spectra of fragment ions.[15] The PEPICO data obtained in this experiment allow a precise characterization of the branching ratios for the formation of CH_3SH^+, CH_3S^+ (or CH_2SH^+), and CH_2S^+ in the unimolecular decomposition of internal-energy-selected CH_3SH^+ in the range of 0-83 kcal/mol.

EXPERIMENTAL

Measurements of TOF Spectra for H, S, SH, CH_3, and CH_2S from the Photodissociation of CH_3SH

The rotatable beam source laser photofragmentation apparatus used in this study has been described in detail previously.[23-25] The apparatus consists of three main components: an ArF excimer laser, a photodissociation chamber in which a rotatable supersonic molecular beam intersects with the laser beam, and a linearly movable ultrahigh vacuum electron ionization quadrupole mass spectrometer (QMS).

In this experiment, a pulsed beam of CH_3SH seeded in He is produced by supersonic expansion through a pulsed valve at ~ 298 K and a total pressure of ~ 1150 Torr. The pulsed valve has a nozzle diameter of 0.5 mm and is operated at 40 Hz. The ratio of the pressure of CH_3SH to that of He is about 0.15. The seeded CH_3SH beam has an angular divergence of ~ 3° which is defined by the opening of the conical skimmer and by the circular aperture between the differential pumping chamber and the photodissociation chamber. The 3° angular spread of the beam corresponds to a beam width of 3 mm in the photodissociation region. All TOF spectra are taken at a flight path of 73.7 cm which is the distance between the photodissociation region and the electron impact ionizer.

The energy of the excimer laser [Questek (Model 2460)] is varied in the range of 90-120 mJ. The laser beam enters the photodissociation chamber through a MgF2 focusing lens and intersects the seeded CH_3SH beam at 90°.

The data acquisition and operation of the apparatus are controlled by an LSI-11/23 mini-computer. The TOF spectrum is recorded on a homemade multichannel scaler (MCS). The firing of the excimer laser is delayed by approximately 450 μs with respect to the triggering pulse for the opening of the pulsed valve. The MCS is started by a second trigger pulse signifying the firing of the laser. The delay timings are controlled by a digital delay unit (SRS, Model DG 535). The laboratory angle (θ) is defined to be the angle between the seeded CH_3SH molecular beam and the detector axis. The laboratory velocity for the parent CH_3SH beam (v_p) is determined by measuring the TOF of the CH_3SH beam pulse at $\theta = 0°$ at two known nozzle-ionizer distances. An aperture of 0.075 mm is used between the photodissociation and detector chambers during the measurement of v_p. The value for v_p is determined before and after the laser photodissociation experiment and the deviation of the two measurements is usually less than 2%. Under the beam expansion conditions used in this experiment, the ratio $\Delta v/v_p$ is estimated to be less than 0.08, where Δv represents the velocity spread [full width at half maximum (FWHM)] of the CH_3SH beam.

The analysis of the TOF data involves the transformation of the laboratory TOF spectra into center-of-mass (c.m.) translational energy (Ec.m.) distributions and has been described in detail.[23-25] We have ignored the effect of the apparatus resolution factors in the transformation.

Measurements of PIE and PEPICO Spectra for CH_2S^+, CH_3S^+, and CH_3SH^+ from CH_3SH

The experimental arrangement of the molecular beam PEPICO apparatus used in these measurements has been reported in detail in previous publications.[26-28] Briefly, the apparatus consists of a 3 m near normal incidence vacuum ultraviolet (VUV) monochromator, a capillary discharge lamp, a tungsten photoelectric VUV light detector, a molecular beam source, a QMS for ion detection, and an electron energy analyzer optimized for threshold photoelectron (TPE) detection.

The grating employed in this study is a Bausch and Lomb 1200 lines/mm Os coated aluminum grating blazed at 1360 Å. The hydrogen many-lined pseudocontinuum is used as the light source.

The CH_3SH gaseous sample is introduced to the photoionization region as a continuous beam of pure CH_3SH produced by supersonic expansion through a stainless steel nozzle with a diameter of 125 μm at a stagnation pressure of ~ 300 Torr. The molecular beam is collimated by a conical skimmer before entering the photoionization chamber. During the experiment, the photoionization chamber is maintained at $\leq 2 \times 10^{-5}$ Torr.

A differential pulsed PEPICO scheme[27] is used for coincidence measurements. The coincidence detection cycle is initiated by an electronic pulse signifying the arrival of a TPE at the electron detector. The electronic pulse triggers two identical extraction pulses (width = 80 ns and height = 120 V) to extract photoions toward the ion detector. The

QMS is used to select the ion of interest for detection. The first and second extraction pulses are delayed by 0 and 40 μs, respectively, with respect to the triggering electronic pulse. The electron flight time from the photoionization region to the electron detector is $\lesssim$ 0.1 μs. In such a short time, the correlated photoion is expected to remain in the photoionization region. Thus, the first extraction pulse serves to extract the correlated photoion as well as background ions, while the second extraction pulse draws out only background ions. The photoionization region is maintained nearly field free, except during the application of the ion extraction pulse. A potential barrier between the photoionization region and the entrance of the QMS ensures that no ions are transmitted to the ion detector without the application of the extraction pulse. The ions arriving at the ion detector are recorded using an MCS. The difference of the ion intensities detected due to the first and second extraction pulses represents the true coincidence signal. The coincidence cycle is completed in a period of 100 μs. The first electronic pulse generated by the electron detector after this period initiates a new coincidence cycle.

All data are obtained with an optical resolution of 1.4 Å (FWHM). The wavelength interval used varies in the range of 0.5-2 Å. The counting time at each data point used for PEPICO measurements is 25 s.

RESULTS AND DISCUSSION

193 nm Photodissociation of CH_3SH

TOF spectra for CH_3 and SH

The TOF spectra for SH and CH_3 at $\theta = 35°$ and CH_3 at $\theta = 45°$ are depicted in Figs. 1(a), 1(b), and 1(c), respectively. The SH and CH_3 TOF peaks shown in these figures are due to process (2).

Based on the conservation of energy,

$$h\nu\ (193\ nm) + E_{int}^{*} = D_o(CH_3\text{-}SH) + E_e + E_v + E_r + E_{c.m.}, \qquad (7)$$

where $h\nu$ is dissociation photon energy (147.9 kcal/mol); E_{int}^{*} is the initial internal energy of the parent CH_3SH molecule, which is assumed to be negligible as a result of supersonic cooling; $D_o(CH_3\text{-}SH)$ is the dissociation energy of the CH_3-SH bond at 0 K; and E_e, E_v, and E_r are the electronic, vibrational, and rotational energies of the photofragments. A value of 75 ± 1.5 kcal/mol is given by Benson[1] for the dissociation energy of the CH_3-SH bond at 298 K [$DH°(CH_3\text{-}SH)$], while a value of 74 ± 1.5 kcal/mol is recommended by McMillen and Golden.[29] Using the latter value and Eq. (7), we have constructed the Newton diagram (Fig. 2) for the formation of SH at $\theta = 35°$ via process (2). Here $v_{c.m.}(SH)$ and $v_l(SH)$ represent the maximum c.m. and laboratory velocities for SH. The velocity circle corresponding to CH_3 is not shown in the figure.

Figure 1. TOF spectra for (a) SH at $\theta = 35°$, (b) CH_3 at $\theta = 35°$, and (c) CH_3 at $\theta = 45°$

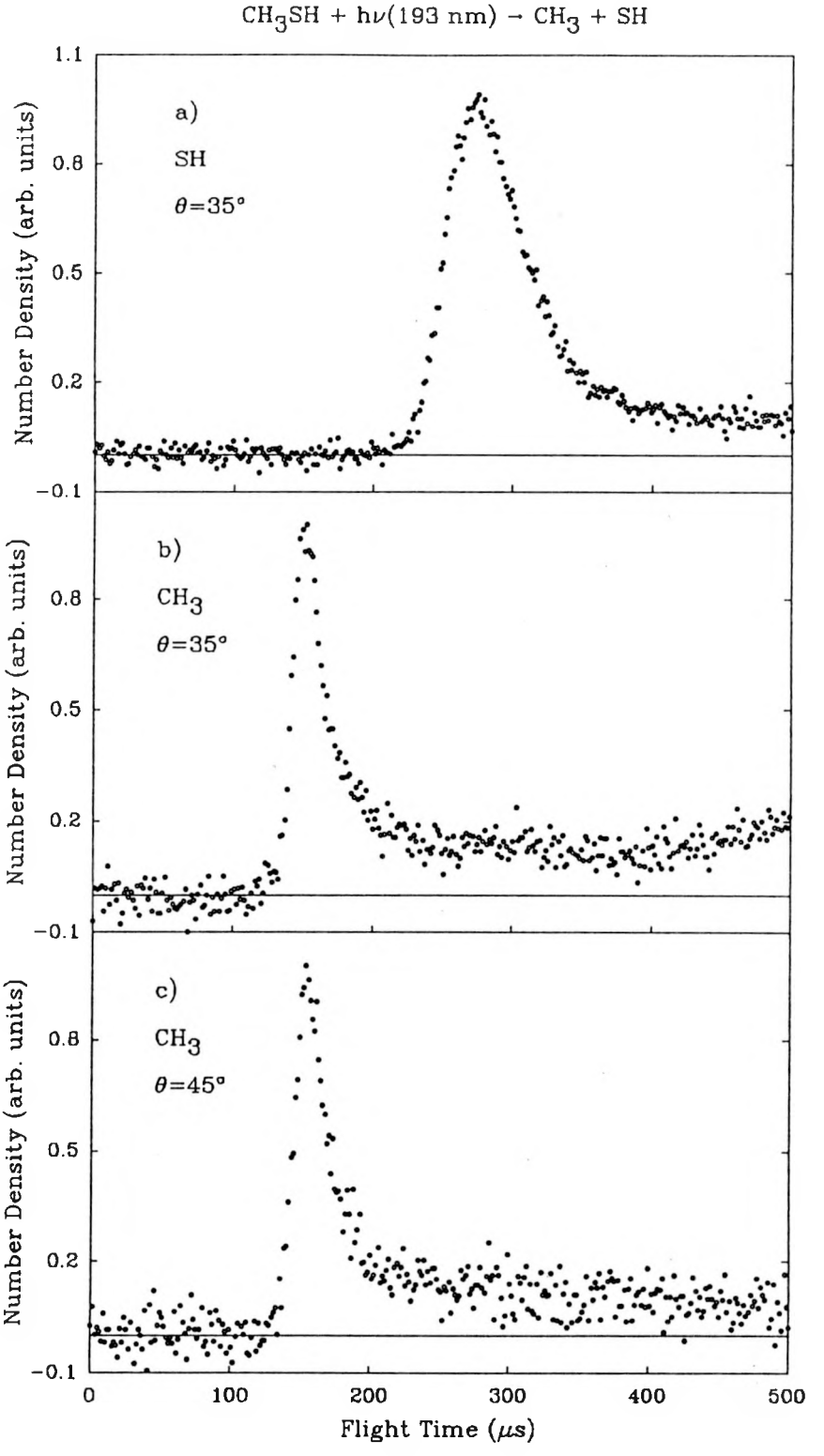
CH3SH + hν(193 nm) → CH3 + SH
a)
SH
θ=35°
b)
CH3
θ=35°
c)
CH3
θ=45°
Number Density (arb. units)
Flight Time (μs)
1.1
0.8
0.5
0.2
−0.1
0
100
200
300
400
500

Figure 2. Newton diagram is shown for the formation of CH_3 + SH and CH_2S + H_2 by the 193 photodissociation of CH_3SH and the sequential formation of S + H by processes (2) and (8) at $\theta = 35°$. Here, v_p is the laboratory velocity for CH_3SH; $v_{c.m.}(SH)$ and $v_l(SH)$ are the maximum c.m. and laboratory velocities for SH, respectively; and $v_{c.m.}[S(^3P)]$, $v_{c.m.}[S(^1D)]$, and $v_{c.m.}[S(^1S)]$ are the maximum c.m. velocities for $S(^3P)$, $S(^1D)$, and $S(^1S)$ formed by process (8).

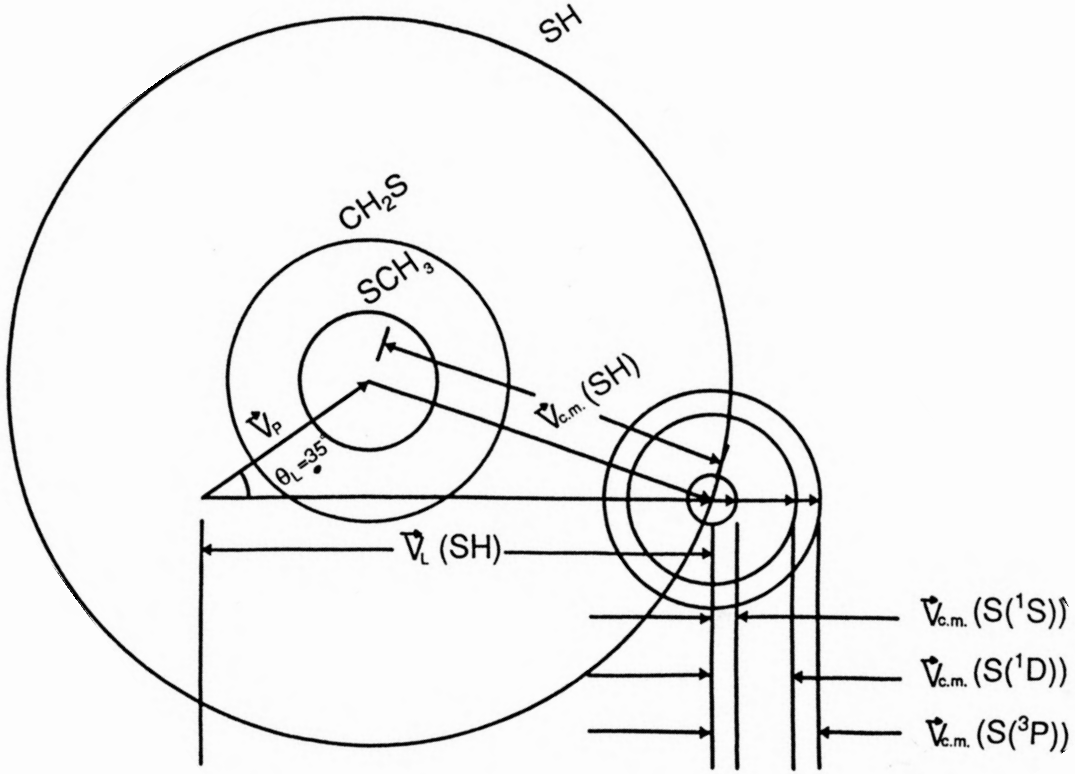
SH
CH2S
SCH3
V⃗p
θL=35°
V⃗c.m.(SH)
V⃗L(SH)
V⃗c.m.(S(1S))
V⃗c.m.(S(1D))
V⃗c.m.(S(3P))

The $E_{c.m.}$ distributions for photofragments of process (2) derived from the TOF spectra for CH_3 at $\theta = 35°$ and 45° are shown in Figs. 3(a) and 3(b), respectively. The threshold energy for the formation of CH_3 is determined to be 75.5 ± 1.5 kcal/mol, yielding a value of 72.4 ± 1.5 kcal/mol for $D_o(CH_3\text{-}SH)$. Assuming that the vibrational and electronic degrees of freedom are not populated at 298 K for CH_3SH, CH_3, and SH, the conversion of $D_o(CH_3\text{-}SH)$ to $DH°(CH_3\text{-}SH)$ requires the addition of 2.1 kcal/mol to $D_o(CH_3\text{-}SH)$.[30] This yields a value of 74.5 ± 1.5 kcal/mol for $DH°(CH_3\text{-}SH)$, in excellent agreement with the literature values.[1,29] The $E_{c.m.}$ distribution peaks at ~ 50 kcal/mol, which corresponds to a value of 24 kcal/mol for the internal excitations of CH_3 and SH. This internal excitation is considerably less than those for photofragments resulting from the $CH_3\text{-}SSCH_3$ and $CH_3\text{-}SCH_3$ bond scissions[24,25] induced by the absorption of a 193 nm photon.

In the 193 nm photodissociation of H_2S to yield H + HS, more than 95% of the available energy is found to appear as $E_{c.m.}$.[31-33] The lack of vibrational excitation is consistent with the observation that the S-H bond distances in H_2S and HS are similar.[31] Since the c.m. of the SH fragment is so close to the S atom, the departing H atom cannot exert appreciable torque on SH, resulting in low rotational excitation for the SH fragment. This expectation has been confirmed by the experiment of Hawkins and Houston.[34] Methyl mercaptan may be viewed as a pseudotriatomic molecule derived from H_2S by substituting a methyl group for an H atom in H_2S. Therefore, the observation that more than 70% of the available energy appears as $E_{c.m.}$ in the 193 nm photodissociation of CH_3SH to CH_3 + SH is in accord with the arguments used in rationalizing the energy distribution of photofragments formed in the 193 nm photolysis of H_2S.

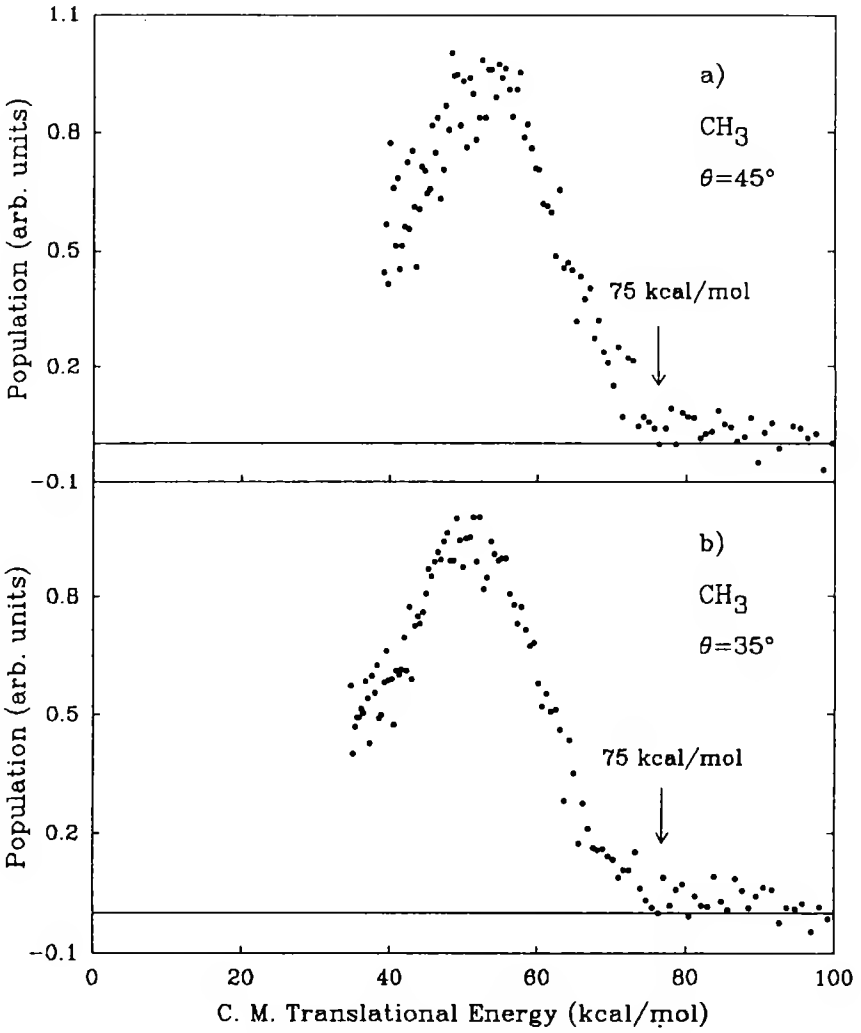

Figure 3. Translational energy distributions for the fragments of process (2) derived from the TOF spectra for CH_3 at (a) $\theta = 45°$ and (b) $\theta = 35°$

TOF spectrum for H

A recent ab initio theoretical study[11] concludes that photochemical fragmentation of the S-H bond is strongly favored over that of the C-H bond. Nevertheless, the formation of H via homolytic cleavage of the C-H bond in CH_3SH cannot be excluded.[18]

Assuming that H atoms are formed by process (1), we have transformed the TOF spectrum of H into the $E_{c.m.}$ distribution as depicted in Fig. 4. The $E_{c.m.}$ distribution exhibits a sharp rise at $E_{c.m.}$ = 58 ± 2 kcal/mol and has a peak at $E_{c.m.}$ ~ 40 kcal/mol. If this rise is taken as the threshold energy for process (1), we arrive at a value of 90 ± 2 kcal/mol for $D_o(CH_3S\text{-}H)$. The latter value corresponds to a value of 91.5 ± 2 kcal/mol for $DH°(CH_3S\text{-}H)$,[30] in excellent agreement with the literature values.[1,29]

A tail in the region of 60-100 kcal/mol is observed in the $E_{c.m.}$ distribution in Fig. 4. This tail is attributed partly to the further dissociation of SH formed in process (2) according to the process,

$$SH + h\nu \rightarrow S(^3P, {}^1D, {}^1S) + H. \qquad (8)$$

The literature value[1] for $DH°(S\text{-}H)$ is 83.6 ± 1 kcal/mol. The formation of S from SH is confirmed by the TOF spectrum for S.

As shown in the Newton diagram (Fig. 2), the photofragment CH_3S resulting from process (1) cannot be observed at $\theta > 21°$ due to energy constraint. Attempts to measure the TOF spectrum for SCH_3 at small angles ($\theta < 21°$) are hindered by the background due to fragmentation of CH_3SH clusters.

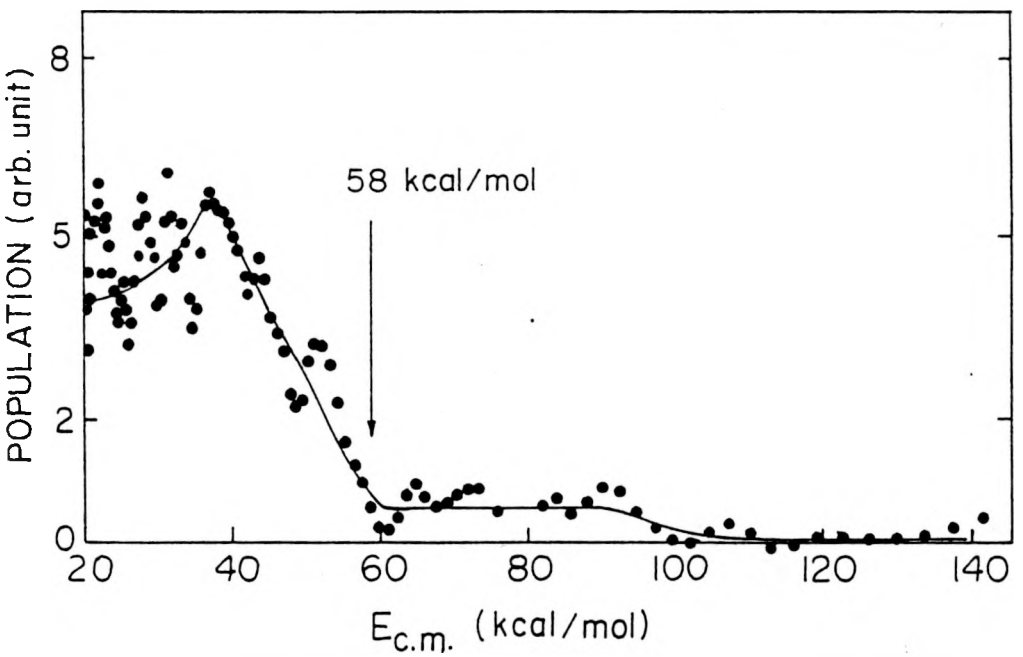

Figure 4. Translational energy distribution for the fragments of process (1) derived from the TOF spectrum for H measured at $\theta = 90°$

TOF spectrum for CH_2S

Process (3) has been investigated in a recent theoretical study[10] which suggests a high activation energy for the 1,2-H_2 elimination dissociation pathway from CH_3SH. The formation of CH_2S is predicted to require at least 20 kcal/mol more than that needed to break the CH_3-SH bond.

The maximum $v_{c.m.}(CH_2S)$ circle associated with process (3) is shown in Fig. 2. At $\theta = 35°$ only the photofragments with $E_{c.m.} \geq 80$ kcal/mol can be probed by the TOF measurement of CH_2S. The overwhelming background due to fragmentation of CH_3SH clusters prevents the measurement of the TOF spectrum for CH_2S at small angles ($\theta < 30°$). The background arising from cluster fragmentation decreases rapidly with increasing θ, but finite contribution from cluster fragmentation to the TOF spectrum for CH_2S can still be identified at $\theta = 35°$. The $E_{c.m.}$ distribution based on the TOF spectrum of CH_2S obtained at $\theta = 35°$ is shown in Fig. 5. The rapid rise at $E_{c.m.}$ below ~ 90 kcal/mol is due to the contribution of cluster fragmentation to the TOF spectrum for CH_2S. The $E_{c.m.}$ distribution has an onset at ~ 122 kcal/mol, a value in accord with the thermochemical threshold of 120 kcal/mol for process (3). The latter value is calculated using the known values[1,35] of -2.9 and 25.1 kcal/mol for $\Delta H_{f0}(CH_3SH)$ and $\Delta H_{f0}(CH_2S)$, respectively. The good agreement between the predicted and observed thresholds for CH_2S is direct evidence for the photochemically driven 1,2-H_2 elimination process (3).

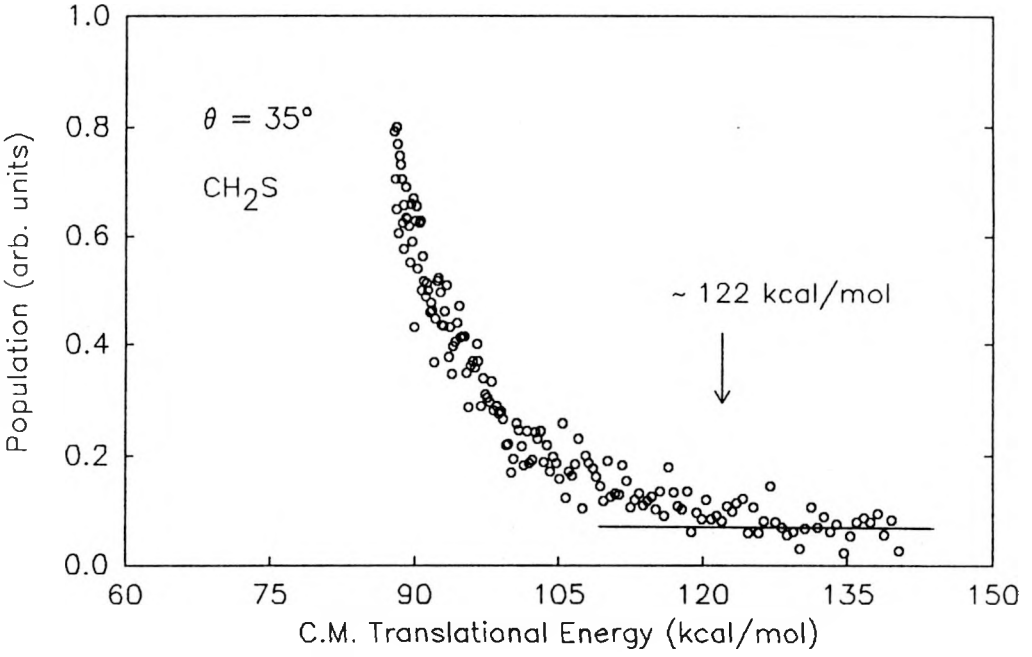

Figure 5. Translational energy distribution for the fragments of process (3) derived from the TOF spectrum of CH_2S measured at $\theta = 35°$

TOF spectrum for S

Figures 6(a) and 6(b) compare the TOF spectra of S and SH. The main TOF peak for S clearly can be attributed to fragmentation of SH. The S signal in the temporal range < 225 μs is due to process (8). The excited metastable $S(^1D)$ and $S(^1S)$ states are 26.4 and 63.4 kcal/mol higher, respectively, than the $S(^3P)$ ground states.[36] Energetically, S formed by process (8) can be in the $S(^3P, ^1D, ^1S)$ states. The Newton diagram for the sequential formation of $S(^3P, ^1D, ^1S)$ according to processes (2) and (8) is also shown in Fig. 2. The maximum laboratory velocities for $S(^3P, ^1D, ^1S)$ observed at $\theta = 35°$ are $v_l[S(^3P)] = v_l(SH) + v_{c.m.}[S(^3P)]$, $v_l[S(^1D)] = v_l(SH) + v_{c.m.}[S(^1D)]$, and $v_l[S(^1S)] = v_l(SH) + v_{c.m.}[S(^1S)]$. A simple calculation gives values of 202, 209, and 230 μs for $v_l[S(^3P)]$, $v_l[S(^1D)]$, and $v_l[S(^1S)]$, respectively. These values are marked in a magnified view of the TOF spectrum for S near the threshold [Fig. 6(c)]. The majority of the SH radicals formed by process (2) are internally excited. Due to kinematic constraint, the laboratory velocities for $S(^3P)$, $S(^1D)$, and $S(^1S)$ arising from the dissociation of internally excited SH radicals are less than $v_l[S(^3P)]$, $v_l[S(^1D)]$, and $v_l[S(^1S)]$. As shown in Fig. 6(c), the experimental threshold for S is in agreement with the thermochemical threshold for the formation of $S(^3P)$, suggesting that the $S(^3P)$ + H is a product channel in the 193 nm photodissociation of $SH(X^2\Pi)$.

Figure 6. (a) TOF spectrum for S measured at $\theta = 35°$; (b) TOF spectrum for SH measured at $\theta = 35°$; (c) a magnified view of the TOF spectrum for S near the threshold region

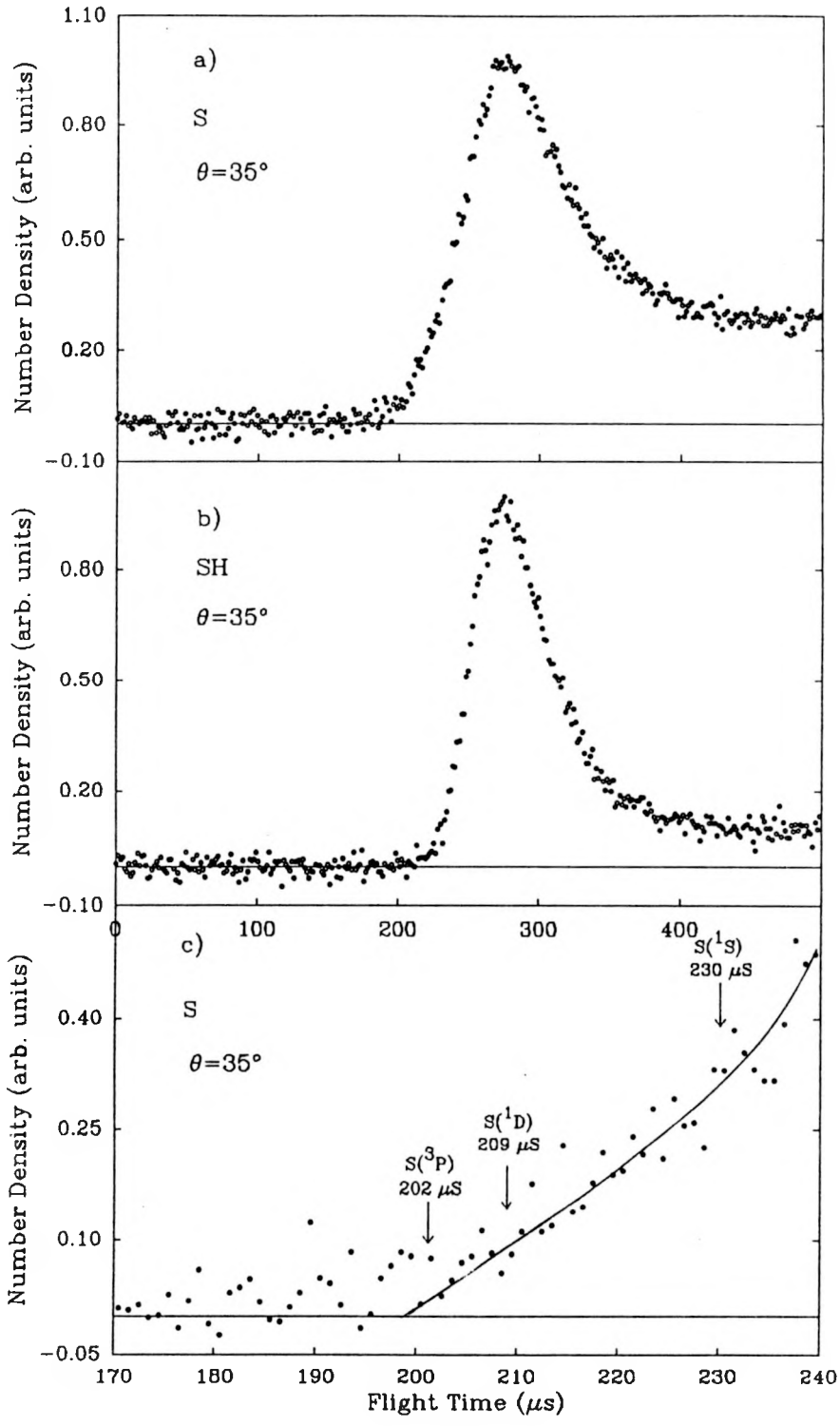
a)
S
θ=35°
b)
SH
θ=35°
c)
S
θ=35°
S(1S)
230 μS
S(1D)
209 μS
S(3P)
202 μS
Number Density (arb. units)
Flight Time (μs)

Photoionization of CH_3SH

PIE spectra for CH_3SH^+, CH_3S^+ (or CH_2SH^+), and CH_2S^+ from CH_3SH

The photoionization mass spectrum for CH_3SH measured at 950 Å is shown in Fig. 7. The major photoions observed are CH_3SH^+ and CH_3S^+ (or CH_2SH^+). The intensity for CH_2S^+ is $\leq 3\%$ that for CH_3S^+ (or CH_2SH^+).

Figures 8(a)-8(c) show the PIE spectra for CH_3SH^+, CH_3S^+, and CH_2S^+ in the region of 925-1360 Å. The general profiles of these spectra are in good accord with previous measurements.[12,13] The IE for CH_3SH and the AE's for CH_3S^+ (or CH_2SH^+) and CH_2S^+ obtained here are compared to previous measurements in Table 1. The IE of CH_3SH and the AE for CH_2S^+ determined in Refs. 12 and 13 are in reasonable agreement. The value of 11.611 ± 0.005 eV for the AE for CH_3S^+ (or CH_2SH^+) obtained by Kutina et al.[13] is 0.24 eV greater than that reported earlier by Akopyan, Serhiev, and Vilesov.[12] The PIE for CH_3S^+ (or CH_2SH^+) increases abruptly at ~ 1070 Å. A magnified view of the PIE spectrum for CH_3S^+ (or CH_2SH^+) near the threshold region reveals a long tail extending to 1125 Å. The value of 11.611 eV (1068 Å) for the AE of CH_3S^+ (or CH_2SH^+) assigned by Kutina et al.[13] is based on the assumption that the weak tail is due to the vibrational and rotational hot band effect. We note that a rapid rise in PIE for CH_2S^+ at ~ 1070 Å is also found in Fig. 8(c). Since the second photo-electronic band for CH_3SH^+ appears at ~ 11.5 eV,[37,38] we believe that the sharp increases in PIEs for CH_3S^+ (or CH_2SH^+) and CH_2S^+ are most likely due to the onset of the second photo-electronic band of CH_3SH^+. The rapid

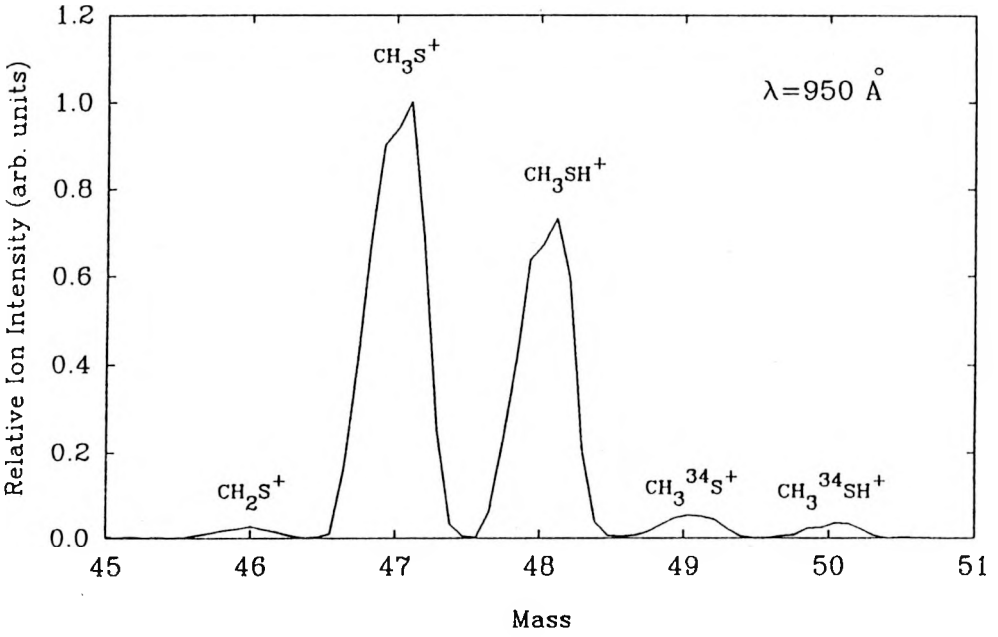

Figure 7. Photoionization mass spectrum for CH_3SH measured at photoionization wavelength of 950 Å

Figure 8. PIE spectra in the region of 925-1360 Å (a) CH_3SH^+; (b) CH_3S^+ (or CH_2SH^+); (c) CH_2S^+

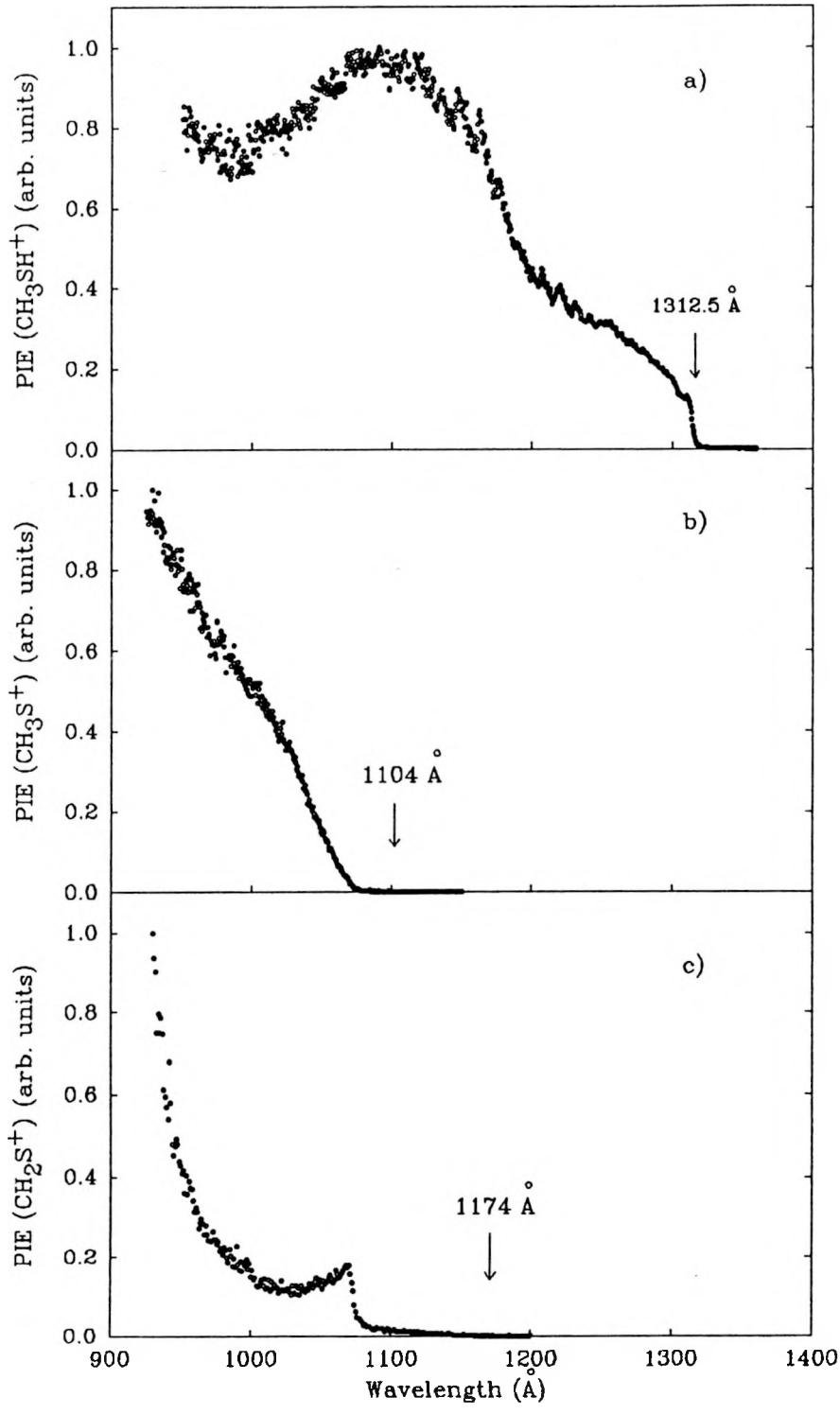
a)
b)
c)
1312.5 Å
1104 Å
1174 Å
PIE (CH_3SH^+) (arb. units)
PIE (CH_3S^+) (arb. units)
PIE (CH_2S^+) (arb. units)
0.0
0.2
0.4
0.6
0.8
1.0
900
1000
1100
1200
1300
1400
Wavelength (Å)

Table 1. IE and AE's determined from photodissociation measurements

Process	AE or IE[a]
$CH_3SH + h\nu(193\ nm) \rightarrow CH_3S + H$	2.52 ± 0.09 eV (58 ± 2 kcal/mol)
$CH_3SH + h\nu(193\ nm) \rightarrow CH_2S + H_2$	5.33 ± 0.13 eV (122 ± 3 kcal/mol)
$CH_3SH + h\nu(193\ nm) \rightarrow CH_3 + SH$	3.27 ± 0.07 eV (75.5 ± 1.5 kcal/mol)
$CH_3SH + h\nu \rightarrow CH_3SH^+ + e^-$	9.446 ± 0.010 eV (1312.5 ± 1.4 Å) 9.44 ± 0.01 eV[b] 9.438-9.441 eV[c]
$CH_3SH + h\nu \rightarrow CH_3S^+ + H + e^-$	11.23 ± 0.05 eV (1104 ± 5 Å) 11.37 ± 0.05 eV[b] 11.611 ± 0.005 eV[c]
$CH_3SH + h\nu \rightarrow CH_2S^+ + H_2 + e^-$	10.58 ± 0.05 eV (1172 ± 5 Å) 10.8 ± 0.1 eV[b] 10.61 ± 0.05 eV[c]

[a]This work.
[b]Reference 12.
[c]Reference 13.

rise of the second electronic band for CH_3SH^+ at ~ 1070 Å is also evident in the TPE spectrum for CH_3SH.

The estimation of the hot band effect in AE determination is a difficult task. Despite efficient rotational cooling for CH_3SH achieved in this experiment, a weak tail extending ~ 20 Å from the IE of CH_3SH, can be observed. Assuming that the AE for CH_3S^+ (or CH_2SH^+) is affected to the same extent, we arrive at a value of 11.23 ± 0.05 (1104 ± 5 Å) for the AE of CH_3S^+ (or CH_2SH^+). The latter value is slightly higher than that reported in Ref. 12.

PEPICO spectra for CH_3SH^+, CH_3S^+ (or CH_2SH^+), and CH_2S^+

The PEPICO spectra for CH_3SH^+, CH_3S^+ (or CH_2SH^+), and CH_2S^+ in the region of 910-1325 Å are shown in Figs. 9(b)-9(d), respectively. After correcting for the ion transmissions through the QMS, the PEPICO intensities for CH_3SH^+, CH_3S^+ (or CH_2SH^+), and CH_2S^+ are summed and shown in Fig. 9(a). This summed PEPICO spectrum is identical to the TPE spectrum of CH_3SH.

Methyl mercaptan has a C_s symmetry. In the ionization energy range similar to that used in this experiment, the HeI photoelectron spectrum for CH_3SH reveals three electronic bands, which are assigned to the removal of an electron from the 3a″, 10a′, and 9a′ molecular orbitals.[37,38] The vertical IE's of 9.46, 12.05, and 13.73 eV for the $CH_3SH^+(3a''^{-1}, 10a'^{-1}, 9a'^{-1})$ electronic bands are marked in Fig. 9(a).

The first PEPICO band for CH_3SH^+ is similar to the ground $CH_3SH^+(3a''^{-1})$ electronic band observed in the HeI photoelectron spectrum of CH_3SH. The CH_3SH^+ PEPICO

Figure 9. (a) The sum of the PEPICO spectra for CH_3SH^+, CH_3S^+ (or CH_2SH^+), and CH_2S^+ after calibrating the ion transmissions for the mass 48, mass 47, and mass 46 ions; PEPICO spectra in the region 910-1325 Å for (b) CH_3SH^+, (C) CH_3S^+ (or CH_2SH^+), and (d) CH_2S^+

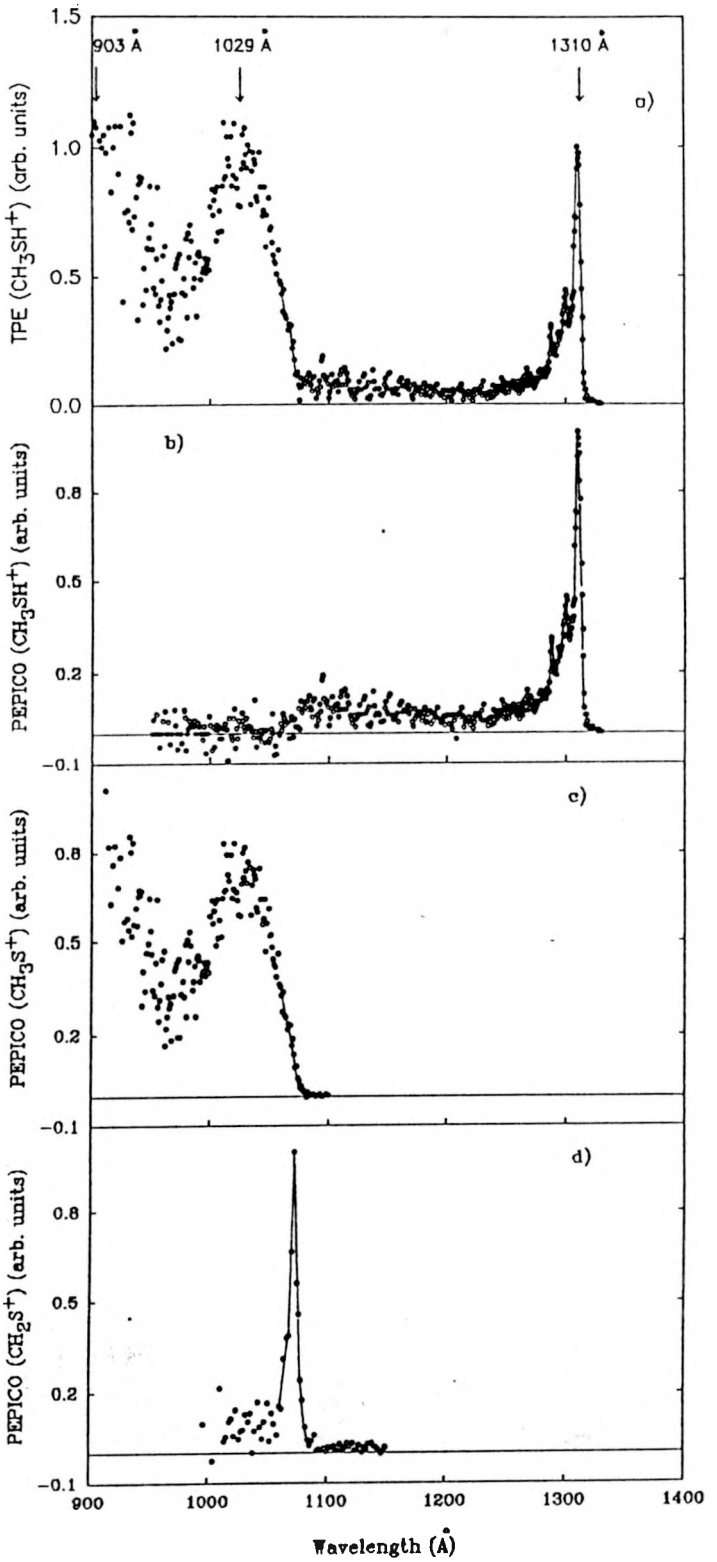
903 Å
1029 Å
1310 Å
a)
b)
c)
d)
TPE (CH_3SH^+) (arb. units)
PEPICO (CH_3SH^+) (arb. units)
PEPICO (CH_3S^+) (arb. units)
PEPICO (CH_2S^+) (arb. units)
1.5
1.0
0.5
0.0
0.8
0.5
0.2
−0.1
900
1000
1100
1200
1300
1400
Wavelength (Å)

intensity drops to the noise level at the onset (1070 Å) of the second $CH_3SH^+(10a'^{-1})$ electronic band. The low energy peak observed in the PEPICO spectrum for CH_3S^+ (or CH_2SH^+) is due to the second $CH_3SH^+(10a'^{-1})$ electronic band. The PEPICO spectrum for CH_2S^+ in the region of 1000-1100 Å consists of a narrow peak near the onset of the second electronic band. Because of very low PEPICO intensities for CH_3S^+ (or CH_2SH^+) and CH_2S^+ at wavelengths > 1080 Å, accurate determination of the AE's of these ions is extremely time consuming. Therefore, the AE's for CH_3S^+ (or CH_2SH^+) and CH_2S^+ presented here are based only on the PIE measurements.

Figures 10(a) and 10(b) compare the magnified views of the PIE and PEPICO spectra for CH_3SH^+ in the region of 1260-1330 Å. The second step observed in the PIE spectrum for CH_3SH^+ is assigned to the excitation of the C-S stretch (ν_4) of CH_3SH^+ because the spacing (642 cm^{-1}) between the second step and the onset of the PIE spectrum is close to the C-S stretching frequency (704 cm^{-1})[39] of CH_3SH. Five vibrational peaks with nearly equal spacings are resolved in the PEPICO spectrum of Fig. 10(b), while only two vibrational peaks have been observed in previous HeI photoelectron spectroscopic measurements. The additional vibrational peaks observed in the PEPICO spectrum may be attributed partly to the rotational cooling of CH_3SH achieved in this experiment. The average vibrational spacing (647 ± 20 cm^{-1}) found in the PEPICO spectrum is consistent with that determined from the PIE spectrum. We note that the value of 9.468 ± 0.025 eV for the vertical IE of CH_3SH obtained from the PEPICO spectrum is slightly higher than the adiabatic IE of 9.446 ± 0.010 eV based on the PIE spectrum. The vertical IE for CH_3SH determined by the PEPICO spectrum for CH_3SH^+ is in good agreement with that

Figure 10. (a) PIE spectrum for CH_3SH^+ in the region of 1260-1340 Å, (b) PEPICO spectrum for CH_3SH^+ in the region of 1260-1330 Å

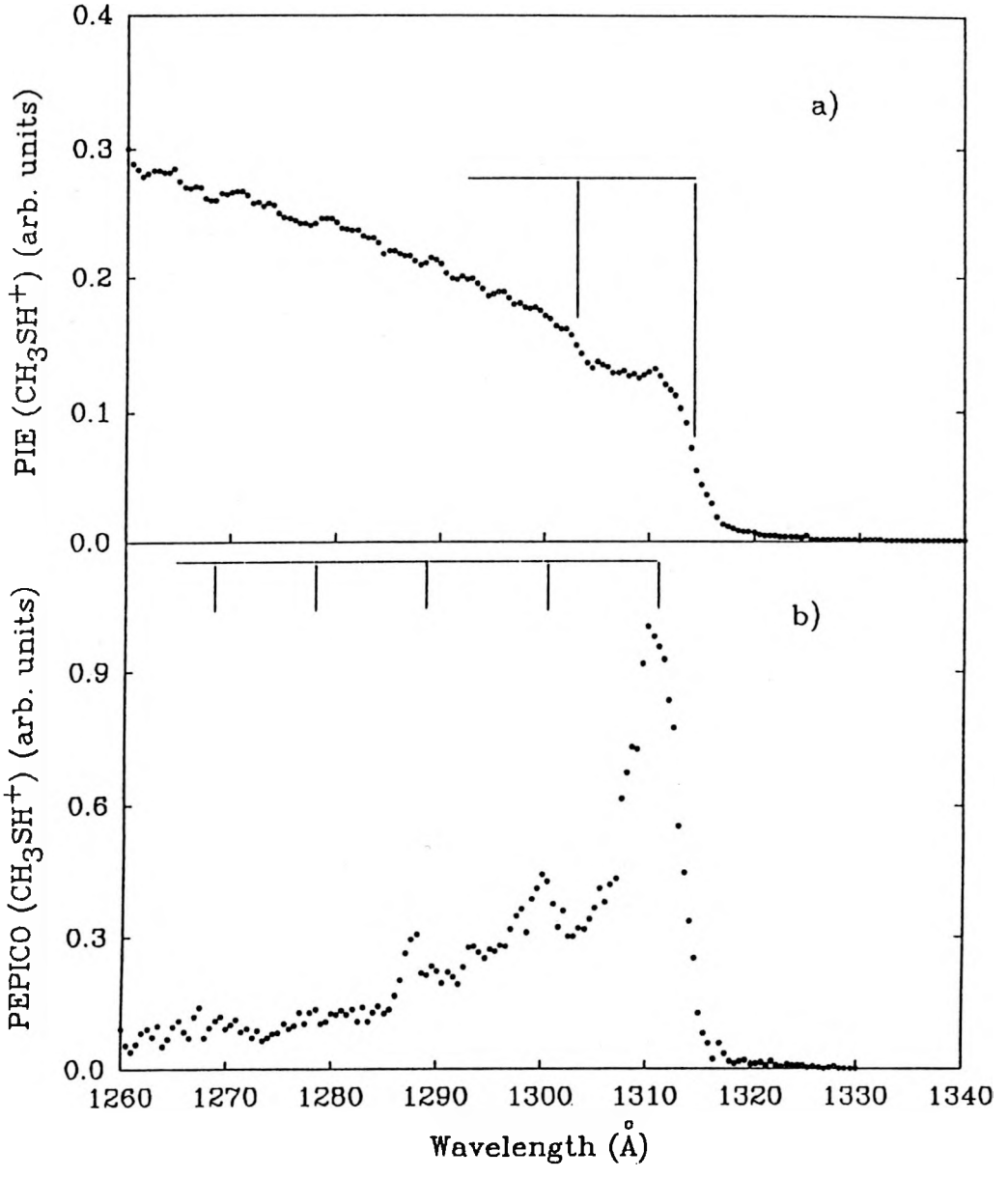
a)
b)
PIE (CH_3SH^+) (arb. units)
PEPICO (CH_3SH^+) (arb. units)
0.0
0.1
0.2
0.3
0.4
0.3
0.6
0.9
1260
1270
1280
1290
1300
1310
1320
1330
1340
Wavelength (Å)

obtained using the HeI photoelectron spectrum.[37,38]

Breakdown diagram for the unimolecular decomposition of CH_3SH^+

After calibrating the ion transmissions through the QMS, we have constructed the breakdown diagram for the unimolecular decomposition of CH_3SH^+ in the wavelength range of 950-1350 Å as shown in Fig. 11. The internal energies of CH_3SH^+ corresponding to the ionization wavelengths are also indicated in the figure.

The breakdown diagram displays a sharp crossover between the mass 48 (CH_3SH^+) and mass 47 (CH_3S^+ or CH_2SH^+) ions at ~ 1075 Å. In the internal energy range of 0-83 kcal/mol, the CH_2S^+ ion only appears as a weak spike in this crossover region. A theoretical breakdown diagram in this energy region, calculated using the QET formulation,[13] is in qualitative accord with the experimental breakdown diagram. However, the QET result, showing that the CH_2S^+ breakdown curve decreases gradually from the crossover region toward higher internal energy, is not consistent with the CH_2S^+ breakdown curve shown in Fig. 11.

The formation of CH_3S^+ (or CH_2SH^+) may be achieved by direct S-H (or C-H) bond rupture, whereas the formation of $CH_2S^+ + H_2$ from CH_3SH^+ necessarily involves 1,2-H_2 elimination. The increase in internal energy of CH_3SH^+ is expected to increase the entropy factor and to suppress the 1,2-H_2 elimination process.

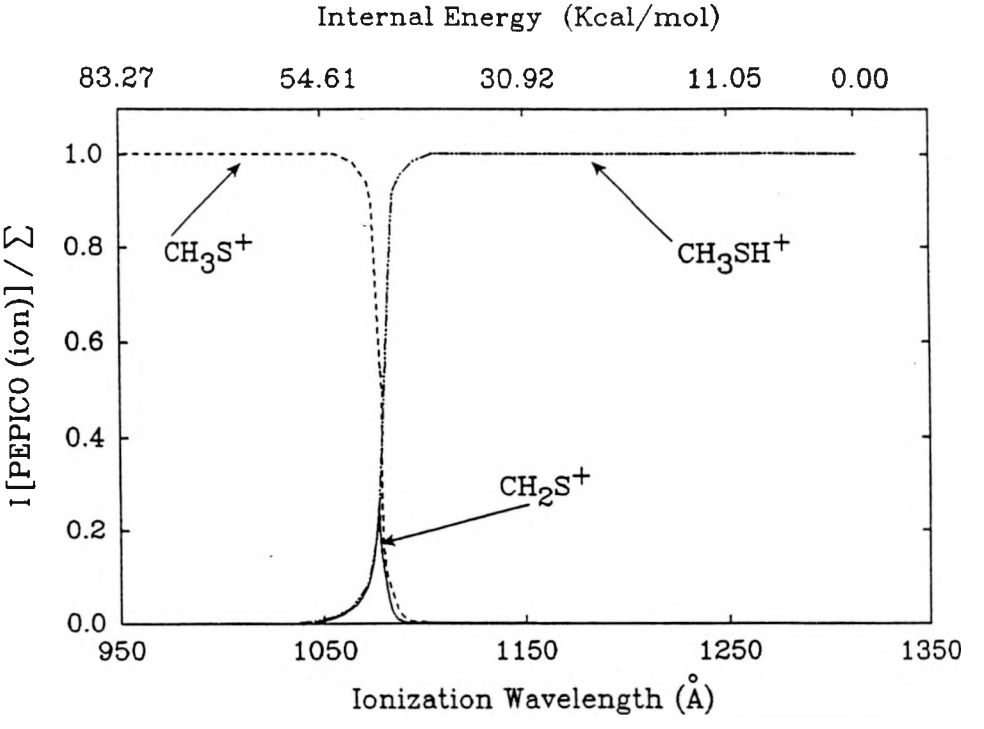

Figure 11. Breakdown diagram for the unimolecular decomposition of energy selected CH_3SH^+, where I[PEPICO(ion)] is the PEPICO intensity of the ion and Σ = I[PEPICO(CH_3SH^+ + CH_3S^+ (CH_2SH^+) + CH_2S^+)]

Thermochemistry of CH_3SH and CH_3SH^+ and their fragments

The values for the heats of formation of the CH_3SH/CH_3SH^+ system determined in this study are listed and compared to the literature values[1,12,13,24,25,29,35,39-43] in Table 2. The values for $\Delta H_{f0}(CH_3S)$ determined by kinetic energy release measurements[24,25] of the photodissociation process $CH_3SCH_3 + h\nu$ (193 nm) $\rightarrow CH_3S + CH_3$ and $CH_3SSCH_3 + h\nu$ (193 nm) $\rightarrow 2CH_3S$ are in excellent agreement with that based on the AE for process (1). The value for $\Delta H_{f0}(SH)$ obtained in this work is also consistent with the literature value.[40]

The ab initio calculation of Nobes, Bouma, and Radom[17] indicates that the mass 47 ion formed in the fragmentation of CH_3SH^+ at the threshold has the mercaptomethyl ion (CH_2SH^+) structure. Assuming that the mass 47 ion observed at the onset of the photoionization process (5) corresponds to CH_2SH^+, we obtain a value of 204.5 ± 1.2 kcal/mol for $\Delta H_{f0}(CH_2SH^+)$. This value is consistent with the value (206.2 ± 1 kcal/mol) calculated using the AE of CH_2SH^+ formed in the photoionization of CH_3SCH_3.[25] These values are in reasonable agreement with values obtained in previous studies.[12,35,41]

Using the AE for process (6), we arrive at a value of 241 ± 1 kcal/mol for $\Delta H_{f0}(CH_2S^+)$. This value is in excellent agreement with the value calculated based on the IE (9.34 eV) of CH_2S,[38] and is consistent with a negligible activation energy for the formation of CH_2S^+ by 1,2-H_2 elimination of CH_3SH^+.

Table 2. Heats of formation for organosulfur molecules and their ions involved in the photodissociation and photoionization of CH_3SH

Molecule	ΔH_{f0}(kcal/mol)	D_o(kcal/mol)
CH_3SH	-2.9[a]	$D_o(CH_3\text{-}SH)$ = 72.9 ± 1.5[b] = 72.9 ± 1.5[c] = 71.9 ± 1.5[d] $D_o(CH_3S\text{-}H)$ = 90 ± 2[b] = 90.5 ± 1.5[c] = 89.2 ± 2[d]
CH_3S	35.4 ± 2[b] 35.1 ± 1.5[e] 35.4 ± 1.5[f] 34.2 ± 1.5[g] 33.2 ± 1.5[h]	
CH_2S	24.3[g] 25.1[i]	
CH_3	34.8 ± 0.3[a]	
SH	35.2 ± 1.5[b]	
S	66.1[a]	
H	51.63[a]	
CH_3SH^+	214.9[b] 214.8[j,k]	
CH_2SH^+	204.5 ± 1.2[b] 206.2 ± 1[l] 205[j] 208[m] 207[n]	
CH_2S^+	241 ± 1[b] 240.5[o] 251.5[p] 233[i]	

Table 2. (continued)

[a]Reference 40.
[b]This work.
[c]Reference 1.
[d]Reference 29.
[e]Reference 25. Based on the energy release measurement of the process, CH_3SCH_3 + hν (193 nm) → CH_3S + CH_3.
[f]Reference 24. Based on the energy release measurement of the process, CH_3SSCH_3 + hν (193 nm) → $2CH_3S$.
[g]ΔH_{f298}, Reference 1.
[h]ΔH_{f298}, Reference 29.
[i]Reference 43.
[j]Reference 12.
[k]Reference 13.
[l]Reference 25. Based on the AE of the process, CH_3SCH_3 + hν → CH_3S^+ (or CH_2SH^+) + CH_3 + e^-.
[m]Reference 35.
[n]Reference 41.
[o]Reference 42. Based on the IE (9.34 ± 0.01 eV) of CH_2S.
[p]Reference 25. Based on the AE of the process, CH_3SCH_3 + hν → CH_2S^+ + CH_4 + e^-.

SUMMARY

The primary product channels in the 193 nm photodissociation of CH_3SH have been identified by the TOF mass spectrometric method. The AE's for processes (1) and (2) provide a direct measure of the values for $D_0(CH_3S\text{-}H)$ and $D_0(CH_3\text{-}SH)$. The TOF measurements also yield information about the kinetic energy distributions for processes (1) and (2). The AE for process (3) is consistent with the thermochemical threshold. The 193 nm photodissociation of SH to yield S + H has also been observed. The TOF threshold for S corresponds to the formation of $S(^3P)$ + H.

The unimolecular decomposition of energy-selected CH_3SH^+ ions in the internal energy range of 0-83 kcal/mol has been investigated using the PEPICO method. The value for $\Delta H_{f0}(CH_2SH^+)$ determined by the AE of process (5) is in excellent agreement with that based on the AE for the process $CH_3SCH_3 + h\nu \rightarrow CH_2SH^+ + CH_3$. The AE observed for process (6) is consistent with the conclusion that the activation energy for the 1,2-H_2 elimination process $CH_3SH^+ \rightarrow CH_2S^+ + H_2$ is negligible.

The threshold values for the photodissociation and photoionization processes determined in this study are summarized in Table 1.

REFERENCES

1. S. W. Benson, Chem. Rev. 78, 23 (1978) and references therein.
2. D. F. Sheraton and F. E. Murray, Can. J. Chem. 59, 2750 (1981).
3. N. P. Skerrett and N. W. Thompson, Trans. Faraday Soc. 37, 81 (1951).
4. T. Inaba and B. de B. Darwent, J. Phys. Chem. 64, 1431 (1960).
5. A. B. Callear and D. R. Dickson, Trans. Faraday Soc. 66, 1987 (1970).
6. R. P. Steer and A. R. Knight, J. Phys. Chem. 72, 2145 (1968).
7. L. Bridges and J. M. White, J. Phys. Chem. 77, 295 (1973).
8. D. Kamra and J. M. White, J. Photochem. 4, 361 (1975).
9. A. Rauk and S. Collins, J. Mol. Spectry. 105, 438 (1984).
10. K. K. Baldridge, M. S. Gordon, and D. E. Johnson, J. Phys. Chem. 91, 4145 (1987).
11. B. Mouflih, C. Larrieu, and M. Chaillet, Chem. Phys. 119, 221 (1988).
12. M. E. Akopyan, Y. L. Serhiev, and F. I. Vilesov, Khim. Vys. Energ. 4, 305 (1970).
13. R. E. Kutina, A. K. Edwards, G. L. Goodman, and J. Berkowitz, J. Chem. Phys. 77, 5508 (1982).
14. B.-O. Jonsson and J. Lind, J. Chem. Soc. Faraday Trans. 2 70, 1399 (1974).
15. J. D. Dill and F. W. McLafferty, J. Am. Chem. Soc. 100, 2907 (1978).
16. J. D. Dill and F. W. McLafferty, J. Am. chem. Soc. 101, 6526 (1979).
17. R. H. Nobes, W. J. Bouma, and L. Radom, J. Am. Chem. Soc. 106, 2774 (1984).
18. M. J. S. Dewar and H. S. Rzepa, J. Am. Chem. Soc. 99, 7432 (1977).

19. F. Bernardi, I. G. Csizmadia, H. B. Schlegel, and S. Wolfe, Can. J. Chem. 53, 1144 (1975).

20. M.-H. Whangbo, S. Wolfe, and F. Bernardi, Can. J. Chem. 53, 3040 (1975).

21. T. Yamabe, K. Yamashita, K. Fukui, and K. Morokuma, Chem. Phys. Lett. 63, 433 (1979).

22. F. Bernardi, A. Bottoni, and N. A. Epiotis, J. Am. Chem. Soc. 100, 7205 (1978).

23. W.-B. Tzeng, H.-M. Yin, W.-Y. Leung, J.-Y. Luo, S. Nourbakhsh, G. D. Flesch, and C. Y. Ng, J. Chem. Phys. 88, 1658 (1988).

24. S. Nourbakhsh, C.-L. Liao, and C. Y. Ng, J. Chem. Phys. 92, 6589 (1990).

25. S. Nourbakhsh, K. Norwood, H.-M. Yin, C.-L. Liao, and C. Y. Ng, J. Chem. Phys. submitted.

26. K. Norwood, J.-H. Guo, G. Luo, and C. Y. Ng, Chem. Phys. 129, 109 (1989).

27. K. Norwood and C. Y. Ng, Chem. Phys. Lett. 156, 145 (1989).

28. K. Norwood, J.-H. Guo, and C. Y. Ng, J. Chem. Phys. 90, 2995 (1989).

29. D. F. McMillen and D. M. Golden, Ann. Rev. Phys. Chem. 33, 493 (1982).

30. S. W. Benson, J. Chem. Ed. 42, 502 (1965).

31. R. Bersohn, J. Phys. Chem. 88, 5146 (1984).

32. R. Bersohn, in "Molecular Photodissociation Dynamics", edited by M. N. R. Ashfold and J. E. Baggott (Royal Society of Chemistry, London, 1987).

33. G. N. A. van Veen, K. A. Mohamed, J. Baller, and A. E. deVries, Chem. Phys. 74, 261 (1983).

34. W. G. Hawkins and P. L. Houston, J. Chem. Phys. 76, 729 (1982).

35. J. J. Butler, T. Baer, and S. A. Evans, Jr., J. Am. Chem. Soc. 105, 3451 (1983).

36. H. Okabe, "Photochemistry of Small Molecules" (Wiley, New York, 1978).

37. K. Kimura, S. Katsumata, Y. Achiba, T. Yamazaki, and S. Iwata, "Handbook of HeI Photoelectron Spectra of Fundamental Organic Molecules" (Halsted Press, New York, 1981).

38. D. C. Frost, F. G. Herring, A. Katrib, C. A. McDowell, and R. A. N. McLean, J. Phys. Chem. 76, 1030 (1972).

39. G. Herzberg, "Molecular Spectra and Molecular Structure. III. Electronic Spectra and Electronic Structure of Polyatomic Molecules" (Van Nostrand, Princeton, 1966), p. 630.

40. H. M. Rosenstock, K. Draxl, B. W. Steiner, J. T. Herron, J. Phys. Chem. Ref. Data Suppl. 6, (1977).

41. M. Roy and T. B. McMahon, Org. Mass Spectrom. 17, 392 (1982).

42. H. W. Kroto and R. J. Suffolk, Chem. Phys. Lett. 15, 545 (1972).

43. J. J. Butler and T. Baer, Org. Mass Spectrom. 18, 248 (1983).

SECTION V.

A 193 nm LASER PHOTOFRAGMENTATION TIME-OF-FLIGHT MASS SPECTROMETRIC STUDY OF CH_3CH_2SH

ABSTRACT

The kinetic energy releases of the photodissociation processes, $CH_3CH_2SH + h\nu$ (193 nm) $\rightarrow CH_3CH_2 + SH$, $CH_3CH_2S + H$, and $CH_3 + CH_2SH$, have been measured by the time-of-flight mass spectrometric method. Based on the thresholds of kinetic energy spectra, the dissociation energies of 72.4 ± 1.5, 90 ± 2, and 100 ± 2 kcal/mol have been obtained for the CH_3CH_2-SH, CH_3CH_2S-H, and CH_3-CH_2SH bonds at 0 K.

INTRODUCTION

Sulfur-containing radicals formed in the ultraviolet (UV) photolysis of organosulfur pollutants, which are produced in coal and oil combustion, are reaction intermediates in atmospheric cycles.[1,2] In order to study the energy disposals and to identify primary UV photodissociation channels of organosulfur compounds, we have carried out a series of excimer laser photofragmentation time-of-flight (TOF) mass spectrometric measurements of CS_2,[3] CH_3SSCH_3,[4] CH_3SCH_3,[5] and CH_3SH[6].

Previous experiments suggest that the primary dissociation channels in the ultraviolet photolysis of ethyl mercaptan (CH_3CH_2SH) involve the scission of the C-S and S-H bonds.[7-12] An ab initio calculation aiming to understand the thermal decomposition pathways of CH_3CH_2SH has been reported.[13] In this article, we present the results of a 193 nm photodissociation TOF mass spectrometric study of CH_3CH_2SH.

$$CH_3CH_2SH + h\nu\ (193\ nm) \rightarrow CH_3CH_2 + SH \qquad (1)$$

$$CH_3CH_2SH + h\nu\ (193\ nm) \rightarrow CH_3CH_2S + H \qquad (2)$$

$$CH_3CH_2SH + h\nu\ (193\ nm) \rightarrow CH_3 + CH_2SH \qquad (3)$$

EXPERIMENTAL

The rotatable beam source laser photofragmentation apparatus used in this study has been described in detail previously.[3,4] The apparatus consists of three main components: an ArF excimer laser, a photodissociation chamber in which a rotatable supersonic molecular beam intersects with the laser beam, and a linearly movable ultrahigh vacuum electron ionization quadrupole mass spectrometer (QMS).

In this experiment, a pulsed beam of CH_3CH_2SH seeded in He is produced by supersonic expansion through a pulsed valve at ~ 298 K and a total pressure of ~ 1150 Torr. The pulsed valve has a nozzle diameter of 0.5 mm and is operated at 40 Hz. The ratio of the pressure of CH_3CH_2SH to that of He is about 0.15. The seeded CH_3CH_2SH beam has an angular divergence of ~ 3° which is defined by the opening of the conical skimmer and by the circular aperture between the differential pumping chamber and the photodissociation chamber. The 3° angular spread of the beam corresponds to a beam width of 3 mm in the photodissociation region. All TOF spectra are taken at a flight path of 73.7 cm which is defined to be the distance between the photodissociation region and the electron impact ionizer.

The energy of the excimer laser [Questek (Model 2460)] used varies in the range of 90-120 mJ. The laser beam enters the photodissociation chamber through a MgF_2 focusing lens and intersects with the seeded CH_3CH_2SH beam at 90°.

The data acquisition and operation of the apparatus is controlled by an LSI-11/23 mini-computer. The TOF spectrum is recorded on a multichannel scaler (MCS). The firing of the excimer laser is delayed by approximately 450 μs with respect to the triggering pulse for the opening of the pulsed valve. The MCS is started by a second trigger pulse signifying the firing of the laser. The delay timings are controlled by a digital delay unit (SRS, Model DG 535). The laboratory angle (θ) is defined to be the angle between the seeded CH_3CH_2SH molecular beam and the detector axis. The laboratory velocity for the parent CH_3CH_2SH beam ($\mathbf{v}_p$) is determined by measuring the TOF of the CH_3CH_2SH beam pulse at $\theta = 0°$ at two known nozzle-ionizer distances. The value for $\mathbf{v}_p$ is determined before and after the laser photodissociation experiment and the deviation of the two measurements is usually less than 2%. Under the beam expansion conditions used in this experiment, the ratio $\Delta v/v_p$ is estimated to be less than 0.08, where Δv represents the velocity spread [full width at half maximum (FWHM)] of the CH_3CH_2SH beam.

The analysis of the TOF data involves the transformation of the laboratory TOF spectra into center-of-mass (c.m.) translational energy ($E_{c.m.}$) distributions and has been described in detail.[3,4] We have ignored the effect of the apparatus resolution factors in the transformation.

RESULTS AND DISCUSSION

TOF Spectra for SH

Figure 1(a) shows the TOF spectrum for SH observed at $\theta = 30°$. The TOF peak centered at ~ 270 μs is due to process (1) and the SH signals in the temporal range $\gtrsim$ 400 μs are attributed to dissociative ionization processes involving dimers and clusters of CH_3CH_2SH in the ionizer. The $E_{c.m.}$ distribution for photofragments of process (1) derived from the TOF spectrum for SH is depicted in Fig. 1(b). A value of 75.5 kcal/mol is obtained for the $E_{c.m.}$ threshold for process (1). Based on two independent measurements, we assign an uncertainty of ± 1.5 kcal/mol to the experimental threshold. This $E_{c.m.}$ threshold yields a bond energy of 72.4 ± 1.5 kcal/mol at 0 K [$D_o(CH_3CH_2\text{-}SH)$]. Assuming that the electronic and vibrational degrees of freedom for CH_3CH_2 and SH are not excited at 298 K,[14] we estimate the bond dissociation energy for $CH_3CH_2\text{-}SH$ at 298 K [$DH°(CH_3CH_2\text{-}SH)$] to be 74.5 ± 1.5 kcal/mol, which is slightly higher than the value of 70.5 ± 1.5 kcal/mol recommended by McMillen and Golden.[15] However, the $DH°(CH_3CH_2\text{-}SH)$ obtained here agrees with the value of 72.0 ± 1.5 kcal/mol given by Benson[16] after taking into account the experimental uncertainties. The ab initio calculation of Baldridge, Gordon, and Johnson predicts a value of 65.1 kcal/mol for the homolytic cleavage of the C-S bond.[13]

Figure 1. (a) TOF spectrum for SH at $\theta = 30°$; (b) $E_{c.m.}$ distribution for process (1) transformed from the TOF spectrum for SH

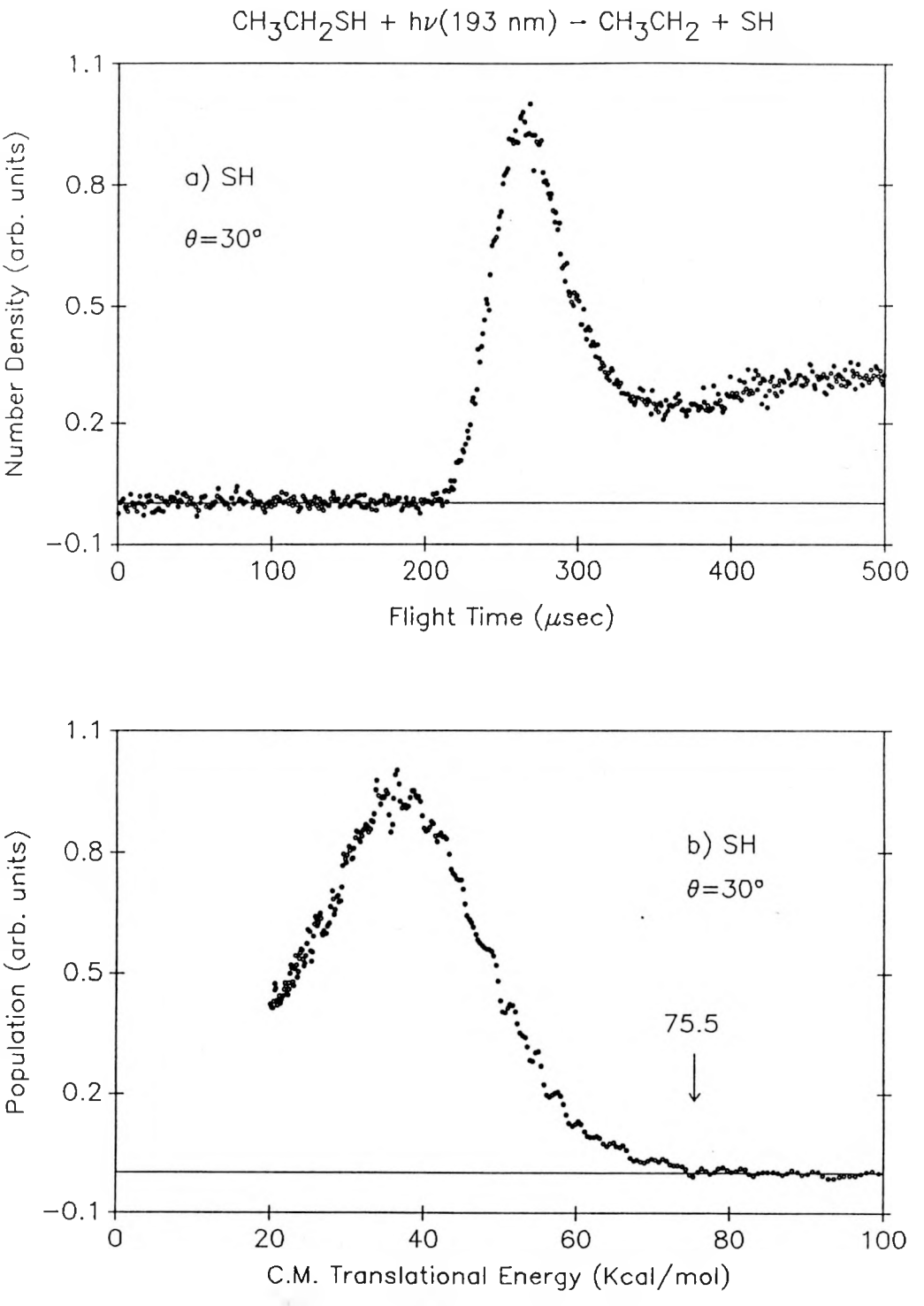
$CH_3CH_2SH + h\nu(193\ nm) \rightarrow CH_3CH_2 + SH$
a) SH
θ=30°
Number Density (arb. units)
Flight Time (μsec)
b) SH
θ=30°
75.5
Population (arb. units)
C.M. Translational Energy (Kcal/mol)

The $E_{c.m.}$ distribution of Fig. 1(b) has a maximum at about 35 kcal/mol, corresponding to a value of 40.5 kcal/mol for the most probable internal excitation (E_{int}) of CH_3CH_2 + SH. Table 1 lists the values for D_o(R-SH) and the percentages of available energies that appear as the most probable $E_{c.m.}$ and E_{int} for R + SH arising from the 193 nm photofragmentation of RSH, where R = H, CH_3, and CH_3CH_2. In the case of H_2S, more than 90% of the available energy appears as $E_{c.m.}$. This observation has been rationalized by a Franck-Condon picture for photodissociation. Since the S-H distances in the SH fragment and H_2S are very similar, the vibrational excitation of the SH fragment is expected to be small. Furthermore, the c.m. of SH is so close to the S atom that the torque exerted to SH by the departing H atom is negligibly small. The high percentage (70%) of available energy appearing as $E_{c.m.}$ in the 193 photodissociation of CH_3SH can also be understood by a similar picture because CH_3SH may be considered as a pseudotriatomic molecule. As shown in Table 1, the percentage for $E_{c.m.}$ (47%) observed in the photodissociation of CH_3CH_2SH is substantially lower than those of H_2S and CH_3SH. The most stable geometry for the CH_3CH_2 radical is quite different from that for the CH_3CH_2 group in CH_3CH_2SH. For example, the C-C bond distance in the CH_3CH_2 radical is expected to be considerably shorter than that in CH_3CH_2SH. Therefore a high degree of internal excitation for the CH_3CH_2 fragment is anticipated, in accordance with the Franck-Condon picture for photodissociation. On statistical grounds, the percentage for E_{int} for the photofragments should be proportional to the number of internal degrees of freedom for the precursor molecule.

Table 1. Partition of available energies in $E_{c.m.}$ and E_{int} of fragments in the 193 nm photolysis of H_2S, CH_3SH, and CH_3CH_2SH

Bond	D_o (kcal/mol)	% $E_{c.m.}$	% E_{int}
H-SH	89.9 ± 1.5[a]	90[b]	10[b]
CH_3-SH	72.4 ± 1.5[c]	70[c]	30[c]
CH_3CH_2-SH	72.3 ± 1.5[d]	46[d]	54[d]

[a]References 15 and 16.
[b]References 17-19.
[c]Reference 6.
[d]This work.

The signal-to-noise ratio of the measured CH_3CH_2 spectrum (not shown here) is poorer than that of the SH spectrum. Nevertheless, the threshold and the most probable $E_{c.m.}$ observed in the $E_{c.m.}$ distribution transformed from the CH_3CH_2 spectrum are consistent with those derived from the SH spectrum.

TOF Spectrum for H

The TOF spectrum for H formed in process (2) is shown in Fig. 2(a) and the corresponding $E_{c.m.}$ distribution for CH_3CH_2S + H derived from the TOF spectrum for H is plotted in Fig. 2(b).

The $E_{c.m.}$ threshold for process (2) is found to be 58 ± 2 kcal/mol, yielding a value of 90 ± 2 kcal/mol for $D_o(CH_3CH_2S\text{-}H)$. The latter value is in excellent agreement with the literature values[15,16] of 92 ± 2 and 91 ± 1.5 kcal/mol for $DH^o(CH_3CH_2S\text{-}H)$. The $E_{c.m.}$ distribution peaks at $E_{c.m.}$ ~ 40 kcal/mol, which corresponds to a most probable E_{int} value of 18 kcal/mol. The slow decrease of the $E_{c.m.}$ distribution from 35 kcal/mol towards low $E_{c.m.}$ indicates that a substantial fraction of CH_3CH_2S fragments are formed with $E_{int} > 23$ kcal/mol.

TOF Spectrum for CH_3

Figures 3(a) and 3(b) show the TOF spectrum for CH_3 and the $E_{c.m.}$ distribution for photofragments of process (3) based on the TOF spectrum for CH_3, respectively. Due to

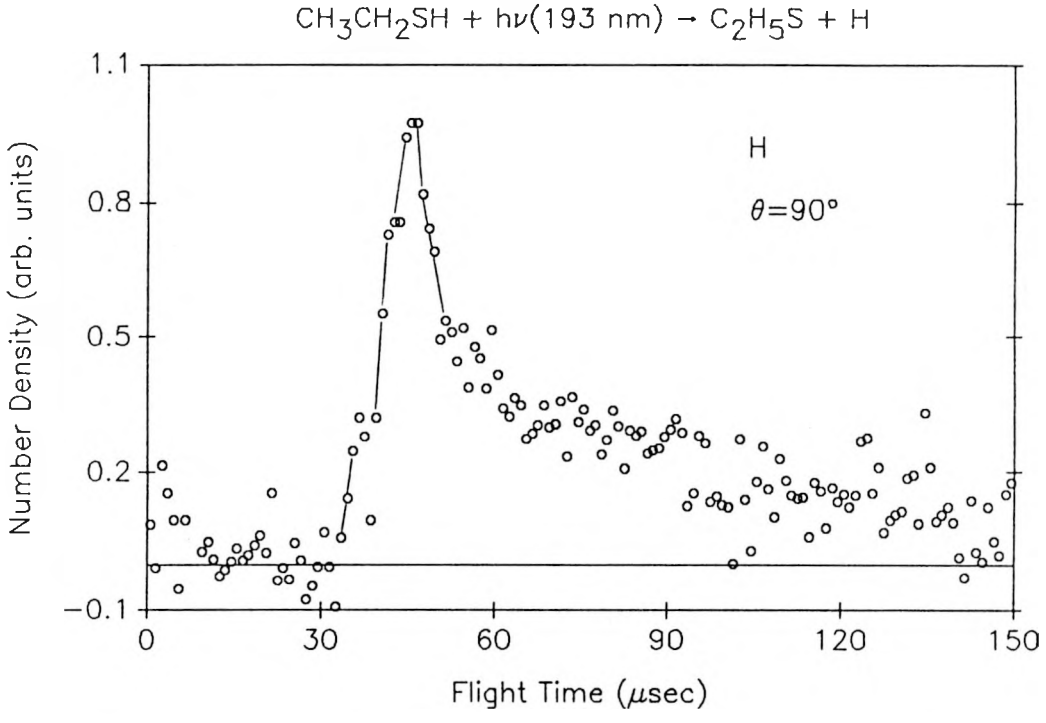

Figure 2(a). TOF spectrum for H at $\theta = 90°$

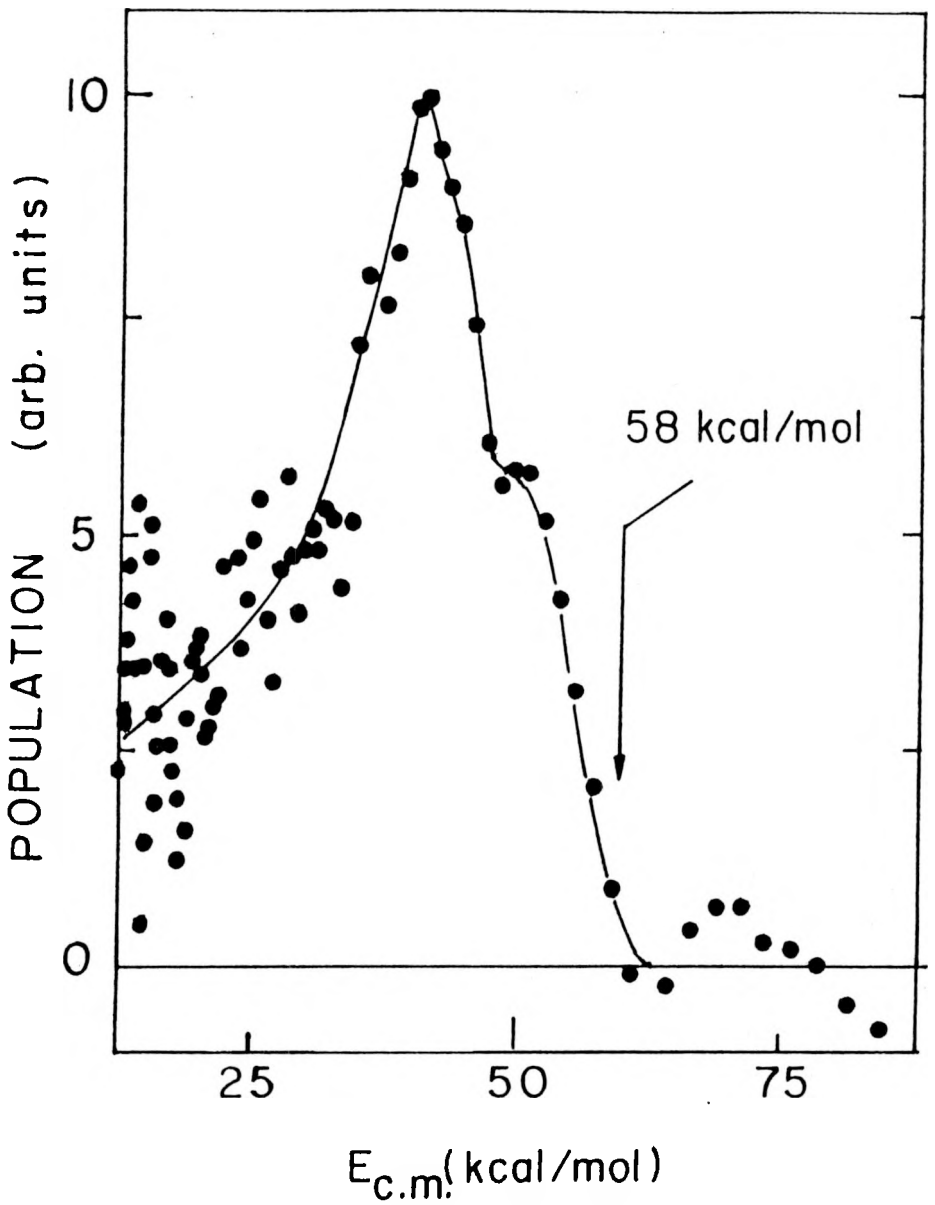

Figure 2(b). $E_{c.m.}$ distribution for process (2) transformed from the TOF spectrum for H

Figure 3. (a) TOF spectrum for CH_3; (b) $E_{c.m.}$ distribution for process (3) transformed from the TOF spectrum for CH_3

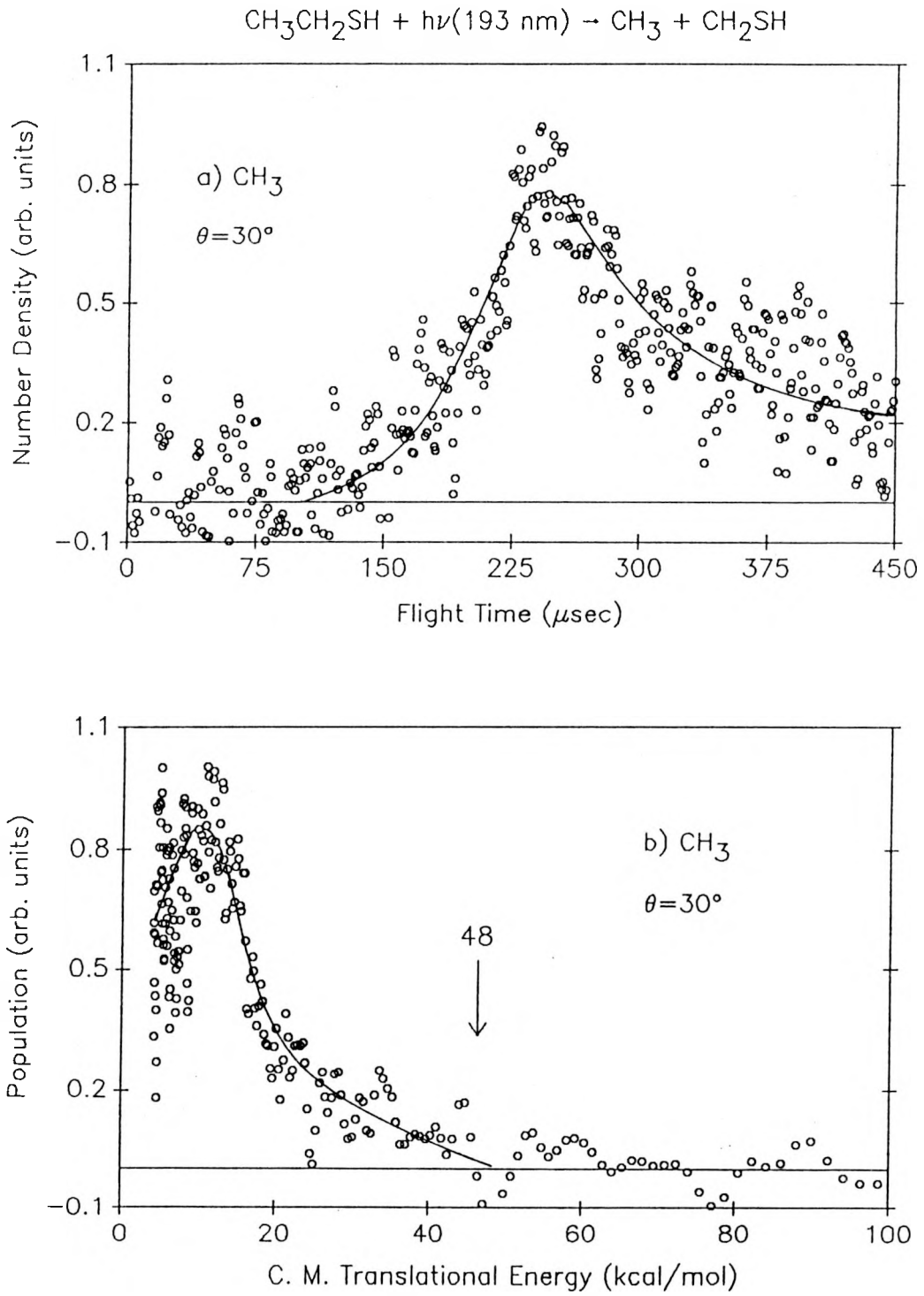
$CH_3CH_2SH + h\nu(193\ nm) \rightarrow CH_3 + CH_2SH$
a) CH_3
θ=30°
Number Density (arb. units)
Flight Time (μsec)
1.1
0.8
0.5
0.2
−0.1
0
75
150
225
300
375
450
b) CH_3
θ=30°
48
Population (arb. units)
C. M. Translational Energy (kcal/mol)
20
40
60
80
100

the poor signal-to-noise of the TOF spectrum for CH_3, the $E_{c.m.}$ threshold of 48 kcal/mol should be viewed as an lower bound. The latter value corresponds to an upper bound of 100 kcal/mol for $D_o(CH_3\text{-}CH_2SH)$.

We note that the $E_{c.m.}$ distribution peaks at a low $E_{c.m.}$(~ 10 kcal/mol), indicating the majority of the available energy for process (3) appears as internal excitations for CH_2SH and CH_3. The high E_{int} for CH_2SH is consistent with the fact that the C-S bond distance in CH_2SH is significantly different from that in CH_3CH_2SH.[13]

REFERENCES

1. A. Levy, E. L. Merryman, and W. T. Reid, Environ. Sci. Technol. 4, 653 (1970).

2. C. F. Cullis and M. F. R. Mulcahy, Combust. Flame 18, 225 (1975).

3. W.-B. Tzeng, H.-M. Yin, W.-Y. Leung, J.-Y Luo, S. Nourbakhsh, G. D. Flesch, and C. Y. Ng, J. Chem. Phys. 88, 1658 (1988).

4. S. Nourbakhsh, C.-L. Liao, and C. Y. Ng, J. Chem. Phys. 92, 6587 (1990).

5. S. Nourbakhsh, K. Norwood, H.-M. Yin, C.-L. Liao, and C. Y. Ng, J. Chem. Phys. submitted.

6. S. Nourbakhsh, K. Norwood, H.-M. Yin, C.-L. Liao, and C. Y. Ng, J. Chem. Phys. submitted.

7. G. Black and L. E. Junsinski, Chem. Phys. Lett. 136, 241 (1987).

8. A. B. Callear and D. R. Dickson, Trans. Faraday Soc. 66, 1987 (1970).

9. J. M. White, R. L. Johnson, Jr., and D. Bacon, J. Chem. Phys. 52, 5212 (1970).

10. R. P. Steer and A. R. Knight, Can. J. Chem. 47, 1335 (1969).

11. M. Meissner and H. W. Thompson, Trans. Faraday Soc. 34, 1238 (1938).

12. W. E. Haines, G. L. Cook, and J. S. Ball, J. Am. Chem. Soc. 78, 5213 (1956).

13. K. K. Baldridge, M. S. Gordon, and D. E. Johnson, J. Phys. Chem. 91, 4145 (1987).

14. S. W. Benson, J. Chem. Ed. 42, 502 (1965).

15. S. W. Benson, Chem. Rev. 78, 23 (1978).

16. D. F. McMillen and D. M. Golden, Annu. Rev. Phys. Chem. 33, 493 (1982).

17. R. Bersohn, J. Phys. Chem. 88, 5146 (1984).

18. G. N. A. van Veen, K. A. Mohamed, J. Baller, and A. E. deVries, Chem. Phys. 74, 261 (1983).

19. W. G. Hawkins and P. L. Houston, J. Chem. Phys. 76, 729 (1982).

SECTION VI.

PHOTOIONIZATION STUDY OF SUPERSONICALLY COOLED CS FORMED IN THE EXCIMER LASER PHOTODISSOCIATION OF CS_2

ABSTRACT

The photoionization efficiency data of supersonically cooled CS have been obtained in the region from 1000-1100 Å. The CS radicals are prepared by 193 nm laser photodissociation of a pulsed supersonic CS_2 beam. Experiments show that internally hot CS molecules initially formed by the photodissociation process relax efficiently in the supersonic expansion.

INTRODUCTION

One of the most important contributions of photoionization mass spectrometric (PIM) experiments is to provide precise thermochemical data, such as the ionization energies (IE) and appearance energies (AE) of photoionization processes. A current focus of PIM studies has been on transient molecules and radicals.[1-3] Because of the reactive nature of radicals, the preparation of a pure radical with sufficiently high concentration for PIM measurements is difficult. Despite these difficulties, a substantial body of photoionization efficiency (PIE) data on radicals has been accumulated over the past decades, due mostly to the sustained efforts of Berkowitz and co-workers.[1] However, considering the diversity of radicals and transient molecular species, and their importance to chemistry, the characterization of radicals and transient molecules by PIM measurements and by photoelectron (PE) spectroscopy is still in its infancy. In previous PIM studies, radicals have been prepared mostly by pyrolysis, discharge, and fast atom reactions in effusive beam conditions. The internal excitations of radicals formed by such processes are often difficult to assess, making it difficult to estimate the hot band effects on the measured IEs and AEs.

RESULTS AND DISCUSSION

In this communication, we report preliminary PIE data of supersonically cooled CS formed in the 193 nm excimer photodissociation of CS_2. HeI PE spectra for CS formed in the microwave discharge of CS_2 have been reported.[4-6] The difficulty of sustaining a discharge in CS_2 for a sufficiently long period of time has prevented the measurement of the PIE spectrum of CS.[7] Excimer photodissociation is an excellent method for preparing specific radicals in high yields.[8,9] It is well-known that CS is produced efficiently by the 193 nm excimer photodissociation of CS_2, and that CS photofragments thus formed are in the CS(X, v = 0-13) states, corresponding to internal excitations up to 45 kcal/mol.[10-13]

The molecular beam photoionization apparatus used has been described in detail.[14,15] In this experiment, a pulsed beam of CS_2 seeded in Ar is produced by supersonic expansion through a pulsed value with a nozzle diameter of 0.5 mm and a total stagnation nozzle pressure (P_o) of 1150 Torr. The partial nozzle stagnation pressure for CS_2 is determined by its vapor pressure (~ 350 Torr) at room temperature. The pulsed valve is operated at 40 Hz. The ArF excimer laser beam intersects the CS_2 free jet at 90° and ~ 2 mm from the nozzle tip. The laser beam is mildly focussed to a pencil shape (cross sectional area ~ 2 x 6 mm^2) in the photodissociation region with the length of the laser cross section aligned along the axis of the CS_2 beam. The energy of the excimer laser varies in the range of 15-25 mJ. The pulsed beam is skimmed by a conical skimmer before entering the photoionization region located ~ 8 cm from the pulsed nozzle tip. The

hydrogen many-lined pseudocontinuum is used as the vacuum ultraviolet (VUV) photoionization light source and the wavelength resolution used is 1.5 Å [full width at half maximum (FWHM)].

Figure 1(a) shows the temporal profile of the CS_2 pulsed beam determined by photoionization at 1068 Å using a multichannel scaler. Time zero of the time-of-flight (TOF) spectrum corresponds to the initiation of the trigger pulse for opening the pulse valve. The triggering pulse for firing the excimer laser is delayed by 500 μs with respect to time zero. The delay time for firing the excimer is chosen to maximize the CS intensity as observed by photoionization. The CS_2 pulse has a width of ~ 1500 μs (FWHM) and its maximum is centered at ~ 1200 μs. The CS^+ ion pulses observed at 1068 Å and P_o = 520, 1150, and 1550 Torr are shown in Fig. 1(b), 1(c), and 1(d), respectively. The accumulation time for each spectrum is 5 min. The vertical scale indicates the actual counts of various channels (channel width = 10 μs). The two peaks at 520 and 630 μs indicated by arrows in Fig. 1(b), which are also found in Figs. 1(c) and 1(d), are attributed to background CS^+ resulting from the ionization effects of the excimer laser. These two peaks are the only feature observed in the TOF spectrum when the VUV photoionization light source is off.[16] The CS pulse observed in Figs. 1(b)-1(d) is ~ 800 μs wide (FWHM) and peaks at nearly the same position as the parent CS_2 pulse. The observed width of the CS pulse is greater than that expected based on the spacial distribution (~ 6 mm) of the photodissociation region and the laser pulse width (~ 8 ns). Since CS molecules initially formed by 193 nm photodissociation of CS_2 have substantial kinetic energies, the greater width of the CS pulse may be attributed to collisions of hot

Figure 1. (a) TOF spectrum of CS_2 showing the CS_2 pulsed beam profile observed at 1068 Å and P_o = 1150 Torr. Part (b), (c), and (d) show the TOF spectra for CS observed at 1068 Å and P_o = 520 Torr, P_o = 1150 Torr, and P_o = 1550 Torr, respectively. For (b), (c), and (d), the firing of the excimer laser is delayed by 500 μs with respect to the trigger pulse for opening the pulsed valve. The excimer pulse energy is 25 mJ and the accumulation time for each spectrum is 5 min.

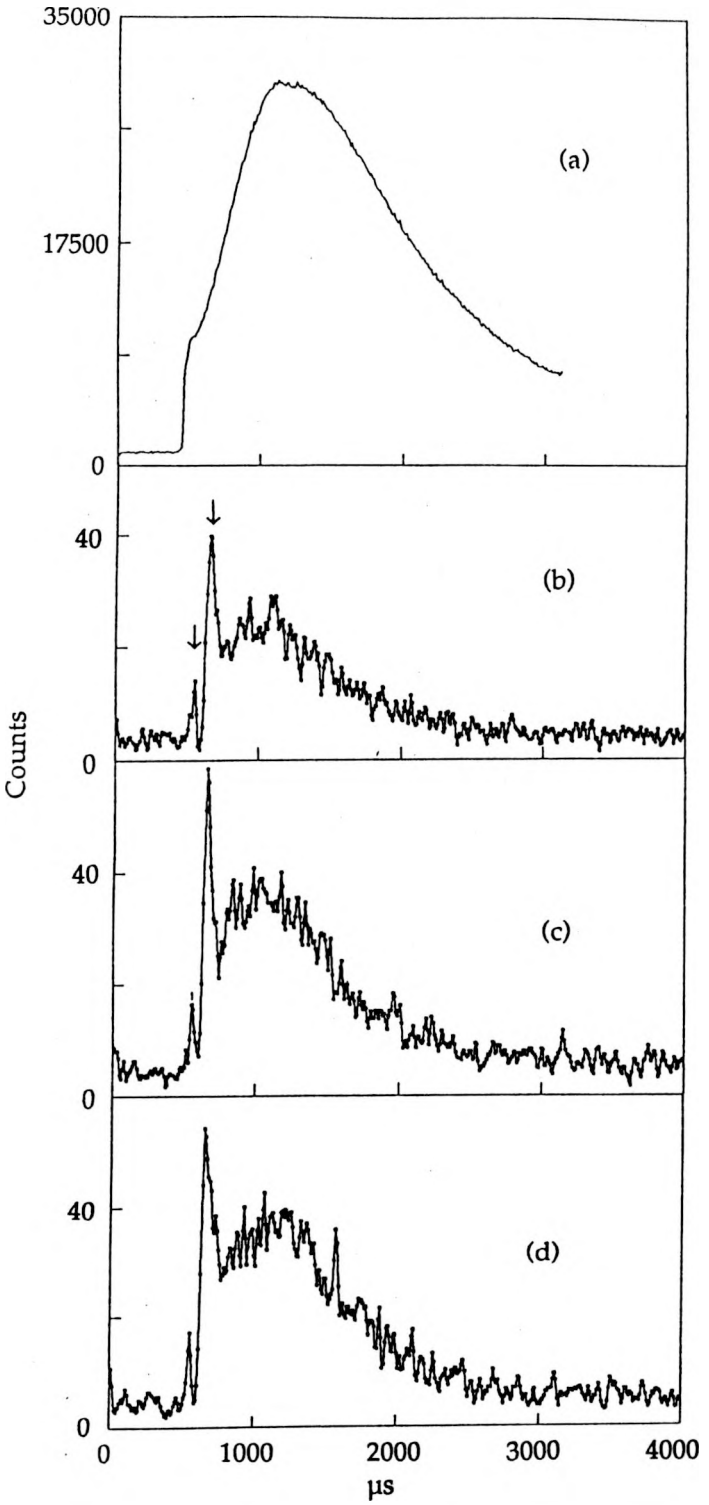
35000
17500
0
(a)
40
0
(b)
40
0
(c)
40
0
(d)
Counts
0
1000
2000
3000
4000
μs

CS molecules with Ar and cold CS_2 molecules in the free jet. This interpretation implies that the density of the free jet is sufficiently high and the pulse width sufficiently wide for complete trapping and cooling of the hot CS molecules produced by photodissociation. The higher intensities for CS observed at P_o = 1150 and 1550 Torr [Figs. 1(c) and 1(d)] compared to that at P_o = 520 Torr [Fig. 1(b)] are consistent with this rationalization.

In order to avoid the CS^+ background due to the excimer laser, the CS^+ ion counts resulting from photoionization of CS and background counts of the ion detector are measured by gating the scaler in the temporal range 0.9-3.9 ms. The background counts of the ion detector are measured by gating the scaler in the range 5.9-8.9 ms. The PIE spectrum for CS in the region of 1000-1100 Å is depicted in Fig. 2. The adiabatic IE for CS is determined to be 11.323 ± 0.010 eV (1095 ± 1 Å), in good agreement with values obtained in previous PE spectroscopic studies.[4-6] The observation that PIEs for CS^+ are in the noise level at photon energies below the IE indicates that CS molecules sampled in the photoionization region have negligible internal energies.

Autoionization features resolved in the PIE spectrum of CS are stronger than those observed in the PIE spectrum of CO measured using the same wavelength resolution.[17] The strong autoionization features resolved near the ionization threshold can be grouped into vibrational progressions I and II which have an average vibrational spacing of 1030 and 1010 cm^{-1}, respectively. These progressions most likely originate from Rydberg states converging to the second ($\tilde{A}^2\Pi$) and third ($\tilde{B}^2\Sigma$) ionization limits of CS^+. The vibrational spacings for the $CS^+(\tilde{A}^2\Pi)$ and $CS^+(\tilde{B}^2\Sigma)$ states are determined to be 970 and 870 cm^{-1}, respectively, by PE spectroscopic studies.[4,6] The slightly greater vibrational spacings for

Figure 2. PIE spectrum for CS in the region of 1000-1100 Å obtained at P_o = 1150 Torr and using a laser pulsed energy ~ 20 mJ. The accumulation time at each data point is 60 s.

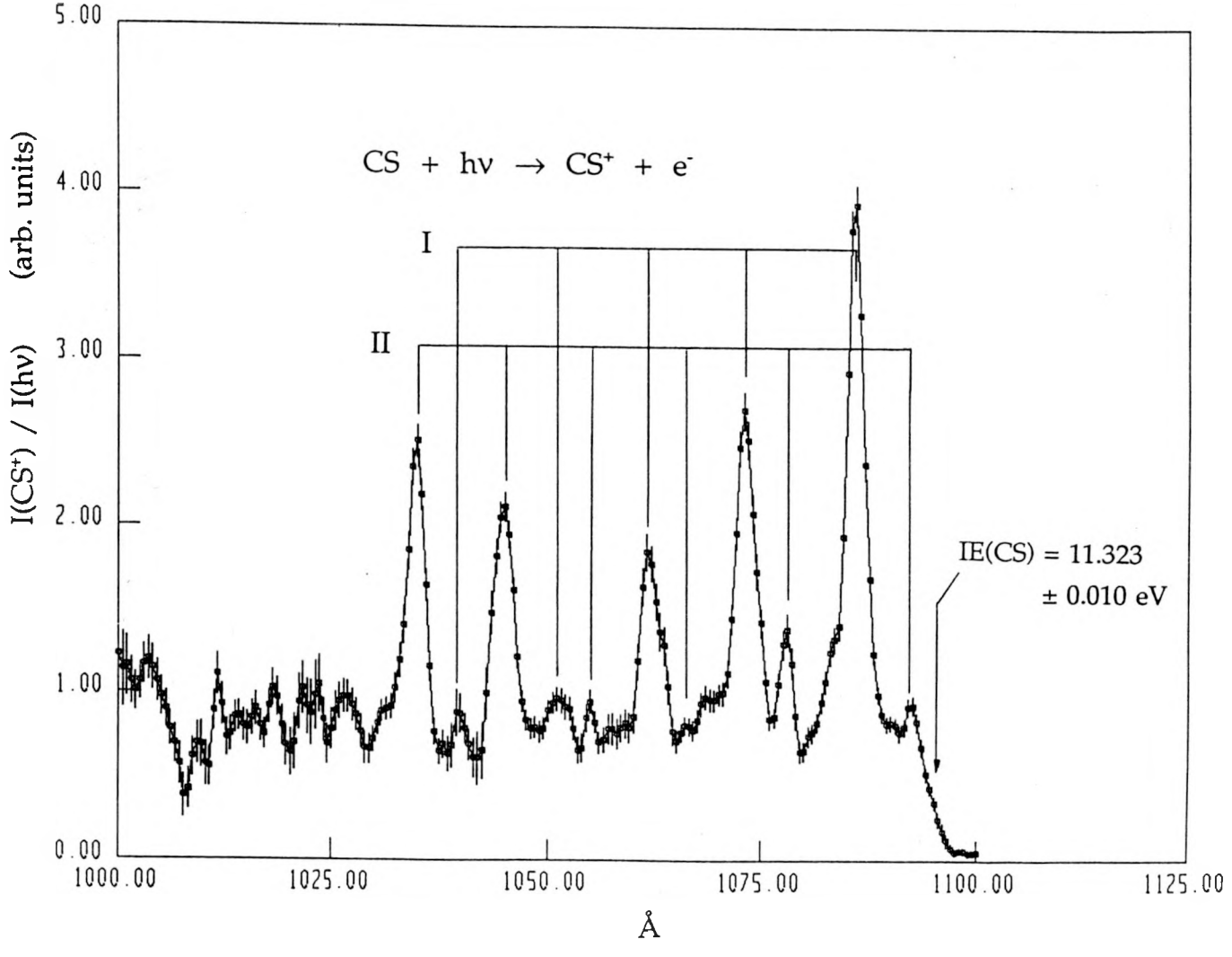
5.00
4.00
3.00
2.00
1.00
0.00
I(CS+) / I(hν) (arb. units)
CS + hν → CS+ + e-
I
II
IE(CS) = 11.323
± 0.010 eV
1000.00
1025.00
1050.00
1075.00
1100.00
1125.00
Å

the Rydberg states compared to the ionic states are consistent with the bonding nature of the 2π and 6σ molecular orbitals for CS.[6] The high resolution PIE spectrum of CO reveals complex autoionization structures.[18] Detailed assignments of the autoionization structure of CS require a photoionization study of CS at higher resolution. A high resolution PIE spectrum for CS can be made by increasing the laser pulse energy and the repetition rate of the pulsed beam and excimer laser. At a repetition rate of 500 Hz, the radical beam is predicted to have a duty factor of 0.5, which is close to a pseudocontinuum. Such a radical source will make possible the photoelectron-photoion coincidence measurements of cold radicals.[19]

REFERENCES

1. J. Berkowitz and B. Ruscic, "Photoionization Mass Spectrometric Studies of Free Radicals", in "Vacuum Ultraviolet Photoionization and Photodissociation of Molecules and Clusters", edited by C. Y. Ng (World Scientific Co., New Jersey, 1991).

2. M. C. R. Cockett, J. M. Dyke, and H. Zamanpour, "Photoelectron Spectroscopy of Short-Lived Molecules", in "Vacuum Ultraviolet Photoionization and Photodissociation of Molecules and Clusters", edited by C. Y. Ng (World Scientific Co., New Jersey, 1991).

3. C. Y. Ng, "Molecular Beam Photoionization and Photoelectron-Photoion Coincidence Studies of High Temperature Molecules, Transient Species, and Clusters", in "Vacuum Ultraviolet Photoionization and Photo-dissociation of Molecules and Clusters", edited by C. Y. Ng (World Scientific Co., New Jersey, 1991).

4. N. Jonathan, A. Morris, M. Okuda, D. J. Smith, and K. J. Ross, Chem. Phys. Lett. 13, 334 (1972); N. Jonathan, A. Morris, M. Okuda, K. J. Ross, and D. J. Smith, Faraday Discuss. Chem. Soc. 54, 48 (1972).

5. G. H. King, H. W. Kroto, and R. J. Suffolk, Chem. Phys. Lett. 13, 457 (1972).

6. D. C. Frost, S. T. Lee, and C. A. McDowell, Chem. Phys. Lett. 17, 153 (1972).

7. A value of 11.33 ± 0.01 for the IE of CS obtained by photoionization was given in J. Drowart, J. Smets, J. C. Reynaert, and P. Coppens, Adv. Mass Spectrom. 7A, 647 (1978). However, the PIE spectrum of CS was no reported.

8. H. Okabe, "Photochemistry of Small Molecules" (Wiley, New York, 1978).

9. M. N. R. Ashfold and J. E. Baggott, eds., "Molecular Photodissociation Dynamics" (Royal Society of Chemistry, London, 1987).

10. W.-B. Tzeng, H.-M. Yin, W.-Y. Leung, J.-Y. Luo, S. Nourbakhsh, G. D. Flesch, and C. Y. Ng, J. Chem. Phys. 88, 1658 (1988).

11. S. Yang, A. Freedman, M. Kawasaki, and R. Bersohn, J. Chem. Phys. 72, 4080 (1980).

12. V. R. McCrary, R. Lu, D. Zakheim, J. A. Russell, J. B. Halpern, and W. M. Jackson, J. Chem. Phys. 83, 3481 (1985).

13. I. M. Waller and J. W. Hepburn, J. Chem. Phys. 87, 3261 (1987).

14. Y. Ono, S. H. Linn, H. F. Prest, M. E. Gress, and C. Y. Ng, J. chem. Phys. 73, 2523 (1980).

15. C. Y. Ng, Adv. Chem. Phys. 52, 265 (1983).

16. The background ion peak appearing at 520 μs is believed to be the result of ionization processes occurring at the photoionization region due to scattered laser light. The second background peak at 630 μs is mostly likely caused by ionization events of highly energetic species formed in the beam due to the interaction of CS_2 molecules and the excimer laser.

17. S. H. Linn, Y. Ono, and C. Y. Ng, J. Chem. Phys. 74, 3342 (1981).

18. J. Berkowitz, "Photoabsorption, Photoionization, and Photoelectron Spectroscopy" (Academic Press, New York, 1979), p. 227.

19. K. Norwood and C. Y. Ng, Chem. Phys. Lett. 156, 145 (1989).

SECTION VII.

PHOTOIONIZATION STUDY OF SUPERSONICALLY COOLED POLYATOMIC RADICALS: HEAT OF FORMATION OF CH_3S^+

INTRODUCTION

The stability of the mercaptomethyl ion, $CH_2{=}SH^+$ (**1**), and the thiomethoxy ion, CH_3-S^+ (**2**), have been the subject of numerous experimental[1-16] and theoretical[1,17-21] studies. A collisional activation experiment[1] of Dill and McLafferty indicates that both these isomers are stable and that (**1**) is more stable than (**2**). This conclusion is supported by a high level ab initio study of Radom and co-workers,[17] predicting that the singlet $CH_2{=}SH^+(^1A')$ lies > 27 kcal/mol below the triplet CH_3-$S^+(^3A_1)$. Despite all this activity, the value for $\Delta H_{f0}(CH_3S^+)$ has not been measured. In this communication, we report a photoionization study of supersonically cooled CH_3S, which yields a value of 9.225 ± 0.014 eV for the ionization energy (IE) of $CH_3S(^2E_{3/2})$[22] to (**2**).

The photoionization apparatus used has been described in detail.[23,24] A pulsed beam of CH_3SCH_3 (vapor pressure ~ 400 Torr) seeded in Ar is produced by supersonic expansion through a pulsed valve with a nozzle diameter of 0.5 mm and a total stagnation pressure (P_o) of 1150 Torr. The pulsed valve is operated at 40 Hz. The ArF laser beam is mildly focussed to a pencil shape (cross section area ~ 2 x 6 mm^2) before intersecting the CH_3SCH_3 jet at 90° and ~ 2 mm from the nozzle tip. The gas beam is skimmed by a conical skimmer before entering the photoionization region. The photoionization wavelength resolution used is 1.5 Å (FWHM).

RESULTS AND DISCUSSION

Figure 1(a) shows the temporal profile of the CH_3SCH_3 pulsed beam recorded by a multichannel scaler after photoionization at 1280 Å. Time zero of the time-of-flight (TOF) spectrum corresponds to the initiation of the trigger pulse for opening the pulsed valve. The triggering pulse for firing the excimer laser is delayed by 500 μs with respect to time zero.[25] The CH_3S and CH_3 TOF spectra observed at 1250 Å for laser pulse energies of 60 and 35 mJ are shown in Figs. 1(b) and 1(c), respectively. The accumulation time for each spectrum is 5 min. The vertical scale indicates the actual counts of various channels (channel width = 10 μs). The peaks indicated by arrows in Figs 1(b) and 1(c) are identified as background ions caused by the excimer laser alone.[26] In order to avoid these background ions, ion counts resulting from photoionization of CH_3S and CH_3 are measured by gating the scaler in the range 0.9-2.9 ms. The observed widths [~ 800 μs (FWHM)] for the CH_3S and CH_3 TOF spectra are lower than that [~ 1500 μs (FWHM)] of the CH_3SCH_3 spectrum, but are greater than that expected based on the spacial distribution (~ 6 mm) of the photodissociation region and the laser pulse width (~ 8 ns). Since the radicals initially formed by photodissociation have substantial kinetic energies, the greater than expected width may be attributed to the collisions of translationally hot radicals with Ar and CH_3SCH_3 molecules in the jet. Using similar expansion conditions, photoionization efficiency (PIE) spectra for SO[27] and CS[28] prepared by 193 nm laser photodissociation[29,30] of SO_2 and CS_2, respectively, show that SO and CS

Figure 1. (a) TOF spectrum of CH_3SCH_3 showing the CH_3SCH_3 pulsed beam profile observed at 1280 Å and P_o = 1150. Part (b) and (c) show TOF spectra of CH_3S and CH_3 observed at 1250 Å and P_o = 1150 Torr for laser energies of 60 and 35 mJ, respectively. For (b) and (c), the firing of the excimer laser is delayed by 500 μs. The accumulation time for each spectrum is 5 min.

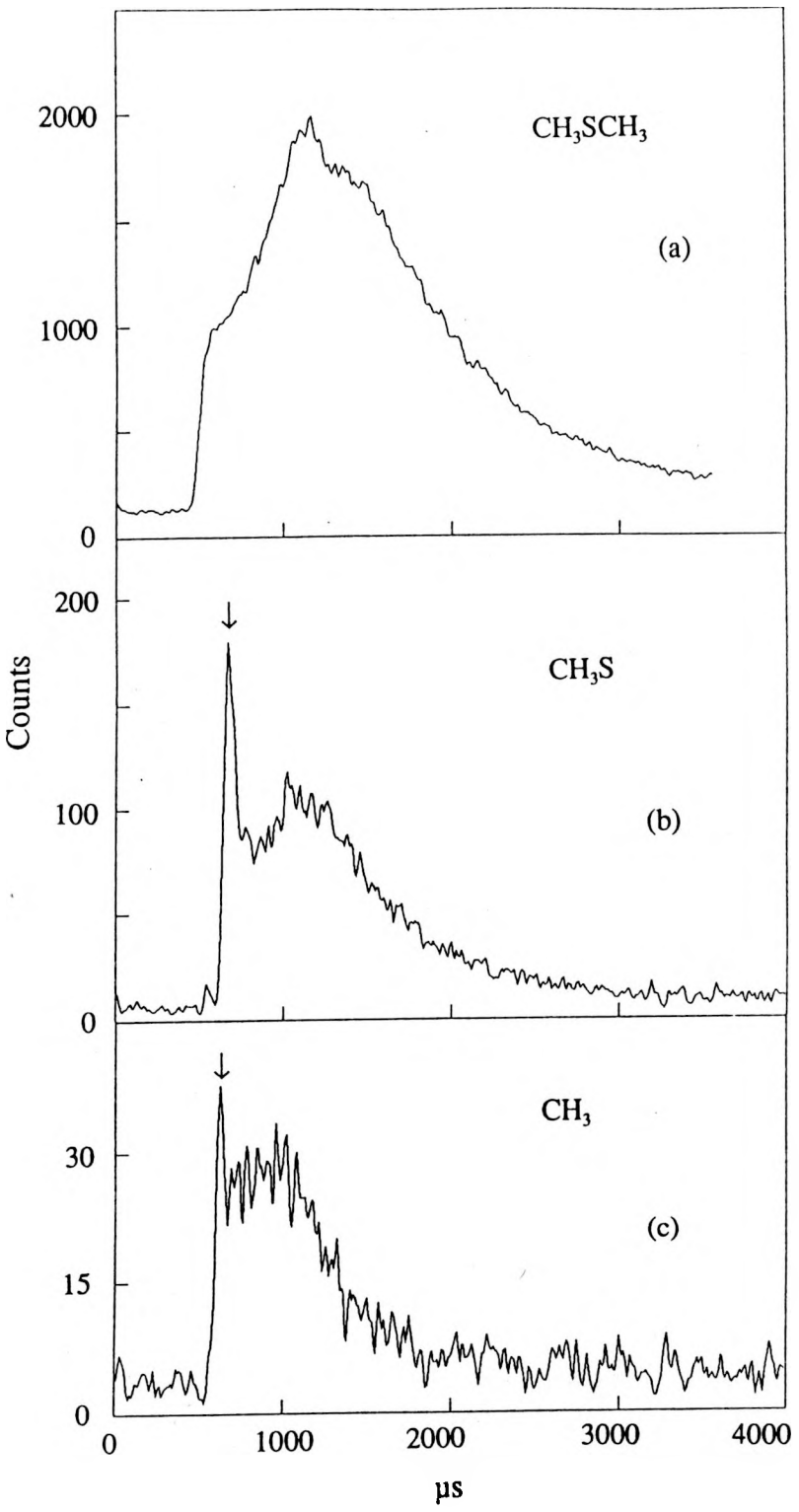
2000
1000
0
CH_3SCH_3
(a)
200
100
0
CH_3S
(b)
30
15
0
CH_3
(c)
Counts
0
1000
2000
3000
4000
μs

sampled in the photoionization region are in the v = 0 states.

The PIE spectra for CH_3S^+ from CH_3S and for CH_3S^+ from CH_3SCH_3 measured in the range of 1200-1470 and 1020-1150 Å are depicted in Fig. 2. The threshold for the formation of CH_3S^+ from CH_3SCH_3 is 1049 Å.[16,31,32] Therefore, the CH_3S^+ observed at wavelength > 1200 Å are due to the photoionization of CH_3S. The PIE spectra for CH_3^+ from CH_3 and for S^+ from S[33] near their thresholds are also shown in the figure. The observed IE of CH_3 and S are consistent with the literature values.[34,35] Since the photoionization of CH_3S involves the removal of an essentially non-bonding electron from S, the threshold is expected to be sharp. As the photon energy is increased, the PIE for CH_3S^+ is found to rise rapidly at 1344 ± 2 Å, which is interpreted as the IE for CH_3S to form (**2**). Based on the recent energy release measurements, $\Delta H_{f0}(CH_3S)$ is determined to be 35.2 ± 1.5 kcal/mol.[16,32] Using this value and the IE for SCH_3 to (**2**), we arrive at a value of 247.9 ± 1.5 kcal/mol for $\Delta H_{f0}(CH_3S^+)$. The literature value for $\Delta H_{f0}(CH_2SH^+)$ is 206-209 kcal/mol.[4,9,16,36] The finding that $\Delta H_{f0}(CH_3S^+)$ is greater than $\Delta H_{f0}(CH_2SH^+)$ by 39-41 kcal/mol is consistent with the theoretical prediction of > 27 kcal/mol.[17]

The PIE of CH_3S in the range of 1344-1470 Å is small and decreases slowly toward lower photon energy, indicating that the Franck-Condon factor for photoionization to the mercaptomethyl ion is unfavorable.

Figure 2. PIE spectra for CH_3S^+ from CH_3S and CH_3SCH_3, for CH_3^+ from CH_3 and for S^+ from S. CH_3S, CH_3, and S are the result of the 193 nm laser (pulse energy = 60 mJ) photolysis of CH_3SCH_3.

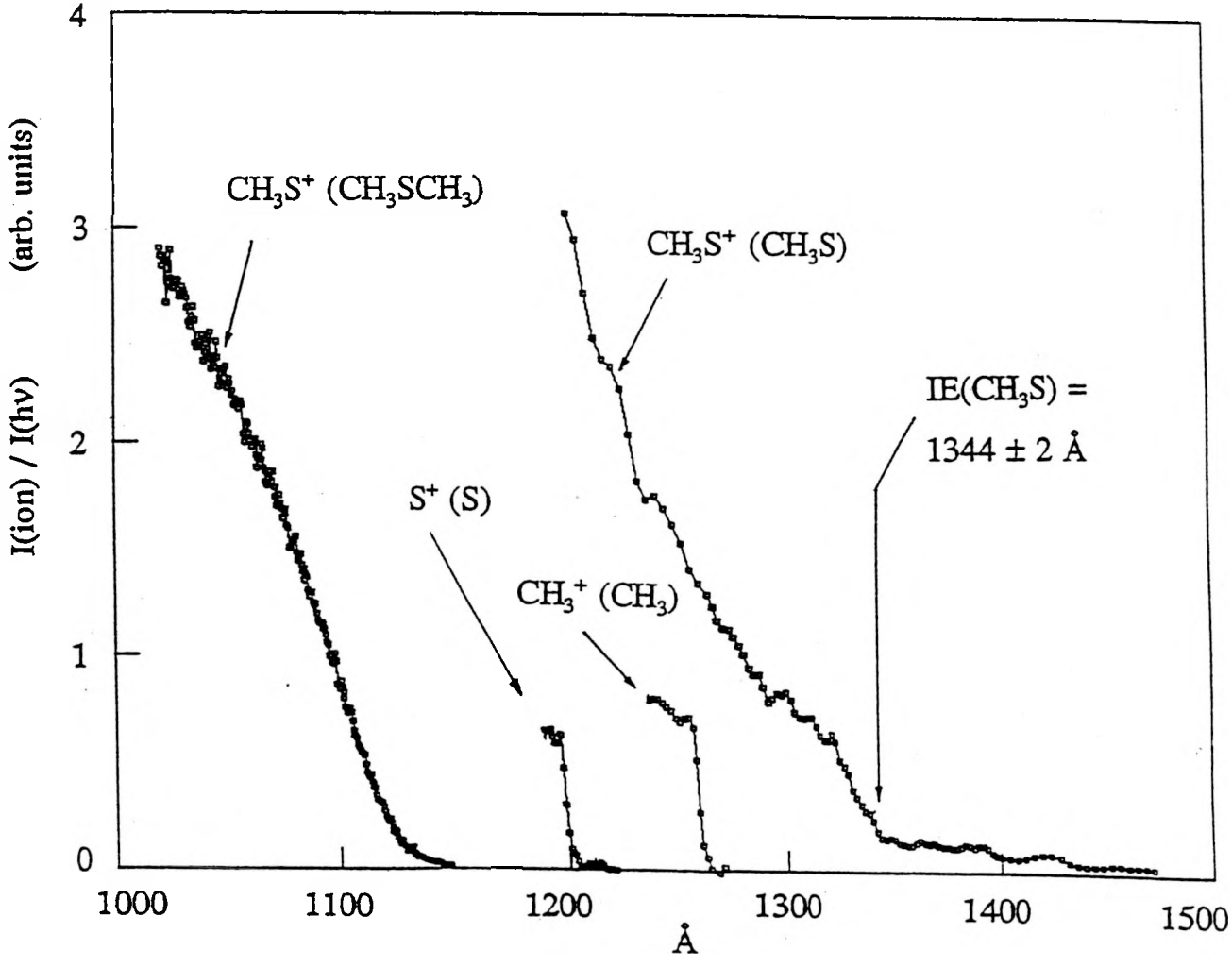
4
3
2
1
0
I(ion) / I(hν) (arb. units)
CH3S+ (CH3SCH3)
CH3S+ (CH3S)
IE(CH3S) =
1344 ± 2 Å
S+ (S)
CH3+ (CH3)
1000
1100
1200
1300
1400
1500
Å

REFERENCES

1. J. D. Dill and F. W. McLafferty, J. Am. Chem. Soc. 100, 2907 (1977); ibid. 101, 6526 (1979).

2. A. G. Harrison, J. Am. Chem. Soc. 101, 4911 (1978).

3. J. R. Gilbert, P. A. M. von Koppen, W. T. Huntress, M. T. Bowers, Chem. Phys. Lett. 82, 455 (1981).

4. M. Roy and T. B. McMahon, Org. Mass Spectrom. 17, 392 (1982).

5. B. G. Hobrock and R. W. Kiser, J. Phys. Chem. 67, 1283 (1963).

6. J. L. Franklin and H. E. Lumpkin, J. Am. Chem. Soc. 74, 1023 (1952).

7. T. F. Palmer and F. P. Lossing, J. Am. Chem. Soc. 84, 4661 (1962).

8. R. W. Taft, R. H. Martin, and F. W. Lampe, J. Am. Chem. Soc. 87 2490 (1965).

9. J. J. Butler, T. Baer, S. A. Evans, J. Am. Chem. Soc. 105, 3451 (1983).

10. B. G. Gowenlock, J. Kay, and J. R. Mayer, Trans. Faraday Soc. 59, 2463 (1963).

11. B. G. Keyes and A. G. Harrison, J. Am. Chem. Soc. 90, 5671 (1968).

12. D. Amos, R. G. Gillis, J. L. Occolowitz and J. F. Pisani, Org. Mass Spectrom. 2, 209 (1969).

13. B.-O. Jonsson and J. Lind, J. Chem. Soc. Faraday Trans. 2, 70, 1399 (1974).

14. D. H. William and G. Hvistendahl, J. Am. Chem. Soc. 96, 6753 (1974).

15. R. E. Kutina, A. K. Edwards, and G. L. Goodman, J. Berkowitz, J. Chem. Phys. 77, 5508 (1982).

16. S. Nourbakhsh, K. Norwood, H.-M. Yin, C.-L. Liao, and C. Y. Ng, J. Chem. Phys., submitted.

17. R. H. Nobes, W. J. Bouma, and L. Radom, J. Am. Chem. Soc. 106, 2774 (1984).

18. F. Bernardi, I. G. Csizmadia, H. B. Schlegel, and S. Wolfe, Can. J. Chem. 53, 1144 (1975).

19. M.-H. Whangbo, S. Wolfe, and F. Bernardi, Can. J. Chem. 53, 3040 (1975).

20. T. Yamabe, K. Yamashita, K. Fukui, and K. Morokuma, Chem. Phys. Lett. 63, 433 (1979).

21. F. Bernardi, A. Bottoni, and N. A. Epiotis, J. Am. Chem. Soc. 100, 7205 (1978).

22. The CH_3S radical prepared by 193 nm laser photodissociation of CH_3SCH_3 has been characterized using the laser-induced fluorescence method. See M. Suzuki, G. Inoue, and H. Akimoto, J. Chem. Phys. 81, 5405 (1984). The vibronic structure of CH_3S has also been examined in a photodetachment experiment and an ab initio calculation. See B. K. Janousek and J. I. Brauman, J. Chem. Phys. 72, 694 (1980).

23. Y. Ono, S. H. Linn, H. F. Prest, and C. Y. Ng, J. Chem. Phys. 73, 2523 (1980).

24. C. Y. Ng, Adv. Chem. Phys. 52, 265 (1983).

25. The excimer laser delay time is chosen to maximize the CH_3S signal as observed by photoionization.

26. These peaks are the only feature in the TOF spectra when the photoionization light source is off.

27. K. Norwood, S. Nourbakhsh, G.-Z. He, and C. Y. Ng, unpublished results.

28. K. Norwood, S. Nourbakhsh, G.-Z. He, and C. Y. Ng, J. Chem. Phys., submitted.

29. The 193 nm laser photofragmentation TOF mass spectrometric study of SO_2 shows that the vibrational distribution of SO for v = 0, 1, 2, and 3 is 0.05:0.23:0.67:0.05. See P. Felder, C. S. Effenhauser, B. M. Haas, and J. R. Huber, Chem. Phys. Lett. 148, 417 (1988).

30. It is known that CS formed in 193 nm laser photofragmentation of CS_2 are in the CS(X, v = 0-13) states, corresponding to internal excitations up to 45 kcal/mol. See W.-B. Tzeng, H.-M. Yin, W.-Y. Leung, J.-Y. Luo, S. Nourbakhsh, G. D. Flesch, and C. Y. Ng, J. Chem. Phys. 88, 1658 (1988) and references therein.

31. M. E. Akopyan, Yu. L. Sergeev, and F. I. Vilesov, Khimiya Vysokikh Energil, 4, 305 (1970).

32. The theoretical study of Radom and co-workers suggests that the singlet $CH_2{=}SH^+(^1A')$ is formed exclusively at the dissociation thresholds from $CH_3SCH_3^+$ and $CH_3SSCH_3^+$. See Ref. 17.

33. Sulfur atoms are produced from 193 nm laser photodissociation of CH_3S. See Ref. 16.

34. W. A. Chupka and C. Lifshitz, J. Chem. Phys. 48, 1109 (1968).

35. S. G. Lias, J. E. Bartmess, J. F. Liebman, J. L. Homes, R. D. Levin, and W. G. Mallard, J. Phys. Chem. Ref. Data 17 Suppl. 1 (1988).

36. S. Nourbakhsh, C.-L. Liao, and C. Y. Ng, J. Chem. Phys. 92, 6587 (1990).

GENERAL CONCLUSION

In 193 nm photofragmentation study of CS_2 there are two energetically allowed channels:

$$CS_2 + h\nu\ (193\ nm) \rightarrow CS(X^1\Sigma^+) + S(^1D),$$

$$CS_2 + h\nu\ (193\ nm) \rightarrow CS(X^1\Sigma^+) + S(^3P).$$

The energies available for $S(^1D)$ and $S(^3P)$ channels have been determined to be 18.7 kcal/mol and 45.0 kcal/mol, respectively. Results calculated from the CS translational energy spectra yield a value of 2.6 for the $S(^3P)/S(^1D)$ branching ratio. This value is consistent with the value of 2.8 ± 0.3 determined by Waller et al[20] using the laser-induced fluorescence method. For photolysis energies between 25-150 mJ/pulse, the S and CS TOF spectra remain the same. Also the C.M. translational energy distribution of S and CS are in good accord. These two observations demonstrate that secondary photolysis of the CS photofragment to form $C(^3P) + S(^3P)$ within the laser pulse is negligible. The measured vibrational distribution for CS(X, v = 0-13) is peaked at v = 3 and the distribution is in agreement with the literature results.[20-22] Photofragments from CS_2 dimers and clusters are observed at small laboratory angles.

Using photofragment translational energy spectroscopy, the primary products in the 193 nm photofragmentation of CH_3SH, CH_3SCH_3, CH_3CH_2SH and CH_3SSCH_3 have been identified. From the onsets of translational energy distributions derived from the TOF data, bond dissociation energies are obtained. The bond dissociation energies determined

in these experiments compare well with the literature values as summarized in table 1. The TOF thresholds for S from the 193 nm photodissociation of SH and SCH_3 reveal that sulfur atoms are formed in the $S(^3P)$ + H and $S(^3P, ^1D)$ + CH_3 channels, respectively. These results are consistent with a recent resonant enhanced multiphoton ionization experiment. Table 2 lists the percent internal and translational energy partitioning among some photofragments. In general, as the size of molecule increases, the percent internal energy increases because there are more degrees of freedom in which to store the energy.

PEPICO spectra have been measured for $CH_3SCH_3^+$, $CH_3SCH_2^+$, CH_3S^+, CH_2S^+ resulting from ionization of CH_3SCH_3, and for CH_3SH^+, CH_3S^+, CH_2S^+ resulting from ionization of CH_3SH. The PEPICO spectra for these ions provide accurate information for ionization and appearance energies, and for the unimolecular decomposition of energy-selected ions. By incorporating the results from photoionization and photodissociation experiments the ionization energy for CH_3S radical has been estimated to be 7.5 eV.

In a new experiment, a laser photolysis radical source has been combined with a VUV photoionization apparatus to study the energetics of free radicals. A high repetition rate ArF excimer laser beam photodissociates molecules at the tip of a pulsed valve. The cold fragments are skimmed before entering the ionization region. Using this method we have successfully obtained a PIE spectra for S, CS, CH_3 and SCH_3 radicals. This experiment can further be modified by incorporating the PEPICO method, and new information on the vibronic states of radical ions can be obtained.

Table 1. Bond dissociation energies for some sulfur molecules

Bond dissociation energies	This work (kcal/mol)	Literature values[a] (kcal/mol)
SC-S	104.1	103.4
CH_3-SH	74.5	75.0
CH_3S-H	91.5	92.0
CH_3S-CH_3	77.3	77.0
CH_3SCH_2-H	93	-
CH_3CH_2-SH	74.5	72.0
CH_3CH_2S-H	92	92
CH_3-CH_2SH	~ 100	-
CH_3S-SCH_3	74.8	74
CH_3SS-CH_3	57.4	57.0
SS-CH_3	46.5	47.5

[a]Reference 23.

Table 2. Energy partitioning among some photofragments

Bond	$E_{available}$ (kcal/mol)	% $E_{c.m.}$	% E_{int}
CH_3-SH	75.5	70	30
CH_3S-CH_3	73.0	58	42
CH_3CH_2-SH	75.5	46	54
CH_3SS-CH_3	92.9	48	52

REFERENCES

1. A. M. Wodtke and Y. T. Lee, "Molecular Photodissociation Dynamics", edited by M. N. R. Ashfold and J. E. Baggott (Royal Society of Chemistry, London, 1987).

2. W.-B. Tzeng, H.-M. Yin, W.-Y. Leung, J.-Y. Luo, S. Nourbakhsh, G. D. Flesch, and C. Y. Ng, J. Chem. Phys. 88, 1658 (1988).

3. K. E. Holdy, L. C. Klotz, and K. R. Wilson, J. Chem. Phys. 52, 4588 (1970).

4. M. Shapiro and R. D. Levine, Chem. Phys. Lett. 5, 499 (1970).

5. M. Shapiro, J. Chem. Phys. 56, 2582 (1972).

6. M. Shapiro, Israel J. Chem. 11, 691 (1973).

7. C. E. Chaplan and M. S. Child, Mol. Phys. 23, 249 (1972).

8. M. J. Berry, Chem. Phys. Lett. 27, 73 (1974); 29, 329 (1974); 61, 3114 (1974).

9. G. A. West and M. J. Berry, J. Chem. Phys. 61, 4700 (1974).

10. S. Mukamel and J. Jortner, J. Chem. Phys. 65, 3735 (1976).

11. G. E. Busch, J. F. Cornelius, R. T. Mahoney, R. I. Morse, D. W. Schlosser, and K. R. Wilson, Rev. Sci. Instrum. 41, 1066 (1970).

12. G. E. Busch and K. R. Wilson, J. Chem. Phys. 56, 3626 (1972); 56, 3638 (1972).

13. A. M. Wodtke and Y. T. Lee, J. Phys. Chem. 89, 4744 (1985).

14. S. Nourbakhsh, C.-L. Liao, and C. Y. Ng, J. Chem. Phys. 92, 6589 (1990).

15. C. C. Hayden, D. M. Neumark, K. Shobatake, R. K. Sparks, and Y. T. Lee, J. Chem. Phys. 76, 3607 (1982).

16. S. Nourbkhsh, K. Norwood, H.-M. Yin, C.-L. Liao, and C. Y. Ng, J. Chem. Phys. submitted.

17. S. Nourbkhsh, K. Norwood, H.-M. Yin, C.-L. Liao, and C. Y. Ng, J. Chem. Phys. submitted.

18. H. B. Rayner and F. E. Murray, Pulp Pap. Mag. Can. 71, 75 (1970).

19. M. D. Bentley, I. B. Douglass, J. A. Lacadie, and D. R. Whittier, J. Air Pollut. Contr. Ass. 22, 359 (1972).

20. I. M. Waller and J. W. Hepburn, J. Chem. Phys. 87, 3261 (1987).

21. J. B. Butler, W. S. Drozdoski, and J. R. McDonald, Chem. Phys. 50, 413 (1980).

22. S. Yang, A. Freedman, M. Kawasaki, and R. Bersohn, J. Chem. Phys. 72, 4048 (1980).

23. R. Benson, Chem. Rev. 78, 23 (1978) and references therein.

APPENDIX A.

TRANSFORMATION OF LABORATORY INFORMATION TO CENTER OF MASS

Transformation of Laboratory (lab) Distribution to Center of Mass (C.M.) Distribution

The relationship between C.M. ($I_{c.m.}$) and laboratory (I_{lab}) flux per unit solid angle per unit velocity is given by

$$I_{c.m.}(U, \theta_{c.m.}) = U^2/V^2 \, I_{lab}(V, \theta_{lab}),$$

where U is the C.M. velocity, V is the laboratory velocity, $\theta_{c.m.}$ is the C.M. angle, and θ_{lab} is the lab angle.

Since an electron impact ionizer is sensitive to number density and not flux, the lab signal (N_{lab}) is given by

$$N_{lab}(V, \theta_{lab}) = V/U^2 \, I_{c.m.}(U, \theta_{c.m.}).$$

Because the lab signal is measured as a function of time (t), it must be converted to center of mass as a function of energy ($E_{c.m.}$). This is accomplished by the following transformation:

$$\underline{I_{c.m.}(E_{c.m.}, \theta_{c.m.}) \propto t^3 \, U \, N_{lab}(t, \theta_{lab}).}$$

Transformation of Recoil Velocity to Center of Mass Energy ($E_{c.m.}$)

In order to interpret the data one must transform the recoil velocity of the fragment in the laboratory frame (V_{lab}) to recoil velocity in the C.M. frame ($V_{c.m.}$). This transformation is necessary in order to take into account the effect of the parent beam velocity (V_{par}) since,

$$\vec{V}_{c.m.} = \vec{V}_{lab} - \vec{V}_{par}.$$

Velocity diagram:

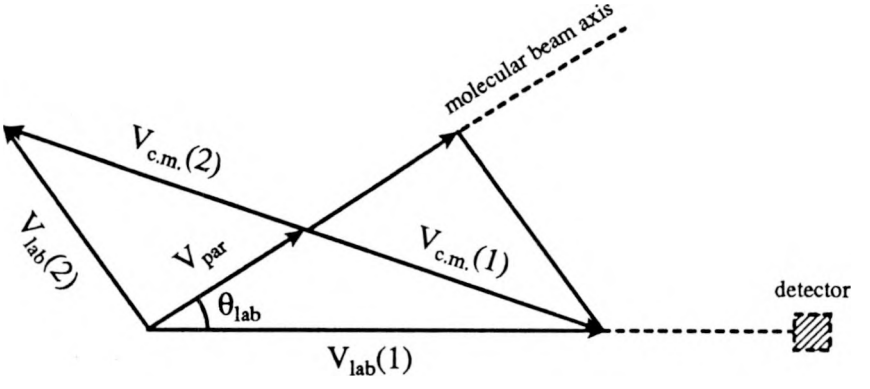

In a photofragmentation experiment one measures V_{lab}, and V_{par}. From conservation of energy,

$$E_{c.m.} + E_{int} = E_{par} + h\nu(193\ nm) - D_o,$$

where $E_{c.m.}$ and E_{int} are the total C.M. and internal energy of the photofragments and E_{par} and D_o are the initial parent energy (~ 0) and bond dissociation energy. From V_{lab}, V_{par}, and θ_{lab} one can determine $E_{c.m.}$, and therefore D_o, since E_{int} is zero in the threshold region of the time of flight spectrum.

APPENDIX B.

SELECTED COMPUTER PROGRAMS

```
C*****************************************************************
C
C      FILENAME: CONV.FOR
C
C      CONV.FOR IS A PROGRAM FOR TOF TO ENERGY CONVERSION
C
C      THIS PROGRAM MAKES CALCULATION FOR WHICHEVER FRAGMENT
C      LABELED MASSA, AND READS THE FIRST 1022 NUMBERS.  ALSO A
C      FOR009.DAT FILE IS GENERATED AT THE END OF PROGRAM FOR
C      PLOTTING PURPOSES.
C
C      THIS PROGRAM USES 2 PEN FOR PLOTTING (USING HGRAPH).
C
C*****************************************************************
C
C      ANGCM  = ANGLE BETWEEN FRAGMENT BEAM AND DETECTOR AXIS
C      IN C.M. FRAME, IN "DEGREE".
C      ANGLAB = ANGLE BETWEEN NOZZLE BEAM AXIS AND DETECTOR
C      AXIS, IN "DEGREE".
C      BAKAVG = AVERAGED NEMBER OF BACHGROUND CHANNELS FOR
C      BACKGROUND SUBTRACTION.
C      DRIFT  = ION DRIFT TIME AT THAT PARTICULAR MASS IN
C      "MICROSECONDS".
C      DWELL  = DWELL TIME PER CHANNEL IN TIME-OF-FLIGHT DATA,
C      IN "MICROSECOND PER CHANNEL".
C      ENGYCM = KINETIC ENERGY OF FRAGMENTS IN C.M. FRAME IN
C      "KCAL/MOL".
C      INTENS = FRAGMENT FLUX IN C.M. FRAME IN "(COUNTS)(CM)
C      (MICROSECOND**2)".
C      PATH   = PRODUCT FLIGHT PATH, IN "CENTIMETER".
C      RDMASS = REDUCED MASS OF SYSTEM, IN "A.M.U.".
C      VELBM  = PARENT BEAM VELOCITY OBTAINED FROM TIME OF FLIGHT
C      MEASUREMENTS, IN "CENTIMETER/SECOND".
C      VELLAB = FRAGMENT BEAM VELOCITY IN "CM/S".
C
C-----------------------------------------------------------------

      REAL*4 MASSFA, MASSFB
      REAL*4 Y(2100), ENGYCM(1050), INTENS(1050), Q2(2), S2(2)
      CHARACTER*30 HEAD
      BYTE  DATE(16), DATVAX(16)
      CHARACTER*47 COMM
```

```
C     CONSTANT C1 IS THE AVOGADRO'S NUMBER.
C     CONSTANT C2 IS A ANGLULAR CONVERSION FACTOR FROM RADIAN
C     TO DEGREE.
C     CONSTANT C3 IS A ENERGY CONVERSION FACTOR FROM ERG TO
C     KCAL/MOL.
      DATA Q2(1),Q2(2),S2(1),S2(2)/-1000,1000,0,0/
      C1 = 6.022045E+23
      C2 = 57.29578
      C3 = 1.43956E+13

      OPEN(UNIT=33, NAME='CONV.PAR', TYPE='OLD')

      READ  (33,35) COMM
35    FORMAT (//,A47)
      READ  (33,40) HEAD
40    FORMAT (A30)
      READ  (33,*)  MIK
      READ  (33,50) DATE
50    FORMAT (16A1)
      READ  (33,*)  IVAX
      READ  (33,50) DATVAX
      READ  (33,*)  ISU
      READ  (33,*)  ISP
      READ  (33,*)  IC
      READ  (33,*)  ID
      READ  (33,*)  XMAX, XMIN, XTIC, YMAX, YMIN, YTIC
      READ  (33,*)  ITC1, ITC2
      READ  (33,*)  IEC
      READ  (33,*)  IPTAVG
      READ  (33,*)  ANT
      READ  (33,*)  SP
      READ  (33,*)  ANGLAB
      READ  (33,*)  MASSFA, MASSFB
      READ  (33,*)  IFIRST, ILAST
      READ  (33,*)  DWELL
      READ  (33,*)  DRIFT
      READ  (33,*)  PATH
      READ  (33,*)  VELBM

      CLOSE (UNIT=33)

C     DECIDING TO USE THE TERMINAL OR THE PRINTER.
      KE=6
```

```
      IF (ISP.EQ.2) KE=7

      OPEN(UNIT=22, NAME=DATE, READONLY, TYPE='OLD')

C     READING THE DATA VALUE
      IX=1
      JJ=10
      DO 30 JB=1,103
      IF (JB.NE.103) GOTO 10
      JJ=1022
10    READ (22,*,ERR=10) LXY, (Y(I), I=IX, JJ)
      IX=IX+10
      JJ=JJ+10
30    CONTINUE

C     READ (22,*) (Y(I), I=1, 1022)

      CLOSE (UNIT=22)

      IF (IPTAVG.EQ.0) GOTO 55
C     MUST MAKE SURE THE NUMBER OF CHANNEL READ MATCHES 1022
C     IN SMOOFT
      CALL SMOOFT(Y,1022,IPTAVG)

55    RDMASS = MASSFA * MASSFB / (MASSFA + MASSFB)

      BAKSUM = 0.
      DO 60 I = IFIRST,ILAST
      BAKSUM = BAKSUM + Y(I)
60    CONTINUE
      BAKAVG = BAKSUM / (ILAST-IFIRST+1)

      BIG=0.
      VBIG=0
      ICON=0
      SENG=1.0E+10
      DO 70 I = 1 , IEC
      DATA = Y(I) - BAKAVG
C     SUBTRACTING 2.0 IS BECAUSE OF QUESTEK DELAY BEFORE IT FIRES.
      TIME =(I * DWELL) - DRIFT - 2.0
      IF (TIME .GT. 0.) THEN
      VELLAB = (PATH / TIME) * 1.0E+6
      VELCMY = VELLAB * SIN(ANGLAB/C2)
```

```
      VELCMX =(VELLAB * COS(ANGLAB/C2)) - VELBM
      ANGCM = ATAN2(VELCMY,VELCMX) * C2
      VELCM = SQRT(VELCMX**2 + VELCMY**2)
      INTENS(I) = (TIME**3) * VELCM * DATA * 1.0E+6
      VEL=VELCM*(MASSFA+MASSFB)/MASSFB
C     CALCULATING THE BOND ENERGY.(193 NM=147.9 KCAL/MOL)
C     ENGYCM(I)=147.9-(.5*C3*(RDMASS/C1)*(VEL**2))
      ENGYCM(I)=(.5*C3*(RDMASS/C1)*(VEL**2))
C     FINDING THE SMALLEST ENERGY AND ITS CORRESPONDING
C     CHANNEL AND INTENSITY.(TO FIND OUT WHEN FOLDING STARTS.)
      IF (ENGYCM(I) .LT. SENG) THEN
      SENG=ENGYCM(I)
      SINT=INTENS(I)
      JU=I
      ENDIF
C     FINDING THE LARGEST ENERGY AND ITS CORRESPONDING CHANNEL
      IF (ENGYCM(I) .GT. VBIG) THEN
      VBIG=ENGYCM(I)
      IVC=I
      ENDIF
C     FINDING THE LARGEST INTENSITY AND ITS CORRESPONDING
C     ENERGY.
      IF (INTENS(I) .GT. BIG)  THEN
      BIG =INTENS(I)
      BENG=ENGYCM(I)
      KZ=I
      ENDIF
      ELSE
C     GETTING RID OF VALUES WITH NEGATIVE TIME, RESULTED FROM
C     DRIFT TIME.
      ICON=ICON+1
      ENGYCM(I)=1.0E+10
      INTENS(I)=0.
      ENDIF
70    CONTINUE

      WRITE (KE,700) DATE
      WRITE (KE,702) COMM
      WRITE (KE,705) MASSFA, MASSFB
      WRITE (KE,710) DWELL
      WRITE (KE,720) DRIFT
      WRITE (KE,730) PATH
      WRITE (KE,740) ANGLAB
```

```
      WRITE (KE,750) VELBM
      WRITE (KE,755) IPTAVG
      WRITE (KE,760) RDMASS
      WRITE (KE,773) IEC
      WRITE (KE,775) IFIRST, ILAST
      WRITE (KE,777) ANT
      WRITE (KE,778) SP
      WRITE (KE,780) BENG, KZ
      WRITE (KE,790) SENG, JU
      WRITE (KE,850) VBIG, IVC
      WRITE (KE,900)

700   FORMAT(X, 'DATE(FILENAME): ',16A1)
702   FORMAT(/,1X,A47)
705   FORMAT(/,1X,'THE CALCULATIONS ARE FOR FRAGMENT: ',F8.3,
     /,1X,'THE MASS OF OTHER FRAGMENT IS: ',F8.3)
710   FORMAT(X, 'THE DWELL TIME PER MCS CHANNEL IN TOF DATA IS
     ',F4.1,' MICROSECONDS')
720   FORMAT(X, 'THE ION DRIFT TIME IS ', F8.3, ' MICROSECONDS.')
730   FORMAT(X, 'THE PRODUCT FLIGHT PATH IS ', F6.2, ' CM. ')
740   FORMAT(X, 'THE LAB ANGLE IS ', F5.1, ' DEGREES.')
750   FORMAT(X, 'THE PARENT BEAM VELOCITY IS ', F9.2, ' CM/S.')
755   FORMAT(X, 'THE NUMBER OF POINTS SMOOTHING BEFORE TRANSFOR
     MATION IS ',I2)
760   FORMAT(X, 'THE REDUCED MASS OF FRAGMENTS IS ', F8.3, ' A.M.U.')
773   FORMAT(X, 'THE LAST CHANNEL CONSIDERED FOR CALCULATIONS IS:
     ',I4)
775   FORMAT(X, 'CHANNEL X1 AND CHANNEL X2 FOR BACKGROUND
     SUBTRACTION ARE: ',I3,' AND ',I3)
777   FORMAT(X, 'THE NOZZLE TEMPERTURE IS (MILLI VOLTS): ',F5.1)
778   FORMAT(X, 'THE STAGNATION PRESSURE IS: ',F6.1)
780   FORMAT(X, 'THE MAXIMUM INTENSITY IS AT ENERGY ', F8.3,
     ' AND CHANNEL ',I4)
790   FORMAT(X, 'THE SMALLEST ENERGY IS ',E10.4,' AT CHANNEL ',I4)
850   FORMAT(X, 'THE LARGEST ENERGY IS ' ,E10.4,' AT CHANNEL ',I4)
900   FORMAT(/,X,'THE CHANNEL, ENERGY, AND INTENSITY VALUES
     REQUESTED ARE:',//)

C     NORMALIZING ONLY THE PART OF DATA THAT DOESN'T FOLD.
      DO 1100 I=1, IEC
C     IF (I .GT. JU) THEN
C     ENGYCM(I)=SENG
C     INTENS(I)=SINT
```

```
C       ENDIF
        INTENS(I)=INTENS(I)/BIG
1100    CONTINUE

        IF (IVAX.NE.1) GOTO 1130
        OPEN (UNIT=11, NAME=DATVAX, TYPE='NEW')
C       WRITING TO UNIT 11 TO TRANSFER TO VAX FOR FURTHER WORK
C       WRITE (11,*) (ENGYCM(I), INTENS(I), I=1,IEC)
        DO 1125 I=(ICON+1),IEC,ISU
        WRITE (11,*) ENGYCM(I), INTENS(I), I
1125    CONTINUE
        CLOSE (UNIT=11)

C       PRINTING THE CHANNEL, ENERGY, AND INTENSITY REQUESTED.
1130    DO 1150 JV=ITC1, ITC2, 2
        WRITE (KE,*) JV, ENGYCM(JV), INTENS(JV),
        JV+1, ENGYCM(JV+1), INTENS(JV+1)
1150    CONTINUE

C       FROM HERE ON WE ARE PLOTTING
        CALL CHOICE (IUNIT)
1200    CALL INIPLT (IUNIT, 10.25, 7.25)
        CALL WINDOW (1.4, 9.6, .9, 6.2)
        CALL SCALE  (XMIN, XMAX, YMIN, YMAX)
        IF (IUNIT.EQ.7) CALL PLTSTR (170, 490, HEAD, MIK, 1, 3)
        CALL PLTSTR (350, 1310, HEAD, 30, 1, 3)
        CALL AXIS   (XTIC, YTIC, 'CENTER-OF-MASS ENERGY (KCAL/MOLE)'
C       CALL AXIS   (XTIC, YTIC, 'BOND ENERGY (KCAL/MOLE)'
        , 33, 2, 0, 'PROBABILITY', 11, 2, 1)
        CALL LINE   (ENGYCM, INTENS, IEC, 1, ID, 1, IC)
        CALL DASHLN (Q2, S2, 2, 0, 0, 1, 1, 1)
        CALL INILGN (6., 11., 5., 6.)
        CALL WRILGN (DATE, 15, 0, 0, 0, 0, 1)
        CALL ENDLGN
        CALL ENDPLT
C       HERE WE ARE GENERATING FOR009.DAT FOR PLOTTER.
        IF (IUNIT.EQ.9) GOTO 1300
        IUNIT=9
        GOTO 1200

1300    STOP
        END
```

```
      SUBROUTINE SMOOFT(Y, N, IPTS)

C*********************************************************************
C
C     NAME: SMOOFT.SUB
C
C     SMOOTH AN ARRAY Y OF LENGTH N WITH A WINDOW WHOSE FULL
C     WIDTH IS OF ORDER PTS NEIGHBORING POINTS, A USER SUPPLIED
C     VALUE, Y IS MODIFIED.
C
C*********************************************************************

      REAL*4 FAC
      PARAMETER(MMAX=1024)
      DIMENSION Y(MMAX)
      M=2
      NMIN=N+2*IPTS
1     IF(M.LT.NMIN)THEN
      M=2*M
      GO TO 1
      ENDIF
      XIPTS=FLOAT(IPTS)
      XM=FLOAT(M)
      CONST=(XIPTS/XM)**2
      Y1=Y(1)
      YN=Y(N)
      RN1=1./(N-1.)
      DO 110 J=1,N
      Y(J)=Y(J)-RN1*(Y1*(N-J)+YN*(J-1))
110   CONTINUE
      IF(N+1.LE.M)THEN
      DO 120 J=N+1,M
      Y(J)=0.
120   CONTINUE
      ENDIF
      M02=M/2
      CALL REALFT(Y,M02,1)
      Y(1)=Y(1)/M02
      FAC=1.
      DO 130 J=1,M02-1
      K=2*J+1
      IF(FAC.NE.0.)THEN
      A=FLOAT(J)
```

```
      B=CONST
      C=(1.-B*A**2)/M02
      FAC=MAX(0.,C)
      Y(K)=FAC*Y(K)
      Y(K+1)=FAC*Y(K+1)
      ELSE
      Y(K)=0.
      Y(K+1)=0.
      ENDIF
130   CONTINUE
      AA=FLOAT(M02)
      BB=(1.-0.25*XIPTS**2)/AA
      FAC=MAX(0.,BB)
      Y(2)=FAC*Y(2)
      CALL REALFT(Y,M02,-1)
      DO 140 J=1,N
      Y(J)=RN1*(Y1*(N-J)+YN*(J-1))+Y(J)
140   CONTINUE
      RETURN
      END


      SUBROUTINE REALFT(DATA,N,ISIGN)

C**********************************************************************
C
C     CALCULATES THE FOURIER TRANSFORM OF A SET OF 2N
C     REAL-VALUED DATA POINTS.  REPLACES THIS DATA (WHICH IS
C     STORED IN ARRAY DATA) BY THE POSITIVE FREQUENCY HALF OF ITS
C     COMPLEX FOURIER TRANSFORM.  THE REAL-VALUED FIRST AND
C     LAST COMPONENTS OF THE COMPLEX TRANSFORM ARE RETURNED
C     AS ELEMENTS DATA(1) AND DATA(2) RESPECTIVELY.  N MUST BE A
C     POWER OF 2.  THIS ROUTINE ALSO CALCULATES THE INVERSE
C     TRANSFORM OF A COMPLEX DATA ARRAY IF IT IS THE TRANSFORM
C     OF REAL DATA.  (RESULT IN THIS CASE MUST BE MULTIPLIED BY
C     1/N).
C**********************************************************************

      REAL*8 WR,WI,WPR,WPI,WTEMP,THETA
      DIMENSION DATA(2*N+2)
      THETA=6.28318530717959D0/2.0D0/DFLOAT(N)
      WR=1.0D0
      WI=0.0D0
```

```
      C1=0.5
      IF (ISIGN.EQ.1) THEN
      C2=-0.5
      CALL FOUR1(DATA,N,+1)
      DATA(2*N+1)=DATA(1)
      DATA(2*N+2)=DATA(2)
      ELSE
      C2=0.5
      THETA=-THETA
      DATA(2*N+1)=DATA(2)
      DATA(2*N+2)=0.0
      DATA(2)=0.0
      ENDIF
      WPR=-2.0D0*DSIN(0.5D0*THETA)**2
      WPI=DSIN(THETA)
      N2P3=2*N+3
      DO 210 I=1,N/2+1
      I1=2*I-1
      I2=I1+1
      I3=N2P3-I2
      I4=I3+1
      WRS=SNGL(WR)
      WIS=SNGL(WI)
      H1R=C1*(DATA(I1)+DATA(I3))
      H1I=C1*(DATA(I2)-DATA(I4))
      H2R=-C2*(DATA(I2)+DATA(I4))
      H2I=C2*(DATA(I1)-DATA(I3))
      DATA(I1)=H1R+WRS*H2R-WIS*H2I
      DATA(I2)=H1I+WRS*H2I+WIS*H2R
      DATA(I3)=H1R-WRS*H2R+WIS*H2I
      DATA(I4)=-H1I+WRS*H2I+WIS*H2R
      WTEMP=WR
      WR=WR*WPR-WI*WPI+WR
      WI=WI*WPR+WTEMP*WPI+WI
210   CONTINUE
      IF (ISIGN.EQ.1) THEN
      DATA(2)=DATA(2*N+1)
      ELSE
      CALL FOUR1(DATA,N,-1)
      ENDIF
      RETURN
      END
```

```
      SUBROUTINE FOUR1(DATA,NN,ISIGN)

C*****************************************************************
C
C     REPLACES DATA BY ITS DISCRETE FOURIER TRANSFORM, IF ISIGN IS
C     INPUT AS 1; OR REPLACES DATA BY NN TIMES ITS INVERSE
C     DISCRETE FOURIER TRANSFORM, IF ISIGN ISINPUT AS -1.  DATA IS A
C     COMPLEX ARRAY OF LENGTH NN OR EQUIVALENTLY, A REAL
C     ARRAY OF LENGTH 2*N.
C     NN MUST BE AN INTEGER POWER OF 2.
C
C*****************************************************************

      REAL*8 WR,WI,WPR,WPI,WTEMP,THETA
      DIMENSION DATA(2*NN)
      N=2*NN
      J=1
      DO 310 I=1,N,2
      IF(J.GT.I)THEN
      TEMPR=DATA(J)
      TEMPI=DATA(J+1)
      DATA(J)=DATA(I)
      DATA(J+1)=DATA(I+1)
      DATA(I)=TEMPR
      DATA(I+1)=TEMPI
      ENDIF
      M=N/2
2     IF ((M.GE.2).AND.(J.GT.M)) THEN
      J=J-M
      M=M/2
      GO TO 2
      ENDIF
      J=J+M
310   CONTINUE
      MMAX=2
3     IF (N.GT.MMAX) THEN
      ISTEP=2*MMAX
      THETA=6.28318530717959D0/(ISIGN*MMAX)
      WPR=-2.D0*DSIN(0.5D0*THETA)**2
      WPI=DSIN(THETA)
      WR=1.D0
      WI=0.D0
      DO 320 M=1,MMAX,2
```

```
      DO 330 I=M,N,ISTEP
      J=I+MMAX
      TEMPR=SNGL(WR)*DATA(J)-SNGL(WI)*DATA(J+1)
      TEMPI=SNGL(WR)*DATA(J+1)+SNGL(WI)*DATA(J)
      DATA(J)=DATA(I)-TEMPR
      DATA(J+1)=DATA(I+1)-TEMPI
      DATA(I)=DATA(I)+TEMPR
      DATA(I+1)=DATA(I+1)+TEMPI
330   CONTINUE
      WTEMP=WR
      WR=WR*WPR-WI*WPI+WR
      WI=WI*WPR+WTEMP*WPI+WI
320   CONTINUE
      MMAX=ISTEP
      GO TO 3
      ENDIF
      RETURN
      END
```

```
      SUBROUTINE MAXMIN (Y, N, YMAX, CMAX, YMIN, CMIN)

C*********************************************************************
C
C     NAME: MAXMIN.SUB
C
C     3-20-88
C
C*********************************************************************

      DIMENSION Y(N)

      YMAX=0
      YMIN=9999999

      DO 100 I=1, N
      IF (YMAX.LT.Y(I)) THEN
      YMAX=Y(I)
      CMAX=I
      ENDIF

      IF (YMIN.GT.Y(I)) THEN
      YMIN=Y(I)
      CMIN=I
      ENDIF
100   CONTINUE

      RETURN
      END
```

```
      SUBROUTINE CHOICE (ORDER)

C*****************************************************************
C
C     NAME: CHOICE.SUB
C
C*****************************************************************

      INTEGER ORDER
      REAL WORD
      ORDER = 0
401   TYPE 1, 'ARE YOU GOING TO USE TERMINAL(TT) OR PLOTTER(PT):'
1     FORMAT(X, A50, $)
      ACCEPT 2, WORD
2     FORMAT(A2)
      IF(WORD .EQ. 'TT') ORDER = 7
      IF(WORD .EQ. 'PT') ORDER = 9
      IF(ORDER .EQ. 0) GOTO 401
      RETURN
      END
```

PARAMETER FILE FOR CONV.FOR PROGRAM

PROGRAM MAKES CALCULATION FOR WHICHEVER FRAGMENT LABELED MASSA.

```
SO2 -------> SO + O    PULSE NOZZLE              COMMENT
ENERGY SO                                    HEADING
9                                         HEADING SIZE
102001.LOG                                  FILE NAME/DATE
1                  CREATE A VAX FILE?     1)YES       2)NO
VM:A.LOG           FILENAME TO BE CREATED FOR VAX
1                  INTERVAL NUMBER OF DATA WRITTEN TO FILENAME.
2                  WRITE TO:              1)PRINTER   2)SCREEN
-1      8=-..-.. 7=-.-. 2-6=DASHED 1=LINE+DOTS 0=LINE -1=DOTS
3              SHAPE OF THE SYMBOLE(0-5) 0=PLUS 1=CROSS 3=CIRCLE
30 0 10 1.1 -.1 .3            XMAX-XMIN-XTIC,YMAX-YMIN-YTIC
210 425 ----------------------------------CHANNELS PRINTOUT
425 ---------------LAST CHANNEL CONSIDERED FOR CALCULATIONS
4 -----------------------------NUMBER OF POINTS AVERAGING
0  ------------------------- NOZZLE TEMPERTURE(MILLI VOLTS)
15 ------------------------------------STAGNATION PRESSURE
30 ------------------------------------------------LAB ANGLE
48.063 15.999 ------------------------------  MASSA, MASSB
10 100  --------------------X1,X2 FOR BACKGROUND SUBTRACTION
2 ---------------------------------CHANNEL WIDTH(MICRO SEC)
28 ----------------------------------DRIFT TIME(MICRO SEC)
84.4 ---------------------------------------PATH LENGTH(CM)
113157.9 ---------------------------------- VELOCITY(CM/SEC)
```

```
C*****************************************************************
C
C      OCTOBER 19 1988
C
C      NAME: NEWTON.FOR
C
C      THIS PROGRAM WILL CALCULATE THE VALUES FOR NEWTON
C      DIAGRAM.
C                              ABC -----> AB + C
C
C*****************************************************************

       DIMENSION B(30),V1(30),V2(30),VE(30),VK(30),VL(30),X1(30),Y(30)

       OPEN (UNIT=22, NAME='NEWTON.PAR', TYPE='OLD')

       READ (22,20) W, XW, YW, XMC, XMAB, EABC, EC, ANL, FP, PV
20     FORMAT (//,F9.3,/,F9.3,/,F9.3,/,F9.3,/,F9.3,/,
       F9.3,/,F9.3,/,F9.3,/,F9.3,/,F9.3)

       ELAS=1239.852/193.3
       EAVA=ELAS-EABC-EC
       RM=(XMC*XMAB)/(XMAB+XMC)
       TV=SQRT((5*1.38066E-16*6.02E23*298)/(XMC+XMAB))
       IF (PV.NE.0) TV=PV
       ANG=ANL/57.29578
       N=0

       WRITE (6,30) W,XW,YW,XMC,XMAB,EABC,EC,ANL,EAVA,RM,ELAS,FP,TV
30     FORMAT(1X,'RESULTS FOR DRAWING NEWTON DIAGRAM FROM
       PROGRAM NEWTON".',//,1X,'REACTION ABC ----> AB(1) + C(2)',//,1X,
       'W  (1/CM) IS: ',F9.3,/,1X,'XW (1/CM) IS: ',F7.3,/,1X,'YW (1/CM) IS:
       ',F7.3,/,1X,'MASS OF C  (G/MOLE) IS: ',F7.3,/,1X,'MASS OF AB (G/MOLE)
       IS: ',F7.3,/,1X,'DISSOCIATION ENERGY (EV) IS: ',F5.3,/,1X,'ENERGY OF C
       (EV) IS: ',F5.3,/,1X,'THE LAB ANGLE IS:',F6.2,/,1X,'MAXIMUM AVAILABLE
       ENERGY (EV) IS: ',F5.3,/,1X,'REDUCED MASS (G/MOLE) IS:
       ',F7.3,/,1X,'ENERGY OF LASER (EV)  IS: ',F5.3,/,1X,'FLIGHT PATH (CM) IS:
       ',F7.3,/,1X,    'BEAM VELOCITY (CM/SEC) [V=SQRT(5KT/M)] IS:
       ',F9.3,/////,3X,'V',3X,'EVIB (EV)',1X,'VCM1(CM/S)',1X,'VCM2(CM/S)'1X,
       'K.E(KCAL/MOLE)',/)

       DO 100 I=1,21
       B(I)=((W*((I-1)+.5))-(XW*((I-1)+.5)**2)+(YW*((I-1)+.5)**3))*1.2398E-4
```

```
      IF (EAVA-(B(I)-B(1)).LT.0) GOTO 105
      N=N+1
      Y(I)=0
      V1(I)=SQRT((((EAVA-(B(I)-B(1)))*1.6022E-12)/
      (.5*(RM/6.02205E23)*(1+(XMAB/XMC))**2)))
      V2(I)=V1(I)*(XMAB/XMC)
      VE(I)=.5*RM*(V1(I)**2)*((1+(XMAB/XMC))**2)/
      (6.02205E23*1.6022E-12)
      VK(I)=VE(I)*23.06
      AA=SQRT((4*TAN(ANG)**2*TV**2)-(4*(1+TAN(ANG
      )**2)*(TAN(ANG)**2*(TV**2-V1(I)**2))))
      BB=((2*TAN(ANG)*TV)+AA)/(2*(1+TAN(ANG)**2))
      VL(I)=BB/SIN(ANG)
      X1(I)=SQRT(TV**2+V2(I)**2-(2*TV*V2(I)*COS(ASIN(BB/V1(I)))))
      WRITE (6,50) I-1, B(I), V1(I), V2(I), VK(I)
50    FORMAT(2X,I2,2X,F9.6,2X,F8.1,2X,F8.1,2X,F9.5)
100   CONTINUE

105   WRITE (6,110)
110   FORMAT(/,3X,'V',2X,'K.E(EV)',1X,'VL1(CM/S)',1X,'VL2(CM/S)',
      3X,'FT1',6X,'FT2',/)
      DO 120 J=1,N
      FT1=(FP/VL(J))*1E6
      FT2=(FP/X1(J))*1E6
      WRITE (6,115) J-1, VE(J), VL(J), X1(J), FT1, FT2
115   FORMAT(2X,I2,2X,F7.4,2X,F8.1,2X,F8.1,2X,F7.2,2X,F7.2)
120   CONTINUE

      XMAX=V2(1)
      V2(N+2)=-TV
      V2(N+1)=0
      CALL INIPLT (9, 10.25, 7.25)
      CALL WINDOW (1.4, 9.3, .4, 6.2)
      CALL SCALE  (-XMAX, XMAX, -1., 1.)
      CALL LINE   (V2, Y, N+2, 0, 1, 1, -1)
      CALL LINE   (V1, Y, N  , 1, 1, 1, -1)
      CALL ENDPLT

      STOP
      END
```

PARAMETER FILE FOR NEWTON.FOR PROGRAM

ABC -----> AB(1) + C(2)
THE FORMAT FOR READING THE DATA IS F9.3 -----.--- (3 DIGIT AFTER DECIMAL)

1149.200	W (1/CM)
5.630	XW (1/CM)
0.000	YW (1/CM)
15.999	MASS OF FRAGMENT C
48.060	MASS OF FRAGMENT AB
5.629	DISSOCIATION ENERGY OF PARENT (EV)
0.000	ENERGY OF FRAGMENT C WHEN FORMED (EV)
30.000	PARENT LAB ANGLE
82.000	FLIGHT PATH
0.000	PARENT VELOCITY (IF YOU WANT TO USE SQRT(5KT/M) ENTER 0) UNITS ARE CM/SEC.